

IAEA TECDOC SERIES

IAEA-TECDOC-1913

Modelling of Fuel Behaviour in Design Basis Accidents and Design Extension Conditions

Proceedings of a Technical Meeting



IAEA

International Atomic Energy Agency

IAEA SAFETY STANDARDS AND RELATED PUBLICATIONS

IAEA SAFETY STANDARDS

Under the terms of Article III of its Statute, the IAEA is authorized to establish or adopt standards of safety for protection of health and minimization of danger to life and property, and to provide for the application of these standards.

The publications by means of which the IAEA establishes standards are issued in the **IAEA Safety Standards Series**. This series covers nuclear safety, radiation safety, transport safety and waste safety. The publication categories in the series are **Safety Fundamentals**, **Safety Requirements** and **Safety Guides**.

Information on the IAEA's safety standards programme is available on the IAEA Internet site

<http://www-ns.iaea.org/standards/>

The site provides the texts in English of published and draft safety standards. The texts of safety standards issued in Arabic, Chinese, French, Russian and Spanish, the IAEA Safety Glossary and a status report for safety standards under development are also available. For further information, please contact the IAEA at: Vienna International Centre, PO Box 100, 1400 Vienna, Austria.

All users of IAEA safety standards are invited to inform the IAEA of experience in their use (e.g. as a basis for national regulations, for safety reviews and for training courses) for the purpose of ensuring that they continue to meet users' needs. Information may be provided via the IAEA Internet site or by post, as above, or by email to Official.Mail@iaea.org.

RELATED PUBLICATIONS

The IAEA provides for the application of the standards and, under the terms of Articles III and VIII.C of its Statute, makes available and fosters the exchange of information relating to peaceful nuclear activities and serves as an intermediary among its Member States for this purpose.

Reports on safety in nuclear activities are issued as **Safety Reports**, which provide practical examples and detailed methods that can be used in support of the safety standards.

Other safety related IAEA publications are issued as **Emergency Preparedness and Response** publications, **Radiological Assessment Reports**, the International Nuclear Safety Group's **INSAG Reports**, **Technical Reports** and **TECDOCs**. The IAEA also issues reports on radiological accidents, training manuals and practical manuals, and other special safety related publications.

Security related publications are issued in the **IAEA Nuclear Security Series**.

The **IAEA Nuclear Energy Series** comprises informational publications to encourage and assist research on, and the development and practical application of, nuclear energy for peaceful purposes. It includes reports and guides on the status of and advances in technology, and on experience, good practices and practical examples in the areas of nuclear power, the nuclear fuel cycle, radioactive waste management and decommissioning.

MODELLING OF FUEL BEHAVIOUR
IN DESIGN BASIS ACCIDENTS
AND DESIGN EXTENSION CONDITIONS

The following States are Members of the International Atomic Energy Agency:

AFGHANISTAN	GERMANY	PAKISTAN
ALBANIA	GHANA	PALAU
ALGERIA	GREECE	PANAMA
ANGOLA	GRENADA	PAPUA NEW GUINEA
ANTIGUA AND BARBUDA	GUATEMALA	PARAGUAY
ARGENTINA	GUYANA	PERU
ARMENIA	HAITI	PHILIPPINES
AUSTRALIA	HOLY SEE	POLAND
AUSTRIA	HONDURAS	PORTUGAL
AZERBAIJAN	HUNGARY	QATAR
BAHAMAS	ICELAND	REPUBLIC OF MOLDOVA
BAHRAIN	INDIA	ROMANIA
BANGLADESH	INDONESIA	RUSSIAN FEDERATION
BARBADOS	IRAN, ISLAMIC REPUBLIC OF	RWANDA
BELARUS	IRAQ	SAINT LUCIA
BELGIUM	IRELAND	SAINT VINCENT AND
BELIZE	ISRAEL	THE GRENADINES
BENIN	ITALY	SAN MARINO
BOLIVIA, PLURINATIONAL STATE OF	JAMAICA	SAUDI ARABIA
BOSNIA AND HERZEGOVINA	JAPAN	SENEGAL
BOTSWANA	JORDAN	SERBIA
BRAZIL	KAZAKHSTAN	SEYCHELLES
BRUNEI DARUSSALAM	KENYA	SIERRA LEONE
BULGARIA	KOREA, REPUBLIC OF	SINGAPORE
BURKINA FASO	KUWAIT	SLOVAKIA
BURUNDI	KYRGYZSTAN	SLOVENIA
CAMBODIA	LAO PEOPLE'S DEMOCRATIC REPUBLIC	SOUTH AFRICA
CAMEROON	LATVIA	SPAIN
CANADA	LEBANON	SRI LANKA
CENTRAL AFRICAN REPUBLIC	LESOTHO	SUDAN
CHAD	LIBERIA	SWEDEN
CHILE	LIBYA	SWITZERLAND
CHINA	LIECHTENSTEIN	SYRIAN ARAB REPUBLIC
COLOMBIA	LITHUANIA	TAJIKISTAN
CONGO	LUXEMBOURG	THAILAND
COSTA RICA	MADAGASCAR	TOGO
CÔTE D'IVOIRE	MALAWI	TRINIDAD AND TOBAGO
CROATIA	MALAYSIA	TUNISIA
CUBA	MALI	TURKEY
CYPRUS	MALTA	TURKMENISTAN
CZECH REPUBLIC	MARSHALL ISLANDS	UGANDA
DEMOCRATIC REPUBLIC OF THE CONGO	MAURITANIA	UKRAINE
DENMARK	MAURITIUS	UNITED ARAB EMIRATES
DJIBOUTI	MEXICO	UNITED KINGDOM OF GREAT BRITAIN AND NORTHERN IRELAND
DOMINICA	MONACO	UNITED REPUBLIC OF TANZANIA
DOMINICAN REPUBLIC	MONGOLIA	UNITED STATES OF AMERICA
ECUADOR	MONTENEGRO	URUGUAY
EGYPT	MOROCCO	UZBEKISTAN
EL SALVADOR	MOZAMBIQUE	VANUATU
ERITREA	MYANMAR	VENEZUELA, BOLIVARIAN REPUBLIC OF
ESTONIA	NAMIBIA	VIET NAM
ESWATINI	NEPAL	YEMEN
ETHIOPIA	NETHERLANDS	ZAMBIA
FIJI	NEW ZEALAND	ZIMBABWE
FINLAND	NICARAGUA	
FRANCE	NIGER	
GABON	NIGERIA	
GEORGIA	NORTH MACEDONIA	
	NORWAY	
	OMAN	

The Agency's Statute was approved on 23 October 1956 by the Conference on the Statute of the IAEA held at United Nations Headquarters, New York; it entered into force on 29 July 1957. The Headquarters of the Agency are situated in Vienna. Its principal objective is "to accelerate and enlarge the contribution of atomic energy to peace, health and prosperity throughout the world".

IAEA-TECDOC-1913

MODELLING OF FUEL BEHAVIOUR
IN DESIGN BASIS ACCIDENTS
AND DESIGN EXTENSION CONDITIONS

PROCEEDINGS OF A TECHNICAL MEETING

INTERNATIONAL ATOMIC ENERGY AGENCY
VIENNA, 2020

COPYRIGHT NOTICE

All IAEA scientific and technical publications are protected by the terms of the Universal Copyright Convention as adopted in 1952 (Berne) and as revised in 1972 (Paris). The copyright has since been extended by the World Intellectual Property Organization (Geneva) to include electronic and virtual intellectual property. Permission to use whole or parts of texts contained in IAEA publications in printed or electronic form must be obtained and is usually subject to royalty agreements. Proposals for non-commercial reproductions and translations are welcomed and considered on a case-by-case basis. Enquiries should be addressed to the IAEA Publishing Section at:

Marketing and Sales Unit, Publishing Section
International Atomic Energy Agency
Vienna International Centre
PO Box 100
1400 Vienna, Austria
fax: +43 1 26007 22529
tel.: +43 1 2600 22417
email: sales.publications@iaea.org
www.iaea.org/publications

For further information on this publication, please contact:

Nuclear Fuel Cycle and Materials Section
International Atomic Energy Agency
Vienna International Centre
PO Box 100
1400 Vienna, Austria
Email: Official.Mail@iaea.org

© IAEA, 2020
Printed by the IAEA in Austria
June 2020

IAEA Library Cataloguing in Publication Data

Names: International Atomic Energy Agency.
Title: Modelling of fuel behaviour in design basis accidents and design extension conditions / International Atomic Energy Agency.
Description: Vienna : International Atomic Energy Agency, 2020. | Series: IAEA TECDOC series, ISSN 1011-4289 ; no. 1913 | Includes bibliographical references.
Identifiers: IAEAL 20-01317 | ISBN 978-92-0-108020-2 (paperback : alk. paper) | ISBN 978-92-0-108120-9 (pdf)
Subjects: LCSH: Nuclear fuels. | Nuclear reactors – Computer programs. | Nuclear reactors — Safety measures. | Computer simulation.

FOREWORD

Increased demands on fuel performance, including transient regimes, higher discharge burnup and longer fuel cycles, have resulted in an increase of loads on fuel and core internals. To satisfy these fuel performance demands while ensuring compliance with safety criteria, new national and international programmes have been launched and advanced modelling codes are being developed. The need for adequate analysis of all aspects of fuel performance to prevent a failure, and to predict fuel behaviour in accident conditions, was evidenced by the accident at the Fukushima Daiichi nuclear power plant.

In response to a recommendation by the Technical Working Group on Fuel Performance and Technology, the IAEA organized a Technical Meeting on Modelling of Fuel Behaviour in Design Basis Accidents and Design Extension Conditions. The meeting, hosted by the China Nuclear Power Technology Research Institute of the China General Nuclear Power Group, in Shenzhen, China, on 13–16 May 2019, was the tenth in the series of IAEA meetings on the topic of fuel performance in accident conditions. The previous meetings were held in 1980 (jointly with OECD Nuclear Energy Agency, in Helsinki), 1983 (Risø, Denmark), 1986 (Vienna), 1988 (Preston, United Kingdom), 1992 (Pembroke, Canada), 1995 (Dimitrovgrad, Russian Federation), 2001 (Halden, Norway), 2011 (Mito, Japan) and 2013 (Chengdu, China). The two most recent meetings focused on modelling of fuel behaviour and modelling under design basis accidents and design extension conditions, reflecting the importance of the subject and the urgent need to accelerate the development and verification of accident related fuel behaviour codes.

The current meeting provided a forum for international experts to review the state of the art of code development for modelling fuel performance of nuclear fuel for water cooled reactors with regard to steady state and transient conditions, for design basis and early phases of severe accidents, including experimental support for code validation for traditional and advanced technology fuels. The meeting was attended by 26 specialists in fuel performance modelling and experimental support from 14 Member States and the Joint Research Centre. Twenty papers were presented at five sessions that covered all topics of the meeting subject. Meeting participants discussed in detail two recently completed coordinated research projects, one on Fuel Modelling in Accident Conditions (FUMAC), held from 2014 to 2018, and one on Analysis of Options and Experimental Examination of Fuels for Water Cooled Reactors with Increased Accident Tolerance (ACTOF), held from 2015 to 2019. A round table discussion on the information exchange in R&D on advanced technology materials helped to define a scope and to outline a new CRP entitled Testing and Simulation for Advanced Technology and Accident Tolerant Fuels (ATF-TS).

The IAEA wishes to thank all participants for their contributions, with special gratitude to the CNPRI hosts for the excellent organization of the meeting including the technical visit to the CNPRI testing facilities. The IAEA officer responsible for this publication was M. Veshchunov of the Division of Nuclear Fuel Cycle and Waste Technology.

EDITORIAL NOTE

This publication has been prepared from the original material as submitted by the contributors and has not been edited by the editorial staff of the IAEA. The views expressed remain the responsibility of the contributors and do not necessarily represent the views of the IAEA or its Member States.

Neither the IAEA nor its Member States assume any responsibility for consequences which may arise from the use of this publication. This publication does not address questions of responsibility, legal or otherwise, for acts or omissions on the part of any person.

The use of particular designations of countries or territories does not imply any judgement by the publisher, the IAEA, as to the legal status of such countries or territories, of their authorities and institutions or of the delimitation of their boundaries.

The mention of names of specific companies or products (whether or not indicated as registered) does not imply any intention to infringe proprietary rights, nor should it be construed as an endorsement or recommendation on the part of the IAEA.

The authors are responsible for having obtained the necessary permission for the IAEA to reproduce, translate or use material from sources already protected by copyrights.

The IAEA has no responsibility for the persistence or accuracy of URLs for external or third party Internet web sites referred to in this publication and does not guarantee that any content on such web sites is, or will remain, accurate or appropriate.

CONTENTS

SUMMARY	1
MAIN RESULTS OF THE CRP FUMAC (Session 1)	
Simulation tools incorporated to DIONISIO in the frame of the FUMAC project	15
<i>M. Lemes, A. Soba, A. Denis</i>	
Qualification of FRAPCON/FRAPTRAN for LOCA fuel behaviour modelling and safety evaluation	29
<i>J. Zhang, A. Dethioux, T. Drieu, C. Schneidesch</i>	
Fuel behaviour modelling in accident conditions in ALCYONE fuel performance code	40
<i>A. Bouloré, C. Struzik, P. Goldbronn, I. Guenot-Delahaie, J. Sercombe</i>	
Qualification of transuranus models for mixed core fuel based on the FUMAC outcome	50
<i>M. Ieremenko, I. Ovdienko</i>	
Main results of FUMAC from CNPRI and sensitivity and uncertainty study of performance of ATF under transient condition	59
<i>Y.R. Xie, Q.S. Ren, Y.D. Zhang</i>	
EXPERIMENTS ON FUEL BEHAVIOUR IN ACCIDENTAL CONDITIONS (Session 2)	
Experimental and modelling results of the QUENCH-19 bundle tests with FeCrAl claddings	71
<i>J. Stuckert, T. Hollands, K. Dolganov</i>	
Oxidation performance and failure behaviour of monolithic and coated ATF claddings under severe accident conditions	86
<i>C. Tang, M. Steinbrueck, M. Grosse</i>	
FUEL PERFORMANCE CODES APPLIED TO DESIGN BASIS ACCIDENTS (DBA) AND TO DESIGN EXTENSION CONDITIONS (DEC) (Session 3)	
Assessment of high conductivity ceramic fuel concept under normal and accident conditions	95
<i>D.S. Gomes, A. Abe, A.T. Silva, R.O.R. Muniz, C. Giovedi, M.R. Martins</i>	
Modelling of accident scenarios with the FINIX fuel behaviour module	102
<i>H. Loukusa, J. Peltonen, V. Tulkki</i>	
Safety analysis of fuel behaviour for implementation licensing	111
<i>H. Papp, K. Kulacsy</i>	
Fuel behaviour during DBA and DEC: analytical and experimental studies for development of ATF	115
<i>A.J. Gaikwad, A. K. Deo, P. Sharma, K. Obaidurrahman, S. Bera</i>	
An introduction to a multidimensional reactor simulation environment with the capability of advanced modelling of nuclear fuel under accident conditions	124
<i>R. Vadi, K. Sepanloo</i>	
Simulation of IFA650.5 experiment using the fully coupled SPACE-FRAPTRAN code system	136
<i>H.C. Kim, S.W. Lee, K.D. Kim</i>	
Thermo mechanical performance of TRISO coated fuel particle used in high temperature Gas Cooled Reactor	145
<i>S. Liu, Y. Zhou, P. Chen, W. Li, S. Gao, H. Pang, C. Tang, X. Qiu</i>	

MAIN RESULTS OF THE CRP ACTOF (Session 4)

Reactivity Initiated Accident assessment for ATF cladding materials.....	155
<i>C. Giovedi, M.R. Martins, A. Abe, R. Reis, A.T. Silva</i>	
Round Robin exercise of the candidate ATF cladding materials within the ACTOF project.....	162
<i>M. Ševeček, J. Krejčí, A. Chalupová, J. Kabátová, F. Manoch, J. Kočí, L. Cvrček,</i> <i>C. Tang, M. Steinbrück, M. Grosse, S. Penttilä, J.-M. Autio, J. Lydman,</i> <i>A. Toivonen, B. Sartowska, W. Starosta, L. Waliś, A. Krześniak, E. Pańczyk,</i> <i>P. Kalbarczyk, K. Kulisa, J. Smolik, J. Mizeracki, Z. Hózer, T. Novotny,</i> <i>E. Perezné Feró, A. Pintér Csordás, M. Horváth, P. Szabó, C. Giovedi, P. Xu</i>	
Introduction of ATF development and main results of the CRP on ACTOF of KAERI	174
<i>C.H. Shin, H.C. Kim, Y.S. Yang</i>	

MODELLING OF TRADITIONAL UO₂ AND ADVANCED ATF FUELS BEHAVIOUR IN INTEGRAL SEVERE ACCIDENT (SA) CODES (Session 5)

Status of ATF modelling and application with ATHLET-CD	183
<i>T. Hollands, L. Lovasz, C. Bals</i>	
Advanced LOCA safety criteria: implementation in mechanistic fuel performance codes and applications	191
<i>M. Veshchunov, A. Boldyrev, V. Shestak</i>	
List of Participants	207

SUMMARY

1. INTRODUCTION

The Technical Meeting (TM) on Modelling of Fuel Behaviour in Design Basis Accidents and Design Extension Conditions, was held on May 13-16, 2019, in Shenzhen, China. It was organised by the IAEA and hosted by China Nuclear Power Technology Research Institute (CNPRI), a company of the China General Nuclear Power Group (CGN).

The objectives were:

- To review Member States' capabilities in modelling, predicting and improving their understanding of the behaviour of nuclear fuel under accident conditions;
- To report on the main results and outcomes of the coordinated research projects (CRPs) on Fuel Modelling in Accident Conditions (FUMAC) and Analysis of Options and Experimental Examination of Fuels with Increased Accident Tolerance (ACTOF);
- To discuss a proposed new CRP on Testing and Simulation of Advanced Technology Fuels (ATF-TS) (planned for 2020-2023).

Twenty-six (26) participants from 14 Member States and 2 International Organizations (IAEA and EC JRC) attended the meeting. The TM was divided in 5 technical sessions:

- Main results of the CRP FUMAC (Chair: Mr. J. Zhang, Belgium);
- Experiments on fuel behaviour in accidental conditions (Chair: Mr. M. Ševeček, Czech Republic);
- Fuel performance codes applied to Design Basis Accidents (DBA) and to Design Extension Conditions (DEC) (Chair: Mr. A. Bouloire, France);
- Main results of the CRP ACTOF (Chair: Ms. T. Liu, China);
- Modelling of traditional UO₂ and advanced ATF fuels behaviour in integral Severe Accident (SA) codes (Chair: Mr. J. Stuckert, Germany).

A total of 20 papers were presented and discussed at the meeting. The main conclusions and recommendations were summarized by the session chairs as follows.

2. SUMMARY OF THE TECHNICAL SESSIONS

2.1. Technical Session 1: Main results of the CRP FUMAC

The first session was chaired by Mr. Jinzhao Zhang, Tractebel (Engie), Belgium.

2.1.1. Overview

This session provided an overview of the recently completed the IAEA Coordinated Research Project on Fuel Modelling in Accident Conditions (CRP FUMAC). Within the FUMAC project, the following achievements were made:

- Verified experimental data set on fuel characteristics in accident conditions (in particular LOCA) and design extension conditions (DEC), supporting fuel rod codes development and validation for potential extension of the IFPE database;
- Better predictive capacities of fuel modelling codes: improved models, material properties and codes for the simulation of nuclear fuel under DBA and severe accident conditions, statistical uncertainty and sensitivity analysis method;
- Extended collaboration between some Member States organisations (examples: INL–POLIMI–JRC collaboration agreement; IFE–IBRAE collaboration and joint presentation at the Enlarged Halden Programme Group Meeting, 2017) beyond the FUMAC project timeframe.

Many participants have acknowledged the IAEA for organising this CRP, which provided an ideal platform to compare their code results with others and especially with experimental data, to which they otherwise would not have had access.

All experimental data analysed reveal a relatively large spread of the measured burst strains, which is not only determined by the local conditions of temperature and pressure, but also by heterogeneities and composition or micro-structural variations in the materials under investigations. An uncertainty analysis of the experimental data was therefore recommended, including those data that have been used for the development and validation of the codes applied.

It has been reiterated that this CRP triggered new collaborations, leading for example to the common development of improved models (e.g. fission gas release model, large strain deformation model, axial fuel relocation model), in particular for those that are used by a larger user group (e.g. FRAPTRAN, TRANSURANUS). It has also enabled to point out differences in the interpretation of some experiments and therefore in the use of the codes, the so-called “user effect”.

The continuous participation of the organisations providing the experimental data was also very instrumental in clarifying various questions raised during the project.

2.1.2. Summary of presentations

A total of six papers were presented in this session.

The first presentation on overview of the CRP FUMAC described the organization and structure of the Project was done by Mr. M. Veshchunov from the IAEA. The CRP was initiated in light of the Fukushima accident under the umbrella of the IAEA Action Plan on Nuclear Safety, following a recommendation of the 2012 meeting of the IAEA Technical Working Group on Fuel Performance and Technology (TWG FPT) to launch a new fuel modelling CRP focusing on accident conditions. The CRP FUMAC was launched in 2014 and ended in 2018. The objectives of the CRP were:

- Analysis and better understanding of fuel behaviour in accident conditions, with a focus on LOCA (DBA), in line with the early stage of the scenario of the Fukushima accident (BDBA);
- Collection of well checked results of accident simulation experiments, and dissemination of experience in the organizations of Member States;
- Identification of best practices in the application of physical models and computer codes used in different Member States for modelling of fuel in accident conditions, and enhancement of predictive capacities of these models and codes.

Twenty-six (26) organizations from 18 Member States participated in the CRP. Selected sets of accident simulation experimental results were provided by the CRP participants and will be integrated into the International Fuel Performance Experiments (IFPE) Database (developed in close co-operation and co-ordination between OECD/NEA, the IAEA and the IFE/OECD/Halden Reactor Project). The codes used for benchmarking ranged from fuel performance codes (ALCYONE, BISON, DIONISIO, FRAPTRAN, FTPAC, RAPTA, TRANSURANUS) to system or severe accident codes (ATHLET-CD, MARS, MELCOR, SOCRAT). An uncertainty and sensitivity analysis was also performed on Halden LOCA test IFA-650.10. The results were compiled and compared with the available experimental data.

The second paper on the simulation tools incorporated to DIONISIO was presented by Mr. M. Lemes from ANEA, Argentina. Several models related to the cladding response in high temperature range: oxidation, hydrogen uptake and release, ballooning and burst, were incorporated to the DIONISIO code within the frame of the IAEA CRP FUMAC) to simulate accidental conditions, in particular the so-called LOCA. A specially designed thermal hydraulic subroutine provides a simplified description of the rod environment in normal or accidental conditions. The heat transfer coefficients corresponding to the different coolant regimes are activated as the corresponding conditions are met. Simulation of different experiments has shown that, despite its simplicity this subroutine gives adequate predictions of the conditions in the channel, not far from those given by specific thermal hydraulic codes. With its incorporation, the description of the fuel rod atmosphere, which may consist of single (liquid or vapor) or double phases, provides quite realistic boundary conditions for the simulation of the fuel rod behavior, without requiring the intervention of external specific thermal hydraulic codes. The calculation scheme divides the rod length into a user-defined number. The physical and chemical parameters in one representative pellet subjected to the local conditions of the segment are solved, with the synchronous work of all the subroutines. Then, a description of the whole rod is obtained by coupling all the segments. This strategy has yielded accurate simulations of a wide variety of cases, either in normal or LOCA type conditions. Exhaustive comparisons were carried out with several thermal hydraulic codes (COBRA-IV, RELAP5-Mod3.1, SOCRAT, ATHLET-Mod 1.1)

and with a number of experiments like those of the IFA-650 series (-1, -2, -9, -10, -11), PUZRY, QUENCH-L0/L1 (for which a new working scheme was specially developed in DIONISIO), CORA-15, IAEA-SPE-4, among others.

The third paper on qualification of FRAPCON/FRAPTRAN for LOCA fuel behaviour modelling and safety evaluation was presented by Mr. J. Zhang, from Tractebel (Engie), Belgium. He presented the model improvements to FRAPTRAN-TE-1.5 code, such as the Quantum Technologies' axial relocation model and errors corrections in the adapted FRAPTRAN-TE-1.5 version. The impacts of the model improvements together with the improvement in the thermal hydraulic modelling by using the imposed thermal hydraulic boundary conditions from SOCRAT calculations and in the thermal boundary conditions (axial power profile, plenum temperature) on the calculation results for the selected Halden LOCA tests IFA-650.9 and 10 were identified and discussed. In addition, the statistical uncertainty and sensitivity analysis has been performed on the FRAPTRAN-TE-1.5 modelling of the selected Halden LOCA test IFA-650.10, which helped the identification of significant input parameters for LOCA fuel behaviour modelling. The final objective was to apply the qualified fuel rod transient analysis codes FRAPCON/FRAPTRAN to develop an efficient methodology for assessing the performance and quantifying the margins for advanced technology fuel designs under design basis accident conditions (in particular LOCAs). The perspectives for further model improvements and benchmarks, as well as the LOCA fuel safety evaluation methodology development and applications were also discussed.

The fourth paper, fuel behaviour modelling in accident condition in ALCYONE fuel performance code, was presented by Mr. A. Bouloure (CEA, France). He presented the CEA development of the ALCYONE fuel performance code for PWR fuel in the PLEIADES software environment. It is dedicated to normal, off-normal and accident conditions such as RIA and LOCA. CEA's participation to the IAEA FUMAC CRP led to an improvement of the fuel modelling in LOCA conditions. Specific developments of the fuel performance code for the LOCA conditions have been done regarding cladding behaviour modelling, fission gas release and stress evaluation in the pellet before and during the tests. The improved code has been used to simulate some of the experiments of interest of the FUMAC project (IFA650.10 and Studsvik 192 LOCA test). For IFA650.10, the cladding outer temperature profile calculated with the SOCRAT code has been used. The results obtained with ALCYONE were in a good agreement with the experimental data. In terms of uncertainty quantification, the uncertainty on the determination of the boundary conditions like cladding outer temperature resulted in a large uncertainty on the cladding deformation and the burst time.

In the fifth paper on qualification of TRANSURANUS models for mixed core fuel based on the FUMAC outcome, Mr. M. Ieremenko (SSTC, Ukraine) presented results of testing of the TRANSURANUS code for modelling the behaviour of WWER nuclear fuel in the LOCA accident conditions. A simulation of a part of the experimental data (MTA-EK data, IFA-650.10, IFA 650.11 and Studsvik 192&198) was performed. Also calculations of some of these data sets and KIT QUENCH-L1 set were carried out by other teams using the TRANSURANUS code (INRNE, Bulgaria; JRC, Germany). TRANSURANUS code demonstrated good possibility to predict behaviour of nuclear fuel rod cladding. Predicted geometry of cladding and time of burst for both general types of cladding (PWR and WWER) showed good correlations with experimental data for such type of regimes. In addition, the experimental data of the FUMAC project contained the results of post-irradiation measurements after operational in commercial reactor. This data was used to test the capabilities of the TRANSURANUS code for modelling of the irradiated fuel rod behaviour in the core.

The last paper on the main results of FUMAC from CNPRI and sensitivity and uncertainty study of performance of ATF under transient condition was presented by Ms. Q. Ren (CGN, China). With the simulation of Halden fuel rod LOCA behaviour tests IFA-650.9/10/11 using FRAPCON/FRAPTRAN, evaluation of integrated performance of fuel rod under LOCA condition was performed. Generally, FRAPCON/FRAPTRAN predicted well the fuel rod behaviour under LOCA condition. Sensitivity and uncertainty study on IFA-650.10 was then performed using the DAKOTA code, for both conventional fuel ($\text{UO}_2 + \text{Zry-4}$) and ATF fuel systems ($\text{UO}_2\text{-BeO} + \text{ODS FeCrAl}$). Based on assumed uncertainty distributions for selected input parameters (5 fuel rod design data in uniform distribution, 12 physical properties and thermal hydraulic conditions), several global sensitivity methods have been tested in order to determine the influence on the clad failure time under LOCA condition. It was found out that the design parameters, especially the pellet diameter have important influence on fuel system's performance during LOCA. Proper adjustment of design parameters can optimize the fuel performance for ATF.

2.1.3. General conclusion

- All experimental data analyzed reveal a relatively large spread of the measured burst strains, which is not only determined by the local conditions of temperature and pressure, but also by heterogeneities and composition or micro-structural variations in the materials under investigations. An uncertainty analysis of the experimental data was therefore recommended, including those data that have been used for the development and validation of the codes applied;
- The fuel rod codes simulate reasonable agreement in the cladding and fuel thermal behaviours but large dispersions in the cladding deformation and burst time;
- Further improvements in the plenum temperature, fuel relocation, cladding deformation and burst models are needed. The thermal hydraulic boundary conditions are also important;
- Uncertainty and sensitivity analysis is helpful in improving the modelling of fuel behaviour during LOCA.

2.1.4. Further recommendations

- More analysis and cases for WWER fuel would be needed, especially in view of recent advanced fuel developments;
- A general interest has been expressed to consider a similar analysis for advanced fuels and cladding materials, including some of the so-called accident tolerant fuels (ATFs);
- For a successful CRP that involves so many cases and participants, the duration of the project meetings may be extended, enabling for instance to analyse better model details and code changes as well as their comparison with more detailed experimental data;
- Deeper analysis of failure criteria with advanced tools, and uncertainty analysis on experimental data is needed;
- Need more quantitative information about fuel fragmentation.

It is also recommended to focus the future CRP in fuel modelling on more practical applications to support the sustainability of nuclear technology, diversification of fuel supply, and innovation in fuel technology development. The final objective is to apply the qualified fuel rod codes to develop a best estimate plus uncertainty analysis (BEPU) type LOCA hot rod fuel safety evaluation methodology (FSEM) for assessment of the performance of the evolutionary Advanced Technology Fuels (eATFs), and verification of the compliance with the applicable LOCA safety criteria (e.g. the USNRC new LOCA criteria 10CFR50.46c).

2.2. Technical session 2: Experiments on fuel behaviour in accidental conditions

The second technical session focused mainly on the experimental investigation of new ATF cladding concepts to support modelling and simulation activities. It was chaired by Mr. Martin Ševeček, Czech Technical University, Czech Republic.

2.2.1. Overview

The session provides an overview of the experimental testing of different ATF cladding materials such as silicon carbide, FeCrAl alloys, and coated cladding. The bundle test with FeCrAl alloy B136Y was supported also by pre- and post test modelling activities using two severe accident codes. The sessions highlighted the expected benefits as well as the remaining challenges of ATF cladding development.

2.2.2. Summary of presentations

Both contributions incorporated into this session were given by researches from the Karlsruhe Institute of Technology (KIT), Germany. The first contribution was focused on the details of the first-ever integral bundle experiment with ATF cladding material including modelling benchmark that followed. The second talk presented experimental results from testing of four different ATF cladding candidates:

- Mr. Juri Stuckert (KIT, Germany) — Experimental modelling results of the QUENCH-19 bundle tests with FeCrAl claddings;

- Mr. Chongchong Tang (KIT, Germany) — Oxidation performance and failure behaviour of monolithic and coated ATF claddings under severe accident conditions.

Mr. Stuckert presented in his talk an overview of the bundle experiment with FeCrAl alloy in the well-known QUENCH facility at KIT. The B136Y alloy was provided by Oak Ridge National Laboratory and the accident scenario was chosen to allow direct comparison between older QUENCH experiments such as QUENCH-15 test with ZIRLO alloy. B136Y alloy is advanced steel from the group of alloys usually titled as FeCrAl. The composition of B136Y is as follows: Fe-80.85, Cr-12.99, Al-6.14, Y-0,003. It is considered as one of the main near-term ATF candidates. There were several challenges found related to testing of this ATF material. These challenges included also a new design of thermocouples that eventually initiated the melting of the bundle. Additionally, there were steam leakages detected from the bundle that caused the wetting of the insulation and related radial heat losses.

Substantial benefits of B136Y were confirmed by the test including reduced oxidation kinetics and hydrogen production. The coping time that can be quantified for this specific design and scenario is on the order of several thousand seconds. However, new issues related to FeCrAl deployment were identified. One issue is related to the higher coefficient of thermal expansion of FeCrAl that is approximately 3 times higher than Zr. When reflooding and quenching, the dimensional changes cause high stresses and failure of the cladding. Additionally, when FeCrAl melts it is not covered with strong oxide layer such as traditional Zr alloys which allows higher mobility of melts. It was also found that when locally melted, FeCrAl interacts with ZrO₂ pellets that were used. This is not observed for Zr alloys and poses an additional challenge and requires more investigation.

The pre- and post test calculations were performed with ATHLET-CD code by GRS. GRS models showed good agreement with experiment, but serious challenges remain. The main inconsistency is related to the oxidation model used. It strongly underpredicts oxidation and hydrogen release. The post test calculation was done also by IBRAE using the SOCRAT code. The uncertainties revealed by calculation emphasize high needs for more experimental data and separate effect experiments to support the development of new correlations.

In the second talk the team at KIT studied various types of ATF cladding candidates and mainly their behaviour in DBA and DEC conditions. The studied materials are — Cr PVD coated Zry-2, Cr cold spray coated Zry-4, FeCrAl alloys, MAX phase coated Zry-4 and SiC. Mr. C. Tang presented a range of tests with FeCrAl that show that the oxidation resistance of this material depends on the heating scenario. This is due to the complex oxide formation. It was shown that with high heating rates the oxidation of FeCrAl can be catastrophic. Additionally, acceleration of oxidation was observed above 1350°C which is probably linked to Al(OH)₃ melting.

MAX phase coated cladding showed the protective nature of the coating up to 1260°C in the transient test but then local delamination and cracking were observed. Cr cold spray cladding showed good resistance against oxidation at a lower temperature but at higher temperatures, local melting and cladding deformation were observed. Tests with SiC provided by General Atomics and Westinghouse Electric Company were performed up to 1750°C. It was found that silica bubbles formed above 1713°C and cladding locally failed at 1750°C. The protective nature of SiC cladding is ensured only if the protective outer CVD SiC stays intact.

2.2.3. General conclusion

This session emphasized the need for more experimental data even for ATF concepts that have been already inserted into commercial reactors. Both presentations revealed new failure modes and phenomena of ATF cladding materials that were not known previously. The talks also highlighted the need for more high-quality experimental data to support modelling and simulation activities.

2.2.4. Further recommendations

The talks both confirmed the safety benefits of ATF cladding materials. Valuable separate effect test data were presented but the claimed benefits of any ATF candidate should be confirmed by an integral bundle test. It was also shown that ATF cladding material properties strongly vary based on the fabrication parameters. The materials produced by fuel vendors and industry have been optimized in order to achieve the best possible performance. Therefore, the transferability of experimental results between commercial and in-laboratory produced materials is questionable. This was confirmed for both FeCrAl (B136Y alloy vs. laboratory alloy) as well as for Cr coated cladding materials (disagreement with data published by fuel vendors). Additionally, new phenomena such as SiC scale melting and excessive hydrogen release, FeCrAl failure during quenching or bending

of Cr cold-spray coated tubes were identified. This confirms that there is still a high need for experimental testing of ATF cladding concepts including support for modelling and simulation activities.

2.3. Technical session 3: Fuel performance codes applied to design basis accidents (DBA) and to design extension conditions (DEC)

The third technical session was chaired by Mr. Antoine Bouloré, CEA, France.

2.3.1. Overview

Whereas the first session was dedicated to the FUMAC CRP, mainly related to fuel behaviour modelling in Design Basis Accidents, this session was focused on the fuel modelling and simulation in both Design Basis Accidents (DBA), but also in Design Extension Conditions (DEC), which, according to IAEA standards, could include conditions without important fuel degradation and conditions with core melting. During the session, participants have presented their experience and their recent developments in relation with this topic. One objective of this technical meeting was to prepare a proposal for the next CRP. So, in the general discussion at the end of the session, some recommendations and general comments have been raised to help prepare this new CRP.

2.3.2. Summary of presentations

Seven presentations were made during this session:

- Assessment of high conductivity ceramic fuel concept under normal and accident conditions (Mr. A. Abe, Brazil);
- Modelling of accident scenarios with the FINIX fuel behaviour module (Mr. H. Loukusa, Finland);
- Safety analysis of fuel behaviour for implementation licensing (Ms. H. Papp, Hungary);
- Fuel behaviour during DBA and DEC: analytical and experimental studies for development of ATF (Mr. A. Gaikwad, India);
- An introduction to a multidimensional reactor simulation environment with the capability of advanced modelling of nuclear fuel under accident conditions (Mr. R. Vadi, Islamic Republic of Iran);
- Simulation of IFA650.5 experiment using the fully coupled SPACE-FRAPTRAN code system (Mr. H. Kim, Republic of Korea);
- Thermo mechanical performance of TRISO coated fuel particle used in high temperature Gas Cooled Reactor (Mr. S. Liu, China).

Mr. A. Abe showed an example of assessment of an advanced fuel concept. This new fuel is made of UO_2 particles surrounded by BeO matrix, in order to enhance the thermal conductivity of the pellet. A simple model for the equivalent thermal conductivity is presented (mixing law) and considering the standard models in FRAPCON/FRAPTRAN code, the effect of the lower temperature on the fission gas release is also presented.

Mr. H. Loukusa presented a multiphysics coupling scheme developed at VTT. The fuel behaviour module FINIX has been coupled to the neutronics code SERPENT2 and to thermal-hydraulics codes TRAB1D, TRAB3D and HEXTRAN. In the presentation, some elements of validation have been shown (IFA650.5) but also some comparisons between stand-alone and coupled calculations. At the moment, the main limitations of the FINIX module is in mechanical modelling, and this will be improved.

The presentation of Ms. H. Papp was an example of safety analysis, and an illustration of a conservative approach in safety criteria assessment. This conservative approach consists in the selection of the most critical rods in operation, and their deterministic simulation to make sure they verify the safety criteria.

A large number of examples of analytical and experimental studies made for ATF were given by Mr. A. Gaikwad. Physical and chemical properties of many types of coated claddings and an evaluation of their effect in simulations were presented.

The next two presentations were about the development of multiphysics coupling schemes. Mr. R. Vadi presented a simulation environment consisting of three codes (a CFD based code for thermal-hydraulics, and two neutronics codes for point kinetics equations and multigroup diffusion equations). Some results were presented for LOCA conditions. In the presentation of H. Kim, a system analysis code (SPACE) was coupled to the fuel performance code (FRAPTRAN). An illustration of this coupling scheme for LOCA test IFA650.5 was presented.

This test shows that the surface-to-surface radiation must be modelled precisely to predict the cladding temperature. So, both presentations contained some elements of validation of the coupling schemes.

The last presentation of the session by Mr. S. Liu was about TRISO coated fuel particles with UN as the kernel. Taking into account the physical and mechanical properties of the different materials involved in such particles (kernel, coatings, ...), the performance of this type of fuel in RIA conditions are assessed. The main conclusion is that the thermal expansion is the dominant factor resulting in the failure of the particle in RIA conditions.

2.3.3. General conclusions

In this session, several papers about fuel performance code developments and fuel behaviour modelling were presented. The subjects covered the following: modelling of advanced fuel concepts, safety analysis example, link between experimental and modelling activities for ATF and multiphysics coupling.

All presentations in this session contained some validation aspects of the codes and coupling schemes developed (comparison between calculation and experimental data), which is a very good point if the computation tools are used for safety analysis.

2.3.4. Further recommendations

One objective of the present technical meeting was also to prepare the proposal for the new CRP following FUMAC and ACTOF. In the discussion of this session, the link between the modelling capabilities of the Member States and the requirements of this next CRP were listed and discussed.

The first important point was about the validity of the codes for transposition to real reactor cases. Fuel performance codes presented in this session are all “single pin” codes, and the calibration of those codes is performed on single pin experimental data. The transposition of the calculated results to real reactor cases raises some questions. This point should be addressed to the next CRP.

In the second point of the discussion, it was mentioned that each fuel performance code has its own validation domain, which is the domain where calculated results can be compared to experimental data. If the code is used out of its validation domain, extended margins have probably to be considered to take into account the lack of knowledge of fuel behaviour out of this domain. The question of the validity of the extrapolation of the validation domain to new concepts and new materials for ATF should be addressed in the next CRP.

In the session, several presentations introduced multiphysics simulation. Up to now, safety analysis is mainly based on the single fuel pin analysis. But the question of the necessity of multiphysics coupling environment is raised, which should be addressed in the next CRP. The two approaches presented (single fuel pin and multiphysics coupling) have their pros and cons.

As mentioned in conclusion of the first session of this meeting, the next CRP will probably be dedicated to the development of a method to quickly assess the performance of advanced technology fuel using simulation and testing. In this framework, this raises the question of the material properties to be used for the new materials or the new concepts tested. If these concepts are new, there will be probably very few data to consider the evolution of those properties with irradiation. So experimental data are required on the new materials and new concepts to make sure the proper material properties are considered in the simulation. This is why both testing and simulation have to be considered in the definition of the next CRP. In the case of complex materials, such as composite or heterogeneous materials, the modelling of the material properties should also be addressed.

The last point mentioned in the discussion for future work was about the uncertainties. In safety analysis, margins must be defined, and a key point that should be addressed in the next CRP is how to take into account epistemic uncertainties, which represent in fact a lack of knowledge of material properties, for example, in the definition of these margins. The modelling of uncertainties is also a key point, as it was already mentioned in the conclusions of the FUMAC project.

2.4. Technical session 4: Main results of the CRP ACTOF

The fourth session was chaired by Ms. Tong Liu, CNPRI, China.

2.4.1. Overview

This session provided an overview of the recently completed IAEA Coordinated Research Project on Analysis of Options and Experimental Examination of Fuels for Water cooled Reactors with Increased Accident Tolerance (ACTOF). The CRP dealt with the acquisition of data through experiments on new fuel types and cladding materials, development of modelling capacity to predict the behaviour of the components and the integral performance of accident tolerant fuel designs under normal and transient conditions and to demonstrate improvements under severe accident conditions. The objective was to provide information to Member States to support decision making on the choices available to improve the safety of Nuclear Power Plants under normal and severe accident conditions.

Various ATF options were analysed resulting in improved understanding of ATF behaviours and developments of ATF technologies in Member States. For example, several coated cladding materials were produced, tested, characterized and analysed. The feedbacks are important for Member States to improve their ATF concepts and development activities.

Fuel performance codes from participating organizations were significantly extended to the analysis of several ATF concepts (including FeCrAl and SiC claddings, coated zircaloy claddings, and U_3Si_2 fuel). Furthermore, a benchmark was organized and finalized where the extended codes were compared for the analysis of fuel rod behaviour under both normal operation and design-basis accident conditions. Additionally, Monte Carlo simulations were carried out to investigate the effect of new claddings and fuel on a potential cycle. Integral codes (ATHLET-CD and SOCRAT) were applied and benchmarked against the severe-accident bundle test QUENCH-19 with FeCrAl claddings of fuel rods.

2.4.2. Summary of presentations

In this session, four presentations were made:

- Main results of the IAEA Coordinated Research Project on Analysis of Options and Experimental Examination of Fuels for Water cooled Reactors with Increased Accident Tolerance (ACTOF) (Mr. M. Veshchunov, IAEA);
- Reactivity Initiated Accident assessment for ATF cladding materials (Ms. C. Giovedi, Brazil);
- Round Robin exercise of the candidate ATF cladding materials within the ACTOF Project (Mr. M. Ševeček, Czech Republic);
- Introduction of ATF development and main results of the CRP on ACTOF of KAERI (Mr. C. Shin, Republic of Korea).

Mr. M. Veshchunov gave an overview of IAEA CRP ACTOF by introducing the background, objectives, participants and current status of ACTOF. The joint actions (including Round Robin tests, benchmark exercises, severe accident experimental and modelling Exercise), the main outputs as well as the perspectives and recommendations for the new CRP were presented.

Ms. Claudia Giovedi presented preliminary results for FeCrAl HbbBO-5 test case by using modified versions of the FRAPCON-FRAPTRAN codes to simulate the fuel behaviour under steady state and RIA conditions. According to the steady state study, FeCrAl showed better performance as compared to Zircaloy-4: higher fuel temperatures, lower internal pressure, gap remained opened, and lower cladding hoop stress. And RIA simulation results showed a good agreement with the experimental results.

In Mr. Martin Ševeček's presentation, main results of Round Robin Test with ATF cladding candidates were presented, including Cr-coated, MAX phase coated, ZrSi-Cr coated, AISI 348. According the experimental results, only Cr coated concept seemed to be promising from perspective of both long term corrosion and high temperature oxidation resistance.

Mr. Changhwan Shin introduced an overview of R&D activities for ATF in Republic of Korea. KAERI focuses on surface modified Zr cladding with ODS treatments and ceramic or metallic microcell UO_2 pellets as the near-term choice. Mechanical Model of FRACAS-CT for multi-layered cladding has been developed and implemented in FRAPCON. The fuel performance analysis with material properties of ATF developed by KAERI

shows ATF has significant advantage in the reduction of the fuel temperature, cladding oxidation thickness, fission gas release, etc. Safety analysis was conducted to study the ATF benefits in LOCA and BDBA.

2.4.3. General conclusion and further recommendations

The following comments and conclusions were made via presentations and related discussions in the session:

- Development of standard methods and testing procedures are needed for all ATF products;
- Further experiments were proposed to carry out to better understand the failure mechanism and establish new failure criteria for FeCrAl cladding under steady state and transient conditions;
- Most participants showed interests to carry out further round robin tests to enhance the database for better understanding and evaluation of ATF behaviour and performance;
- A new CRP on testing and simulation of advanced technology fuels (ATF-TS) (2020-2023) was proposed.

2.5. Technical session 5: Modelling of traditional UO₂ and advanced ATF fuels behaviour in integral severe accident (SA) codes

The fifth session was chaired by Mr. Juri Stuckert, KIT, Germany.

2.5.1. Overview

This session provided an overview of the results of the benchmark on post test analyses of the CORA-15 bundle test with the system codes ATHLET-CD and SOCRAT, the status of ATF modelling and application in ATHLET-CD, and advanced cladding embrittlement criteria, which could be implemented in mechanistic fuel performance and safety codes and applications.

2.5.2. Summary of presentations

This session included three presentations.

The first paper presented by Mr. J. Stuckert (KIT) described the results of the benchmark on post test analyses of the CORA-15 bundle test with the system codes ATHLET-CD and SOCRAT. The CORA-15 test was conducted under transient conditions typical of many CORA-PWR tests, with bundle containing two (Ag, In, Cd) absorber rods. In contrast to other CORA bundles, all fuel rod simulators with and without heater (16 + 7) were filled with helium and were brought to a pressure of 60 bar before the transition. During the transition process, all the rods were ballooned and burst. Balloons developed over about 100 s. Bursts occurred within 150 s in the temperature range of 650 to 850°C. The most probable burst elevation is a bundle height of 750 mm (the hottest bundle level on the onset of burst). At temperatures above 1800°C, molten Zr formed in the gap between UO₂ and ZrO₂ was partially moved downwards with concurrent dissolution of oxides and partially released through the destroyed zirconium oxide layer. The resulting melt, which mainly contains U, Zr, O, moves downwards in the form of a slug and hardens between 400 and 550 mm in the form of a large porous structure. Above the Inconel lattice spacer at 500 mm, a maximum bundle blocking was observed (almost 100%). The absorber melt, which have a much lower solidus temperature, solidified at a lower bundle level of about 150 mm. Investigations performed after the test showed only slight oxidation of claddings up to bundle elevation of 350 mm. The cladding tubes were completely oxidized between 480 and 1000 mm. The maximum value of hydrogen rate (210 mg/s) was measured at the transient end (4800 s). The total hydrogen mass released during the test was 145 ± 15 g.

The latest version of the ATHLET CD code was used to simulate the CORA-15 test, with very similar set of input data and simulation options as for CORA-13 (pressure free rods; it was subject of the international problem IS-31). In general, for both tests, a good agreement was obtained between the calculated and measured data concerning the temperature evolutions, with a slight underestimation at the top of bundle and a slight overestimation at the bundle bottom. The behavior of pressurized rods in CORA-15 was adequately predicted by the code. The calculated time of the cladding burst, bundle elevation and temperature of the cladding tubes at the burst position were within the experimental ranges. Hydrogen release was determined within the uncertainty of the measured data, overestimating the generation rate during the oxidation acceleration between 4000 and 4500 s. One discrepancy in the calculated results is due to the lack of model of melt retention at spacer grids, which leads to a shift in the blockage profile and overestimation of temperatures at bundle levels below grid spacers.

To analyze the CORA-15 test, the current version V3 of the SOCRAT code was used. From a comparison of the simulation results with the CORA-15 experimental data, it can be concluded that the SOCRAT code reproduces quite well the temperature history of cladding tubes and tends to easily overestimate the temperature of the claddings at the upper end of the heated region. The calculated parameters of bursts (time, temperature, pressure, and bundle elevation), the total mass of hydrogen, and bundle blockage due to relocation and solidification of melt are in good agreement with the data, taking into account the measurement accuracies.

Following the modeling of the experiment CORA-15, it is therefore established that the experimental data are fairly good simulated (temperature history, parameters of bursts, total hydrogen release, final bundle degradation). The results reached during the CORA-15 analysis by both system codes SOCRAT and ATHLET-CD showed a good agreement with the measurements and with each other.

The materials of this presentation on the results of the CORA-15 test and the corresponding post-test analyses with ATHLET CD and SOCRAT were recently published: J. Stuckert, H. Austregesilo, Ch. Bals, Th. Hollands, A. Kiselev, D. Tomashchik, T. Yudina, "Post-test analyses of the CORA-15 bundle test with the system codes ATHLET-CD and SOCRAT", Nuclear Engineering and Design 342 (2019), pp. 320-335, and for this reason are not included the current TECDOC.

The second paper, presented by Mr. L. Lovasz (GRS), described status of ATF modelling and application with ATHLET-CD.

The QUENCH-19 bundle test with FeCrAl claddings was accompanied by post test analyses at GRS with the AC² module ATHLET-CD. The QUENCH-19 test was conducted at KIT similarly to the QUENCH-15 test for comparing the oxidation behaviour of FeCrAl and ZIRLO claddings at high temperatures. In contrast to the test QUENCH-15, which showed a sharp escalation after start of quenching resulting in temperatures up to 1900°C, no escalation occurred during QUENCH-19 and peak cladding temperatures of only about 1450°C were reached. For the post test simulations an oxidation correlation for the KANTHAL APMT alloy was available. One simulation used the oxidation kinetic defined by constants given for KANTHAL APMT, the other used the same constants, but the reaction rate was multiplied by 300. Both approaches were implemented in ATHLET-CD with the assumption that only Al₂O₃ layer was formed at the outer cladding surface, but no other oxides. Compared to oxidation of Zr alloys both approaches gave orders of magnitude lower oxidation rates.

In general, the results of the post test simulation show good agreement of the thermal behaviour. While the maximum temperature well reproduced an underestimation of only about 50°C, the radial temperature profile was significantly underestimated by 150-200°C compared to the measured data. The comparison of the hydrogen production of in total 9 g in the test and less than 1 g for both oxidation approaches in the simulation shows that the oxidation model for FeCrAl in the code must be improved. A sharp increase in the hydrogen release was observed at approximately 800 s before the quenching; one possible trigger for this event could be the failure and melting of the steel cladding of thermocouples and following partial dissolution of claddings. This was not considered in the post test calculations. For a detailed evaluation of the calculated hydrogen generation the post test examination of the bundle is necessary to know which components contribute to the total value.

The third paper, presented by Mr. M. Veshchunov (IAEA), discusses advanced cladding embrittlement criteria, which could be implemented in mechanistic fuel performance and safety codes and applications.

The analysis of experiments on direct quenching after isothermal oxidation at high temperatures showed that the ECR 17% criterion notably underestimates cladding capability to withstand thermal shock during LOCA reflood. On the other hand, the tests (impact, ring compression and 3-point bend) on the capability of the cladding to withstand anticipated loads during fuel handling and transport of the assemblies showed that the 17% criterion notably overestimates ductile-to-brittle transition oxidation level. For this reason, the alternative more advanced and physically based Chung-Kassner criteria as well as the KAERI criterion for post-quench embrittlement are considered for practical applications.

The advanced Chung-Kassner criteria are based on a more physical consideration (related to the thickness of ductile β -Zr phase) and were validated by the authors of the criteria against a very wide set of quenching tests in a wide temperature range (up to 1500–1900°C) that is far beyond LOCA conditions, and thus can be broadened to Design Extension Conditions (DEC). For practical applications of these advanced criteria in fuel performance codes, mechanistic diffusion models of cladding oxidation under high temperature transient conditions should be applied. It allows modelling oxygen and hydrogen radial distributions in the cladding under normal and transient conditions with consideration of cladding-fuel interactions. Utilization of the advanced criteria in the mechanistic SVECHA/QUENCH code allows reasonable predictions not only for LOCA conditions, but also for oxidation and

quenching under severe accident conditions of KIT (with fresh Zry-4 claddings) and RIAR tests (with irradiated WWER fuel fragments).

The second Chung-Kassner criterion on capability to withstand fuel handling, transport and storage should be supplemented with an additional condition related to secondary hydriding, revealed in the KIT QUENCH-LOCA tests (brittle fracture of claddings with local hydrogen content more than 1500 wppm during tensile tests).

The applicability of the KAERI advanced failure criteria (with some potential modifications) for oxidized Zr alloy claddings with Cr coatings was confirmed in the recent ring compression tests performed within the IAEA Coordination Research Project (CRP) ACTOF. On this base it is assumed that extension of the mechanistic oxidation model to consideration of the coated claddings will allow verifying applicability of the advanced Chung-Kassner and KAERI criteria (as well as the KIT complementary criterion) on the base of future tests on the coated cladding quenching (which are foreseen, e.g. in the subsequent CRP on ATF in 2020–2023).

2.5.3. *General conclusions and further recommendations*

The development of mechanistic models for traditional and advanced fuel materials should be continued.

It would be very important to use results of conducted and planned bundle experiments with ATF materials for the organization of benchmarks involving different codes.

A new CRP on ATF materials should include various single effect tests on:

- Determination of oxidation kinetics for reactor relevant FeCrAl alloys, especially near to the melting point of these materials;
- Investigation of Cr coating behaviour at high temperatures for coated Zr alloy claddings.

3. CONCLUDING REMARKS AND RECOMMENDATIONS

In this Technical Meeting, participants exchanged their view on national perspectives, R&D progress and results via paper presentations and discussion forums.

The general remarks were as follows:

- The IAEA CRPs on FUMAC and ACTOF provided an excellent platform to collect relevant experimental data and compare the fuel performance and integral code calculation results with others and especially with experimental data;
- The participation of the organisations providing the experimental data was very useful in clarifying various questions raised during the projects;
- An uncertainty analysis of the experimental data was necessary, including those data that have been used for the development and validation of the codes applied;
- Efforts are needed to clarify differences in the interpretation of some experiments and in the use of the same codes, the so-called “user effect”;
- Efforts should be made to apply the validated computer codes and uncertainty analysis methods to evaluate the fuel behaviours and performance of advanced technology fuels (ATFs) in nuclear power plants (NPPs).

It was recommended to focus the new CRP on the testing and simulation of evolutionary Advanced Technology Fuel (ATF-TS), consisting of Round Robin mechanical tests of coated cladding and other concepts, integral out-of-pile bundle tests with coated cladding, code adaptation and validation for ATFs, and development and application of simplified methodology for ATF hot rod LOCA fuel safety evaluation.

Most participants showed interests to participate in this new CRP. It was recommended to hold a Consulting Meeting to finalize the CRP programme and launch the proposal evaluation process by end 2019 and start this project in 2020.

MAIN RESULTS OF THE CRP FUMAC

(Session 1)

Chairperson

J. ZHANG

Belgium

SIMULATION TOOLS INCORPORATED TO DIONISIO IN THE FRAME OF THE FUMAC PROJECT

M. LEMES, A. SOBA, A. DENIS
Sección Códigos y Modelos,
Gerencia Ciclo del Combustible Nuclear,
Comisión Nacional de Energía Atómica,
Avenida General Paz 1499, 1650 San Martín,
Provincia de Buenos Aires, Argentina

Abstract

Several models were integrated to the DIONISIO code within the framework of the IAEA Research Project “Fuel Modeling in Accident Conditions (FUMAC)”, to take account of accidental conditions, in particular the loss of coolant accidents (LOCA). A specially designed thermal-hydraulic subroutine provides a simplified description of the rod environment in normal or accidental conditions. The heat transfer coefficients that account for the different coolant regimes, in single or double phases, are activated as the corresponding conditions occur. The simulation of a considerable number of experiments has shown that, despite its simplicity this subroutine gives adequate predictions of the conditions in a vertical cooling channel, quite similar to those given by the thermal-hydraulic codes. The description of the fuel rod atmosphere is improved with the incorporation of this subroutine since it provides fairly realistic boundary conditions for the simulation of the fuel rod behavior, without requiring the intervention of external specific codes. Models of high temperature oxide growth (ZrO₂) and hydrogen capture and release by the cladding in steam were also included. Moreover, the model of cladding creep predicts the conditions for ballooning and eventually, those for catastrophic failure (burst) and its localization. The calculation scheme makes a partition of the rod length into a number of segments defined by the user. In each segment the local conditions are considered to calculate, with the synchronous work of all the subroutines, the physical and chemical parameters in one representative pellet. Then, a description of the whole rod is obtained by coupling all the segments. This strategy has yielded accurate simulations of a wide variety of cases, either in normal or LOCA type conditions. Exhaustive comparisons were carried out with several thermal-hydraulic codes (COBRA-IV, RELAP5-Mod3.1, SOCRAT, ATHLET-Mod 1.1) and with a number of experiments like those of the IFA-650 series (-1,-2,-9,-10,-11), PUZRY, QUENCH-L0/L1 (for which a new working scheme was specially developed in DIONISIO), CORA-15, IAEA-SPE-4, among others.

1. INTRODUCTION

The DIONISIO code simulates the behavior of a typical PWR fuel rod under irradiation. It starts from the linear power history and environmental temperature profiles to predict temperature, stress and strain (either in the elastic or plastic regimes) distributions in the rod, creep, densification, swelling, release of fission products (noble gases, cesium and iodine) to the internal free volume of the rod, gas mixing, pressure increase, cladding irradiation growth, superficial oxide layer development, hydrogen capture and release, pellet restructuring and grain growth and pellet-cladding mechanical interaction. The effects cladding corrosion due to the internal or external atmosphere are also considered.

In its present version, the code is able to simulate a fuel rod in its whole length. To this end, the bar is axially divided into a quantity of sectors defined by the user. In each one the linear power and external temperature are assumed uniform. The domain formed by one pellet and the corresponding segments of cladding and gap is considered. The differential equations describing all the features of the problem are solved in each rod segment under the local external conditions, using the finite element method in a two-dimensional system, assuming symmetry around the longitudinal axis and with respect to the pellet mid-plane. At every time step the code provides the local values of temperature, stress, strain and every other significant parameter, conforming a net of interconnected and mutually dependent subroutines. The results of the individual segments are then merged to give the time evolution of the global rod features.

The wide temperature range displayed through the radius of the fuel pellet is responsible for the highly non-linearity of most of the models employed to describe the diverse phenomena.

Several improvements have been carried out on DIONISIO during the recent years, with the intention of widening its predicting capability. To give account of the high burnup range, several models were incorporated represent the radial distribution within the pellet of power density, burnup, and concentration of U and Pu nuclides [1–4].

Several types of accidents can occur in the core of a nuclear power reactor. One of considerable gravity is that named Loss of Coolant Accident (LOCA). Fortunately, the safety systems normally act with short delay interrupting the nuclear reaction, but the heat accumulated in the fuel rods and that still produced by radioactive decay represent a large amount that has to be removed in possibly defective conditions.

During an excursion of this type, high temperature values can be reached in the rod. The consequent fast cladding oxidation goes together with the release of a considerable amount of hydrogen, some of which dissolves in the coolant and the rest in the metallic cladding, usually of Zry. Both situations involve severe risks, either due to H₂ accumulation in the reactor containment or to cladding material embrittlement due to hydrides precipitation and justify the necessity of accurate predictions in this respect. The consequent coolant temperature increase can give place to different conditions: turbulent flow of liquid water, birth of water vapor bubbles adjacent to the cladding wall, breakup of the boundary layer and several more that can develop simultaneously at different places along the rod and also at a given location during an accidental event until the equilibrium is restored.

Quite recently, a subroutine was developed and included in DIONISIO to analyze and quantify the coolant behavior in terms of the system pressure and coolant velocity. A vertical channel containing one fuel rod and the corresponding volume of surrounding coolant is modeled. The purpose is to describe in a simple manner the conditions in the cooling channel, including single phase, either liquid or vapor, or two phase flow, thus avoiding the use of specific thermal-hydraulic programs. The comparisons carried out with a considerable number of experiments and with diverse reactor codes have given stimulating results, despite of the comparatively great simplicity of the new subroutine.

2. MODELS AND PARAMETERS INVOLVED

To calculate the temperature distribution in the pellet-gap-cladding system, the heat equation in cylindrical symmetry is solved. Fissions and radioactive decay in the pellet and oxidation of the external cladding surface are considered as heat sources [1–5].

Heat is assumed to flow only in the radial direction. Simulation of the oxidation kinetics plays a significant role since the oxide layer represents a thermal barrier between the rod and the coolant. Models allowing for either normal (with unlimited oxygen supply) or accidental (with the rod in a steam starved atmosphere) conditions are considered [5]. On the other hand, the convective cladding-coolant heat transfer coefficient, h_{eff} [W/(m K)] needs also to be considered.

The thermal-hydraulic, complex codes describe the wide diversity of flow regimes that can be met during a power excursion and/or along a vertical channel with water flowing upwards in typical PWR fuels [6–9]. The objective of DIONISIO is focused on the simulation of the fuel behavior that requires realistic boundary conditions. For this reason the thermal-hydraulic analysis is restricted to those modes regarded as the more representative [5] and is condensed in a code subroutine.

- Forced single-phase convection to subcooled liquid;
- Saturated nucleate boiling;
- Post-critical transition boiling;
- Post-critical film boiling;
- Forced single-phase convection to superheated vapor.

The dissociation of water molecules caused by oxidation of the cladding, particularly rapid in accident conditions, results in a considerable increase of dissolved hydrogen in the coolant and in the cladding material. During a sudden cooling of the bar, a fraction of the hydrogen in solid solution can precipitate and form hydrides, which can be the cause of serious damage to the material.

The model included in DIONISIO [10] involves two different mechanisms of hydrogen absorption by the cladding: chemical reaction with H₂ present in the coolant and rapid diffusion of H⁺ through the oxide layer and the consequent discharge into the oxide-metal interface via the capture of an electron released in the oxidation reaction [11–16].

To estimate the effective cladding creep rate, a temperature dependent empirical correlation [16] was adopted. In a LOCA type scenario, the temperature, clad ductility and tangential stress can combine in such a way that the increase of internal rod pressure and depressurization of the primary circuit, can lead to a local strain sufficiently high as to make the cladding adopt a shape similar to a balloon. This phenomenon can eventually cause catastrophic clad rupture, which is assumed to occur when the hoop stress exceeds a limit value for which the

empirical correlation [16, 17] was adopted. Specific subroutines have been included in the code to predict clad ballooning and burst occurrence and localization.

The models expressing each phenomenon have been codified in subroutines that were separately tested prior to their insertion in the code [5, 10].

3. RESULTS

After the introduction of the accident modules in DIONISIO, several complex experiments were simulated, all of them taken from the IAEA database.

3.1. Simulation of IFA tests

The fuel designs and cladding materials developed in recent years, as well as the tendency to increasing burnup, determined the need to re-examine and update the traditional safety criteria for LOCA accidents, which had been developed on the basis of experiments performed in the 70s. This was the objective of the integral experiments of IFA (Instrumented Fuel Assembly) that were carried out in the Halden Reactor (Norway), designed to evaluate aspects such as the cladding temperature, the relocation of the fragmented sediment, cladding ballooning, hydriding and oxidation, under simulation LOCA conditions. They included a sharp pressure drop and low refrigerant flow [18].

The IFA 650-1 and -2 tests were performed in 2003 and 2004 respectively, with fresh fuel rods that were electrically heated in a heavy water and high pressure circuit. Unlike these, subsequent experiments of the IFA 650 series used pre-irradiated fuel rods in PWR or BWR type reactor reactors that had reached intermediate or high burnup levels [19–21].

To simulate the experimental conditions of both tests, the thermal-hydraulic model incorporated to DIONISIO was applied, taking as input data the power history, the geometric characteristics of the rod (radii of the pellet and cladding, rod length) and aspects of the coolant (flow, pressure, inlet temperature).

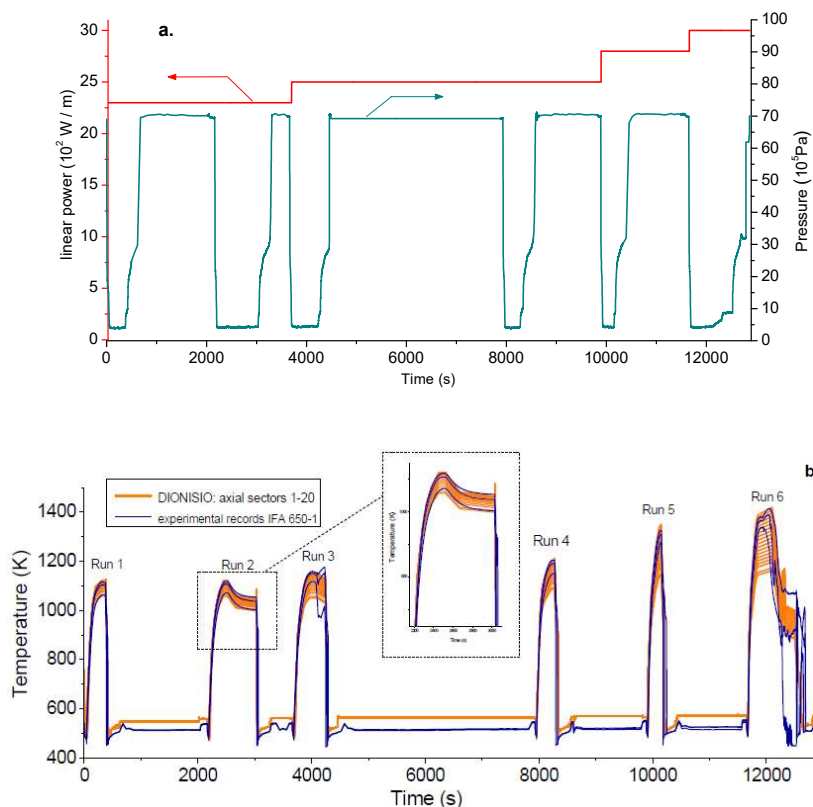


FIG. 1. IFA 650-1 experiment. a.) linear power (red) and pressure history (dark green); b.) temperature evolution: experimental results in blue and simulations with DIONISIO in orange.

In Figure 1(a), the red curve shows the linear power in the IFA 650-1 experiment, which consisted of four constant power steps. In the same interval, six pressure drops followed by stationary periods occurred, which are shown in the dark green curve. Thermocouples placed at three axial positions recorded the temperature throughout the experiment. They are shown in the blue curves in Figure 1(b). In the same figure, the temperature calculated by DIONISIO at the 20 axial positions selected for the simulations [5] are shown in the orange curves. The very good agreement between both sets of curves is visible. In particular, the small frame inserted in figure b shows a magnification of step 2.

In IFA 650-2, the experimental device was a loop filled with heavy water containing a rod segment. It was instrumented with a pressure sensor and thermocouples to record the external cladding wall temperature. Accidental conditions were simulated by valves opening, thus leaving the channel almost empty in about 30 s. The coolant pressure decreased to 3–4 bar and hence the temperature rose. The linear power was kept at an almost constant value of 23 kW/m until 464 s after valves opening, when scram occurred to end the test. The steep external pressure drop, that can be appreciated in Fig. 2, corresponds to the accident initiation ($t = 0$). For the simulations the rod is divided into 20 axial segments [5]. The curves plotted in Fig. 2 represent the temperature calculated at the axial segments that better coincide with the thermocouples locations. The figure shows that clad ballooning and burst occurred during the heat up period. In this respect, a band is plotted to indicate the time interval for which the code predicts an accumulated creep sufficient to produce tube ballooning. During the experiment, burst occurrence triggered the injection of a water spray to stabilize the temperature, as evidenced by the change of slope of the curves. The good coincidence between measured and calculated temperature results can be appreciated.

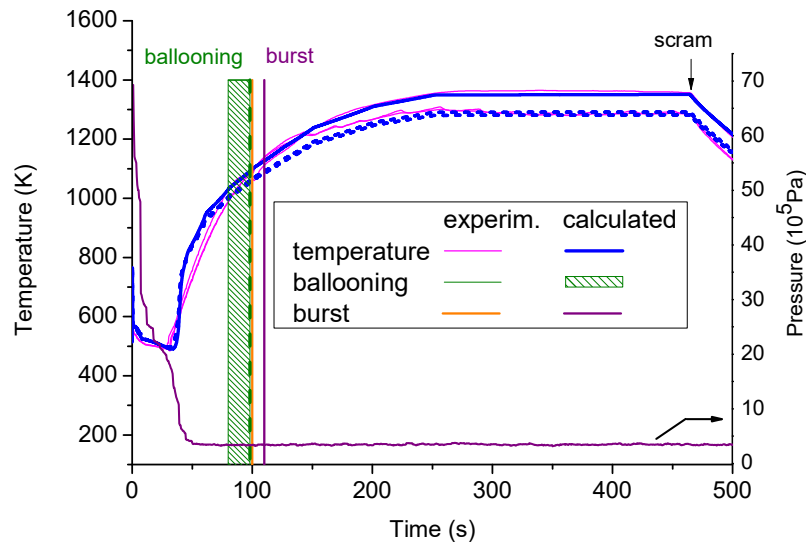


FIG. 2. Comparison between the experimental data of IFA 650-2 and the calculations of DIONISIO. Cladding temperature at three axial positions and pressure evolution; ballooning and burst times as well as the scram are indicated.

Figure 3(a) shows the measured and calculated internal rod pressure in IFA 650-2. The abrupt internal pressure drop reveals the burst event. According to the experimental report [18], the He pressure should have then dropped to about 3 bar, which is the rig pressure. The simulation is carried out under this assumption. The experimental curve shows a different value which is probably due to the sensor design, which is unable to measure pressures below 56 bar (indicated with the horizontal line in Fig. 3(a). Burst occurrence is predicted at $t = 110$ s while the experimental report indicates 99 s. The decrease in pressure evidenced in the experimental curve before the outbreak is attributed to the effect of ballooning [18]. It needs to be mentioned that the mechanical models included in the code assume that the deformations are small. DIONISIO is not able to reproduce this effect, since it involves large strains. A model suitable for these cases will be incorporated in the future. Figure 3(b) shows the experimental and calculated values of the cladding lengthening as functions of the time measured from the pressure drop. The experimental curve evidences an axial contraction that is associated with agglomeration. The abrupt interruption of the contraction is attributed to burst occurrence, at 99 s [18]. The images obtained after the conclusion of the test show an important relocation that is surely responsible for the significant contraction of the

rod observed in the final part of the experiment. This phenomenon, which implies large deformations and involves the entire bar, cannot be taken into account in DIONISIO for reasons similar to those mentioned in relation to Fig. 3(a). This explains the significant deviation between simulation and measurement after 80 s. Before that, the agreement is quite good.

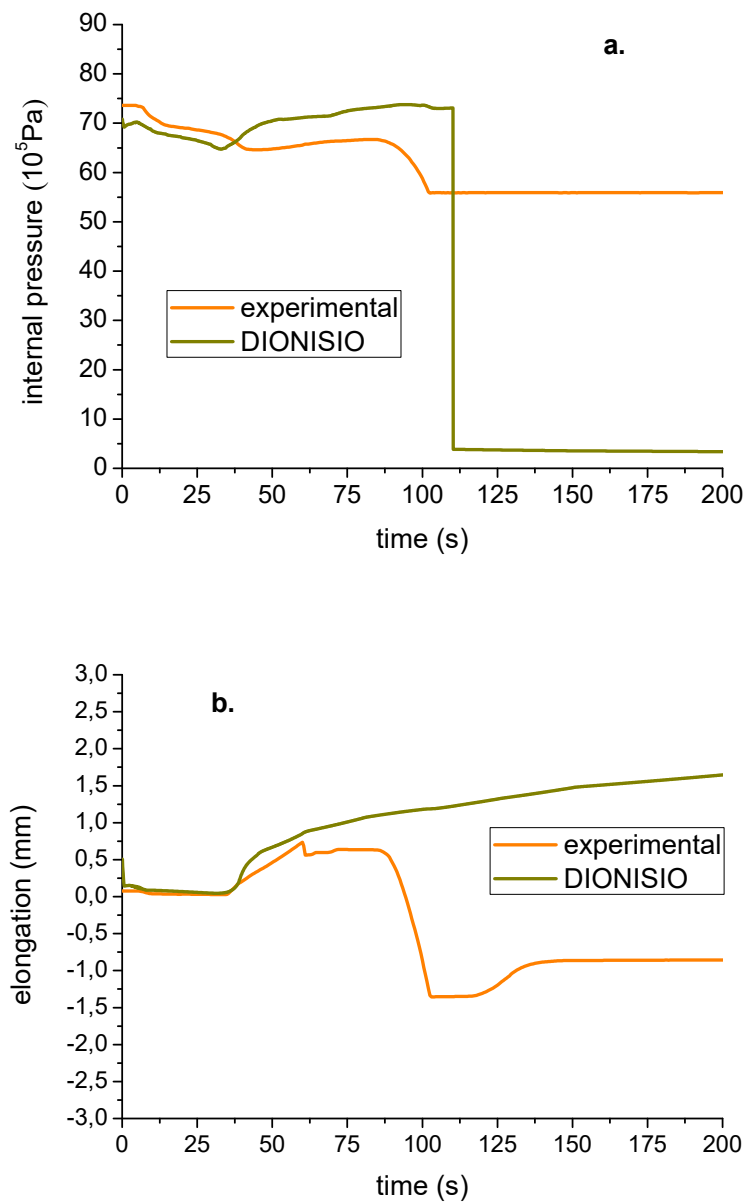


FIG. 3. Comparison between the experimental data of IFA 650-2 and the calculations of DIONISIO. a.) internal rod pressure and b.) clad elongation.

TABLE 1. MAIN CHARACTERISTICS OF THE BASE IRRADIATIONS OF THE RODS IFA 650-9, 10 AND 11.

Experiment	Fuel type	Base irradiated at	Up to a burnup of (MWd/kgU)
IFA 650-9	PWR	Gösgen NPP (Switzerland)	89.9
IFA 650-10	PWR	Graveline 5 (France)	61
IFA 650-11	WWER-440	Loviisa NPP (Finland)	56

For the IFA 650-9, -10 and -11 experiments, short rods cut from commercial fuels that had been previously irradiated in different reactors were instrumented and further irradiated. The main characteristics of the base irradiations are listed in Table 1. The three experiments started with forced coolant circulation until the temperature was stabilized. Then, the cooling was changed to natural circulation.

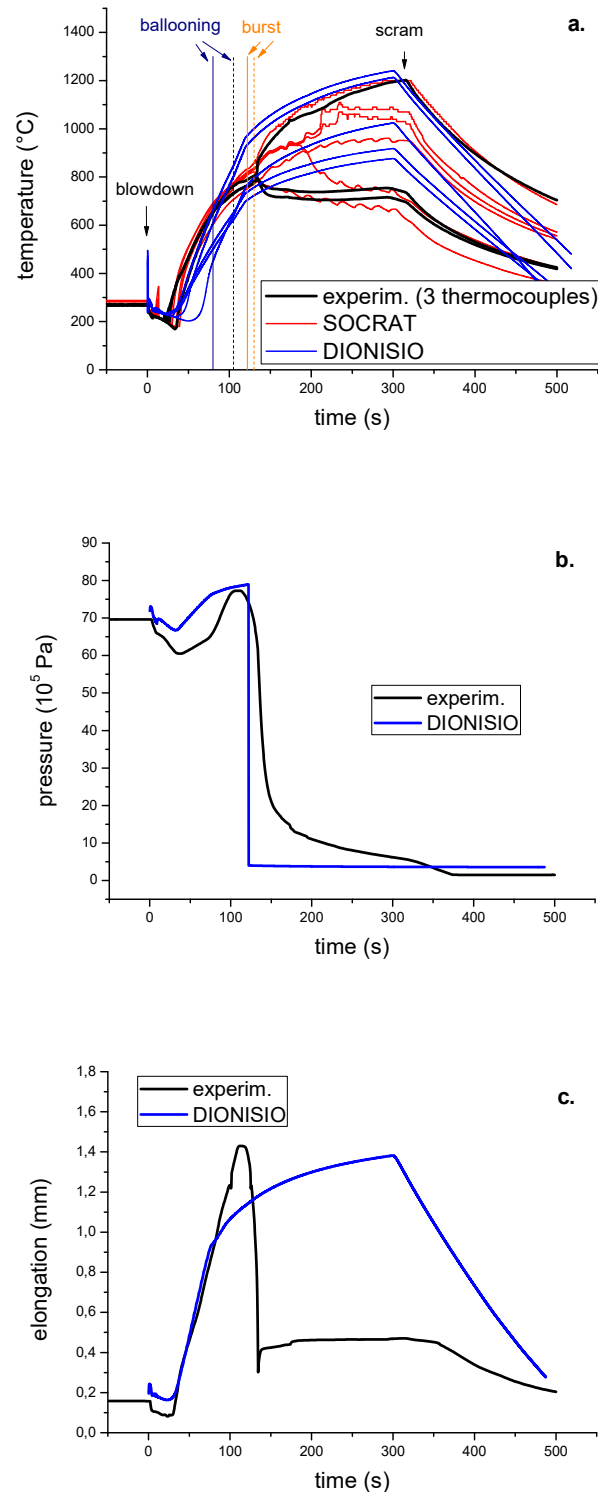


FIG. 4. Comparison between the experimental data of IFA 650-9 and the calculations of DIONISIO a) Cladding temperature at different axial positions vs. time after accident initiation; ballooning, burst and scram times are also indicated. The predictions of SOCRAT are superimposed. b) Internal rod pressure and c) Cladding elongation.

To perform the simulations with DIONISIO, input data of these tests like power history and geometric rod characteristics (pellet and cladding radii, rod length, etc.) are provided. The thermal hydraulic model described in Section 2 was applied to simulate the experimental conditions in the coolant like flow, pressure and temperature. The predictions obtained are compared with the experimental results reported in the data basis and with those calculated with the integral severe accident code SOCRAT, in particular those corresponding to the rod temperature.

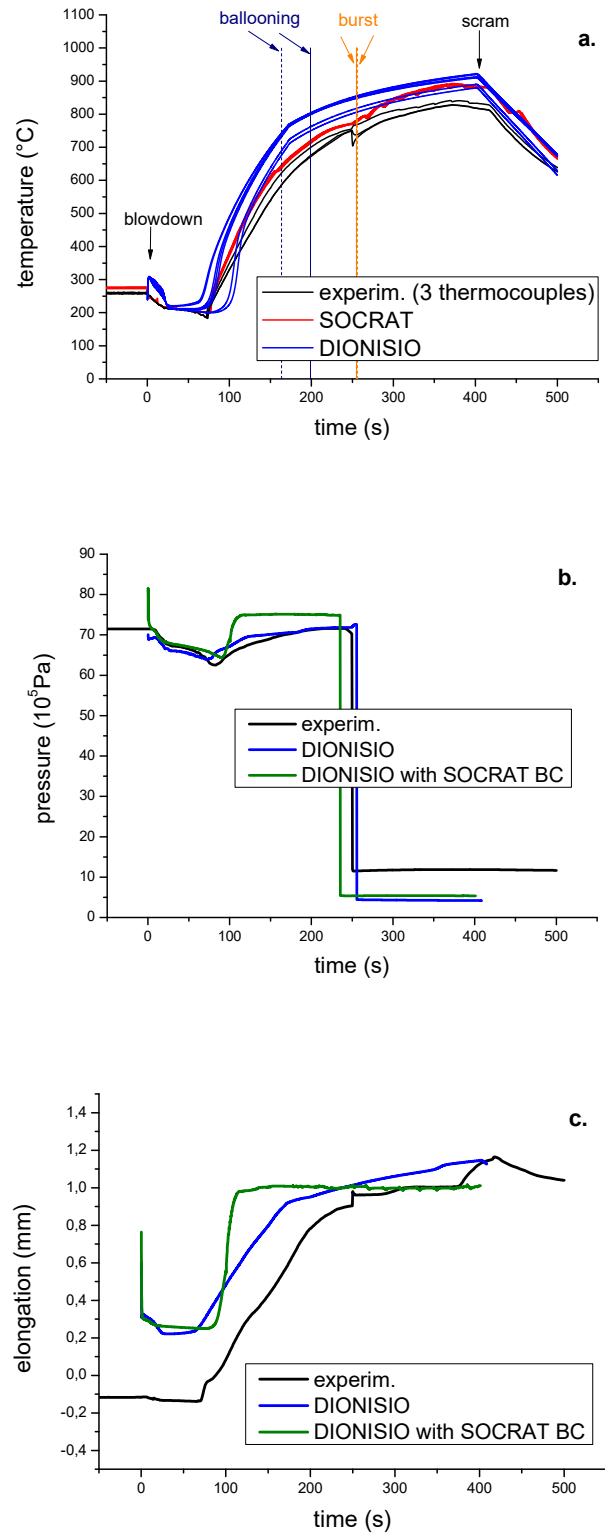


FIG. 5. Idem Fig. 4. but for IFA 650-10.

The cladding temperature evolution predicted by DIONISIO for the IFA 650-9, -10 and -11 tests at different axial positions is represented in Figs 4(a), 5(a) and 6(a) together with the experimental records of three thermocouples. The evaluations of the SOCRAT code at similar locations are superimposed for comparison. These figures also show the times for initiation of blowdown, ballooning, burst and scram, measured and predicted by DIONISIO.

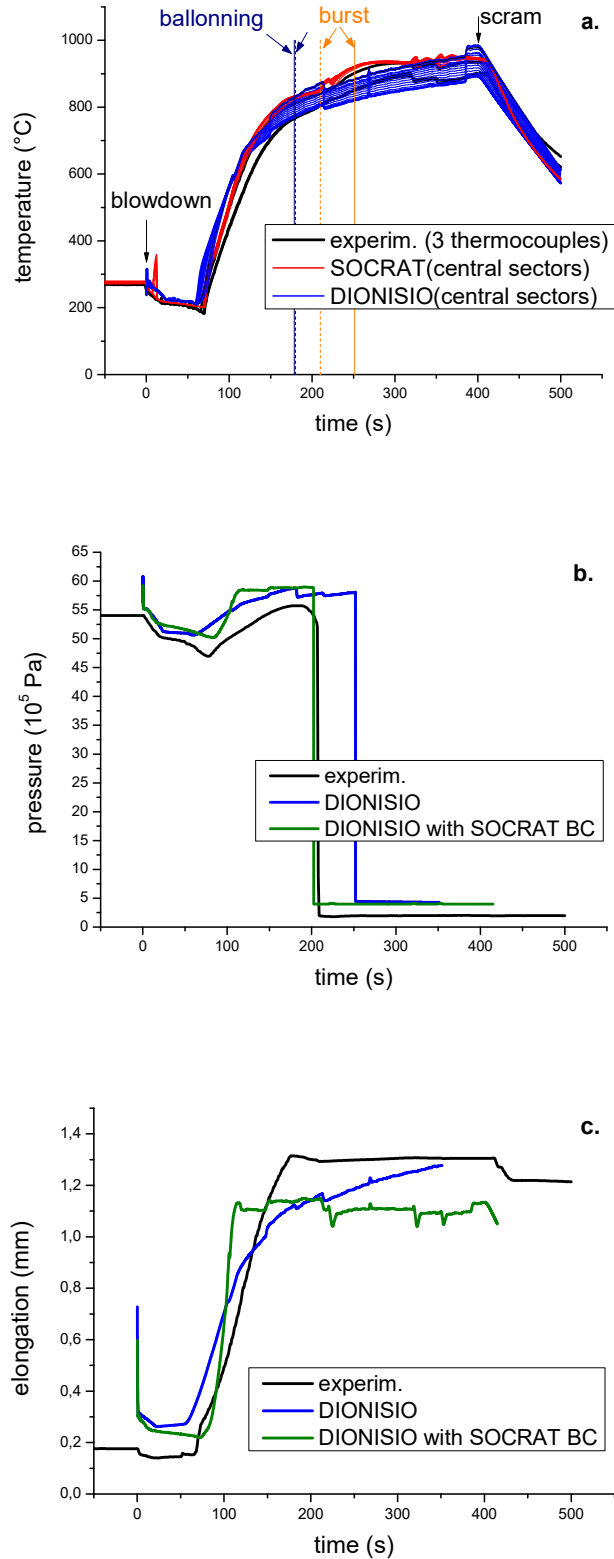


FIG. 6. Idem Fig. 4 but for IFA 650-11.

Figures 4(b), 5(b), 6(b) show the experimental and calculated internal rod pressures for the three tests. As in Fig. 3(a), the steep internal pressure drop indicates burst occurrence. Figures 4(c), 5(c) and 6(c) show the corresponding values of cladding elongation. A good coincidence is in general appreciated. In particular, in Fig. 4(c) the agreement is good only before ballooning. After that, the calculations predict a slower elongation rate. The steep contraction experimentally observed is probably due to relocation, as explained in connection with Fig. 3(b), but this fact is not yet included in the simulation.

With the purpose of testing the quality of the thermal-hydraulic subroutine of DIONISIO, simulations of the internal rod pressure and clad elongation in IFA 650-10 and -11 were performed in two different conditions: with the subroutine incorporated and replacing its outputs with those provided by the SOCRAT code, which operated as boundary conditions (BC) for the fuel behavior simulation with DIONISIO. Figs 5(a) and (b), and Figs 6(a) and (b) show the comparison between the measurements and both types of calculations for the internal pressure and axial elongation. The agreement is good in general, although the predictions seem to be better when DIONISIO is run with the embedded thermal-hydraulic subroutine.

Table 2 shows the time elapsed since accident initiation until ballooning and burst occurrence, measured [22–24] and predicted by SOCRAT and DIONISIO.

TABLE 2. COMPARISON OF THE PREDICTIONS OF SOCRAT AND DIONISIO WITH EXPERIMENTAL DATA FOR THE TIME FOR BALLOONING AND BURST

	IFA 650-9		IFA 650-10		IFA 650-11	
	Ballooning (s)	Burst (s)	Ballooning (s)	Burst (s)	Ballooning (s)	Burst (s)
DIONISIO	79.89	121.2	163.7	256.2	178.4	251.4
SOCRAT	—	—	109.7	235.4	118.2	202.4
Experimental	105	130	199	255	180	210

3.2. Simulations of PMK tests

The PMK experiments were carried out in the mid-1980s on a scale model of the Paks Nuclear Power Plant (Budapest, Hungary). They had been designed to study the safety margins of WWER reactors and validate the ATHLET, CATHARE and RELAP 5 thermal-hydraulic simulation codes. The reactor core was simulated by a bundle of electrically heated bars. In particular, the IAEA-PMK-2 test aimed to investigate processes after small and medium size breaks (from 1% to 22%) [25]. For this end, a hole was opened in the primary circuit to initiate the accidental sequence. Approximately 200 s afterward the cooling device acted by steam discharge. The coolant temperature and pressure recorded during the experiment are shown in Fig. 7 together with the predictions of the RELAP, ATHLET and DIONISIO codes.

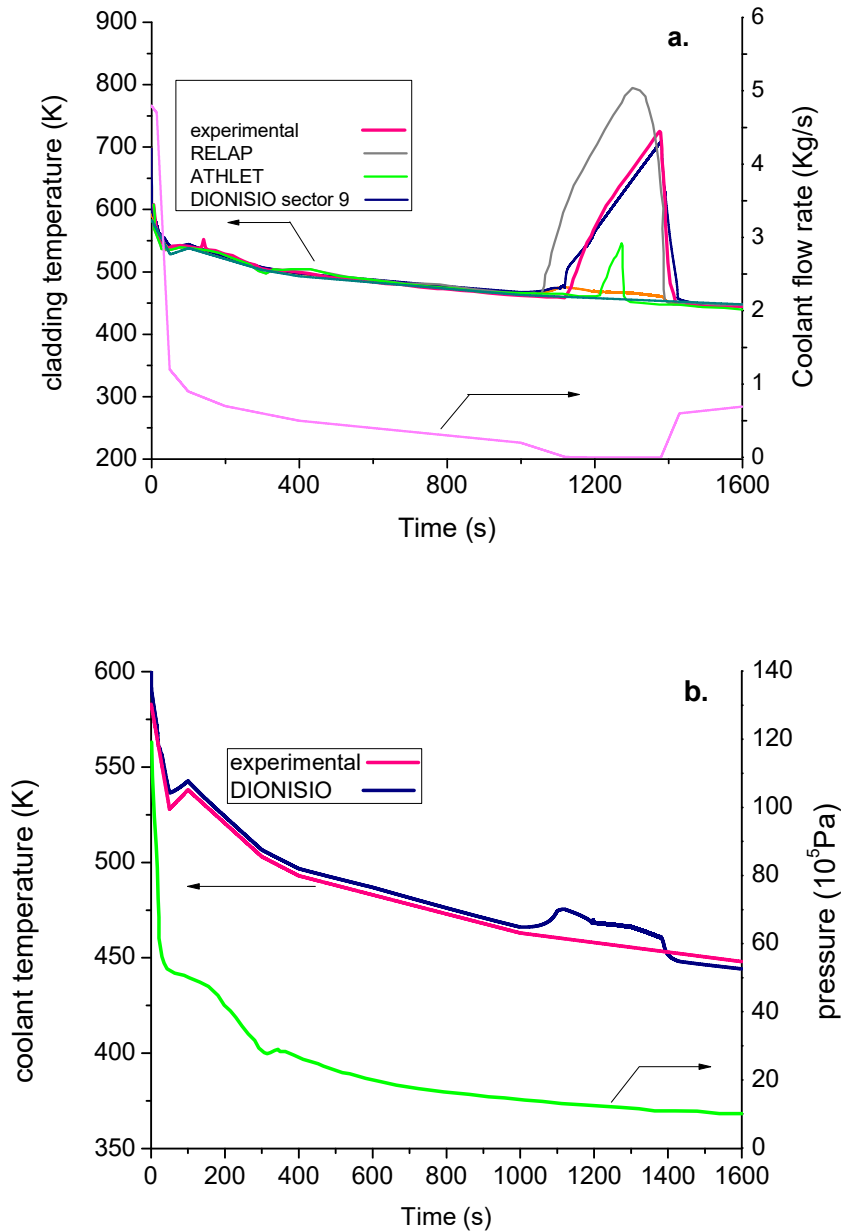


FIG. 7. Comparison between the experimental data of the PMK tests and the calculations of RELAP, ATHLET and DIONISIO; a.) Cladding temperature at different axial positions; b.) Coolant temperature and pressure history.

The different heat transfer modes that were described in Section 2 and are included in the DIONISIO thermal-hydraulic subroutine are activated during the experiment and along the rods axis to provide a realistic simulation of the conditions met in the transient.

3.3. Simulation of QUENCH experiments

In the QUENCH-LOCA facilities of the Karlsruhe Institute of Technology (KIT), a series of tests are carried out to investigate the ballooning and burst behavior, as well as oxidation and hydrogen uptake in design basis accident conditions. Instrumented fuel rods are used, internally heated with tungsten wires connected to DC generators. In particular, results of the QUENCH-L0 and L1 experiments are shown in Figs 7, 9, 10 and compared with the corresponding simulations performed with DIONISIO. The device consists of 21 rods, the 10 internal ones alimeted with high and the 11 external rods with low electrical power.

To investigate the influence of the pressure on the involved processes, the fuel rods in QUENCH-L0 were loaded with internal pressures of 35, 40, 45, 50, and 55 bar, respectively [26]. The experimental determinations of pressure evolution are shown in Fig. 8(a) along with the predictions of DIONISIO. In Fig. 8(b) the measured and predicted time for burst are compared. It is seen that the rods subjected to high power, i.e., at high temperature, fail before than those at low power. No significant effect of the initial internal pressure is visible. The experimental determinations show that burst occurs in the temperature range 1049–1123K while for DIONISIO a similar range of 1062–1123K is predicted.

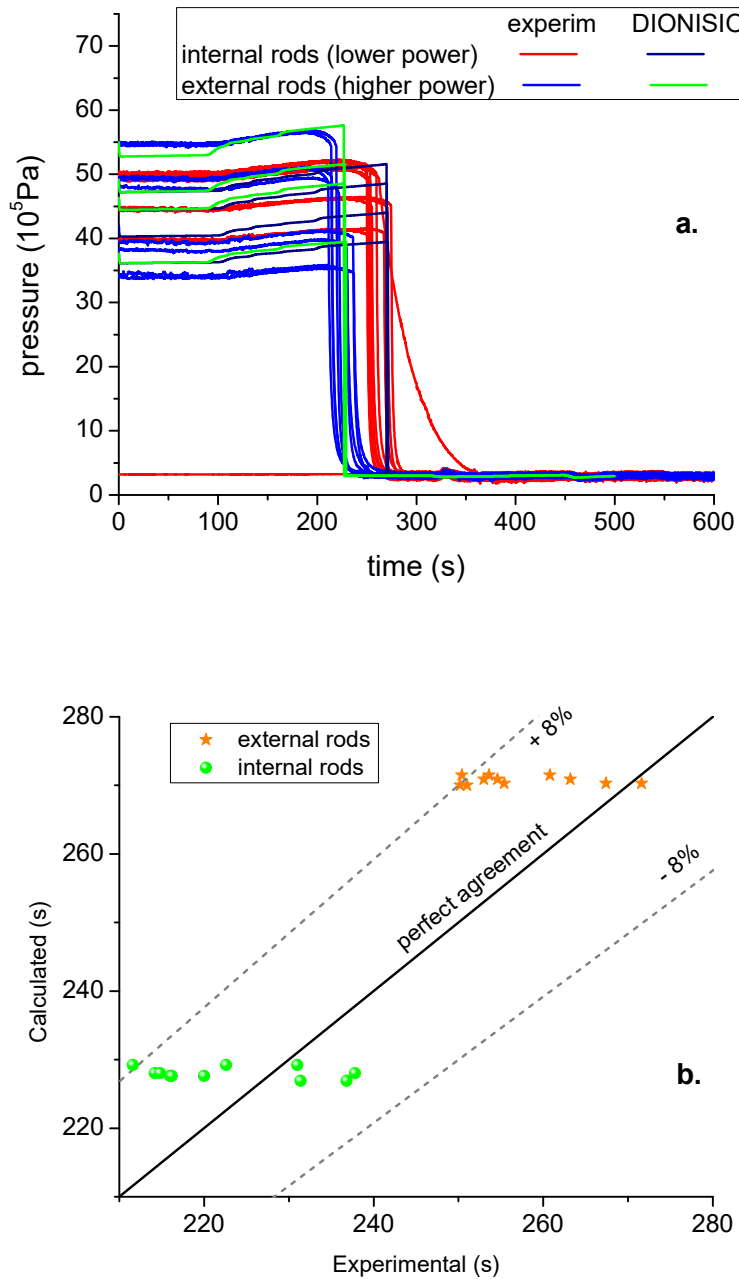


FIG. 8. Comparison between the experimental data of the QUENCH-L0 test and the calculations of DIONISIO. a.) Evolution of the internal pressure. b.) Measured and predicted time for burst.

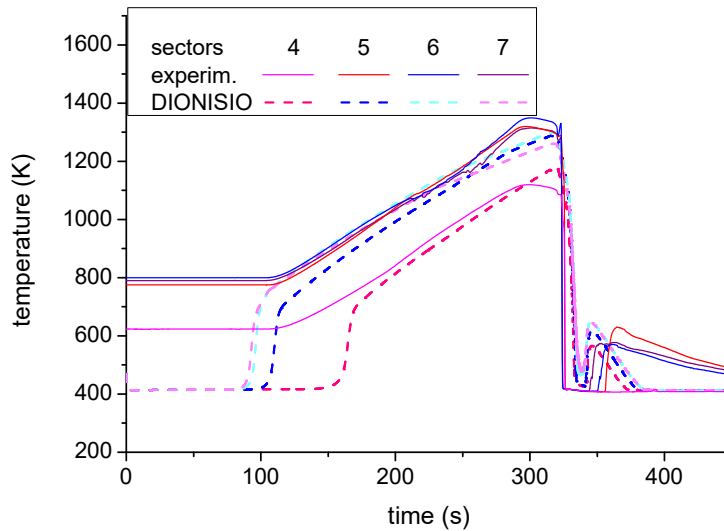


FIG. 9. Comparison between the experimental data of the QUENCH-L0 bundle test and the calculations of DIONISIO. Cladding temperature in selected sectors of rod 4.

Figure 9 shows the temperature evolution in different sections of rod 4 of the QUENCH-L0 experiment. A partition in 10 segments is used for the simulation with DIONISIO. They are numbered starting from bottom in such a way that sectors 5–7 fall in the middle of the rod. After burst, the temperature is drastically reduced by ceasing the power supply and increasing the cooling. However, the residual heat is sufficient to provoke water evaporation and a further temperature increase. This is counteracted with the injection of vapor with argon, which is visible in the tail of the curves.

Measured [26] and calculated hydrogen release in rod 4 are compared in Fig. 10. The sudden liberation accompanying the fast experimental temperature drop is well accounted for by the simulation. However, a disagreement between both at the final portion of the curves is visible. It is surely originated by the mismatch in temperature in that portion of the test. Moreover, while the experimental data correspond to the whole bundle, the simulation with DIONISIO took into account only rod 4 and then the results were extrapolated to the entire bundle. This fact can contribute to the observed disagreement, especially in the final stage of the experiment.

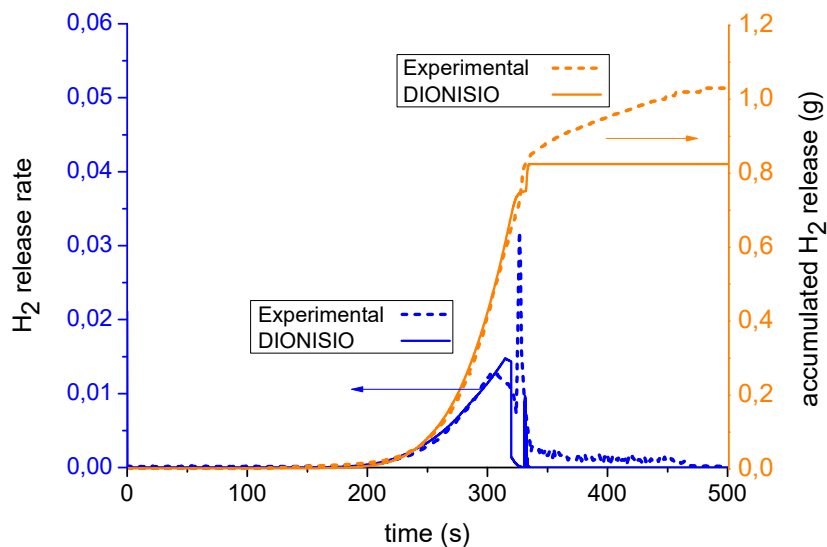


FIG. 10. Comparison between the experimental data of the QUENCH-L1, rod 4, and the calculations of DIONISIO of the instantaneous hydrogen release rate and accumulated amount of hydrogen released vs. time.

4. CONCLUSIONS

Several subroutines have been introduced in DIONISIO in the recent times to give account of individual phenomena related to the cladding response in the high temperature range: oxidation, hydrogen uptake and release, ballooning and burst. They have been all subjected to separate testing plans and then incorporated to the general code.

Moreover, with the purpose of providing realistic boundary conditions to simulate the fuel behavior, a subroutine was developed to give account of the different scenarios that can be met in the coolant, particularly during an accidental excursion. Although this is the specific task of the complex thermal-hydraulic codes, the strategy was adopted of introducing a simplified calculation scheme that could be embedded within DIONISIO, thus avoiding the use of external inputs. This challenging task has been adequately fulfilled as evidenced by the considerable number of experiments simulated, many of which are shown in this report, where a good agreement is verified with the existent experimental data or with the simulations provided by the specific codes.

ACKNOWLEDGMENTS

This work is performed within the frame of the IAEA Research Contract N°18536 which forms part of the Research Project “Fuel Modeling in Accident Conditions (FUMAC)”, and is partially supported by **PICT 2018-01568**, CONICET — Argentina.

REFERENCES

- [1] SOBA, A., DENIS, A., DIONISIO 2.0: New Version of the Code for Simulating a Whole Nuclear Fuel Rod under Extended Irradiation, *Nuclear Engineering and Design* **292** (2015) 213–221.
- [2] SOBA, A., DENIS, A., ROMERO, L., VILLARINO, E., SARDELLA, F., A High Burn-up Model Developed for the DIONISIO Code, *Journal of Nuclear Materials* **433** 1–3 (2013) 160–166.
- [3] SOBA, A., LEMES, M., DENIS, A., An Empirical Formulation to Describe the Evolution of the High Burnup Structure, *Journal of Nuclear Materials* **456** (2015) 174–181.
- [4] SOBA, A., LEMES, M., GONZÁLEZ, M.E., DENIS, A., ROMERO, L., Simulation of the Behavior of Nuclear Fuel under High Burnup Conditions, *Annals of Nuclear Energy* **70** (2014) 147–156.
- [5] LEMES, M., SOBA, A., DAVERIO, H., DENIS, A., Inclusion of Models to Describe Severe Accident Conditions in the Fuel Simulation Code DIONISIO, *Nuclear Engineering and Design* **315** (2017) 1–10.
- [6] U.S. NUCLEAR REGULATORY COMMISSION, International Agreement Report, Heat Transfer Processes During Intermediate and Large Break Loss-Of-Coolant Accidents (LOCAs), 1986.
- [7] MOCHIZUKI, H., Thermal Hydraulics in Nuclear Reactors, International graduate course, Tokyo Institute of Technology, 2009.
- [8] ODAR, F., Assessment of the TRAC-M Codes Using Flecht-Seaset Reflood and Steam Cooling Data, U.S. Nuclear Regulatory Commission, 2001.
- [9] TODREAS, N., KAZIMI, M., Nuclear Systems. Thermal Hydraulic Fundamentals, Massachusetts Institute of Technology, USA, 1989.
- [10] LEMES, M., DENIS, A., SOBA, A., Simulation of nuclear fuel behavior in accident conditions with the DIONISIO code, *Journal of Nuclear Engineering and Radiation Science* **5** 2 (2019).
- [11] VESHCHUNOV, M., BERDYSHEV, A., Modelling of Hydrogen Absorption by Zirconium Alloys During High Temperature Oxidation in Steam, *Journal of Nuclear Materials* **255** (1998) 250–262.
- [12] COX, B., Oxidation of Zirconium and its Alloys, *Advances in Corrosion Science and Technology* **5** (1976) 173–391.
- [13] VESHCHUNOV, M., SHESTAK, V., Modeling of Zr Alloy Burst Cladding Internal Oxidation and Secondary Hydriding under LOCA Conditions, *Journal of Nuclear Materials* **461** (2015) 129–142.
- [14] COX, B., “Mechanisms of Hydrogen Absorption by Zirconium Alloys”, Atomic Energy of Canada Limited, AECL (Report), (January 1985).
- [15] ADAMSON, R., GARZAROLLI, F., COX, B., STRASSER, A., RUDLING, P., Corrosion Mechanisms in Zirconium Alloys, *Adv. Nuclear Technology International*, Skultuna, Sweden (2007).
- [16] MANNING, T., JERNKVIST, L.O., MASSIH, A., Evaluation of Loss-of-Coolant Accident Simulation Tests with the Fuel Rod Analysis Code FRAPTRAN-1.4. Quantum Technologies AB, Report TR11-008V1 (2011).
- [17] ROSINGER, H., A Model to Predict the Failure of Zircaloy-4 Fuel Sheathing during Postulated LOCA Conditions. *Journal of Nuclear Materials* **120** 1 (1984) 41–54.
- [18] EK, M., LOCA testing at Halden; the second experiment IFA-650.2, HWR-813, (2005).
- [19] LESTINEN, V., KOLSTAD, E., WIESENACK, W., LOCA testing at Halden, Trial runs in IFA-650, Nuclear Safety Research Conference Washington, (2003).

- [20] LESTINEN, V., LOCA testing at Halden, first experiment IFA-650.1 HWR-762, (2004)
- [21] EK, M., LOCA testing at Halden; the second experiment IFA-650.2, HWR-813, (2005)
- [22] CHOMONT, F., HWR-917 LOCA TESTING AT HALDEN, THE NINTH EXPERIMENT IFA-650.9, (2009)
- [23] LAVOIL, A., HWR-974 LOCA testing at Halden, the tenth experiment IFA-650.10, (2010)
- [24] LAVOIL, A., HWR-976 LOCA testing at Halden, the VVER fuel experiment IFA-650.11, (2010)
- [25] SZABADOS, L., EZSÖL, G., PERNECZKY, L., KREPPER, E., PRASSER, H., SCHÄFER, F., Two Phase Flow Behavior during a Medium Size Cold Leg LOCA Test on PMK-2 (IAEA SPE-4). KFKI Atomic Energy Research Institute, Budapest, Hungary, (1995)
- [26] HOLLANDS, T., BALS, C., AUSTREGESILO, H., Simulation of QUENCH-L0 with ATHLET-CD, International Quench Workshop, November, (2011).

QUALIFICATION OF FRAPCON/FRAPTRAN FOR LOCA FUEL BEHAVIOUR MODELLING AND SAFETY EVALUATION

J. ZHANG, A. DETHIOUX, T. DRIEU, C. SCHNEIDESCH
Tractebel (ENGIE),
Boulevard Simon Bolivar 34–36, 1000,
Brussels, Belgium

Abstract

As part of the Tractebel contribution to the IAEA FUMAC project, Tractebel has used the updated FRAPTRAN-TE-1.5 code for simulation of selected Halden LOCA tests IFA-650.9 and IFA-650.10, together with the improvement in the thermal hydraulic modelling by using the imposed thermal hydraulic boundary conditions from SOCRAT calculations and in the thermal boundary conditions (axial power profile, plenum temperature). In particular, the impacts of the model improvements such as the Quantum Technologies' axial relocation model and errors corrections in the adapted FRAPTRAN-TE-1.5 version on the calculation results were identified and discussed. In addition, the statistical uncertainty and sensitivity analysis has been performed on the FRAPTRAN-TE-1.5 modelling of the selected Halden LOCA test IFA-650.10, which helped the identification of significant input parameters for LOCA fuel Behaviour modelling. The final objective is to apply the qualified fuel rod transient analysis codes FRAPCON/FRAPTRAN to develop an efficient methodology for assessing the performance and quantifying the margins for advanced technology fuel (ATF) designs under design basis accident conditions (in particular LOCAs).

1. INTRODUCTION

As the owner's engineer for the utility (Electrabel) that owns and operates 7 nuclear power plants (NPPs) in Belgium, Tractebel needs to qualify and apply fuel rod codes for fuel behaviour modelling and safety evaluation during normal and off normal conditions. For this purpose, Tractebel has been working on the qualification of the FRAPCON and FRAPTRAN codes since 2010 [1]. This has been achieved partly by participation in international benchmarks (such as the IAEA's FUMEX-III and FUMAC coordinated research projects and the OECD/NEA's fuel rod codes RIA benchmarks), performing selected benchmark exercises using FRAPCON and FRAPTRAN codes and sharing experience and information with other participants [1, 2].

The FUMAC (Fuel Modelling in Accident Conditions) project has been launched by IAEA as a new Co-ordinated Research Project (CRP) in 2014–2017 [3]. It is a continuation of the previous FUMEX-III project with the focus on the modelling of fuel behaviours in design basis and severe accidents, in particular, Loss-Of-Coolant Accidents (LOCAs), which are of particular interests after the Fukushima accidents.

Tractebel participation in the FUMAC project consists partly in simulation of the integral single rod LOCA tests IFA-650.9 [4] and IFA-650.10 [5] performed at the Halden reactor, using the USNRC fuel performance codes, FRAPCON-3.5 [6, 7] and FRAPTRAN-1.5 [8, 9]. In particular, following the scoping studies [10], the Quantum Technologies' axial fuel relocation model [11] and errors corrections [12] were implemented in the adapted FRAPTRAN-TE-1.5 version [13, 14], and the impacts of the model improvements on the calculation results were identified and discussed. In addition, the statistical uncertainty and sensitivity analysis has been performed on the FRAPTRAN-TE-1.5 modelling of the selected Halden LOCA test IFA-650.10.

The final objective is to qualify FRAPTRAN for simulating relevant behaviours of high burnup fuel under LOCAs, in order to use the code for assessment of margins regarding to the new USNRC acceptance criteria for LOCA (10CFR50.46c), for Belgian operating nuclear power plants (NPPs). For this purpose, an efficient methodology will be developed in the future project for assessing the performance and quantifying the margins for advanced technology fuel designs under design basis accident conditions (in particular LOCAs).

This paper will summarize the contribution of Tractebel to the IAEA's FUMAC project and present the proposal for future development.

2. MODEL IMPROVEMENTS IN FRAPTRAN-TE-1.5

The FRAPCON-3.5 [6] and FRAPTRAN-1.5 [8] fuel rod performance and transient analysis codes have been developed in the framework of reactor safety research programme conducted for the U.S. Nuclear Regulatory Commission (NRC) by Pacific Northwest National Laboratory (PNNL). FRAPCON-3.5 analyses the thermal mechanical behaviour of LWR fuel rods under steady state and power ramp operating conditions, while FRAPTRAN-1.5 code analyses the thermal mechanical behaviour of LWR fuel rods under transient and accident conditions including LOCA and RIA. Experimental data are used for assessing the FRAPCON-3.5 and FRAPTRAN-1.5 capabilities [7, 9]. The worldwide community also contributes to the development, testing and assessment of models.

In the FUMAC project, Tractebel intends to improve and use the FRAPTRAN-1.5 code for better simulation of the fuel behaviours during LOCA, including the axial relocation. TE has reviewed the capability of FRAPTRAN-1.5 and made the preliminary assessment for LOCA simulation. The preliminary scoping parametric analyses recommended improving certain models in FRAPTRAN-1.5, in particular the axial relocation model and the thermal hydraulic boundary conditions [10].

Therefore, Tractebel requested Quantum Technologies to implement their axial fuel relocation model [11] and error corrections [12] in the Tractebel version of FRAPTRAN-TE-1.5 [13, 14], in order to perform further model validation.

3. SIMULATION OF THE HALDEN LOCA TESTS IFA-650.9 AND IFA650.10

3.1. Input models and assumptions

Detailed specifications on the Halden LOCA tests IFA-650.9 and IFA650.10 can be found in [4, 5]. In both FRAPCON and FRAPTRAN input models, most of the data are set according to the specifications of IFA-650 tests (design data, initial data and measured test data) or the code manual recommended values.

In order to simulate the fuel rod conditions before the LOCA tests, FRAPCON input models are built to generate initial conditions for FRAPTRAN analysis. The refabricated rodlet FRAPCON-3.5 input model was validated by comparing with available measured data. The refabricated rodlet FRAPTRAN-1.5 initialization file was the output of FRAPCON-3.5 input model which contained gas data from the initial father rod and subsequent Fission Gas Release (FGR) history data. The number of moles of new gas mixture and the relative amount of each gas species in the refabricated rodlet was adapted to match the calculated and measured initial rod internal pressure.

The measured rod power is imposed. The rod axial power profile in the rodlet is nearly symmetric, with an axial peak to average power factor of 1.04–1.05. The heater is not simulated.

The most important and difficult is the modelling of the test rod thermal hydraulic boundary conditions [10]. As there exist too large uncertainties in the measured inlet coolant temperature and flowrate, and a lack of validation of the FRAPTRAN built-in heat transfer models, it was recommended to use system thermal hydraulic codes (such as RELAP5, TRACE) to calculate the realistic T/H boundary conditions for FRAPTRAN.

Within framework of the FUMAC project, IBRAE has used the integral system thermal hydraulic code SOCRAT (System Of Codes for Realistic Assessment of severe accidents) to simulate the IFA-650 Halden experiments, in order to provide the FUMAC project participants with the thermal hydraulic boundary conditions for fuel rod code benchmarking [15]. In the current study, the calculated coolant temperatures and coolant-cladding heat transfer coefficients from SOCRAT are imposed by using the “Heat” option, and FRAPTRAN will calculate the cladding temperatures. The clad to coolant heat transfer coefficients are determined from the SOCRAT calculated total heat flux (radiative + convective), namely $HTC = Q_{tot} / (T_{clad} - T_{cool})$, for each axial node. For simplicity, only 3 pairs of the SOCRAT calculated thermal hydraulic conditions are imposed at bottom, mid and top of the test rod, consistent with the cladding temperature measurements as in the tests.

The rodlet plenum gas temperature as imposed in the external volume (T_{plenum}) are taken directly from the measurement, or from the SOCRAT calculated coolant temperature at the plenum level.

The father fuel rod and the re-fabricated rodlet have the same number of nodalization: 45 radial nodes and 40 axial nodes both in FRAPCON and FRAPTRAN.

A steady state period of at least 100 s is imposed for the simulations: the LOCA transient is assumed to occur at 100 s and to end at the scram time (600 s). The maximum time step is 0.1 s during the steady state and 0.001 s during the transient.

3.2. Parametric studies on the FRAPTRAN-TE-1.5 model options

The reference case (P0) considers the default properties and models in FRAPTRAN-TE-1.5, namely:

- The FRACAS-I rigid pellet and cladding deformation models (finite difference model) for fuel rod mechanical response;
- The BALON2 high temperature clad failure model based on empirical strain and stress limits for the burst;
- The fuel thermal conductivity, thermal expansion, specific heat models;
- The cladding thermal conductivity, thermal expansion, specific heat models;
- The fuel initial radial deformation and relocation due to densification, solid swelling and gas swelling (from FRAPCON);
- The cladding initial radial deformation (from FRAPCON);
- The Massih model for fission gas release (FGR);
- The gap conductance model due to gap gas conductivity, fuel/cladding emissivity and cladding hardness;
- The Cathcart-Pawel (C-P) model for high temperature oxidation;
- The non-protective initial oxide layer option.

In order to test the model improvements in FRAPTRAN-TE-1.5, the following parametric studies are performed on the model options:

TABLE 1. PARAMETRIC STUDIES ON FRAPTRAN-TE-1.5 MODEL OPTIONS

Case	Clad mechanical	Clad burst failure	Axial fuel relocation
P0	FRAGAS-I	BALON2 (empirical strain and stress limits)	Off
P1	FRAGAS-I	<i>noball</i> (Instability strain)	Off
P2	FRAGAS-I	<i>noball</i> (Instability strain)	On
P3	FEA (finite element analysis)	<i>noball</i> (Instability strain)	On

For the cases with the new “axial relocation” model, the following calibrated parameters are used in order to obtain correct clad ballooning and burst behaviour and fuel packing fraction:

TABLE 2. SUMMARY OF THE AXIAL RELOCATION MODEL CALIBRATED PARAMETERS

Parameters	IFA650.9	IFA650.10
Sigburststrain	1	0.45
Sigcladanneal	0.15	0.1
Sigcladyieldstress	1.05	1.30
Packing fraction	0.72	0.72

3.3. Parametric studies results and discussions

The calculated results of the parametric studies with FRAPTRAN-TE-1.5 (P0-P3) are compared with the available experimental data (Measurement) in Fig. 1 for IFA-650.9, which indicated significant axial fuel relocation. Fig.1 (a) and (b) show cladding temperatures, (c) and (d) coolant temperatures, (e) plenum temperature, (f) rod internal pressure, (g) cladding elongation and (h) rod radius.

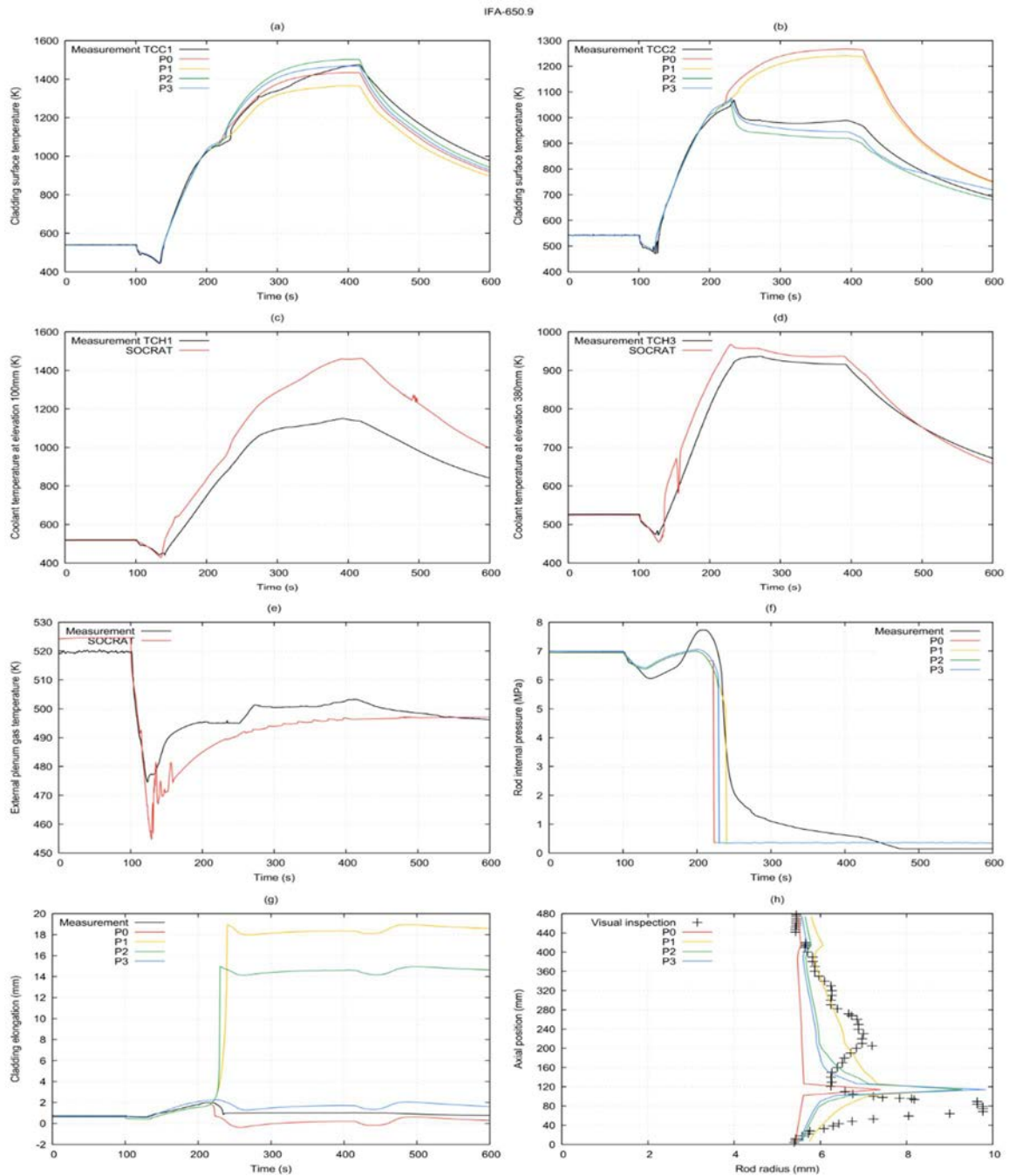


FIG.1. The parametric study results for IFA-650.9.

It can be observed that:

- The measured cladding temperatures at bottom (Fig. 1(a)) and top (b) are well predicted only by using the FRAPTRAN-TE-1.5 axial relocation model (P2 and P3), the SOCRAT calculated coolant temperatures (Fig. 1(c) and (d)) and heat transfer coefficients. However, without the axial relocation model (P0 and P1), FRAPTRAN-TE-1.5 fails to predict the decreased cladding temperature at top (b), even though the SOCRAT calculated coolant temperatures are correct (d).
- The SOCRAT calculated coolant temperatures are quite close to the measured heater temperature at heater top (d) and the rod plenum temperature (e), but significantly higher than the measured heater temperature at bottom after 210 s (c). This can be attributed to the mechanistic relocation model used in the SOCRAT calculation [15].
- The default BALON2 ballooning (with high temperature clad failure criterion based on empirical strain and stress limits for the burst) (P0) predicts earlier burst than the default deformation model (with burst criterion

- based on the cladding effective plastic strain) (P1) as shown in the rod internal pressure (f), lower deformation as shown in the cladding elongation (g) and radius (h).
- The finite element analysis (FEA) model (P3) enables FRAPTRAN-TE-1.5 to better predict the cladding deformation (g and h).
 - The evolution of the rod internal pressure (f) during the cooldown and heatup period and following the burst is poorly predicted in all cases. Since the plenum temperature is well imposed (e), one can attribute this to the poorly predicted deformation (g, h) and the possible axial gas transportation from the plenum to the ballooned and burst region (not simulated in FRAPTRAN-TE-1.5).
 - FRAPTRAN-TE-1.5 fails to predict the “double balloons” as observed in the test (h). This may be attributed to the coarse mesh for the thermal hydraulic boundary conditions. Indeed, with much refined axial meshes in the test rod, SOCRAT is able to predict the “double balloons” [15].

Similar observations are made for IFA650.10, except that no differences are observed between the calculated cases cladding temperature at top as there is almost no axial fuel relocation in this case.

It can be concluded that:

- The default mechanical model (FRACAS-I) with ballooning model under predicts the ballooning but predicts better the rupture behaviour.
- The default mechanical model (FRACAS-I) without ballooning model over predicts the ballooning but predicts later rupture behaviour.
- The default mechanical model (FRACAS-I) without ballooning but with relocation model predicts better the cladding temperatures (in particular for IFA-650.9), the ballooning and rupture behaviour (in particular IFA-650.10).
- Only the FEA model without ballooning but with relocation model predicts better the cladding elongation.

4. STATISTICAL UNCERTAINTY AND SENSITIVITY ANALYSIS ON IFA-650.10

4.1. Specifications

A detailed specification has been made for the uncertainty and sensitivity analysis on IFA-650.10, where uncertain input parameters in fuel rod manufacturing data, operation and test boundary conditions, physical properties and key physical models were identified, with their ranges and distributions defined [16].

The probabilistic input uncertainty propagation method is selected due to its simplicity, robustness and transparency. A total of 200 FRAPTRAN code runs are made, and the input parameters are obtained following a Simple Random Sampling (SRS) of the defined PDFs uncertainty ranges and distributions and assuming independence between input parameters. A lower and upper uncertainty bound of the 5% and 95% percentiles at confidence level higher than 95% are estimated by the 196th and 5th rank, respectively, by using the order statistics method [16].

Besides statistical uncertainty analysis, a global sensitivity analysis is also performed to get qualitative insights on the most influential input parameters, using the previously obtained 200 code runs. The identification is based on selected sensitivity indices and significance thresholds [17].

4.2. Implementation on FRAPTRAN-TE-1.5 using DAKOTA

The DAKOTA (Design Analysis Kit for Optimization and Terascale Applications) tool [18], which is developed by the Sandia National Laboratory and has been used by Tractebel for uncertainty analysis in multi physics modelling [10], is used for performing the uncertainty and sensitivity analysis on the FRAPTRAN-TE-1.5 simulation of IFA-650.10. The above specifications were implemented except for some minor adaptations. In particular, the relocation model related parameters based on the previously calibration for IFA-650.9 (see Table 2) are kept for IFA-650.10, in order to have single calibrated model parameters for the future applications.

For each uncertain input parameter, the information includes a mean value, a standard deviation and a type of distribution. In order to avoid unphysical numerical values, a range of variation (lower and upper bounds) is also provided. The sampling is performed between the upper and lower bounds, i.e. the distributions are truncated. In order to simplify the current benchmark application, a normal distribution is assigned to all the considered input parameters. Their standard deviation is taken as the half of the maximum of the absolute value of the difference between their nominal value and their upper or lower bound for all input parameters.

The DAKOTA tool has been used to sample these input parameters and generate corresponding 200 input models for FRAPTRAN-TE-1.5. After running these 200 cases, the relevant output parameters were collected, the lower and upper bounds were determined by using the order statistics, and the important input uncertainty parameters were identified through the partial rank correlation coefficients (PRCC) obtained by the global sensitivity analysis.

4.3. Uncertainty analysis results and discussion

The FRAPTRAN-TE-1.5 calculation results of the first 200 successful runs are collected, and the 5th and 196th ranks are chosen to estimate the upper/lower (95% / 5%) uncertainty bounds (LB, UB) of the output parameter of interest. The reference case results (Best-Estimate or BE) are also presented, using all input parameters at their mean (or nominal) values. The calculated reference, upper and lower bounds are compared with the available measured data (Experimental) in Fig 2(a) for rod internal pressure, (b) cladding outer surface temperature, (c) for cladding axial elongation, and (e) for rod diameter.

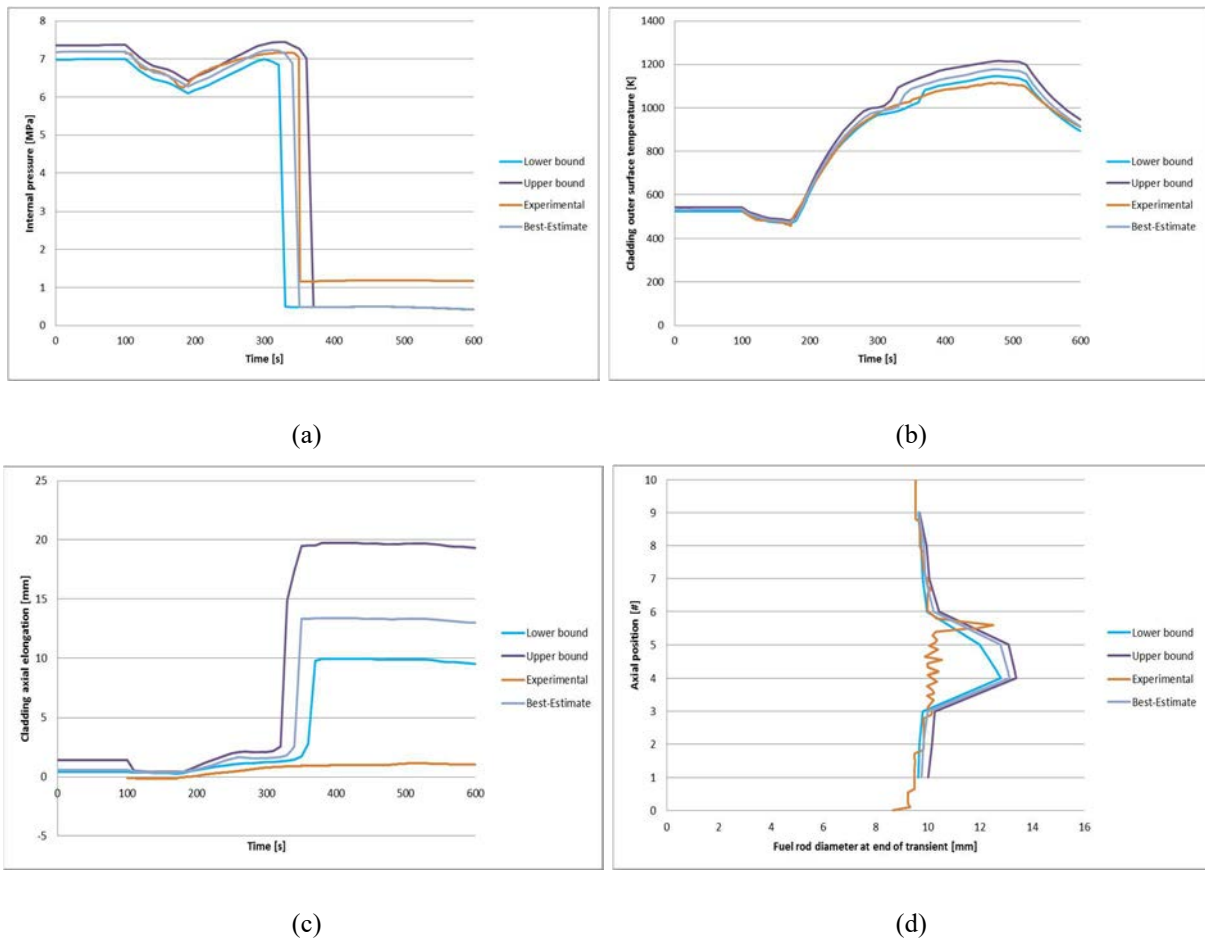


FIG.2. Uncertainty analysis results for IFA-650.10 with relocation model.

It can be observed that:

- The BE rod internal pressure agrees remarkably well with the experimental data, which is well bounded by the uncertainty bands. The pressure is a little underestimated just after the blowdown, but both burst instant and peak pressure are well predicted. This confirms that the fuel thermal aspects are well modelled by FRAPTRAN. Since the fuel axial relocation and deformation are known to be much weaker in this test, the weaknesses in the mechanical deformation models have no impact on the rod internal pressure.
- In the heatup phase, the calculated cladding outer surface temperatures (BE, LB and UB) are above the experimental data, even when the uncertainties are accounted, due to probably the consideration of axial relocation in the calculation. Indeed, it is suspected that some small axial relocations occurred during the test

but were not detected in the 3 cladding temperature measurements. More precise measurements are recommended in the future LOCA tests.

- The predicted clad elongation has large initial uncertainty, which nearly disappears with blowdown. The difference could be due to that the definition of the starting points are different in the calculations and in the experiment. The measurements are overestimated by far and this confirms the need to work on the mechanical deformation models. Use of FEA may also improve the prediction.
- The uncertainties on the cladding diameter are rather weak, except for in the bottom part. This means that there are more phenomena of interest occurring in that bottom part, leading to larger uncertainties. The fact that the uncertainty analysis does not cover the experimental data confirms that the models used are not adequate for all phenomena. There is a balloon of the appropriate radial size, but of exaggerated axial size. This confirms the results on the oversized elongation, but also the choice of the axial relocation model.

4.4. Sensitivity analysis results and discussion

The partial rank correlation coefficients (PRCC) measures the monotonic relation between the output parameter and the input parameter, while adjusting for the effects of the other input parameters. As the FRAPTRAN code have very complex models, and there are certain interactions between input parameters, these coefficients can only be considered as qualitative and relative index for screening the important input parameters.

The PRCC values change during the transient. Based on the PRCCs at their maximum absolute values, the important input parameters are identified for each output as shown in Table 3, where “H” (green) cell means that the input parameter has a significant impact on *at least one* of the related output parameters ($PRCC > 0.5$), “M” (orange) cell means a medium effect ($0.25 \geq PRCC \leq 0.5$), and “L” (white) cell means a low effect ($PRCC < 0.25$). Note that the significance thresholds of 0.25 and 0.5 are chosen arbitrarily for simplicity, as specific guidance and interpretation of the significance depends on the number of samples, number of variables, and analysis tolerance.

The following observations can be made:

- The fuel thermal behaviour (TFC, TFO) and rod internal pressure (RIP) are significantly impacted by the rod gap geometry (fuel diameter and cladding inner diameter), gap gas conductivity, filling gas pressure, plenum gas temperature, fuel thermal conductivity, heat capacity and axial relocation related parameters (clad yield stress, fuel fragment packing ratio and clad annealing), test conditions (relative transient power, coolant temperature, coolant to clad HTC).
- The cladding thermal behaviour (TCI, TCO) and cladding equivalent reacted (ECR) are significantly impacted by clad thickness, steady state corrosion and high temperature oxidation, fuel heat capacity and axial relocation related parameters, test conditions (relative transient power, axial power profile, coolant temperature, coolant to clad HTC).
- The cladding and fuel mechanical behaviour (DCO, CES, ECT and EFT) are significantly impacted by rod gap geometry, fill gas pressure, gap gas conductivity, fuel/clad related properties and models (fuel thermal conductivity, densification, swelling, fuel/clad thermal expansion), steady state corrosion and high temperature oxidation, axial relocation related parameters, test conditions (relative transient power, axial power profile, coolant temperature, coolant to clad HTC).

It is clear that the clad, gap and fuel geometry, initial states, test conditions (relative transient power, axial power profile, coolant temperatures and clad-to-coolant heat transfer coefficients) and axial fuel relocation related parameters (clad yield stress, fuel fragment packing fraction and clad annealing) are important for nearly all output parameters. This means that a good simulation of the fuel behaviours in Halden LOCA tests need a better characterisation of the test rods, better measurements or calculations of the thermal hydraulic boundary conditions, and a realistic axial relocation model.

TABLE 3. IMPORTANCE RANKING OF EACH PARAMETER FOR IFA-650.10

Input uncertainty parameter	Fuel Thermal Behaviour + RIP	Clad Thermal Behaviour + ECR	Mechanical Behaviour	Overall
Cladding outside diameter (mm)	L	H	H	H
Cladding inside diameter (mm)	H	H	H	H
Pellet outside diameter	H	M	H	H
Fuel theoretical density (kg/m ³ at 20°C)	M	M	L	M
U235 enrichment (%)	L	L	L	L
Filling gas pressure (MPa)	H	M	H	H
Relative power during base irradiation	L	L	L	L
Relative power during test	H	H	H	H
Test rod power profile	L	H	H	H
Cladding temperature (°C)				
Coolant temperature (°C)	H	H	H	H
Clad-to-Coolant heat transfer coefficient	H	H	H	H
Fuel thermal conductivity model	H	M	M	H
Clad thermal conductivity model	L	M	L	M
Fuel thermal expansion model	L	L	H	H
Clad thermal expansion model	L	L	H	H
Fuel densification model	M	L	H	H
Fuel solid swelling model	M	L	H	H
Fuel gaseous swelling model	M	L	H	H
Clad Yield stress	H	H	H	H
Fuel heat capacity	H	H	M	H
Cladding heat capacity	L	L	L	L
Cladding elastic modulus	L	L	L	L
Cladding corrosion model during steady state operation	L	H	H	H
Cladding hydrogen pickup fraction during steady state operation	L	L	L	L
Cladding oxidation model at high temperature	L	H	H	H
Thermal conductivity of the oxide layer	L	L	L	L
Fission gas release	L	L	L	L
Gap gas conductivity	H	M	H	H
Fuel/cladding emissivity	L	L	L	L
Fuel radial relocation	L	L	L	L
Fuel fragment packing fraction	H	H	H	H
Cladding strain threshold for fuel mobility	L	L	L	L
Cladding Meyer hardness	L	L	L	L
Cladding annealing	H	H	H	H
Cladding burst criteria	L	L	L	L
Cladding burst strain criteria	L	L	L	L
Plenum gas temperature [°C]	H	M	H	H

5. PROPOSAL FOR DEVELOPMENT OF A METHODOLOGY FOR SAFETY EVALUATION OF ADVANCED TECHNOLOGY FUEL DESIGNS UNDER LOCAS

The final objective is to apply the qualified fuel rod codes FRAPCON/FRAPTRAN to develop a best estimate plus uncertainty analysis (BEPU) type hot rod LOCA fuel safety evaluation methodology (FSEM), in order to verify the compliance with the applicable LOCA safety criteria (e.g. the USNRC new LOCA criteria 10CFR50.46c).

In this FSEM methodology, the important phenomena or input parameters that affect the LOCA fuel behaviour modelling will be first identified by means of the PIRT (phenomena identification and ranking table) technique, and the FRAPTRAN simulation model will be developed for a Pressurized Water Reactor (PWR) fuel rod based on the thermal hydraulic boundary conditions (e.g. local coolant temperatures and cladding to coolant heat transfer coefficients) from the qualified system thermal hydraulic codes (such as RELAP5 or TRACE, CATHARE, MARS or SPACE), as obtained from the most limiting cases for the final safety analysis report (FSAR) the design basis LOCA safety analysis.

The uncertainties related to the FRAPTRAN fuel rod simulation model input parameters and the thermal hydraulic boundary conditions will be identified and defined. Their importance will be confirmed by using the GSA (global sensitivity analysis) technique. The uncertainties on the important input parameters will be combined statistically in the FRAPTRAN calculated upper bound values of peak cladding temperature (PCT) and maximum local oxidation (MLO) or equivalent cladding reacted (ECR), by using the input uncertainty propagation and order statistics methods (such as the method used in the FUMAC project).

This methodology will be used to quickly assess the LOCA performance and the margins of the advanced technology fuel (ATF) rod, without the need to perform complex LOCA safety analyses.

6. CONCLUSIONS

As part of the Tractebel's contribution to the IAEA FUMAC project, two selected Halden LOCA tests IFA-650.9 and IFA-650.10 have been simulated using the updated FRAPTRAN-TE-1.5, in order to qualify the FRAPTRAN-1.5 code for LOCA fuel behaviour modelling. In addition, uncertainty and sensitivity analysis has been performed on the FRAPTRAN-TE-1.5 simulation of the IFA-650.10 test.

It was concluded that:

- The updated FRAPTRAN-TE-1.5 can well simulate the LOCA fuel thermal behaviours as observed in the Halden LOCA tests IFA-650.9 and IFA-650.10, using adequate thermal hydraulic boundary conditions and the axial relocation model.
- The updated FRAPTRAN-TE-1.5 does not well simulate the LOCA fuel mechanical deformation as observed in the Halden LOCA tests IFA-650.9 and IFA-650.10, using the default FRACAS-I model.
- The uncertainty analysis on FRAPTRAN-TE-1.5 simulation of the IFA-650.10 test confirms that the FRAPTRAN-TE-1.5 thermal models, axial relocation model, the heat transfer boundary conditions and gas temperature model are adequate for simulating the thermal behaviour of the Halden LOCA tests, and their impacts can be well considered by statistical uncertainty analysis. However, the mechanical models for the cladding deformation still need to be improved for simulating the Halden LOCA tests, and the coverage of the experimental data.
- The sensitivity analysis on the FRAPTRAN-TE-1.5 simulation of the IFA-650.10 test helps to identify the most influential input fuel rod data, test conditions, physical properties or models. The parameters related to the axial relocation model (when applied) are also important. However, the situation of strain threshold for fuel mobility and burst criteria is more dubious, as they have low correlation coefficients, but should be of importance according to the physics and the modelling. More detailed analysis is needed to examine this, e.g. by considering the scatter plots or using other sensitivity indices (such as Sobol's).

In conclusion, substantial progress has been made in achieving the FUMAC project objectives and the agreed work plan for Tractebel. The following recommendations can be made:

- Further improvements or validation should be made to FRAPTRAN code for LOCA fuel mechanical behaviour modelling: the ballooning and burst models, the finite element analysis model for cladding, and if possible the axial gas transportation model.

- Further improvements could be made to FRAPTRAN code for LOCA fuel rod to coolant heat transfer modelling: this may be overcome by coupling with a system thermal hydraulic code, using a refined nodding scheme.
- The QT's axial fuel relocation model could be improved by obtaining a unique set of model related parameters based on all available Halden LOCA tests with significant fuel relocation.
- More detailed uncertainty and sensitivity analysis should be performed after the code improvements.

It is recommended to apply the validated FRAPTRAN code and the statistical uncertainty and sensitivity analysis method to development of an efficient BEPU type LOCA fuel performance and safety evaluation methodology for new or advanced technology fuel design assessment and licensing. This would enhance the sustainability of nuclear technology and ensure the diversification of fuel supply. This development will be proposed for the new IAEA CRP as a continuation of the FUMAC and ACTOF projects.

ACKNOWLEDGEMENTS

This work was funded by the Nuclear Development Division (NDD) of the ENGIE group as part of the IAEA Coordinated Research Project Fuel Modelling in Accident Conditions (FUMAC). The authors are also grateful to Dr. Lars Olof Jernkvist (Quantum Technologies) for his assistance in the implementation of the Quantum Technologies axial relocation model and other error corrections in the Tractebel version of FRAPTRAN-TE-1.5 code, and to Dr. A.E. Kiselev (IBRAE) for providing the thermal hydraulic boundary condition calculations with SOCRAT code.

REFERENCES

- [1] UMIDOVA, Z., DETHIOUX, A., ZHANG, J., "Qualification Of FRAPCON/FRAPTRAN Codes for Fuel Rod Design Verification and Fuel Safety Evaluation," ENS Conference Proceedings TopFuel 2012, Manchester, UK, 2–6 September 2012.
- [2] ZHANG, J., UMIDOVA, Z., DETHIOUX, A., "Simulation of fuel behaviours under LOCA and RIA using FRAPTRAN and uncertainty analysis with DAKOTA", in "Modelling of Water Cooled Fuel Including Design Basis and Severe Accidents, Proceedings of a Technical Meeting Held in Chengdu, China, 28 October–1 November 2013", IAEA-TECDOC-CD-1775, 2015.
- [3] VESHCHUNOV, M., STUCKERT, J., VAN UFFELEN, P., WIESENACK, W., ZHANG, J., "FUMAC: IAEA's Coordinated Research Project on Fuel Modelling in Accident Conditions," ENS Conference Proceedings TopFuel 2018, Prague, Czech Republic, 30 September–04 October 2018.
- [4] BOLE DU CHOMONT, F., "LOCA Testing at Halden, the Ninth Experiment IFA-650.9", HWR-917, OECD Halden Reactor Project, October 2009.
- [5] LAVOIL, A., "LOCA Testing at Halden, the Tenth Experiment IFA-650.10", HWR-974, OECD Halden Reactor Project, December 2010.
- [6] GEELHOOD, K.J., LUSCHER, W.G., "FRAPCON-3.5: A Computer Code for the Calculation of Steady-State, Thermal mechanical Behaviour of Oxide Fuel Rods for High Burnup", NUREG/CR-7022, Vol. 1, Revision 1, USNRC, May 2014.
- [7] GEELHOOD, K.J., LUSCHER, W.G., "FRAPCON-3.5: Integral assessment", NUREG/CR-7022, Vol. 2, Revision 1, USNRC, May 2014.
- [8] GEELHOOD, K.J., LUSCHER, W.G., CUTA, J. M., "FRAPTRAN-1.5: A Computer Code for the Transient Analysis of Oxide Fuel Rods", NUREG/CR-7023, Vol. 1, Revision 1, USNRC, (May 2014).
- [9] GEELHOOD, K.J., LUSCHER, W.G., "FRAPTRAN-1.5: Integral assessment", NUREG/CR-7023, Vol. 2, Revision 1, USNRC, (May 2014).
- [10] ZHANG, J., DETHIOUX, A., OURY, L., SCHNEIDESCH, C., "FRAPTRAN 1.5 Modelling of the Halden LOCA Tests IFA650.9 and 10: Scoping Parametric Studies and Perspectives", in Proc. Enlarged Halden Programme Group Meeting Sandefjord, Norway, 8th–13th May, 2016.
- [11] JERNKVIST, L.O., MASSIH, A.R., ALVESTAV, A.: "Axial relocation of fragmented and pulverized fuel and its effects on fuel rod heat load during LOCAs", Top Fuel 2015, paper A0059, (2015).
- [12] JERNKVIST, L.O., "Observed and corrected errors in source code and algorithms of FRAPTRAN-1.5," Report TR15-002V2, Quantum Technologies AB, (March 2016).
- [13] ZHANG, J., "Code modification requirements specifications (CMR.S) for extension and adaptation of FRAPTRAN-1.5 for LOCA fuel behaviour modelling," Internal report FUELROD/4DO/0437004/000/00, Tractebel, Brussels, Belgium, February 2016.
- [14] JERNKVIST, L.O., "The FRAPTRAN-TE-1.5 computer programme", Report TR16-001, Quantum Technologies AB, March 2016.

- [15] KISELEV, A.E., "Short Information on the Results of IFA-650.9, IFA-650.10 and IFA-650.11 Calculations with SOCRAT code", Technical Note, version 2, IBRAE, December 2016.
- [16] ZHANG, J., "Specifications for Uncertainty Analysis on Modelling of the Halden LOCA Test IFA-650.10", Internal report DDN/4NT/0520044/000/00, Tractebel, Brussels, Belgium, July 2017.
- [17] MCKAY, M.D., "Sensitivity and uncertainty analysis using a statistical sample of input values," Ch. 4, Uncertainty Analysis, (Ronen, Y. Ed.), CRC Press, Florida, USA, (1988).
- [18] ADAMS, B.M., Multilevel parallel object oriented framework for design optimization, parameter estimation, uncertainty quantification, and sensitivity analysis: Version 5.4 user's manual. Technical Report SAND2010-2183, Sandia National Laboratories, Albuquerque, NM, (Nov. 2013).

FUEL BEHAVIOUR MODELLING IN ACCIDENT CONDITIONS IN ALCYONE FUEL PERFORMANCE CODE

A. BOULORÉ, C. STRUZIŁ, P. GOLDBRONN, I. GUENOT-DELAHAIE, J. SERCOMBE
CEA/DEN/DEC Cadarache,
13108 Saint-Paul-lez-Durance,
France

Abstract

CEA is developing the ALCYONE fuel performance code for PWR fuel in the PLEIADES software environment. It is dedicated to normal, off-normal and accident conditions such as RIA and LOCA. CEA's participation to the IAEA FUMAC CRP led to an improvement of the fuel modelling in LOCA conditions. Specific developments of the fuel performance code for the LOCA conditions have been done regarding cladding behaviour modelling, fission gas release and stress evaluation in the pellet before and during the tests. The improved code has been used to simulate some of the experiments of interest of the FUMAC project (IFA650.10 and Studsvik 192 LOCA test), the paper summarizes the results. For IFA650.10, the cladding outer temperature profile calculated with the SOCRAT code and provided to the participants of the FUMAC CRP has been used. The results obtained with ALCYONE are in a good agreement with the experimental data. In terms of uncertainty quantification, it seems that the uncertainty on the determination of the boundary conditions like cladding outer temperature results in a large uncertainty on the cladding deformation and the burst time. Recent developments have also been done in ALCYONE to improve the modelling of fuel behaviour in RIA conditions, in particular about fuel mechanical behaviour and the consequences on fission gas release.

1. INTRODUCTION

"ALCYONE [1] is a multi dimensional fuel performance code co-developed in the PLEIADES [2] platform by the CEA, EDF and FRAMATOME. It is dedicated to the modelling of the in-reactor Behaviour of PWR fuel rods during normal (base irradiation) and off-normal (power ramps and accidental situations) operating conditions and incorporates three calculation schemes. A one dimensional reference scheme, based on a one dimensional axisymmetric description of the fuel element associated to a discrete axial decomposition of the fuel rod in stacked independent fuel slices, is used to study the Behaviour of the complete fuel rod [3]. A two-dimensional scheme, which describes Pellet cladding Interaction (PCI) at the mid-pellet plane of a pellet fragment, is available to assess precisely stress concentration in the cladding near a pellet crack tip [4]. A three dimensional model of the complete pellet fragment and overlying cladding is also of interest when detailed studies of PCI at pellet-pellet interfaces are required [5]. The different schemes use the Finite Element (FE) code Cast3M to solve the thermo mechanical problem and share the same physical material models at each node or integration points of the FE mesh" [22] Figure 1 presents the flows chart of ALCYONE 1 D. On the figure the different tests of convergence loops are identified in blue, the models in the thermo physical loop are in beige and the other models are in green if they are calculated before the thermo physical loop or in grey pink if after.

Base irradiation code result has been extensively validated on PWR rods (UO₂ and MOX fuel up to 80 GWj/tm, cladding Zry-4 or M5) irradiated in the frame of the French survey programme. Power ramp tests performed in MTR are used to validate the Behaviour of the fuel rod in case of power transient regime. Calculated results are confronted to experimental values at different scales, from overall measurements on the whole rod such as overall fission gas release or geometrical changes to the local measurements on the fuel pellet by SIMS and EPMA. Moreover, fuel temperature calculations are validated specifically on MTR experiments which present a thermocouple in the fuel centre [3].

More recently, specific developments, summarized in this paper, have been done in the code in order to simulate accident conditions such as LOCA and RIA transients. This improved version of the code has been used in the FUMAC CRP benchmark to simulate two experiments. The paper summarizes the results of these simulations.

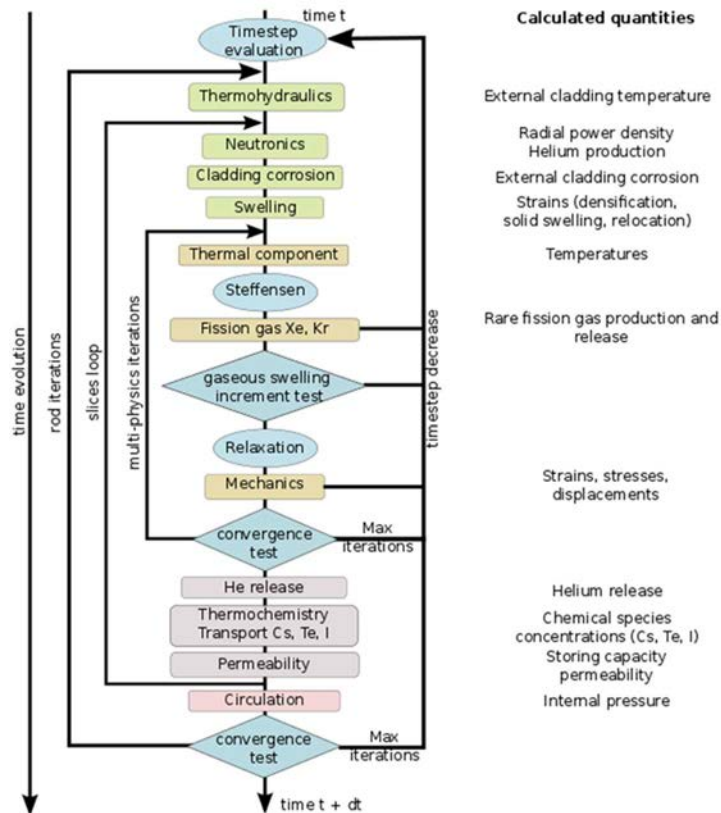


FIG. 1. ALCYONE flow chart.

2. ALCYONE MODELLING FOR ACCIDENT CONDITIONS

2.1. Specific developments for LOCA conditions

Up to now, LOCA studies have been performed using 1.5 D scheme. For LOCA transient analysis, ALCYONE is not able to calculate the cladding temperature evolution with time, so this information has to be provided as input data. Nevertheless, the coupling of ALCYONE [6] with the system code CATHARE will be available in a near future. For the LOCA studies point of view, the evaluation of the rod internal pressure is crucial. To do so, it is necessary to have a good description of the fuel at the end of base irradiation. Then, it is essential to have a correct evolution of the different components of the free volume (plenum, gap, ...) and of the fission gas Behaviour. On the other hand, the evaluation of the quantity of fuel which could be fractured in fine pieces during the accident phase (i.e. at least the fuel zone which are restructured (HBS) or in restructuration) is also important. This description is done by two fission gas models CARACAS [7] or MARGARET [8] (more phenomenological). Both models describe the fission gas production, release and swelling and also the HBS formation. In the grain, dissolved gas, nanometric bubbles, precipitated bubbles (up to 0.1 μm) are considered; the gas atom diffusion and bubbles diffusion are modelled. Trapping of gas atom by bubbles is taken into account. On the grain boundary gas is considered to be precipitated into bubbles and the release could happen by inter-connection of bubbles or fracture by overpressure on a weakened grain boundary. In each point of the pellet, the fraction of HBS is calculated by the balance between defaults accumulation due to fission spike and thermal recovery. These entire phenomena are very sensitive to fuel temperature, fission rate and local stresses.

2.1.1. Cladding behaviour modelling

The EDGAR model [9] describes the viscoplastic behaviour of a zirconium alloy tube under a pressure imposed loading and at high temperature (more than 950 K). This model also gives the phase fractions evolution (2 phases are considered: alpha and beta and a mixed transition domain, alpha + beta).

For its introduction into ALCYONE, the EDGAR model has been turned into a constitutive law suitable for a mechanical analysis: basically, the EDGAR model appears as a modified Norton viscoplastic behaviour with the total strain being split into an elastic and a viscoplastic part. The viscoplastic strain is then traceless which, for

small strains, guarantees that the cladding deformation is isochoric (no volume change), as it is classically assumed, based on experimental facts, in metal plasticity and viscoplasticity.

The mechanical behaviour is expressed in the logarithmic strain framework proposed by Miehe et al [11]. Integration of this formalism in ALCYONE is discussed in a dedicated paper [10]. Once those changes were made, the EDGAR experiments were simulated using ALCYONE to validate this implementation.

2.1.2. Stress distribution in the pellet

The 1D code generally considers that for a solid pellet, the radial displacement of the central point is not authorised. This hypothesis has no impact in hot conditions during base irradiation or power ramp regime. Indeed, the radial stress is in a compressive state in the whole pellet, due to the thermal gradient and that is all the truer when the fuel to cladding gap is closed.

In case of LOCA, the thermal gradient is significantly lower, and the gap is calculated open (even if at very high burnup, the gap, strictly speaking, is closed between cladding and fuel due to internal zirconia layer, but a reopening occurs inside the pellet at about hundred microns from the edge). Then the calculated radial stress tends to be in a tensile state in the central part of the pellet if the hypothesis of the central node blockage is done. This induces wrong input data for fission gas behaviour modelling. We have then decided to consider that the central point of the pellet is able to move radially.

Figure 2 presents stress distribution in the pellet when the gap is open in the cold conditions at the end of a base irradiation with the two hypotheses. During a LOCA, stresses distribution is likely to be in the same shape, as the thermal gradient remains low in the fuel pellet. Nevertheless, the actual value of the stress level depends on the fission gas swelling contribution and then on the base irradiation power history.

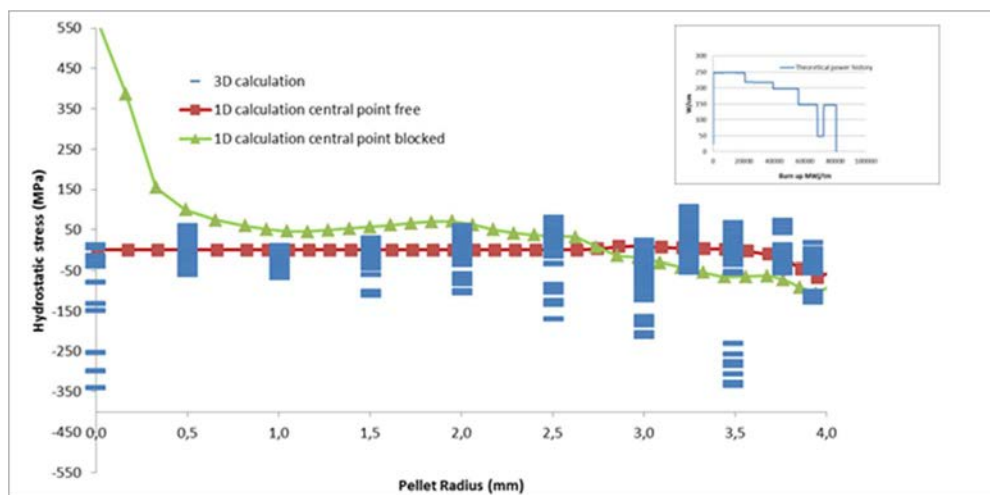


FIG. 2 : Hydrostatic stresses distribution in the pellet at room temperature.

2.1.3. Fission gas release

The fission gas model used in the ALCYONE calculations is CARACAS [7], which considers the following fission gas populations:

- Nanometric intragranular bubbles;
- Precipitated intragranular bubbles;
- Intergranular bubbles;
- Rim structure formation and rim bubbles evolution.

This model is validated in base irradiation conditions and power ramp conditions for UO₂ up to 70 GWd/tM.

During the first part of the LOCA transient, fuel temperature remains low enough to affect only the intergranular gas. A specific criterion for intergranular fracturation initiation has been developed. It is based on the evaluation of stress applied to grain boundary resulting from macroscopic hydrostatic stress and from stress induced by over pressurized intergranular bubbles (tensile stress). If the tensile stress on the grain boundary

induced by intergranular bubbles is higher than the grain boundary yield stress, partial or total fracturation of the grain boundaries is supposed to be possible. This allows fission gas release.

We also assume that grain boundary yield stress is reduced by irradiation (fission gas atoms dissolved on the grain boundary).

This criterion depends primarily on the amount of fission gas precipitated into bubbles after base irradiation (thus before transient), and thus on the initial fuel state and the fission gas distribution between the different populations.

It must be mentioned that this model has been developed to make most of the intergranular gas available for release in transient conditions. Even if the model results in a fraction of opened grain boundaries, it must not be used for now to evaluate a fuel fragment average size. The total fraction of opened grain boundaries being between 10 and 50%, it would result in very fine fragmentation (a few grains) which is not always observed, and particularly has not been observed in the IFA650-10 experiment.

2.2. Specific developments for RIA conditions

ALCYONE pulse-irradiation simulation capability is based on [12]:

- the solving of the thermal heat balance equation and mechanical equilibrium for the pellet-gap cladding system in non-steady state conditions;
- the solving of the thermal and mass balance equations for sodium or water coolant in non-steady state conditions;
- material laws describing the nonlinear mechanical behaviour of irradiated claddings (Zry-4, M5) submitted to RIA loading conditions;
- the addition, to fuel pellet creep and cracking modelling, of grain boundary cracking modelling;
- the use of a specific hypothesis as regards the release of fission gases of the high burnup structure (HBS) zone.

Some of these features are summarized in the following sections.

2.2.1. *Non-steady water heat and mass transport*

"Solving the heat and mass balance equations requires the estimation of the linear heat rate received by the water coolant from the fuel rod, based on the heat exchange between the cladding outer surface and the water, which involves the clad-to-water coolant heat transfer coefficient (HTC) in particular. The HTC is either given together with the coolant bulk temperature or calculated using ALCYONE's built-in thermal-hydraulics models". The model is detailed in [12].

2.2.2. *Suitable constitutive law for claddings*

Loading conditions during a RIA are quite peculiar, especially in terms of clad temperature and strain rates. Constitutive laws for Zry-4 [15] and M5 [14] cladding types and applicable to fast transient conditions and high temperatures representative of RIA spectrum, have been incorporated in ALCYONE [12].

"The models can account precisely for the impact of temperature, strain rate, and irradiation damage on the ultimate stress, on the strain hardening exponent (up to uniform elongation) and on the plastic anisotropy of the material. They are suitable for simulations of unfailed rods. The assumed isotropic elastic deformation is described by Hooke's law assuming a temperature-dependent Young's modulus." [12]

2.2.3. *Suitable constitutive law for UO₂ fuel*

The model proposed by Salvo [16, 17] to describe the Behaviour of uranium dioxide within a range of temperatures (1100–1700°C) and strain rates (10^{-4} – 10^{-1} /s) representative of RIA loading conditions is used in ALCYONE. This model consists of a hyperbolic sine model for the creep strain rate, completed by a Drucker – Prager yield criterion with associated plastic flow to account for the porosity increase induced by grain boundary cracking. The yield criterion is a temperature dependent function identified from the compression tests performed on fresh UO₂ at high strain rates and high temperatures that showed significant development of grain boundary cracking. In this case, the samples' porosity and diameter were found to increase significantly showing that grain

boundary cracking proceeds with pore volume increase. The latter is described in the model by the so-called “plastic” porosity.

“The creep and grain boundary cracking models are completed by a smeared crack model to describe pellet cracking in tension. The resulting constitutive law is particularly relevant for RIA loading conditions where biaxial compression and tensile stress states are commonly encountered.”[12]

2.2.4. Modelling of fission gas release

The fission gas model CARACAS [7] is so far not able to reproduce the FGR under RIA conditions. As this phenomenon has been evidenced as able, especially for high burnup fuels [18], to contribute to clad straining during RIAs, in particular through rod internal pressure increase potentially leading to clad ballooning, ALCYONE related improvement has been done. It aims at relating the FGR to grain boundary cracking and thus to the local mechanical damage of the oxide fuel generated by excessive compressive stresses. This coupling is based upon the following assumptions:

- The cracking of the grain boundaries generated by excessive compressive stresses and described by the plastic porosity (cf. Section 2.2.3) is used by the CARACAS model as the (mechanical) main criterion for the instantaneous release of intergranular gas (i.e. at the grain boundaries) contained in the fuel pellet rings where the criterion is met.
- In case of high burnup fuel where a HBS (characterized by an extremely fine grained structure and an increased quantity of gases at the grain boundaries) has developed during base irradiation in the peripheral regions of the pellet, a temperature criterion is adopted to be consistent with annealing tests which showed FGR from the HBS at temperatures as low as 900 K [19]. In case the temperature threshold is reached, all the fission gas content of the HBS (inter- and intragranular gas) is released instantaneously. The Intragranular gas of the HBS is assumed to be released instantaneously because the grain size is too small for diffusion to be rate-limiting.
- The plastic porosity which models the deformation induced by grain boundary cracking is added to the strains in the thermo mechanical computation scheme of ALCYONE and contributes therefore to the clad loading.

3. SUMMARY OF THE RESULTS OBTAINED IN THE FUMAC CRP

3.1. IFA650.10

This experiment presented in the HWR report [20] has been performed in the IFA650 device. The whole instrumentation of the experiment gives a large amount of valuable data which are used to build the input data for calculation. Nevertheless, it remains difficult to evaluate the temperature axial profile of the cladding, even with the use of fine thermohydraulic modelling.

About the cladding outer temperature profile during the experiment, two different sets of assumptions have been made:

- The temperature difference between the coolant and the cladding is proportional to the fissile power. Then, available measurements at two levels of the fissile rod (TCC1 (95 mm/bfc), TCC2 & TCC3 (360 mm/bfc)) allow the cladding temperature calculation for the whole rod and it is exact at the two TC levels. This set is mentioned as “ALCYONE boundary conditions” in the following;
- The cladding temperature profile provided by SOCRAT calculations.

The considered creep behaviour and phase transformation laws are the ones for “fresh” material. For the determination of the uniform strain limit at failure, we consider the value recommended for irradiated material.

The calculation is performed considering transient condition to evaluate the thermal exchanges. Cladding burst is not calculated directly by ALCYONE but determined by post processing the calculated internal pressure, cladding radius and cladding temperature.

The possibility of the grain boundary fracturation due to the gas bubble action is tested.

Figs 3 and 4 present the evolution of axial cladding elongation and pressure. Up to burst time, the agreement between the experiment results and calculation is rather good, but both boundary conditions sets slightly delay the burst time compared to the experiment. This result validates the hypothesis of perfect communication of the gases between the plenum and the free volumes of the rod for this case (fast plenum depressurization).

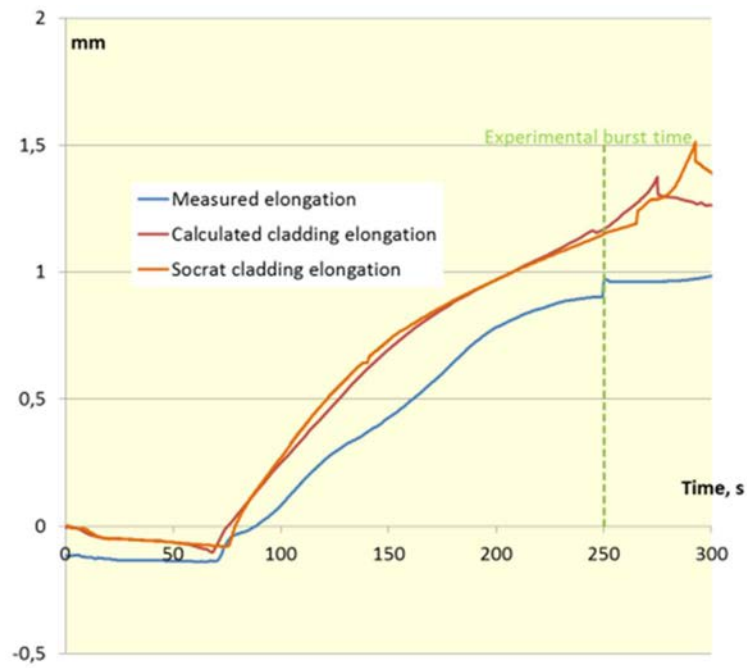


FIG. 3. Cladding elongation evolution.

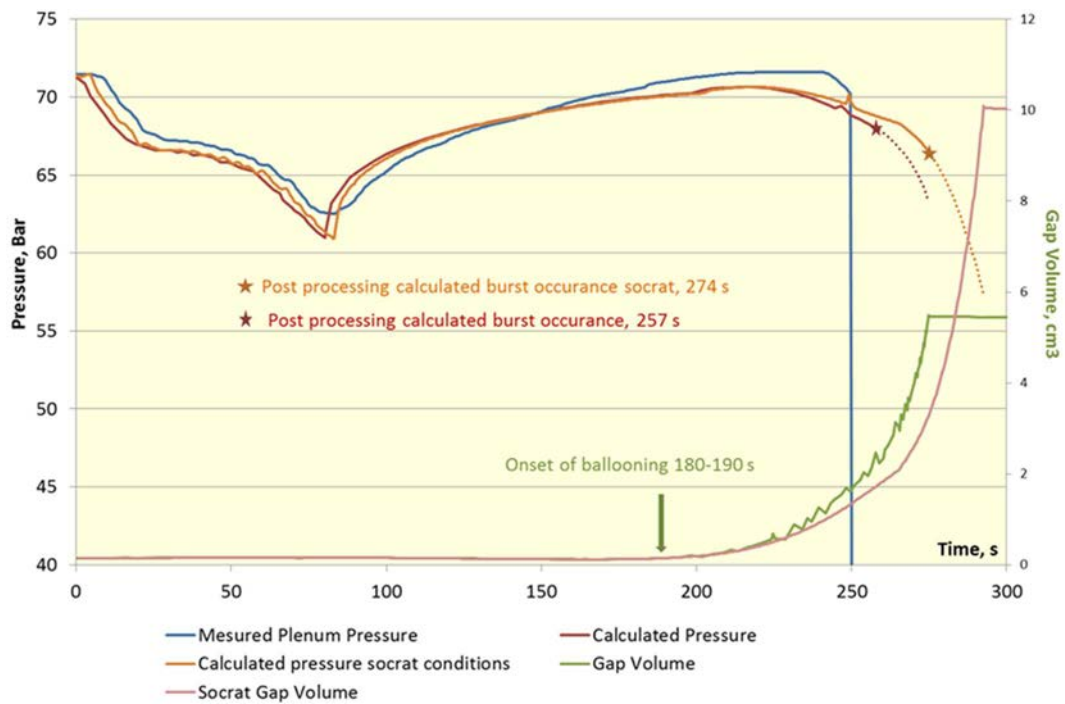


FIG. 4. Rod pressure evolution.

Figure 5 presents the cladding diameter calculated at burst time. Two times are considered: the experimental burst time and the calculated one. It appears that the tendency is correct (calculated diameter is slightly underestimated compared to the two measured diameters). With the SOCRAT thermal hydraulics boundary conditions, the rod diameter is underestimated at experimental burst time. Also, a little depletion of the rod profile is calculated at 2502 mm, and this result has to be related to the provided boundary conditions where this little depletion exists.

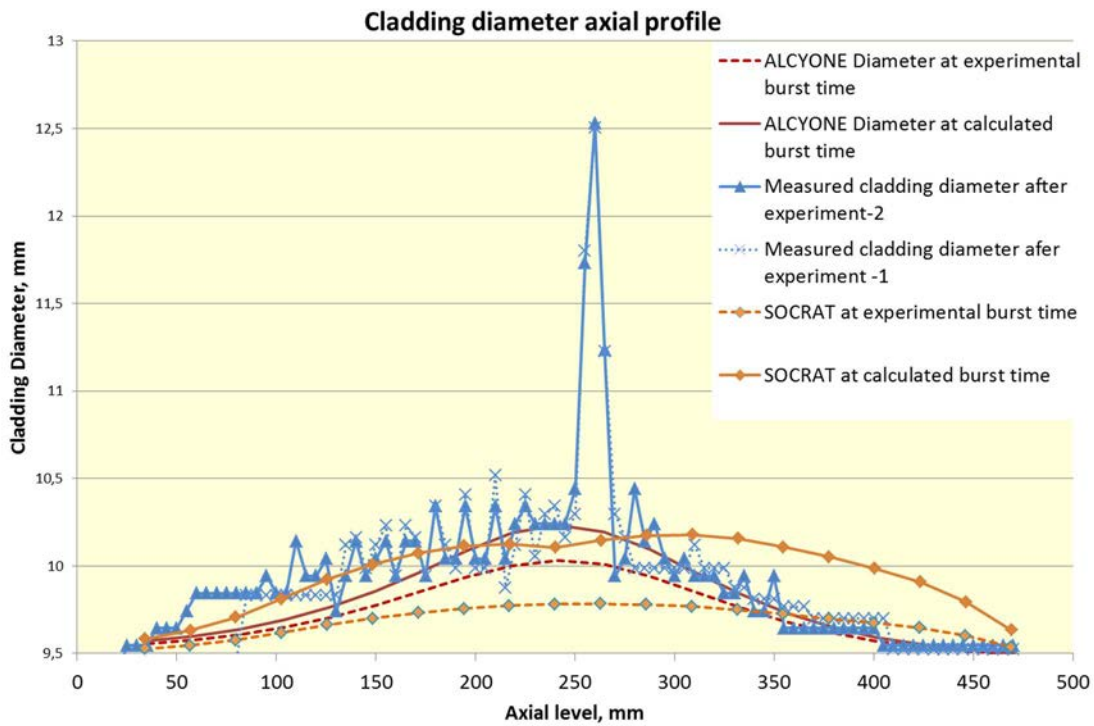


FIG. 5. Cladding diameter at burst time.

Fuel fragmentation due to the over pressurized intergranular bubbles occurs in the simulation in the HBS zones (outer parts of the pellet) and in some central parts. Fuel fragmentation also occurs after the cladding burst which leads to a fast decrease of the inner pressure of the rod.

The amount of gas released during the test is about 8 cm³, and it has a negligible effect on the evolution of the pressure during the test.

The parameters of the fragmentation model still have to be calibrated, to better assess the quantification of fuel fragmentation after burst. Results of this fragmentation model will provide inputs for a proper fuel fragment relocation model.

3.2. Studsvik 192 test

Same as for IFA650.10 experiment, the outer cladding axial temperature profile is imposed (given in the data sheet) in the data file. So is the initial inner pressure in the rodlet.

The plenum temperature is imposed during the experiment. All the different components of the free volume of the rodlet are assumed connected (plenum, gap, open porosity) so that the pressure in the rod is uniform during all the experiment.

Figure 6 presents the calculated evolution of the pressure in the rodlet and the cladding temperature evolution during the test. The calculated burst time is slightly delayed compared to the experiment (about 20 seconds later). In the calculation, burst occurs for a cladding temperature higher of 100°C than the temperature at experimental burst. This can be explained by the fact that the real cladding of the experiment is irradiated ZIRLO, whereas we use the mechanical Behaviour law of the fresh Zry-4.

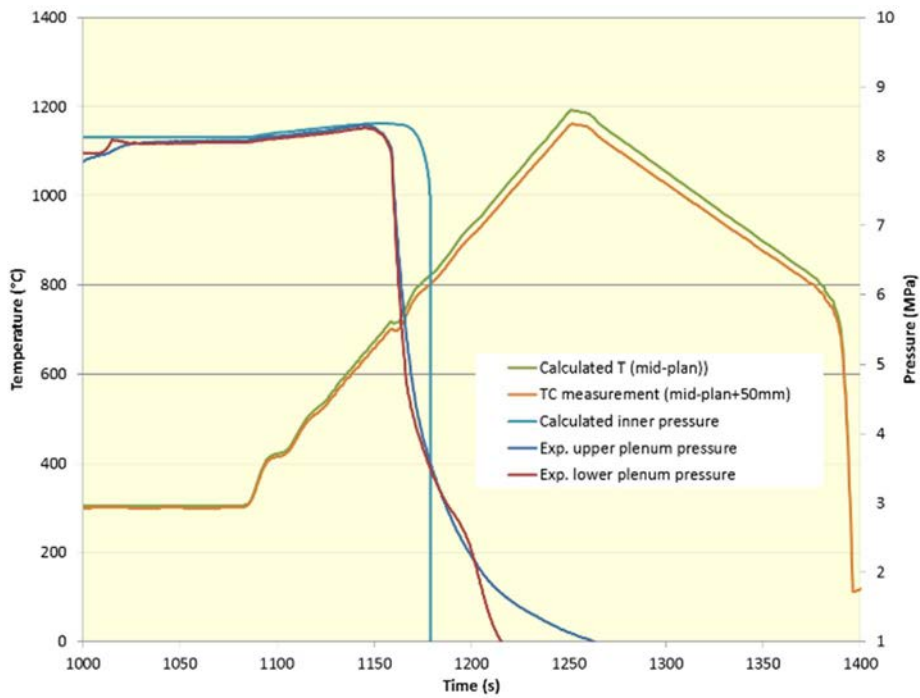


FIG. 6. Rod pressure evolution (Studsvik 192 test).

But the cladding profile calculated just before burst is in good agreement with the measured cladding profiles after the test (Fig. 7).

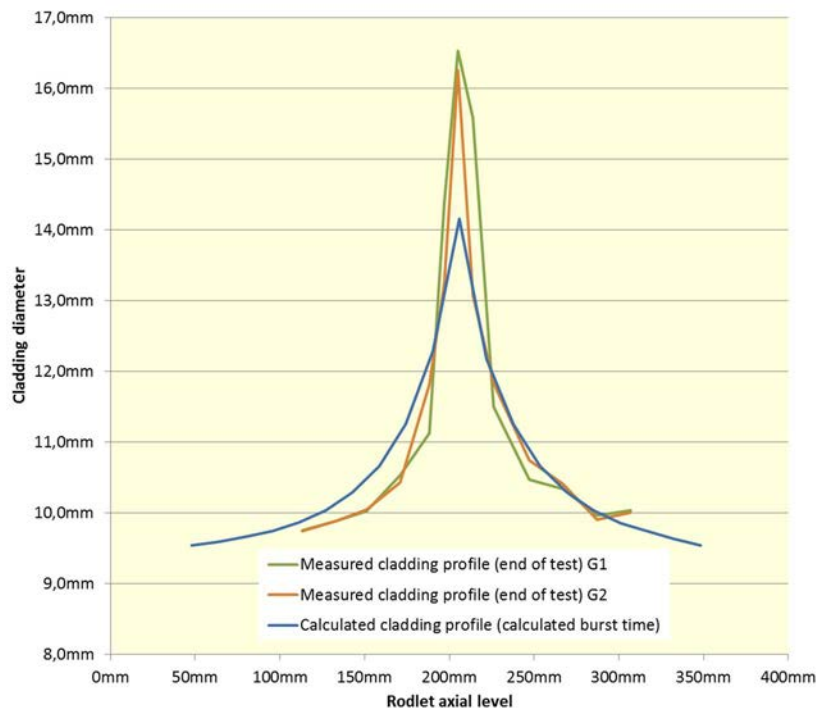


FIG. 7. Cladding profile after test (Studsvik 192 test).

Fuel fragmentation before burst occurs only in high burnup structure zones (edge of the pellet). But after burst, because of the fast decrease of the pressure in the rod, intergranular fragmentation occurs in HBS zones and central zones of the pellet as shown on Fig. 8.

The fragmentation criterion is based on the calculation of the stress applied on the grain boundary due to the overpressurized intergranular bubbles. So, it is closely related to the amount of gas on the grain boundary (in

bubbles in the CARACAS model) at the end of the steady state irradiation and to the fraction of bubbles interconnected to the free volume of the rod.

But as the fission gas model is based on the description of an average grain of the microstructure with spherical shape, the fractured grain boundary ratio cannot be used to quantify a fuel fragment size. In its current development state, the “fragmentation model” can only be used as a fission gas release mechanism.

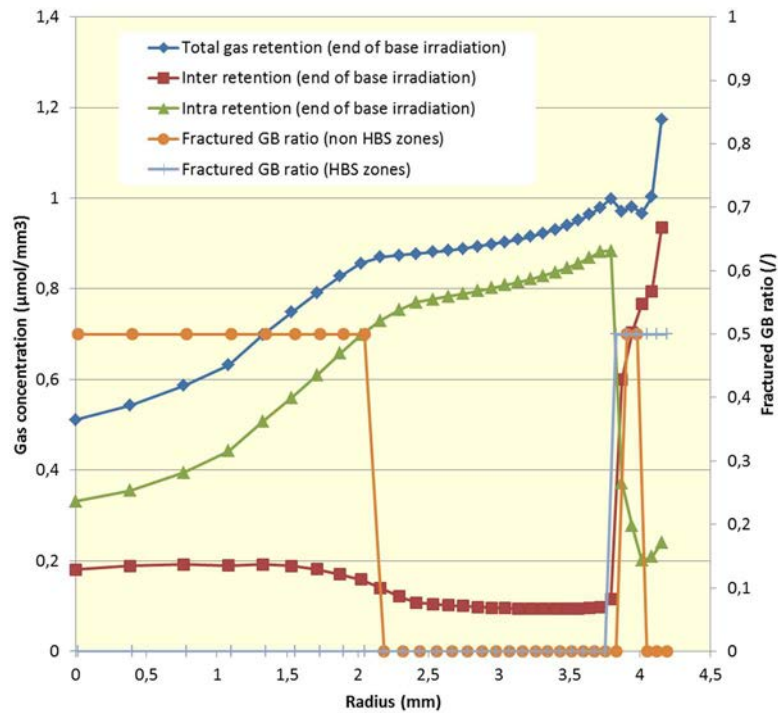


FIG. 8. Fuel fragmentation and fission gas distribution (Studsvik 192 test).

4. CONCLUSION

Some improvements have been done in the ALCYONE fuel performance code to better assess the fuel Behaviour in LOCA conditions. Specific developments have also been done to better assess the behaviour of fuel rod in RIA conditions.

In the framework of the FUMAC CRP, the simulation of IFA650.10 and Studsvik 192 test have been done successfully until the cladding burst with ALCYONE. The calculated results are in relative good agreement with the experimental data, especially if we consider the uncertainties on boundary conditions. Uncertainty quantification and sensitivity analysis, performed using the URANIE software [21], not reported in this paper, showed that for example burst time cannot be estimated more precisely than $\pm 10-15$ seconds. Improvement in the determination of the boundary conditions of such experiments is strongly required.

For future work, it would be interesting to integrate a fuel fragmentation/relocation model in ALCYONE in order to be able to perform the simulation until the end of the experiment. Cladding oxidation during the experiment has also to be represented.

REFERENCES

- [1] MARELLE, V., et al., “Thermo mechanical modeling of PWR fuel with ALCYONE”. in proceedings of Top Fuel 2011, Chengdu, China, (2011).
- [2] MARELLE, V., et al., “New developments in ALCYONE 2.0 fuel performance code.” in proceedings of Top Fuel Boise Idaho USA, (2016).
- [3] STRUZIK, C., et al., “Validation of fuel performance CEA code ALCYONE, scheme 1D, on extensive data base.” in proceedings of Top Fuel 2012, Manchester, United Kingdom of Great Britain and Northern Ireland, (2012).
- [4] SERCOMBE, J., et al., Power ramped cladding stresses and strains in 3D simulations with burnup-dependent pellet-clad friction, Nuclear Engineering and Design **242** (2012) 164.

- [5] MICHEL, B., et al., 3D fuel cracking modelling in pellet cladding mechanical interaction, *Engineering Fracture Mechanics* **75** (2008) 3581.
- [6] MARELLE, V., Validation of PLEIADES/ALCYONE 2.0 fuel performance code. WRFPM2017, Jeju Island Korea, (2017).
- [7] JOMARD, G., et al., “CARACAS: an industrial model for the description of fission gas Behaviour in LWR-UO₂ fuel.” in Proceedings WRFPM 2014, Sendai (Japan), (2014).
- [8] NOIROT, L., et al., MARGARET: A comprehensive code for the description of fission gas behaviour, *Nuclear Engineering and design* **241** (2011).
- [9] FORGERON, T., et al., “Experiment and modeling of advanced fuel rod cladding Behaviour under LOCA conditions: Alpha-beta phase transformation kinetics and EDGAR methodology”. *Zirconium in the Nuclear Industry: Twelfth International Symposium*. ASTM International (2000, January).
- [10] HELFER, T., Extension of monodimensional fuel performance codes to finite strain analysis using a Lagrangian logarithmic strain framework, *Nuclear Engineering and Design* **288** (2015) 75–81
- [11] MIEHE, C., APEL, N., LAMBRECHT, M., Anisotropic additive plasticity in the logarithmic strain space: modular kinematic formulation and implementation based on incremental minimization principles for standard materials, *Computer Methods in Applied Mechanics and Engineering* **191** (2002) 47–48.
- [12] GUENOT-DELAHAIE, I., et al., Simulation of RIA transients on UO₂-M5 fuel rods with ALCYONE V1.4 fuel performance code”. *Nuclear Engineering and Technology* **50** (2018) 268–279.
- [13] GOLDBRONN, P., et al., Avancées de la simulation du comportement du combustible nucléaire en 3D et en transitoire rapide, *Congrès français de mécanique*, Bordeaux, France (2013).
- [14] MOAL, A., et al., *Nucl. Eng. Des.* **280** (2014).
- [15] LE SAUX, M., et al., *J. Nucl. Mat.* **378** (2008) 60.
- [16] SALVO, M., et al., *J. Nucl. Mat.* **456** (2015) 54.
- [17] SALVO, M., et al., *J. Nucl. Mat.* **460** (2015) 184.
- [18] LEMOINE, F., *J. Nucl. Mat.* **248** (1997) 238.
- [19] HIERNAUT, J-P., *J. Nucl. Mat.* **377** (2008) 313.
- [20] LAVOIL, A., HWR 974, LOCA testing experiment at Halden (IFA650.10).
- [21] GAUDIER, F., “URANIE : The CEA/DEN Uncertainty and Sensitivity Platform”. *Procedia Social and Behavioural Sciences* **2** (2010) 7660–7661.
- [22] SERCOMBE, J., MASSON, R., HELFER, T., Stress concentration during pellet cladding interaction: Comparison of closed-form solutions with 2D (r, θ) finite element simulations, *Nuclear Engineering and Design* **260** (2013) 175-187.

QUALIFICATION OF TRANSURANUS MODELS FOR MIXED CORE FUEL BASED ON THE FUMAC OUTCOME

M. IEREMENKO, I. OVDIHENKO

State Scientific and Technical Centre for Nuclear and Radiation Safety,
Kyiv, Ukraine

Abstract

This paper presents the results of TRANSURANUS [1–2] code testing for modelling the Behaviour of WWER nuclear fuel in LOCA accident conditions. The code was tested using data of the IAEA Coordinated Research Project Fuel Modelling in Accident Conditions (FUMAC, [4]). Fuel pins of Westinghouse and TVEL design are currently relevant for Ukrainian NPPs. Fuel from both vendors is presented in the FUMAC project. A part of the experimental data (MTA-EK data, IFA 650.10, IFA 650.11 and Studsvik 192&198) was simulated at SSTC NRS. Some of these data sets and KIT QUENCH-L1 set were calculated by other teams using the TRANSURANUS code (INRNE, Bulgaria; JRC, Germany). TRANSURANUS code demonstrated good capabilities for predicting the Behaviour of nuclear fuel rod cladding. The predicted cladding geometry and time of burst for both general types of cladding (Westinghouse and TVEL) show good correlations with the experimental data for such regimes. In addition, experimental data of the FUMAC project contained the results of post irradiation measurements after operation in a commercial reactor. These data were used to test TRANSURANUS code capabilities for modelling the fuel rod Behaviour in the core under burnup.

1. INTRODUCTION

The diversification of nuclear fuel is currently ongoing at Ukrainian operating NPPs in accordance with the European Energy Security Strategy. Nuclear power supplies almost half of Ukraine's electricity. Therefore, the diversification of fuel supplies is a strategic area for ensuring the uninterrupted operation of nuclear facilities and is one of the main aspects of energy security in Ukraine. As of today (May 2019), six of the 13 WWER-1000 units have Westinghouse FAs (WFAs) in the core (the core of one unit is fully loaded with WFA and 2/4–3/4 of the core is loaded by WFAs at other five units). Moreover, the operator of Ukrainian NPPs plans to extend Westinghouse FA supplies also to Rivne NPP unit 3. The potential use of Westinghouse fuel for the WWER-440 reactor is also under consideration (outcome of the ESSANUF project [3]).

Significant efforts have been made to license alternative fuel designs for WWER NPPs in Ukraine. SSTC NRS as the technical support organization of the Ukrainian regulatory authority takes part in the licensing process for the implementation of new FA types. The TRANSURANUS code is used for independent confirmatory calculations of fuel pin behaviour characteristics. Considering this fact, the adaptation and qualification of TRANSURANUS models to new fuel types are a necessary part of up-to-date calculations, including fuel pin modelling in LOCA. FUMAC project results were used to achieve this goal.

FUMAC — Fuel Modelling in Accident Conditions — IAEA's Coordinated Research Activities (CRP), Code T12028. The main objective of this project is to support the Member States in their efforts to analyze and better understand the Behaviour of water cooled power reactor fuel in LOCA conditions by sharing experimental data and best practices in the application of fuel modelling computer codes. FUMAC covers a wide range of fuel characteristics and vendors. Fuel pins of Westinghouse and TVEL designs are relevant now for Ukrainian NPPs. Fuel from both vendors is included into the FUMAC project.

According to the FUMAC project results, the TRANSURANUS code demonstrated a good capability to predict the behaviour of nuclear fuel rod cladding. The predicted cladding geometry and time of burst for both general cladding types (PWR and WWER) show good correlation with experimental data for such regimes.

SSTC NRS improved the capabilities for modelling nuclear fuel rods in LOCA conditions for both types of cladding: typical WWER cladding and cladding for Westinghouse fuel design.

2. MODELLED CASES

An objective of the FUMAC project is to collect well checked results of accident simulation experiments and distribute them among the participants. The following data were selected for this purpose:

- Ballooning and burst tests performed at MTA EK predecessor including 31 experiments [4], [5–8];
- Halden Reactor test series IFA-650 with fresh PWR rod, IFA-650.1 [9] and IFA-650.2 [10];

- Halden Reactor test series IFA-650 with irradiated PWR and WWER rod, IFA-650.9 [11], IFA-650.10 [12] and IFA-650.11 [13];
- Two out-of-reactor LOCA simulation tests performed by Studsvik Nuclear AB, Sweden, under contract with the U.S. Nuclear Regulatory Commission (U.S. NRC), NRC-192&198, [14–20];
- QUENCH-LOCA-1 test (QUENCH-L1, [21]) with electrically heated bundle (tantalum (Ta) heaters inside each of the 21 rods) performed by KIT in accordance with a temperature/time scenario typical for LOCA.

This data list provided in the FUMAC project is incomplete. This list is formed in terms of the ability to test the TRANSURANUS code. Additionally, the FUMAC project contains experimental data simulating fuel rod melt (CORA-15). However, this is beyond the TRANSURANUS code capabilities and is not covered in this paper.

Table 1 presents common experimental data available in the FUMAC project and suitable for TRANSURANUS code validation. The calculation results obtained by other codes are available (code-to-code comparisons, see Table 2) in addition to the experimental data for TRANSURANUS validation.

TABLE 1. COMMON CHARACTERISTICS OF EXPERIMENTAL SETS

	MTA EK	IFA- 650.1	IFA- 650.2	IFA- 650.9	IFA- 650.10	IFA- 650.11	NRC 192	NRC 198	QUENCH- L1
Cladding	Zry-4	Zry-4	Zry-4	Zry-4 duplex	Zry-4	E110	ZIRLO	ZIRLO	Zry-4
Burnup, MWd/kgU	0	0	0	89.9	61	56	68.2	55	0
Vendor	—	—	—	AREVA	EDF	TVEL	Westing house	Westing house, IFBA rod	—
T, °C	700- 1200	800- 1100	1050	1100	850	935	1185	1185	1100
Clad elongation	Y	Y	Y	Y	Y	Y	Y	Y	Y
Ballooning size	Y	Y	Y	Y	Y	Y	Y	Y	Y
Pressure	Y	Y	Y	Y	Y	Y	Y	Y	Y
Time of burst	Y	N	Y	Y	Y	Y	Y	Y	Y
Position of burst	—	N	Y	Y	Y	Y	Y	Y	Y
Modelling by TRANSURANUS	SSTC, JRC	—	—	—	SSTC, JRC, INRNE	SSTC, JRC, INRNE	SSTC	SSTC	JRC

TABLE 2. AVAILABLE DATA FOR CODE-TO-CODE COMPARISONS

	IFA-650.9	IFA-650.10	IFA-650.11	NRC 192	QUENCH-L1
Integral fission gas release	Y	Y	Y	Y	—
Cladding oxide thickness	Y	Y	Y	Y	Y
Equivalent cladding reacted	Y	Y	Y	Y	Y
Diametral gap	Y	Y	Y	Y	—
Fuel fragmentation volume	Y	Y	N	Y	—
Hydrogen content in cladding	N	N	N	N	Y

The following experiments were selected for modelling by FUMAC participants:

- Six cases of MTA EK (PUZRY-8, 10, 12, 18, 26 and 30);
- IFA-650.9, IFA-650.10 and IFA-650.11;
- NRC-192;
- KIT QUENCH-L1.

Considering the complexity of IFA-650.9 (very high burnup and complicated T/H conditions, an axial relocation model is also required), the participants agreed to use IFA-650.10 as the case for the uncertainty and sensitivity analysis (UASA), see Annex I [4].

All 31 experiments of MTA EK sets and NRC-198 were modeled at SSTC NRS by the TRANSURANUS code [5].

In addition to the FUMAC data obtained with LOCA experimental sets IFA-650.9, .10, and .11, NRC-192 and 198 contain data obtained by fuel rod re-fabrication: rod geometry, cladding oxide thickness, hydrogen content.

3. MODELLING RESULTS

3.1. Separate Effect Tests (MTA-EK Burst tests)

The analyses of MTA-EK series tests using the TRANSURANUS (v1m1j11–SSTC NRS and v1m2j17–JRC) code are presented in this section. The calculation results are compared with the measured data for the following parameters:

- Time to burst failure;
- Pressure of cladding rupture.

SSTC NRS modelled all experimental data sets (31 experiments). JRC team modeled six experiments.

The results in terms of time to burst for the MTA EK cases are reported in Figure 1. The results in terms of cladding inner pressure at the time of burst failure are presented in Figure 2. Experimental data are also included in both figures. Predicted time and pressure of cladding burst show good correlation with the experimental data for such regimes. Additional results of hoop strain at the axial peak position (burst location) on the cladding outer surface at the time of burst failure are available in the FUMAC final report [4] and the participant final reports (Annex II [4]).

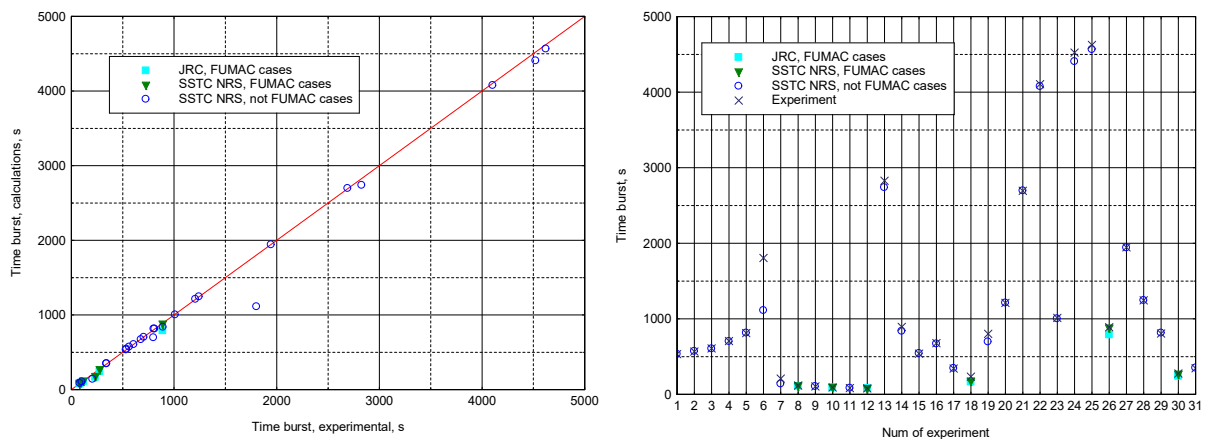


FIG.1. Calculation result. Time to burst failure.

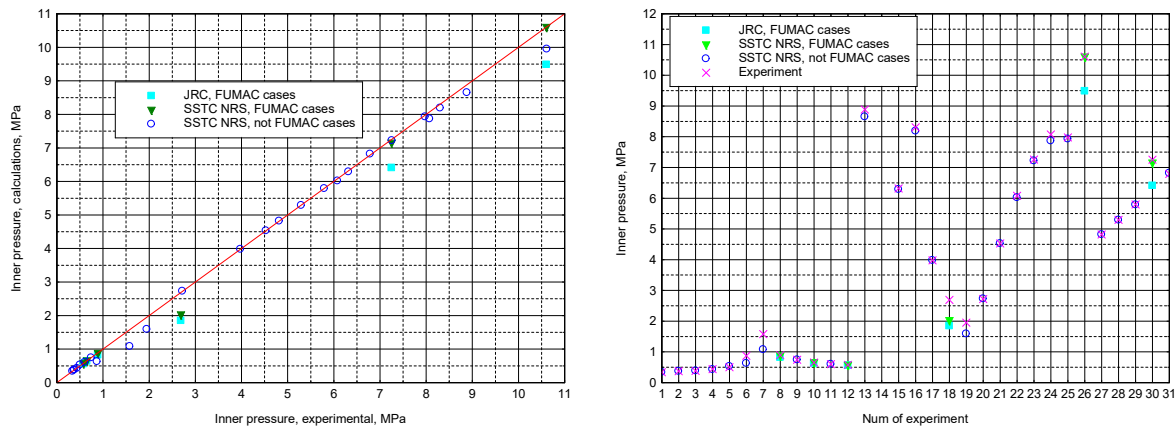


FIG.2. Calculation result. Pressure of cladding burst failure.

3.2. Halden LOCA tests IFA-650.10

The computer analyses of the considered Halden IFA 650.10 tests were carried out in two steps. Pre-irradiation of a full (or father) fuel rod that was later re-fabricated into a test rodlet was modelled in the first step using TRANSURANUS (v1m1j17). The results calculated by TRANSURANUS defining pre-test conditions for the test fuel rodlet were used as input to the second analysis step [5]. Spent fuel storage in a water pool hardly influences the characteristics of cladding and fuel pellets.

The input data for the test rodlet were developed using full (father) rod pre-irradiation history. The following parameters for the father rod are used: linear power, in-cladding pressure, cooling temperature. Using the restart option of the TRANSURANUS code, change of in-cladding gas composition before LOCA experiment was simulated (not for all calculations, a part of tasks was performed with in-cladding gas pressure as boundary conditions [5]).

It should be noted that no computer programme was used to calculate transient thermal hydraulic boundary conditions required for fuel rod analyses with TRANSURANUS. These boundary conditions were derived from measured temperatures or from pre-calculated data distributed by FUMAC participants (calculated by the SOCRAT code).

Figure 3(a) shows the calculated and measured evolution of rod plenum gas pressure during Halden IFA-650.10 test and diameter profiles at the end of the LOCA test. The calculated gas pressure is a little higher than measurements for results of all teams. The calculated diameter profiles are close to measurements. Additional results of the pre-irradiation history and LOCA transient (total fission gas release, clad axial elongation, cladding oxide thickness, equivalent cladding reacted, etc.) are available in the FUMAC final report [4] and the participant final reports (Annex II [4]).

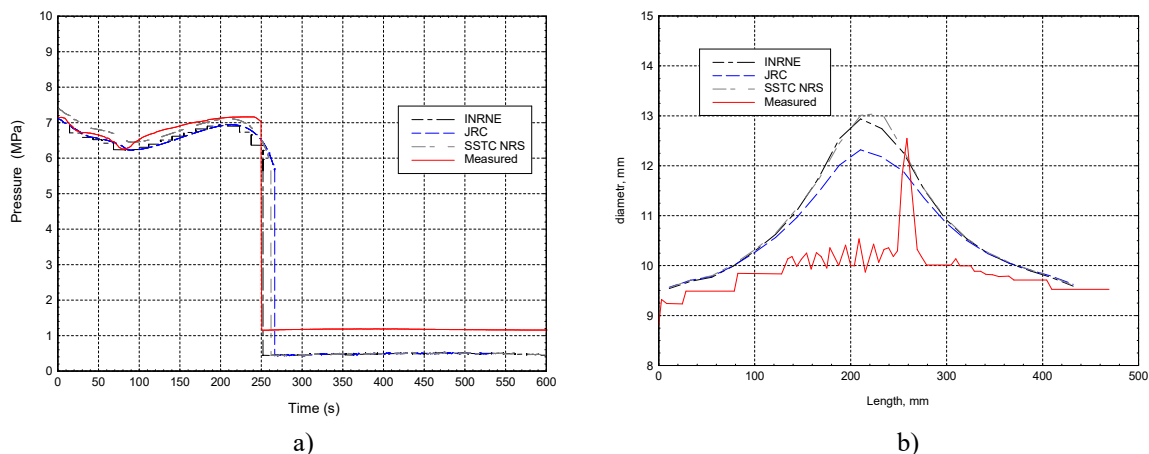


FIG.3. Calculated evolution of rod plenum gas pressure (a) and diameter profiles (b) in comparison with measurements for IFA-650.10 test rodlet.

3.3. Halden LOCA tests IFA-650.11

As for IFA 650.10, the computer analyses of the considered Halden IFA 650.11 tests were carried out in two steps: pre-irradiation of a full (or father) fuel rod and test rodlet simulations at LOCA.

Figure 4(a) shows the calculated and measured evolution of rod plenum gas pressure during Halden IFA-650.11 test and diameter profiles at the end of LOCA test. The calculated gas pressure is a little lower than measurements for results of all teams. The calculated diameter profiles are close to measurements. Additional results of the pre-irradiation history and LOCA transient (total fission gas release, clad axial elongation, cladding oxide thickness, equivalent cladding reacted, etc.) are available in the FUMAC final report [4] and the participant final reports (Annex II [4]).

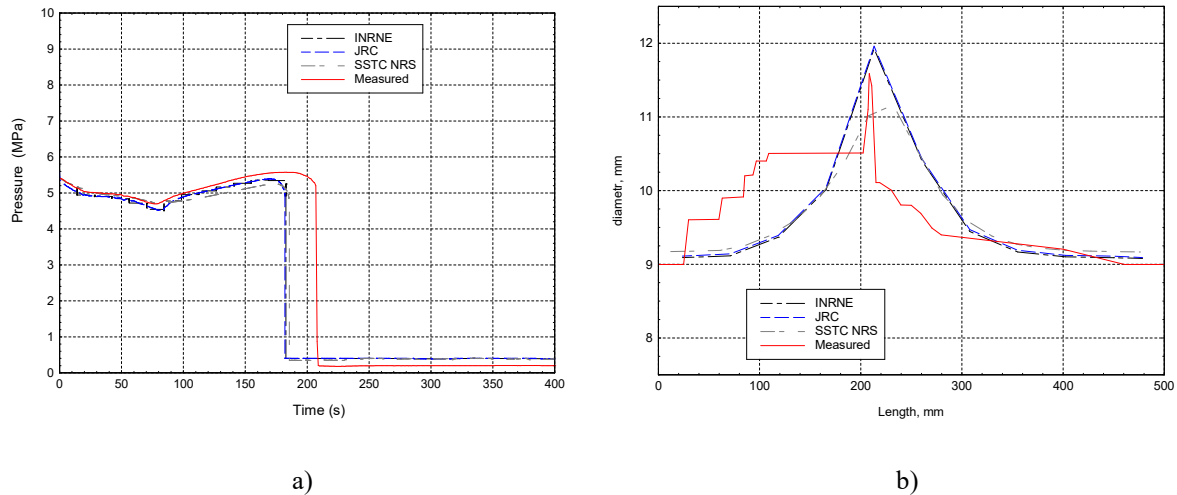


FIG.4. Calculated evolution of rod plenum gas pressure (a) and diameter profiles (b) in comparison with measurements for IFA-650.11 test rodlet.

3.4. Studsvik LOCA test NRC-192

As for IFA 650.10 and 11, the computer analyses of the considered NRC-192 tests were carried out in two steps: pre-irradiation of a full (or father) fuel rod and test rodlet simulations during LOCA. Details and features of pre-irradiation modelling by SSTC NRS are presented in [5].

Figure 5(a) shows the calculated and measured evolution of rod plenum gas pressure during NRC-192 test and diameter profiles at the end of LOCA test. The calculated gas pressure is a little higher than measurements. The calculated diameter profiles are smaller than measurements. Additional results of the pre-irradiation history and LOCA transient (total fission gas release, clad axial elongation, cladding oxide thickness, equivalent cladding reacted, etc.) are available in the FUMAC final report [4] and the participant final reports (Annex II [4]).

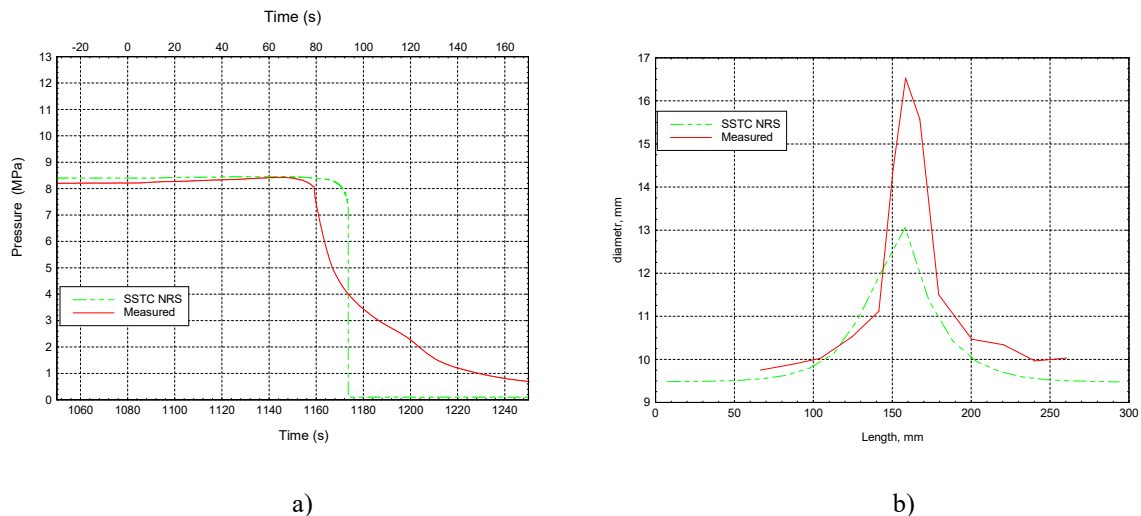


FIG.5. Calculated evolution of rod plenum gas pressure (a) and diameter profiles (b) in comparison with measurements for NRC-192 test rodlet.

3.5. Studsvik LOCA test NRC-198

As for the above cases, the computer analyses of the considered NRC-198 tests were carried out in two steps: pre-irradiation of a full (or father) fuel rod and test rodlet simulations during LOCA. The details and features of pre-irradiation modelling by SSTC NRS are presented in [5].

It should be noted that Westinghouse IFBA fuel rod was used for NRC-Studsvik 198 test. Fuel pellets of this rod were coated by burnable absorber: zirconium diboride ZrB_2 . However, the characteristics of this burnable absorber were not present in 198 test specifications [20]. This burnable absorber in the form of a thin layer works through the (n, α) reaction; e.g. helium is produced and considered in the gas composition of free volume of fuel rod. As a result, the in-cladding pressure depends on the characteristics of the zirconium diboride layer (thickness or mass per fuel length), and so is cladding geometry for test rodlet. Figure 13(b) in [5] shows the influence of ZrB_2 thickness under in-cladding pressure during full rod pre-irradiation history. The thickness of ZrB_2 multiplied or divided by 2 results in the in-cladding pressure change of $\approx 20\%$.

Figure 6(a) shows the calculated and measured evolution of rod plenum gas pressure during NRC-198 test and diameter profiles at the end of LOCA test. The calculated gas pressure is a little higher than measurements. The calculated diameter profiles are close to measurements.

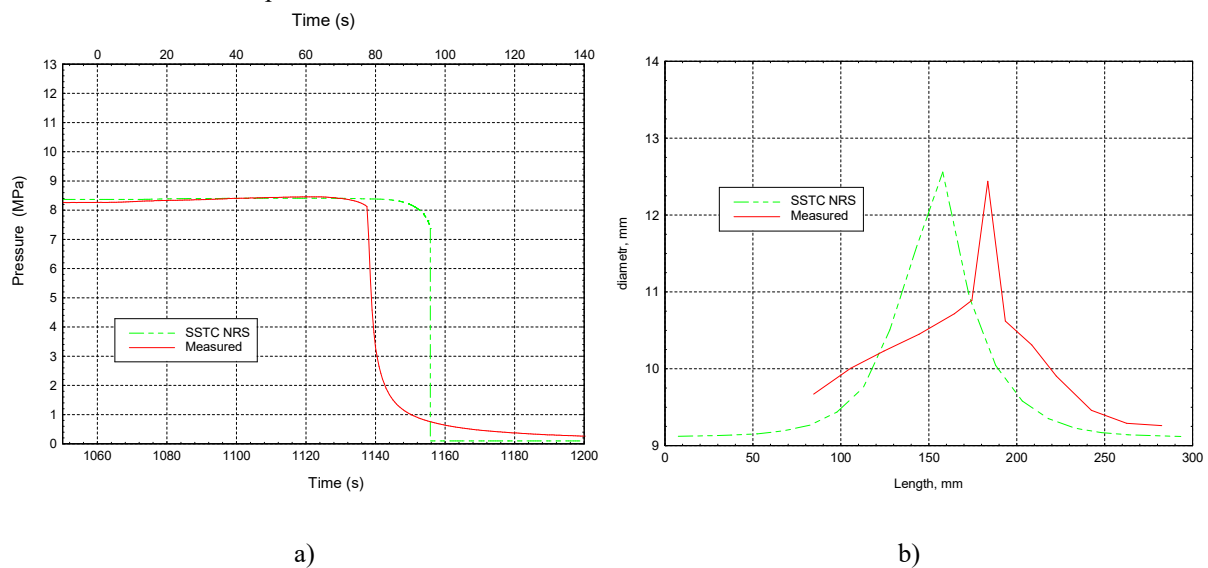


FIG.6. Calculated evolution of rod plenum gas pressure (a) and diameter profiles (b) in comparison with measurements for NRC-198 test rodlet.

3.6. KIT QUENCH-L1 bundle test

Analyses of QUENCH-L1 test using the TRANSURANUS (v1m2j17-JRC) code are presented in this section. The calculation results are compared with measured data for the following parameters:

- Time to burst failure;
- Pressure of cladding rupture.

JRC modelled QUENCH-L1 test.

Figure 7(a) shows the calculated and measured evolution of rod plenum gas pressure during QUENCH-L1 test and diameter profiles at the end of LOCA test. The calculated gas pressure is a little higher than measurements. The calculated diameter profiles are close to measurements. Additional results of LOCA transient (cladding hoop stress, cladding oxide thickness, equivalent cladding reacted, hydrogen content in cladding etc.) are available in the FUMAC final report [4].

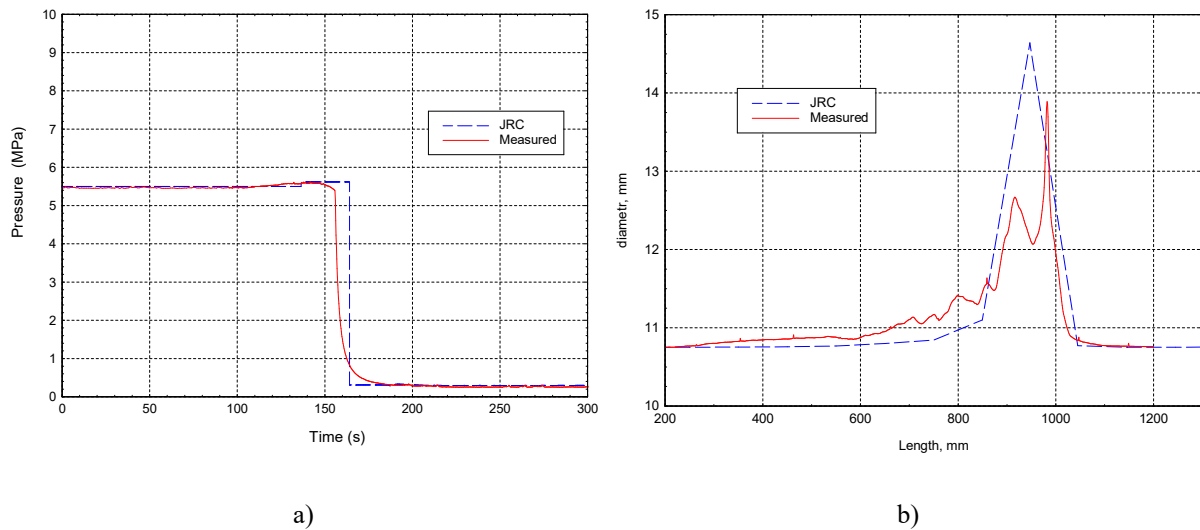


FIG.7. Calculated evolution of rod plenum gas pressure (a) and diameter profiles (b) in comparison with measurements for QUENCH-L1 test rodlet.

3.7. Common remarks on results

Table 3 presents the predicted failure time differences among the participants with the TRANSURANUS code (JRC, INRNE and SSTC NRS). TRANSURANUS-predicted time of cladding burst for both general types of cladding (PWR and WWER) shows good correlations with the experimental data for such regimes.

Table 4 presents differences in the cladding outer diameter after the test among the participants with the TRANSURANUS code. TRANSURANUS results show good correlation with the experimental data for such regimes.

The addition data of comparing TRANSURANUS results with the experimental data and code-to-code comparisons are available in the FUMAC final report [4] and the participant final reports (Annex II [4]).

TABLE 3. BURST TIME. DIFFERENCES WITH MEASURED VALUE

	MTA EK 6 cases	IFA-650.10	IFA-650.11	NRC 192	NRC 198	QUENCH- L1
JRC	<13% (27% for PUZRY-18)	6%	—	—	—	6%
INRNE	—	1%	12%	—	—	—
SSTC	<3% (19% for PUZRY-18)	4%	11%	21%	23%	—

TABLE 4. CLADDING OUTER DIAMETER AFTER TESTS (FOR MTA EK - BURST PRESSURE). DIFFERENCES WITH MEASURED VALUE

	MTA EK (burst pressure) 6 cases	IFA-650.10	IFA-650.11	NRC 192	NRC 198	QUENCH- L1
JRC	<11% (31% for PUZRY-18)	4%	—	—	—	5%
INRNE	—	4%	3%	—	—	—
SSTC	<2% (24% for PUZRY-18)	4%	4%	22%	1%	—

FUMAC results show some features in modelling fuel rod Behaviour in LOCA by the TRANSURANUS code:

- Due to some differences in the fuel rod plenum design, test rodlet and fuel rod for commercial nuclear reactors, the temperature of plenum gas in the TRANSURANUS model is described as boundary conditions from measurement data or from calculations by other code. Considering this aspect, inn-cladding gas pressure predicted by TRANSURANUS can be compared with the measured value with some limitations;
- TRANSURANUS model for prediction of fuel for plenum temperature in LOCA mode should be additionally tested in view of fuel rod design for commercial nuclear reactors;
- Boundary conditions should be predicted by thermal hydraulic codes for modelling of nuclear fuel rods in LOCA by TRANSURANUS code;
- TRANSURANUS model for Westinghouse IFBA fuel rod was not fully tested due to insufficient data in FUMAC set.

4. CONCLUSION

TRANSURANUS code demonstrated good capability to predict the Behaviour of nuclear fuel rod cladding. The predicted cladding geometry and time of burst for both general types of cladding (PWR and WWER) show good correlation with the experimental data for such regimes.

SSTC NRS improved the capability for modelling the nuclear fuel rod in LOCA for both types of cladding: typical WWER cladding and cladding for Westinghouse fuel design. The experience and the TRANSURANUS models obtained during the FUMAC project will be used to perform calculations in the framework of licensing mixed cores.

The FUMAC project contains experimental data and calculation results obtained by other participants of the project to continue testing of the TRANSURANUS code.

REFERENCES

- [1] TRANSURANUS HANDBOOK. Document Number Version 1 Modification 1 Year 2017 ('V1M1J17'). European Commission. Joint Research Centre. Directorate G - Nuclear Safety & Security. PO Box 2340. D-76125 Karlsruhe, (January 2017).
- [2] LASSMANN, K., TRANSURANUS: A Fuel Rod Analysis Code Ready for Use, J. Nucl. Mater. **188** (1992) 295.
- [3] ESSANUF Project.
<http://www.essanuf.eu/>
- [4] INTERNATIONAL ATOMIC ENERGY AGENCY, Fuel Modelling in Accident Conditions (FUMAC). Final Report of a Coordinated Research Project CRP T12028 (2014–2018), IAEA – TECDOC -1889, Vienna, (2019).
- [5] IEREMENKO, M., Testing of the TRANSURANUS Computer Code by Joint Solution of Test Problems within FUMAC Project. Annex II to [4] (draft, now preparing to publish)
- [6] HÓZER, Z., GYUÓRI, C., HORVÁTH, M., NAGY, I., MARÓTI, L., MATUS, L., WINDBERG, P., FRECSKA, J., Ballooning Experiments with VVER Cladding, Nuclear Technology **152** 3 (2005) 273–285.
- [7] PEREZ-FERÓ, E., GYÓRI, C., MATUS, L., VASÁROS, L., HÓZER, Z., WINDBERG, P., MARÓTI, L., HORVÁTH, M., NAGY, I., PINTÉR-CSORDÁS, A., NOVOTNY, T., Experimental Database of E110 Claddings Exposed to Accident Conditions, Journal of Nuclear Materials **397** 1–3 (2010) 48–54.
- [8] PEREZ-FERÓ, E., HÓZER, Z., Experimental Database of E110 Claddings under Accident Conditions. EK-FRL-2011-744-01/04 Budapest, (April 2012).
- [9] LESTINEN, V., LOCA Testing at Halden, First Experiment IFA-650.1. Technical Report HWR-762, OECD Halden Reactor Project, (2004).
- [10] EK, M., LOCA Testing at Halden, the Second Experiment IFA-650.2. Technical Report HWR-813, OECD Halden Reactor Project, (2005).
- [11] DU CHOMONT, F.B., LOCA Testing at Halden, the Ninth Experiment IFA-650.9. Technical Report HWR-917, OECD Halden Reactor Project, (2009).
- [12] LAVOIL, A., LOCA Testing at Halden, the Tenth Experiment IFA-650.10. HWR-974. OECD HALDEN REACTOR PROJECT. (December 2010).
- [13] LAVOIL, A., LOCA Testing at Halden, the VVER Fuel Experiment IFA-650.11. HWR-976. OECD HALDEN REACTOR PROJECT (December 2010).
- [14] JERNKVIST, L.O., Computational Assessment of LOCA Simulation Tests on High Burnup Fuel Rods in Halden and Studsvik. Technical Report. March (2017).

- [15] HELIN, M., FLYGARE, J., NRC LOCA tests at Studsvik: Design and Construction of Test Train Device and Tests with Unirradiated Cladding Material, Report STUDSVIK/N-11/130, Studsvik Nuclear AB, Studsvik, Sweden (2012).
- [16] Studsvik LOCA test machine data sheet.xlsx. FUMAC website shared documents.
<https://nucleus.iaea.org/sites/nefw-projects/fumaccrp/Shared%20Documents>
- [17] FLANAGAN, M., “NUREG-2160: Post test Examination Results from Integral, High-Burnup, Fueled LOCA Tests at Studsvik Nuclear Laboratory,” U.S. Nuclear Regulatory Commission, (August 2013).
- [18] FLANAGAN, M., ASKELJUNG, P., Observations of Fuel Fragmentation, Mobility and Release in Integral, High-Burnup, Fueled LOCA Tests. Halden Workshop on LOCA. Lyon, France (29–30 May 2012).
- [19] NRC-Studsvik LOCA test 192 data sheet. FUMAC’s website shared documents.
<https://nucleus.iaea.org/sites/nefw-projects/fumaccrp/Shared%20Documents>
- [20] NRC-Studsvik LOCA test 198 data sheet. FUMAC’s website shared documents
<https://nucleus.iaea.org/sites/nefw-projects/fumaccrp/Shared%20Documents>
- [21] STUCKERT, J., GROBE, M., RÖSSGER, C., STEINBRÜCK, M., WALTER, M., Results of the LOCA Reference Bundle Test QUENCH-L1 with Zircaloy-4 Claddings. KIT-SR 7651, Karlsruher Institut für Technologie (2018).

MAIN RESULTS OF FUMAC FROM CNPRI AND SENSITIVITY AND UNCERTAINTY STUDY OF PERFORMANCE OF ATF UNDER TRANSIENT CONDITION

Y.R. XIE, Q.S. REN, Y.D. ZHANG
China Nuclear Power Technology Research Institute,
Shenzhen, China

Abstract

The safe, reliable and economic operation of nuclear power reactor fleet has always been a top priority for worldwide nuclear industry. Typically, fuel rod Behaviour in accident conditions is one of the main concerns. After the severe Fukushima accidents, enhancing the accident tolerance of light water reactor (LWRs) became a hot issue in the world. Particularly, the fuel materials are expected to improve accident tolerance. Fuel performance is influenced by design parameters, physical properties and thermal hydraulic condition. In this report, the main result on FUMAC which is in order to better understand fuel rod Behaviour under LOCA condition and assess the predictive ability of the code, was present. Furthermore, take case IFA-650.10 for example, sensitivity and uncertainty study is performed to evaluate the ATF fuel system's (UO₂-BeO + ODS FeCrAl) performance under LOCA condition, and find out an optimal design by using the statistical tool DAKOTA coupling with fuel performance analysis code.

1. INTRODUCTION

Fuel rod represents the primary and the essential safety barrier for nuclear safety. Safety criterion for accident condition is of vital importance. Several LOCA experiments have been performed at Halden reactor to reexamine the current criterion. According to the FUMAC work programme CNPRI was to perform simulations of IFA-650 Halden experiments with FRAPCON/FRAPTRAN to better understand fuel rod Behaviour under LOCA condition and assess the predictive ability of the code. Main results of FUMAC are presented in this report.

After the sever Fukushima accidents in 2011, the concept of accident tolerant fuel (ATF) has been put forward with the intention of improving the fuel performance under transient condition while maintaining or improving the fuel performance during normal operation. Fuel performance is influenced by design parameters, physical models and thermal hydraulic condition. Different factors have different impacts. Sensitivity and uncertainty study can offer an efficient approach to evaluate the impacts of different factors and sort out the important ones. Fuel Behaviour under transient condition is of vital important for the fuel assessment. In this research, sensitivity and uncertainty study is applied to find out the important factors for typical ATF fuel system's (UO₂-BeO pellet+ ODS FeCrAl cladding) failure time under LOCA condition and obtain an optimal design.

2. MAIN RESULTS OF FUMAC

Simulations of IFA-650.9/10/11 were performed in FUMAC work programme. The test rods used in IFA-650.9/10/11 Halden experiments were segments cut from the standard PWR or WWER fuel rod of different burnup. Main characteristics of the test rods are show in Table 1.

TABLE 1. MAIN CHARACTERISTICS OF THE TEST RODS [1–3]

	IFA-650.9	IFA-650.10	IFA-650.11
Reactor type	PWR	PWR	WWER
Burnup, MWd/kgU	89.9	61	56
Stack length, mm	480	440	480
Enrichment, wt%U235	3.5	4.49	3.6
Fuel density, % of T.D.	95	95.32	97
Fuel diameter, mm	9.13	8.21	7.55
Fuel length, mm	8	10	10
Cladding type	DX Zr2.5Nb (duplex) Zry-4 (base)	Zry-4	E110
Cladding outer diameter, mm	10.75	9.5	9.13
Cladding inner diameter, mm	9.3	8.36	7.77
Plenum volume, cm ³	19	16–17	16–17
Gas pressure (RT), bar	40	40	30

Table 2 and Figs 1–3 illustrate the overall comparison of calculated results and corresponding measured values in 3 cases. It implies that variation of cladding temperature, cladding outer diameter, rod internal pressure as well as cladding failure are generally well predicted. The predicted maximum rod pressure and its corresponding cladding hoop stress as well as cladding failure temperature are close to the measured value. Failure time predicted by FRAPTRAN is close to the value that it was actually measured in case 650.10 and 650.11. Due to its very high burnup, significant fuel relocation and the complicated thermal hydraulic boundary condition, the 650.9 case is rather complex. Consequently, deviations between the predicted and measured results are relatively large in case 650.9.

TABLE 2. OVERALL COMPARISON OF FRAPTRAN CALCULATED RESULTS AND CORRESPONDING MEASURED VALUES

	650.9		650.10		650.11	
	MEAS.	CAL.	MEAS.	CAL.	MEAS.	CAL.
Cladding deformation start time, s	106	78	228	211	183	212
Cladding failure time, s	133	87	249	233	207	217
Maximum rod pressure, MPa	7.73	7.08	7.16	7.00	5.57	5.36
Maximum rod pressure corresponding hoop stress, MPa	47.2	47.1	49	48.6	29.5	29.0
Cladding failure temperature, K	1083	1066.7	1028	944.7	1112	1075.4

The sudden decrease of rod pressure indicates the failure of fuel rod. For the IFA tests, the total free volume of gas was practically all located in the plenum, outside the heated region [4]. FRAPTRAN can model an external plenum, and the external plenum gas temperature data is imposed as initial condition. However, the predicted plenum gas temperature is higher than the measured values. It's because that in FRAPTRAN, there is 2 options for defining the plenum gas temperature: assume the gas temperature to be 10°F higher than the axial local coolant temperature; a more detailed model to concern the interactions between the plenum gas and the top pellet surface, hold down spring, and cladding wall [5]. In these temperature calculation processes, the input plenum gas temperature hasn't been used. The input plenum gas temperature history is only used for defining the sum of

volume over temperature terms in gas gap pressure equation. Difference in plenum gas temperature might cause the deviation of other parameters.

The predicted cladding outside temperature shows similar trend with the measured values. The little difference can be accounted by the difference in nodalization and the simplification of the models. Besides, using the thermal properties of light water to replace those of heavy water might have some effect on the results.

The predicted axial variation of cladding outer diameter shows similar trend with the measured one. Deviation of the ballooning node may be accounted by the difference in nodalization of boundary conditions. In case 650.9, measured results indicate that cladding ballooning occurred on 2 portions of the rod while the predicted result show that cladding ballooning occurred only at the upper part of the rod. This difference is due to the calculation method of FRAPTRAN. Once the ballooning has been predicted in one node, no further strain calculations would be performed for any nodes, the further calculation focuses only on the ballooning node [5]. Thus, it could only predict the primary ballooning.

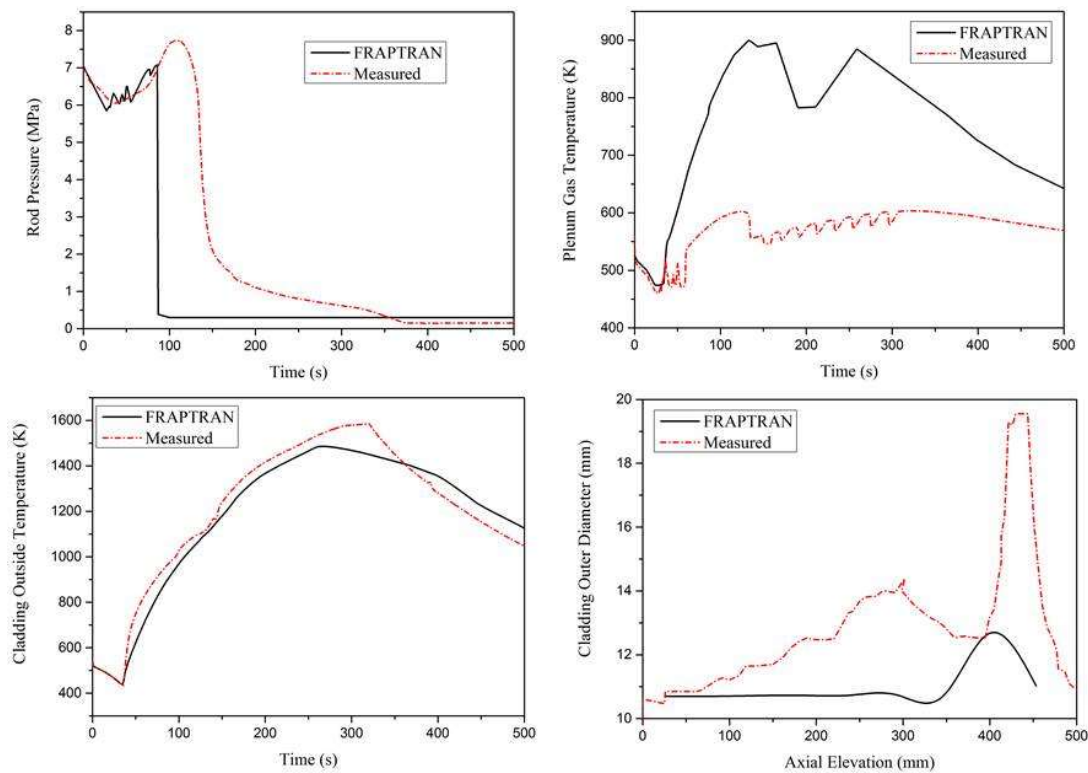


FIG. 1. Variation of rod pressure, plenum gas temperature, cladding outside temperature, cladding outer diameter of case 650.9.

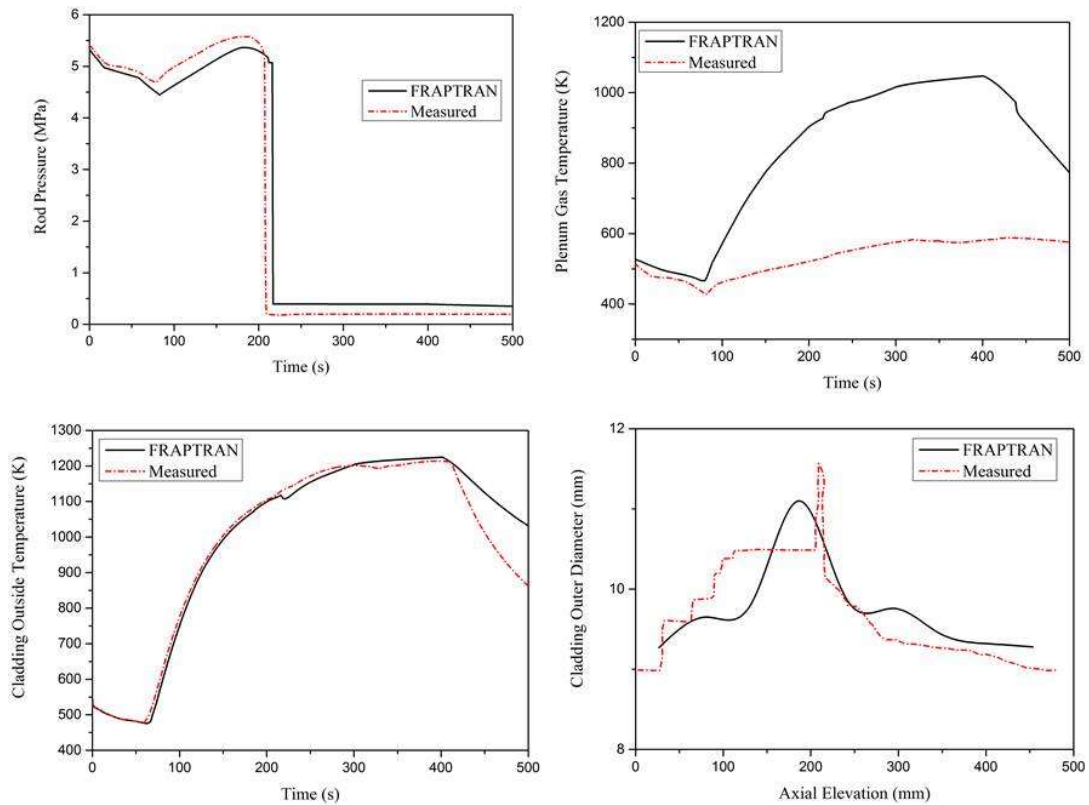


FIG. 2. Variation of rod pressure, plenum gas temperature, cladding outside temperature, cladding outer diameter of case 650.10.

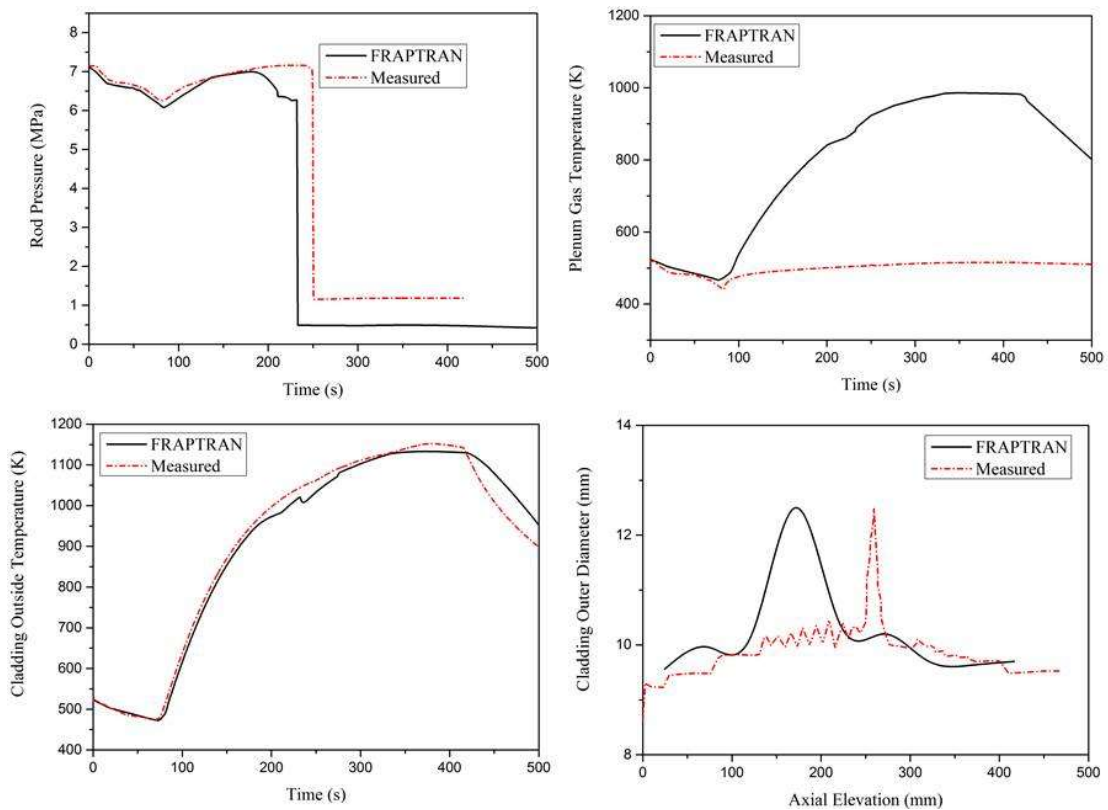


FIG. 3. Variation of rod pressure, plenum gas temperature, cladding outside temperature, cladding outer diameter of case 650.11.

3. SENSITIVITY AND UNCERTAINTY STUDY OF ATF WITH IFA-650.10

3.1. Choice of input and output of uncertainty study

The uncertain parameters of uncertainty study are the variables with uncertainty, giving the upper bound, lower bound as well as the distribution. The uncertain parameters can usually be quantified by the probability distribution function (PDF), which often depends on the engineering experience or experimental results. Moreover, we can use the correlation coefficient to represent how closely the two variables co-vary.

The ATF fuel system (ODS FeCrAl+UO₂-BeO) studied in this report is planning to be applied in the present commercial pressure water reactor, thus, the parameters of fuel rod configuration and thermal hydraulic condition of reactor are not considered in this report. As shown in Table 3, 17 uncertain variables are chosen, including 5 design parameters and 12 physical property models.

As for the distribution of uncertain variables, we consider the uncertainty of physical property models is normal distribution, and the bounds are $\pm 3\sigma$. Otherwise, the uncertainty of design parameters is uniform distribution.

The uncertainty module in FRAPCON and FRAPTRAN are used for the physical property models analysis.

TABLE 3. INFORMATION OF UNCERTAIN VARIABLES

No.	Variable	Value	Lower Bound	Upper Bound	Distribution
1	Pellet diameter	0.00821	0.0078	0.008333	Uniform
2	Cladding thickness	0.00057	0.000542	0.000579	Uniform
3	Plenum length	0.3006	0.28557	0.31563	Uniform
4	Pellet density	95.32	94.32	96.32	Uniform
5	Enrichment	4.49%	3.50%	5.50%	Uniform
6	Fuel thermal conductivity	0	(Relative) 8.8%	$\pm 3\sigma$	Normal
7	Fuel thermal expansion	0	(Relative) 10.3%	$\pm 3\sigma$	Normal
8	Fuel swelling	0	(Absolute) 0.08%	$\pm 3\sigma$	Normal
9	Cladding creep	0	(Relative) 14.5%	$\pm 3\sigma$	Normal
10	Cladding corrosion	0	(Absolute) 5 μ m	$\pm 3\sigma$	Normal
11	Cladding hydrogen pickup	0	(Absolute) 23 ppm	$\pm 3\sigma$	Normal
12	Fuel thermal conductivity (Transient)	1	1.50%	$\pm 3\sigma$	Normal
13	Fuel thermal expansion (Transient)	1	1.50%	$\pm 3\sigma$	Normal
14	Fuel specific heat (Transient)	1	1.50%	$\pm 3\sigma$	Normal
15	Cladding thermal conductivity (Transient)	1	1.50%	$\pm 3\sigma$	Normal
16	Cladding thermal expansion (Transient)	1	1.50%	$\pm 3\sigma$	Normal
17	Cladding surface heat transfer coefficient (Transient)	1	1.50%	$\pm 3\sigma$	Normal

During LOCA accident, the evaluation of fuel rod Behaviour mainly focuses on: 1) variation of cladding and fuel temperature; 2) cladding and fuel strain; 3) cladding oxide thickness; 4) fuel rod pressure and cladding ballooning failure time. In this report, the cladding ballooning failure time is used to evaluate the fuel performance under LOCA condition.

The statistical analysis is performed with the software Dakota-6.4.0 which is a free interface with open code developed by the Sandia National Laboratories. Dakota includes methods for global sensitivity and variance analysis, parameter estimation, uncertainty quantification, and verification, as well as meta level strategies for surrogate based optimization, hybrid optimization, and optimization under uncertainty. It can be coupled with engineering analysis software.

Based on the results shown in Section 2, case 650.10 uses the PWR fuel rod segment for test and can be well predicted by FRAPCON/FRAPTRAN. Thus, the following study is performed with case 650.10.

3.2. Results

3.2.1. Reference calculation

Table 4 shows the overall comparison of different fuel systems under LOCA condition (case 650.10). All the inputs are the same except the fuel and cladding material. It suggests that during LOCA, the ATF system reduces the system temperature, pressure and delays the fuel rod failure. We take these results as reference to make a comparison with the latter calculation.

TABLE 4. REFERENCE CALCULATION RESULTS

Fuel type	UO ₂ +Zry-4	ODS FeCrAl+UO ₂ -BeO
Cladding deformation start time, s	211	280
Cladding failure time, s	233	302
Maximum rod pressure, MPa	7.00	3.78
Maximum fuel temperature, K	1013.21	1002.59
Maximum cladding temperature, K	861.00	856.73

3.2.2. Monte Carlo sampling and correlation coefficient

By applying the Wilks based sample size criterion, the number of samples in Monte Carlo random sampling calculation is set to 93. The definition of mean, standard deviation, skewness and kurtosis of n samples are as follows:

$$\bar{X} = E(X) = \frac{1}{n} \sum_i^n X_i, \quad (1)$$

$$\sigma = \sqrt{E[(X - \bar{X})^2]} = \sqrt{\frac{1}{n} (\sum_i^n X_i^2 - n\bar{X}^2)} \quad (2)$$

$$skew = E \left[\left(\frac{X - \bar{X}}{\sigma} \right)^3 \right] = \frac{1}{n} \sum_i^n \left(\frac{X_i - \bar{X}}{\sigma} \right)^3 \quad (3)$$

$$kurt = \frac{E[(X - \bar{X})^4]}{E[(X - \bar{X})^2]^2} = \frac{1}{n} \sum_i^n \left(\frac{X_i - \bar{X}}{\sigma} \right)^4 \quad (4)$$

The results of 93 samples are shown in Table 5. Fig. 4 shows the Pearson correlation coefficient and Spearman correlation coefficient of the 17 uncertain variables. According to the results, cladding failure time is greatly influenced by pellet diameter, cladding thickness, plenum length as well as fuel specific heat. However, material properties such as cladding corrosion, cladding hydrogen pickup, fuel thermal conductivity as well as cladding thermal conductivity shows relative slight effect on cladding failure time. Under LOCA condition, fuel rods fail due to large cladding hoop strain which is resulted from the high rod pressure caused by the high temperature. Increase properly the thickness of cladding and pellet diameter can enhance the cladding mechanical resistance and reduce the thermal gradient in fuel rod. Furthermore, high fuel specific heat can slow down the fuel temperature increase so that reduce the fuel system temperature.

TABLE 5. RESULTS OF 93 SAMPLES

	Mean	Standard Deviation	Skewness	Kurtosis
Max fuel temperature, K	1007.00	-12.17	-18.63	-16.92
Max cladding temperature, K	857.11	-17.30	-17.39	-17.74
Max plenum pressure, MPa	4.22	0.51	0.01	0.01
Failure time, s	293.34	9.46	-1.11	0.15

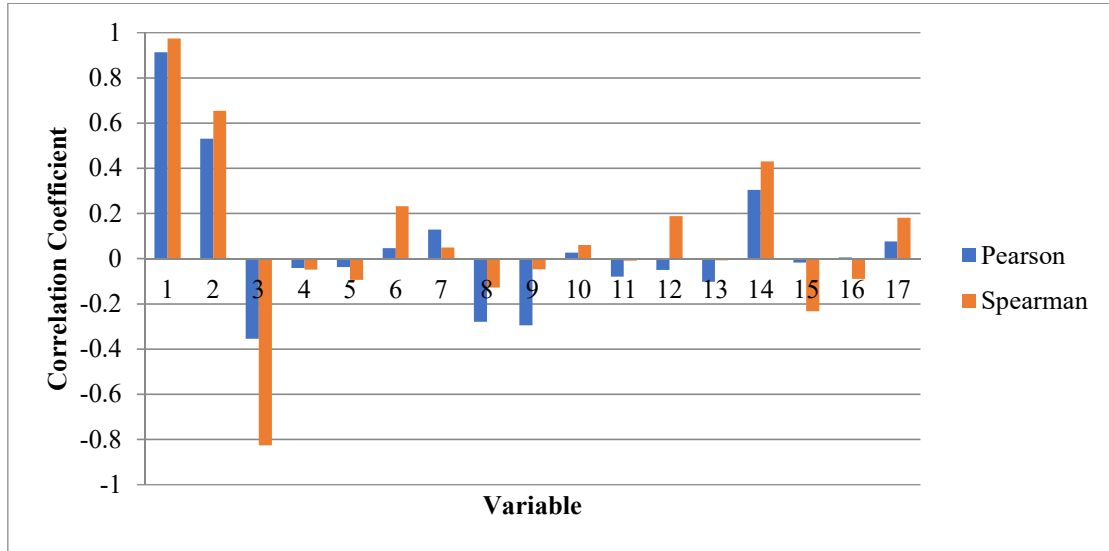


FIG. 4. Pearson & Spearman correlation coefficient.

3.2.3. Screening of low impact factor with Morris method

Morris one-at-a-time sensitivity study (elementary effects (EE) method) is a simple but effective way of screening the important factors among the many that can be contained in a model. It proposes two sensitivity measures: the overall influence assessed by the mean and the interaction effect with other factor estimated by standard deviation [6].

By using Morris method with 108 samples, two sensitivity factors were obtained. The distribution of failure time covers a large range as shown in Fig. 5. The average failure time is 286 s. It suggests that fuel performance under LOCA condition is sensitive to the uncertainty of parameters.

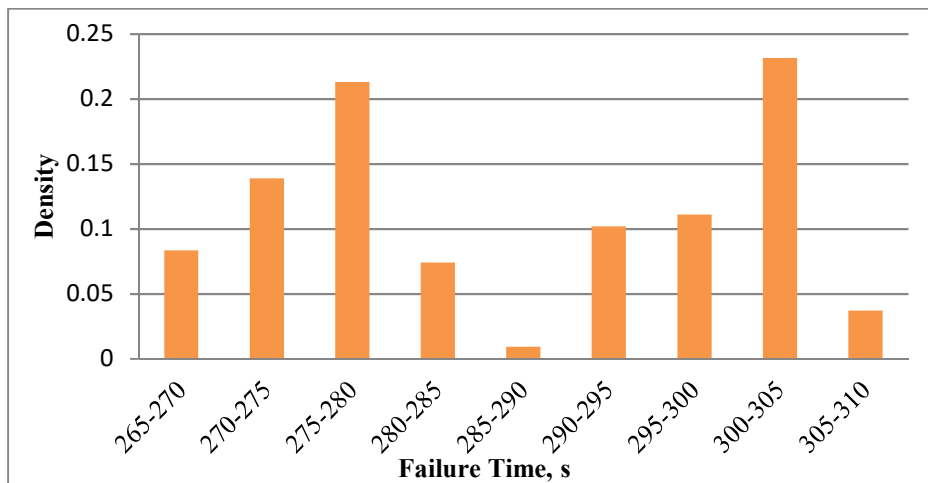


FIG. 5. Failure time distribution.

Figure 6 presents the overall influence (mean) and the interaction effect (standard deviation) calculated by Morris method. In Fig. 6, Variable locates at the top right corner is the high impact factor while variable locates at the low left corner is the low impact factor. For better illustrate, Table 6 shows the data calculated in order of the overall influence, from high to low. The results show that pellet diameter has strong impact on the cladding failure time. Cladding thickness, plenum length, fuel density, enrichment, fuel thermal conductivity (steady + transient), fuel thermal expansion, cladding corrosion, fuel specific heat, cladding surface heat transfer coefficient (transient) are the factors that have some influence. The other 6 factors are the factor of low interest and will not be considered in the following study.

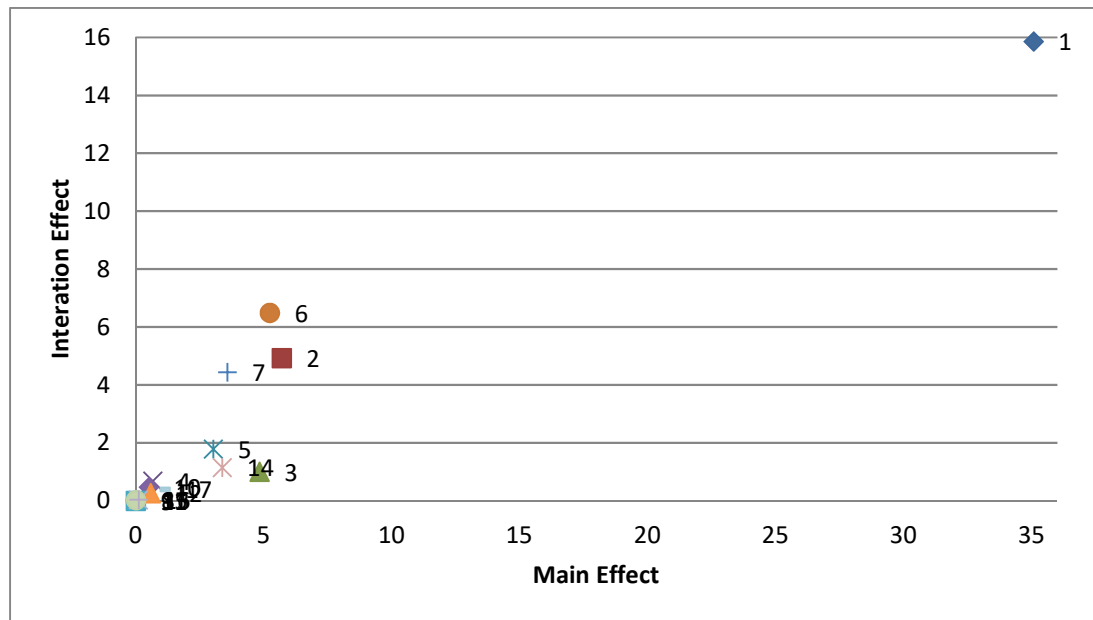


FIG. 6. Overall influence (mean) and interaction effect (standard deviation) calculated by Morris method.

TABLE 6. OVERALL INFLUENCE (MEAN) AND THE INTERACTION EFFECT (STANDARD DEVIATION) CALCULATED BY MORRIS METHOD (IN ORDER OF THE OVERALL INFLUENCE)

No.	Variable	Mean	Standard Deviation
1	Pellet diameter	35.065	15.865
2	Cladding thickness	5.6975	4.9284
6	Fuel thermal conductivity	5.24	6.483
3	Plenum length	4.8425	0.99848
7	Fuel thermal expansion	3.575	4.4381
14	Fuel specific heat (Transient)	3.3825	1.1467
5	Enrichment	3.0325	1.7916
17	Cladding surface heat transfer coefficient (Transient)	0.965	0.39965
4	Pellet density	0.6625	0.68288
12	Fuel thermal conductivity (Transient)	0.5875	0.26705
10	Cladding corrosion	0.52	0.46945
16	Cladding thermal expansion (Transient)	0.1125	0.036435
13	Fuel thermal expansion (Transient)	0.105	0.031464
8	Fuel swelling	0.035	0.029496
15	Cladding thermal conductivity (Transient)	0.015	0.018974
9	Cladding creep	0	0
11	Cladding hydrogen pickup	0	0

3.2.4. Sobol' indices based on PCE method and quantitative analysis of uncertainty

Variance based decomposition is a global sensitivity method that summarizes how the uncertainty in model output can be apportioned to uncertainty in individual input variables [7]. The Sobol' indices are the variance-based sensitivity indices, including the main effect sensitivity index S_i and the total effect index T_i . The main effect sensitivity index corresponds to the fraction of the uncertainty in the output that can be attributed to input x_i alone [7]. The total effects index corresponds to the fraction of the uncertainty in the output that can be attributed to input x_i and its interactions with other variables [7].

Traditional calculation method of Sobol' indices is time consuming. For the case of $N=100$ samples and $k=10$ input, it needs $N \times (k+2)$ times of calculation. Usually, in order to reduce the computational expense, some alternative methods would be applied, for example, the emulator, high dimensional model representations (HDMR.), Fourier Amplitude Sensitivity Test (FAST). Here, the polynomial chaos expansion (PCE), which is an emulator, was applied. It captures the functional relationship between a set of output response metrics and a set of input random variables [7]. With the functional relationship established by PCE, we can perform a large-sample-size sensitivity analysis in much less time and with high reliability.

Efficient Global Optimization (EGO), which is a global reliability method, was developed to search for multiple points on or near the limit state throughout the random variable space [7]. It can evaluate the bounds of the response functions' distribution. This method is based on the iteration of the Gaussian process model.

With the PCE method based on 100 samples, 10000 calculations were performed and obtained the Sobol' indices as shown in Table 7. Same as the above analysis, it demonstrates that pellet diameter is the most influential factor for fuel rod failure during LOCA event. The others show similar effect.

TABLE 7. SOBOL' INDICE CALCULATED BY THE PCE METHOD

No.	Variable	Main Effect	Total Effect
1	Pellet diameter	0.822327328	0.853180919
2	Cladding thickness	0.016790807	0.036137951
3	Plenum length	0.030328453	0.049212338
4	Pellet density	0.000519525	0.017796019
5	Enrichment	0.004103068	0.018385835
6	Fuel thermal conductivity	0.005870458	0.045248346
7	Fuel thermal expansion	0.001270478	0.024899446
8	Cladding corrosion	0.002053417	0.01255415
9	Fuel thermal conductivity (Transient)	0.000495797	0.016435852
10	Fuel specific heat (Transient)	0.002025291	0.008276226
11	Cladding surface heat transfer coefficient (Transient)	0.003789049	0.030197664

With further screening, fuel specific heat (transient), fuel thermal conductivity (transient) and cladding corrosion were no longer considered. EGO analysis was performed with the rest 8 factors. It concludes that the interval of failure time is (258.6 s, 306.93 s) by changing these 8 factors in the given range.

3.2.5. Optimal design

Based on the above analysis, it suggests that fuel rod design parameters play important roles in the fuel performance under LOCA condition. Thus, in this section, EGO analysis is performed with the 5 design parameters to find out an optimal design. It indicates that with the optimal design shown in Table 8, cladding failure time can be delayed to 306.39 s.

According to the comparison of performance under steady state, shown in Table 9, the optimal design improves also the fuel system performance under steady state that enhances the nuclear safety.

TABLE 8. OPTIMAL DESIGN GIVEN BY EGO METHOD

No.	Variable	Reference Value	Optimal Value
1	Pellet Diameter, mm	8.21	8.33
2	Cladding Thickness, mm	0.57	0.5785
3	Plenum Length, mm	300.6	285.58
4	Pellet density, %	95.32	95.65
5	Enrichment, %	4.49	3.5

TABLE 9. COMPARISON OF PERFORMANCE UNDER STEADY STATE

Variable	Optimal Design	Reference Design
Max fuel rod pressure, MPa	3.90	4.14
Max fuel centerline temperature, °C	794.99	822.48
Fission gas release, %	2.02	2.22

4. CONCLUSIONS

With the simulation of Halden fuel rod LOCA behaviour tests IFA-650.9/10/11 using FRAPCON/FRAPTRAN, evaluation of integrated performance of fuel rod under LOCA condition is performed. Generally, FRAPCON/FRAPTRAN predicts well the fuel rod behaviour under LOCA condition. Sensitivity and uncertainty study of ATF fuel system's (UO₂-BeO + ODS FeCrAl) failure time under LOCA condition, found out that the design parameters, especially the pellet diameter have important influence on fuel system's performance during LOCA. Proper adjustment of design parameters can optimize the fuel performance.

ACKNOWLEDGEMENTS

The report performed under IAEA research Agreement No.18514, which forms part of the IAEA Coordinated Research Project "Fuel Modelling in Accident Conditions (FUMAC)". This research was supported by the National Science and Technology Major Project (2015ZX06004001), and High safety ATF Engineering Laboratory of Shenzhen.

REFERENCES

- [1] DU CHOMONT, F.B., LOCA Testing at HALDEN, the Ninth Experiment IFA-650.9, Report on OECD HALDEN Reactor Project No HWR-917, (October 2009).
- [2] LAVOIL, A., LOCA Testing at HALDEN, the Tenth Experiment IFA-650.10, Report on OECD HALDEN Reactor Project No HWR-974, (December 2010).
- [3] LAVOIL, A., LOCA Testing at HALDEN, the VVER Fuel Experiment IFA-650.11, Report on OECD HALDEN Reactor Project No HWR-976, (December 2010).
- [4] GEELHOOD, K.J., LUSCHER, W.G., "FRAPTRAN-2.0: Integral Assessment," U.S. Department of Energy under Contract DE-AC05-76RL01830.
- [5] GEELHOOD, K.J., LUSCHER, W.G., CUTA, J.M., PORTER, I.A., "FRAPTRAN-2.0: A Computer Code for the Transient Analysis of Oxide Fuel Rods," U.S. Department of Energy under Contract DE-AC05-76RL01830.
- [6] SALTELLI, A., RATTO, M., ANDRES, T., CAMPOLONGO, F., CARIBONI, J, et, al., "Global Sensitivity Analysis." The Primer[M]. John Wiley & Sons, Ltd, (2008).
- [7] DAKOTA, A., Multilevel Parallel Object oriented Framework for Design Optimization, Parameter Estimation, Uncertainty Quantification, and Sensitivity Analysis: Version 6.8 Theory Manual.

EXPERIMENTS ON FUEL BEHAVIOUR IN ACCIDENTAL CONDITIONS

(Session 2)

Chairperson

M. ŠEVEČEK
Czech Republic

EXPERIMENTAL AND MODELLING RESULTS OF THE QUENCH-19 BUNDLE TESTS WITH FeCrAl CLADDINGS

J. STUCKERT

Karlsruhe Institute of technology (KIT),
Germany

T. HOLLANDS

Gesellschaft für Reaktorsicherheit (GRS),
Germany,

K. DOLGANOV

Nuclear Safety Institute of the Russia Academy of Sciences (IBRAE),
Russian Federation.

Abstract

The QUENCH-19 test with the bundle including twenty four electrically heated fuel rod simulators with FeCrAl(Y) claddings was conducted at KIT on 29th August 2018. Additional bundle parts were four FeCrAl(Y) spacer grids as well as eight KANTHAL APM corner rods; the test bundle was surrounded by KANTHAL APM shroud. The objective of the experiment was the comparison of FeCrAl(Y) and ZIRLO claddings under similar power and gas flow conditions, simulating an early phase of hypothetical severe accident. Comparable with the previous QUENCH-15 test, the electrical power was the same during both pre-oxidation and transient stages. After increase of the power to 18.12 kW, this power value was kept constant during about 2000 s. At the end of this test stage the maximal peak cladding temperature of about 1500°C was reached. Much lower heating rate in comparison to the QUENCH-15 test was measured. Sharp increase of hydrogen release rate was observed above 1400°C. The experiment was terminated with reflood by injecting of about 48 g/s of water from the bundle bottom. The total hydrogen mass measured during the whole test was 9.2 g compared to 47.6 g in the QUENCH-15 experiment performed with much shorter high electrical power stage. The observation by endoscope showed the failure of cladding tubes at the bundle elevations between 850 and 1000 mm. The claddings were failed either due to melting (central rods), or due to interaction with melted thermocouples, or by spalling of small annular cladding segments. The post-test analyses were performed at GRS and IBRAE by means of the integral system codes ATHLET-CD and SOCRAT. The results of these simulations show that both codes are able to predict the temperature history. However, compared to the radial temperature profile of up to 300 K observed in the experiment, both codes calculate less of 50 K. The hydrogen generation was strongly underestimated due to lack of correct FeCrAl oxidation kinetics above 1300°C.

1. INTRODUCTION

The important accident management measure to terminate a severe accident progress in a Light Water Reactor (LWR) is the water injection into the uncovered degraded core [1]. The QUENCH experiments are devoted to the investigation of the hydrogen source term and materials interactions during LOCA and the early stages of severe accidents including the reflood stage.

Zircaloy-4 was used as cladding tube material in 12 out of 19 QUENCH tests. QUENCH-12 was performed with Nb-bearing E110 cladding material in WWER geometry and QUENCH-14 with M5 in the frame of the Advanced Cladding Materials (ACM) experimental series in the standard PWR-type bundle arrangement. QUENCH-15 as the second ACM experiment was conducted to check the effect of ZIRLO cladding material on bundle oxidation and core reflood, in comparison with tests QUENCH-06, QUENCH-12, and QUENCH-14. The arrangement of the QUENCH-15 bundle was different due to cladding outer diameter and pitch; the bundle was consisted of 24 heated rods with ZIRLO claddings, eight corner rods, and a Zr-702 shroud. The QUENCH-15 experiment was performed with the same test protocol as QUENCH-06, -12 and -14, so that the effects of different cladding materials could be observed [2].

The QUENCH-19 experiment was the worldwide first large-scale bundle test with Accident Tolerant Fuel (ATF) claddings. It was conducted with FeCrAl(Y) claddings (alloy B136Y3 supplied by ORNL). The test objective was the comparison of FeCrAl(Y) and ZIRLO claddings under similar power and gas flow conditions. The QUENCH-15 experiment was used as the reference test.

2. EXPERIMENTAL RESULTS

2.1. Test facility

The scheme of the test section is given in Fig. 1. The arrangement of the test rods presented in Fig. 2. The length of the test bundle is about 2.5 m; there are 24 heated fuel rod simulators. Heating is electric by central tungsten heaters with 5 mm diameter and length of 1024 mm. Electrodes of molybdenum/copper are connected to the tungsten heaters and to the cables leading to the DC electrical power supply. The tungsten heaters are surrounded by annular ZrO₂ pellets, which can simulate UO₂ pellets concerning the similar heat capacity.

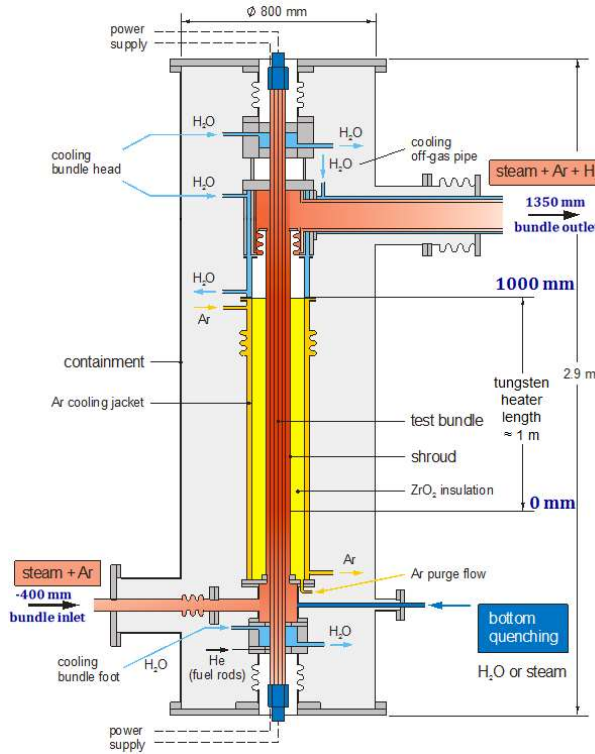


FIG. 1. QUENCH test section.

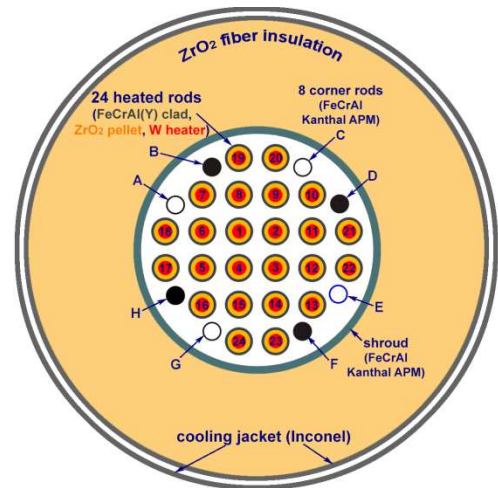


FIG. 2. Cross section of bundle, top view.

The rods are held in position by five grid spacers (at elevations 200, 50, 550, 1050 and 1410 mm). The lower grid spacer was the standard Inconel spacer; the other four spacers were manufactured by ORNL from the same material as the cladding tubes. The cladding outside diameter was 9.52 mm, the inner diameter 8.76 mm. All rods were filled with Kr at a pressure of 0.23 MPa after bundle heating to peak cladding temperature of 800 K.

Seven corner rods were installed at the bundle periphery. Four of them, i.e. rods “A”, “C”, “E”, and “G”, are made of a solid rod (Kanthal APM, Ø6 mm) at the top and a tube at the bottom (Kanthal D, Ø 6 mm, wall thickness 0.4 mm). The bottom part was used for thermocouple instrumentation. The other three corner rods, i.e. rods “B”, “D”, and “F” (solid rods with diameter 6 mm), could be withdrawn from the bundle during the test to check the oxidation degree and hydrogen absorption.

“The test bundle is surrounded by a shroud of Kanthal APM with a 34 mm thick ZrO₂ fibre insulation extending from the bottom (-300 mm) to the upper end of the heated zone (+1024 mm) and a double-walled cooling jacket of Inconel 600 (inner)/stainless steel (outer) over the entire length. The annulus between shroud and cooling jacket is purged and then filled with stagnant Ar. The annulus is connected to a flow- and pressure-controlled argon feeding system in order to keep the pressure constant at the target of 0.23 MPa and to prevent a penetration of steam into the annulus after shroud failure. The annulus of the cooling jacket is cooled by Ar flowing from the upper end to the bottom of the bundle, and by water in the bundle head. Both the absence of porous zirconia insulation above the heated zone and the water cooling allow to avoid too high temperatures in that region” [2]

The thermocouple accuracies are:

- at bundle elevations between 0 and 500 mm (NiCr/Ni thermocouples): ± 2 K (up to 600 K), $\pm 0.005T$ (above 600 K);
- at bundle elevations between 600 and + 1300 mm (W/Re thermocouples): ± 5 K (up to 700 K), $\pm 0.01T$ (above 700 K).

The release of hydrogen is analysed by a quadrupole mass spectrometer Balzers “GAM300” connected to the off-gas pipe of the facility. The ion currents representing the concentrations of the analysed gases are determined. From these measurements, the production rates of different gases (especially hydrogen) are calculated with the ratio of the partial pressure of the particular gas and that one of Ar (carrier gas) and multiplied by the Ar flow rate through the bundle.

2.2. Test conduct and first results

In the QUENCH-19 experiment the test sequence can be distinguished in the following stages:

- Pre-oxidation 0000–6018 s (similar to QUENCH-15);
- Heat-up 6018–7127 s (similar to QUENCH-15);
- Extended period 7127–9100 s (constant electrical power);
- Quench ≈ 9115 –9285 s with water flow rate 48 g/s (similar to QUENCH-15).

The power history for the QUENCH-19 experiment together with the measured peak cladding temperature is shown in Fig. 3.

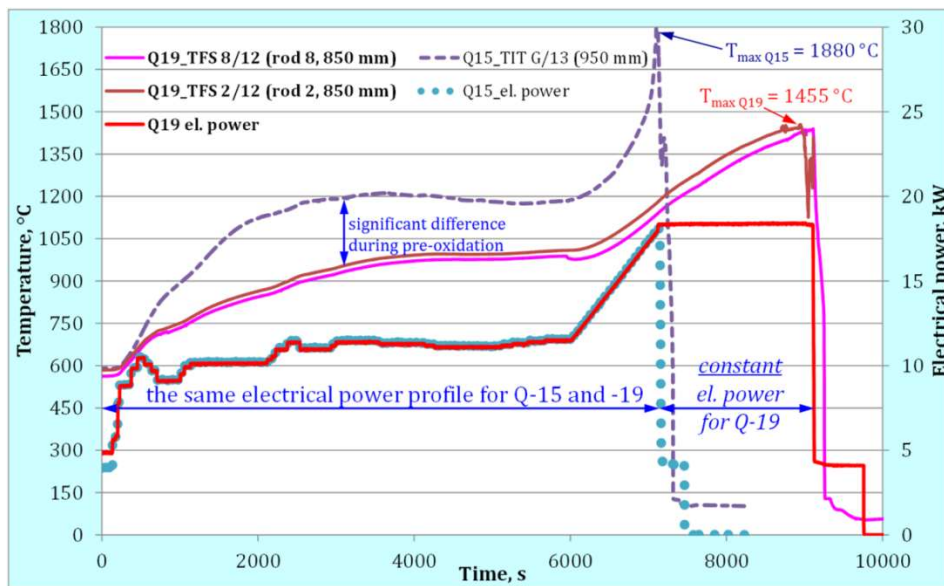


FIG. 3. QUENCH-19 and QUENCH-15 test progresses.

Ar and steam flows, as well as system pressure values are shown in Fig. 4. QUENCH-15 and -19 tests have similar gas inlet conditions except the inlet gas temperature: while the QUENCH-15 gas temperature was constant during the whole test (720 K), the corresponding gas temperature during QUENCH-19 increased from 640 to 700 K.

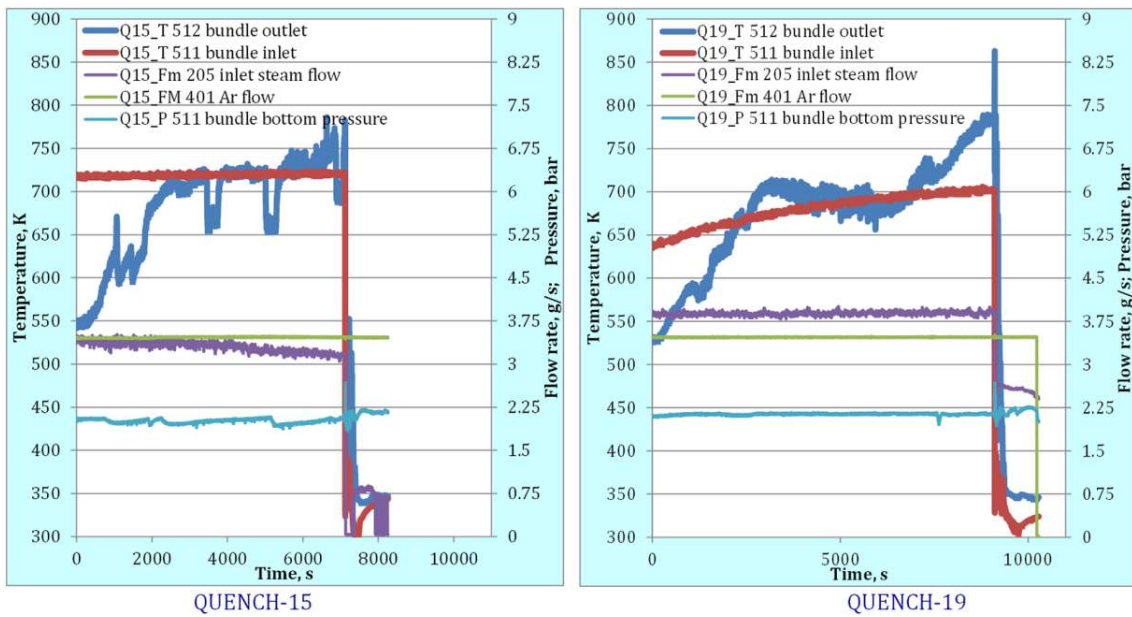


FIG. 4. Comparison of QUENCH-15 and QUENCH-19 gas parameters at bundle inlet and outlet.

The boundary conditions were different for two bundle tests (Fig. 5). Whereas the porous heat insulation of QUENCH-15 was filled with dry argon, the QUENCH-19 insulation contained water due to leakage of steam through the small gap at the upper shroud flange during pre-tests.

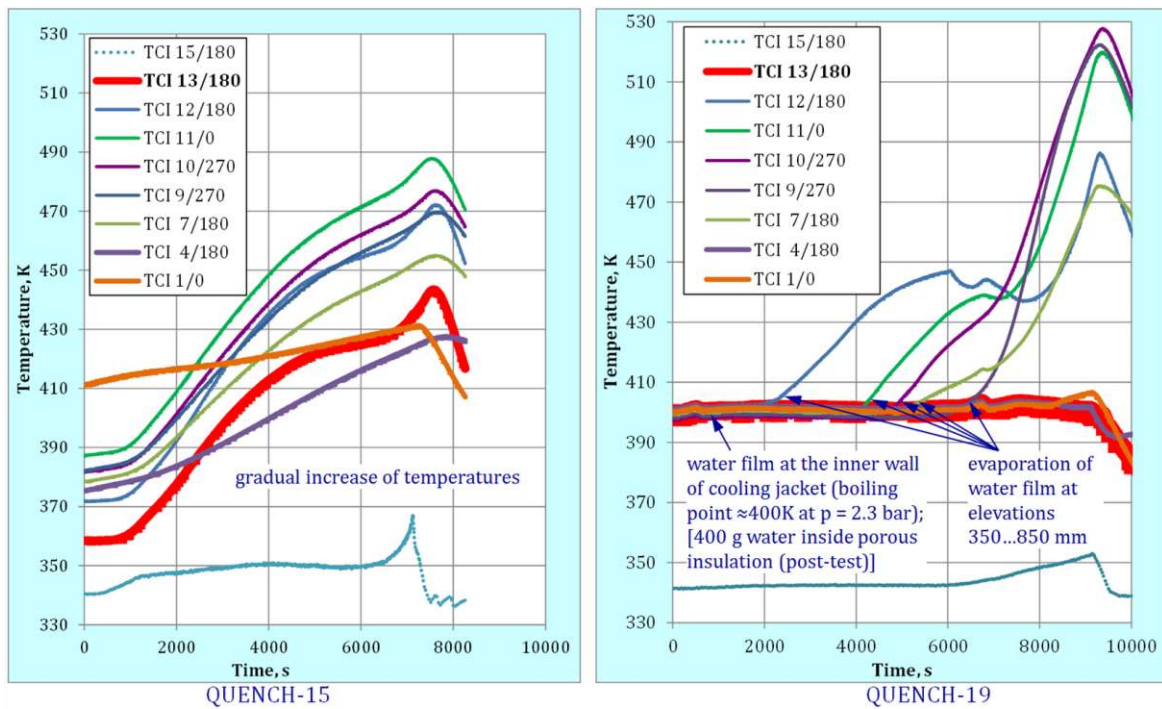


FIG. 5. Readings of thermocouples at different bundle elevations during transient stage.

These different boundary conditions should be the main reason for the fact, that the peak cladding temperature was about 210 K lower during the pre-oxidation stage in comparison to QUENCH-15 (Fig. 6). Additionally, the radial temperature gradient across the QUENCH-19 bundle was larger than the radial gradient for QUENCH-15. In contrast to QUENCH-15, no temperature escalation during extended transient stage of the QUENCH-19 experiment was observed.

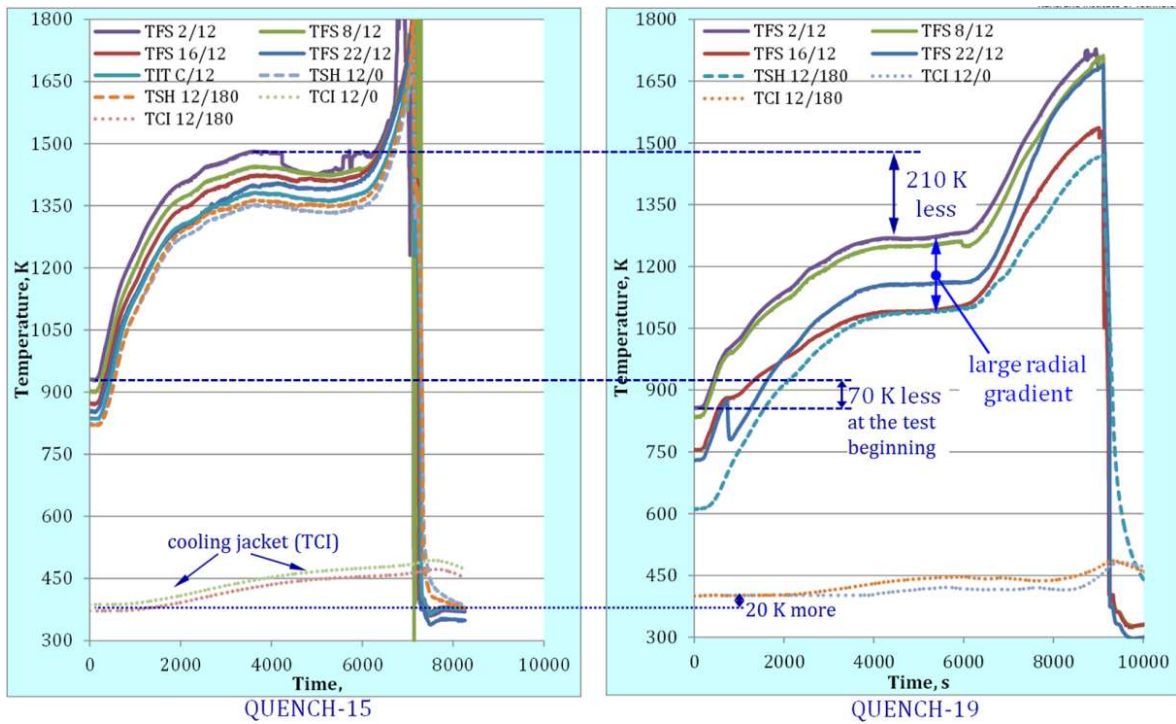


FIG. 6. Readings of thermocouples at 850 mm.

At the beginning of the transient stage, the lower temperatures were observed at all elevations of the QUENCH-19 bundle in comparison to QUENCH-15 (Fig. 7). The hottest elevation of the QUENCH-19 was the level 850 mm unlike 950 mm for QUENCH-15. At the end of transient, the temperatures were very similar between -250 and 650 mm, whereas at higher elevations the QUENCH-15 temperatures were significantly higher due to strong exothermal reaction ZIRLO/steam in this bundle at $T > 1500$ K.

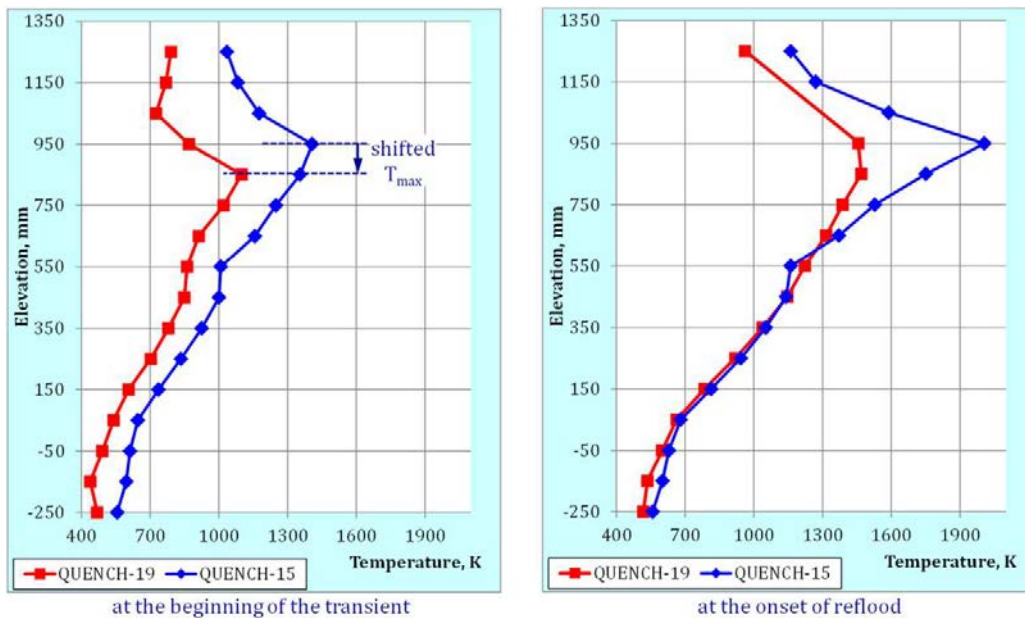


FIG. 7. Readings of thermocouples at 850 mm.

Due to higher temperatures at the onset of reflood, the initial evaporation rate was higher in QUENCH-15 (Fig. 8). Therefore, the duration of water level increases up to the bundle head was shorter in QUENCH-19 (270 s instead 330 s in QUENCH-15).

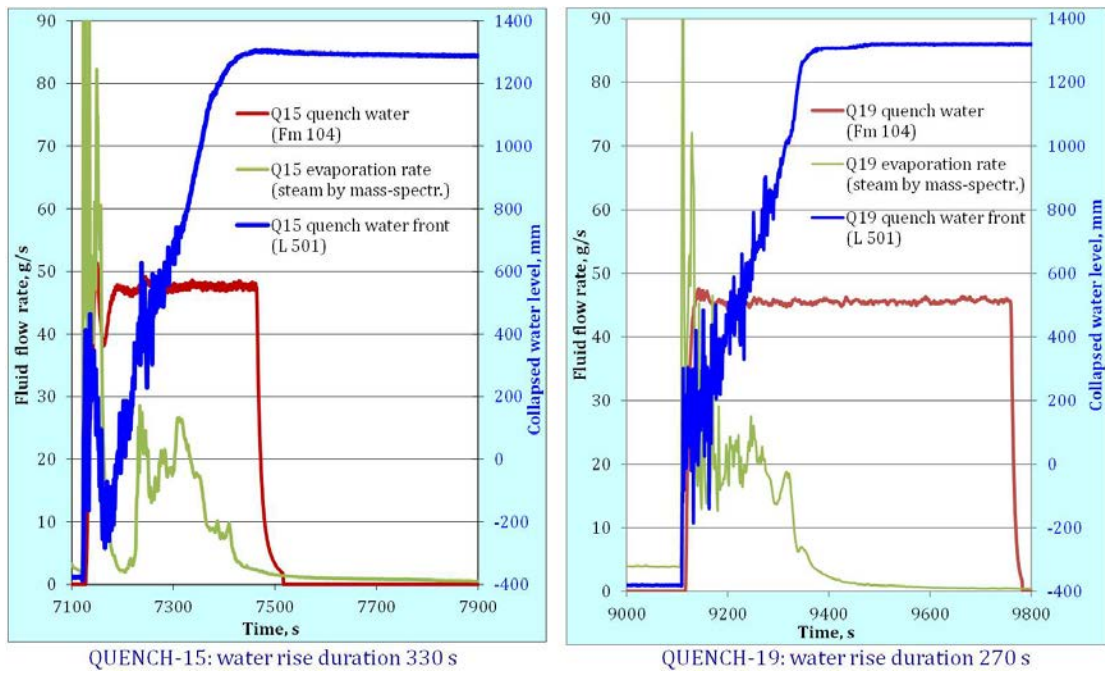


FIG. 8. Reflood stage: evaporation of injected water and progress of collapsed water front propagation.

The wetting of cladding surface thermocouples TFS occurred early than the collapsed water front reached the corresponding thermocouple elevation (Fig. 9). The reason is the relatively high region of two-phase fluid.

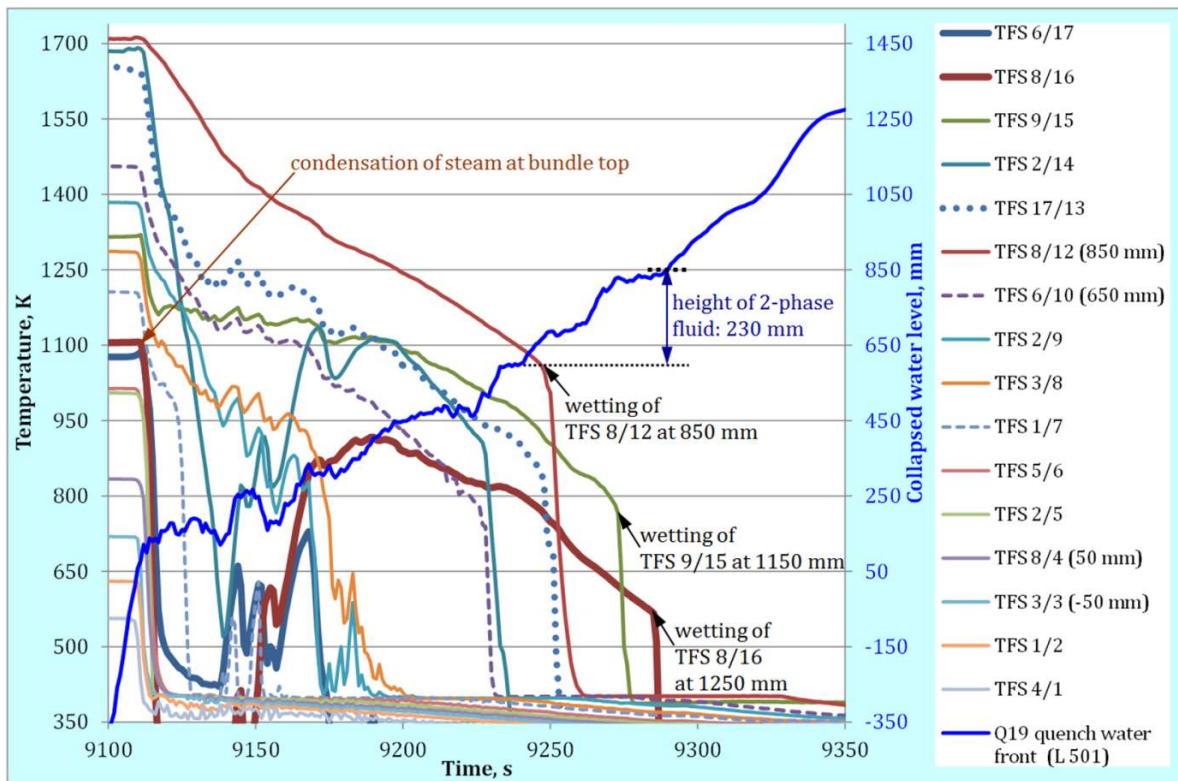


FIG. 9. QUENCH-19: wetting of thermocouples by two-phase fluid.

2.3. Post-test investigations

The inspection of some peripheral rods by videoscope showed absence of cladding circumferential segments with the height up to 12 mm, probably spalled after thermal axial expansion followed by quench shrinkage (Fig. 10). However, several other peripheral rods remained intact.

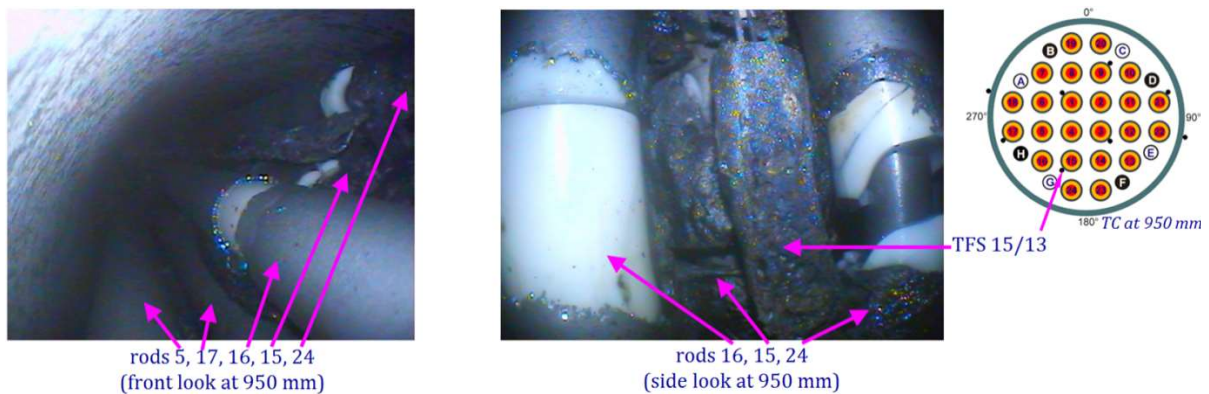


FIG. 10. QUENCH-19: videoscope observations of damaged claddings at upper part of heated zone.

The other damage character of claddings was found by the visual inspection of the post-test bundle. The claddings of the thermocouples made of the AISI-304 stainless steel (melting range 1400–1450°C) and located at the elevations 850, 950 and 1050 mm were melted. The relocated melt attacked the FeCrAl claddings and caused partial melting of these claddings (Fig. 11).



FIG. 11. QUENCH-19 bundle at bundle elevations between 900 and 1100 mm: cladding damages by molten thermocouple steel (AISI 304) sheaths.

The generation rate of hydrogen released due to oxidation of cladding tubes, corner rods, shroud, grid spacers and thermocouples showed the maximal value of 280 mg/s at the end of the transient (QUENCH-15: 1830 mg/s). The total hydrogen mass measured at the end of the test was 9.2 g, what corresponds about 20% of total hydrogen in QUENCH-19 (Fig. 12).

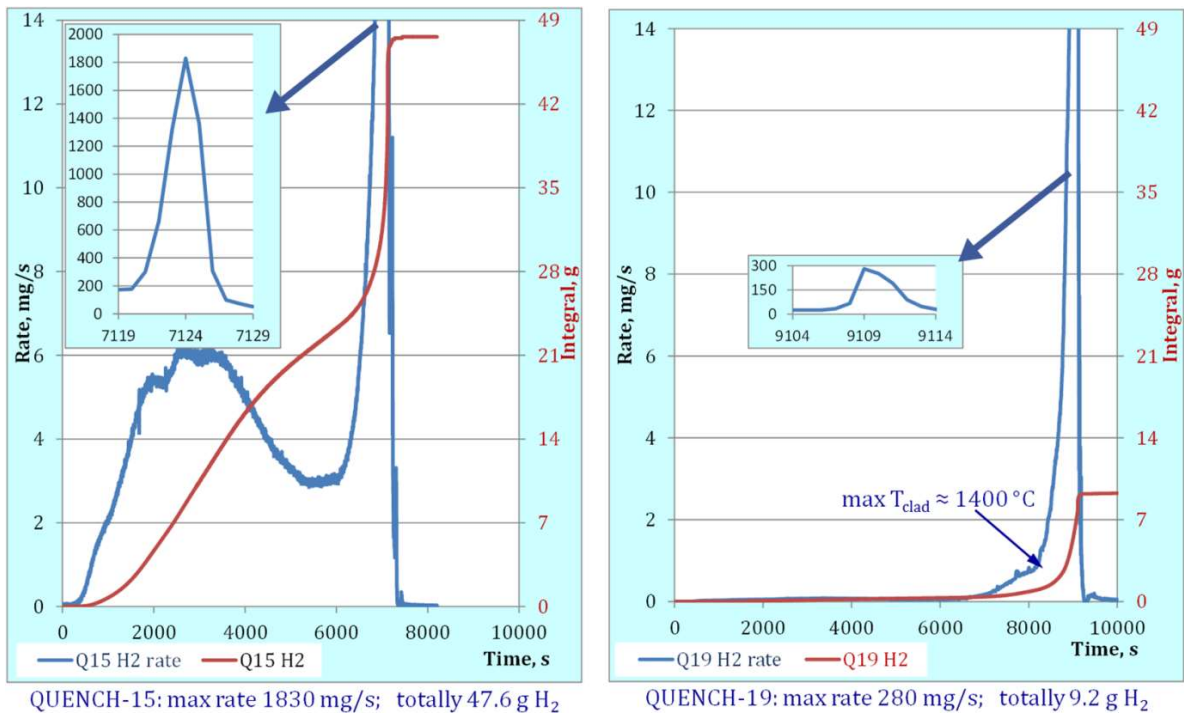


FIG. 12. Hydrogen release during QUENCH-15 and QUENCH-19.

3. SIMULATION RESULTS

3.1. Simulation with ATHLET-CD

ATHLET-CD (Analysis of THERmal-hydraulics of LEaks and Transients with Core Degradation) [5] describes the thermal-hydraulic response of reactor coolant system during severe accidents, including core damage progression as well as aerosol and fission product behavior, to calculate the source term for containment analyses, and to evaluate accident management measures. This code is developed by GRS in cooperation with IKE, University of Stuttgart.

3.1.1. Input data and model options

The post-test calculation used the same nodalization and as far as possible the same modelling options as for the earlier QUENCH-15 simulation. The input model for the QUENCH facility comprises among others the bundle fluid channel, subdivided into 20 axial nodes (10 nodes within the heated length). The rod bundle is simulated within the code module ECOPE by three concentric rings, an inner ring (ROD1) containing four heated rods, an intermediate ring containing eight heated rods (ROD2) and an outer ring with twelve heated rods (ROD3). In addition, the 5 spacer grids, the 8 corner rods, the shroud with its ZrO₂ thermal insulation, and the outer cooling jacket were simulated. The argon and steam flows, as well the quenching by water have been simulated by fill junctions at the bottom of the bundle or at the top of the bundle (injection of argon after start of flooding).

For the simulation of QUENCH-19 input parameters and modelling options as recommended by the code user's manual have been applied. For the external resistance of each heated rod, which takes into account the voltage drop across the sliding contacts at the rod extremities as well as at the cables connecting the sliding contacts to DC power supply, a value of 5 mΩ was applied.

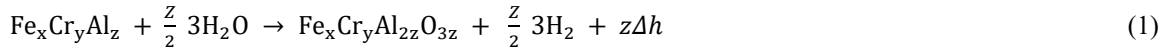
3.1.2. Assumptions and model changes for FeCrAl

In the input data deck for the simulation of the test the material properties of Zr were replaced by the values for FeCrAl given by KIT for the Kanthal APM alloy with a composition of 69% Fe, 21.6% Cr, 4.9% Al (+ 4.5% others) [6]. With the assumption that no other oxides are produced by oxidation beside Al₂O₃ and material data for aluminum oxide taken from [7] the following material properties have been used (Table 1):

TABLE 1. MATERIAL PROPERTIES USED FOR ATHLET-CD

Material property	FeCrAl	Al ₂ O ₃
Density (kg/m ³)	7.1×10 ³	3.9×10 ³
Thermal conductivity (W/mK)	11 (323 K) → 35 (1673 K)	35
Specific Heat (J/kg K)	460 (293 K) → 800 (1673 K)	880

The modification of the oxidation model for FeCrAl components with this specific composition was considered in ATHLET-CD within the ECOPE module for the claddings and within the HECU module for corner rods, spacer grids and shroud. Corresponding to the chemical reaction



with an energy release of $\Delta h = 9.3 \times 10^5 \text{ J/mol} = 9.32 \times 10^6 \text{ J/kg}_{\text{FeCrAl}}$ (molar weight $M_{\text{FeCrAl}} = 99.8 \times 10^{-3} \text{ kg/mol}$) heat and hydrogen were produced. Due to the composition of FeCrAl with the molar masses of $x=1.307$, $y=0.404$ and $z=0.215$ [6] the amount of hydrogen production was calculated. The mass of the resulting oxide Al₂O₃ (molar weight $M_{\text{Al}_2\text{O}_3} = 102.0 \times 10^{-3} \text{ kg/mol}$) determined the layer thickness of the oxide corresponding to its density and the given geometry of the rods.

The oxidation rate was treated as a parabolic law as derived from the analytical solution of the diffusion equation in the same way as used for the oxidation of Zr:

$$dW^2 = K \cdot dt \rightarrow \frac{dW}{dt} = \frac{K}{2W} \quad (2)$$

with $W = m_{\text{ox}}/\text{surf. area}$ in kg/m², K = reaction rate in kg²/m⁴s, t = time in s.

The reaction rate K is defined by an Arrhenius formulation $K = A \exp(-B/RT) \cdot g(p_s)$ with $R = 8.314 \text{ J/(mol}\cdot\text{K)}$ (gas constant), T is cladding temperature in K, $g(p_s)$ is reduction factor to consider steam starvation ($0 \leq g(p_s) \leq 1$) and the rate constants A, B as given by KIT for KANTHAL APMT [6]: $A = 3.1 \text{ kg}^2/\text{m}^4\text{s}$, $B = 2.78519 \times 10^5 \text{ J/mol}$. Additionally to this data, a second rate with a multiplication factor of 300 was used, which was derived from [3]. Fig. 13 compares the resulting oxidation rates with the standard options of ATHLET-CD used for the oxidation of Zr.

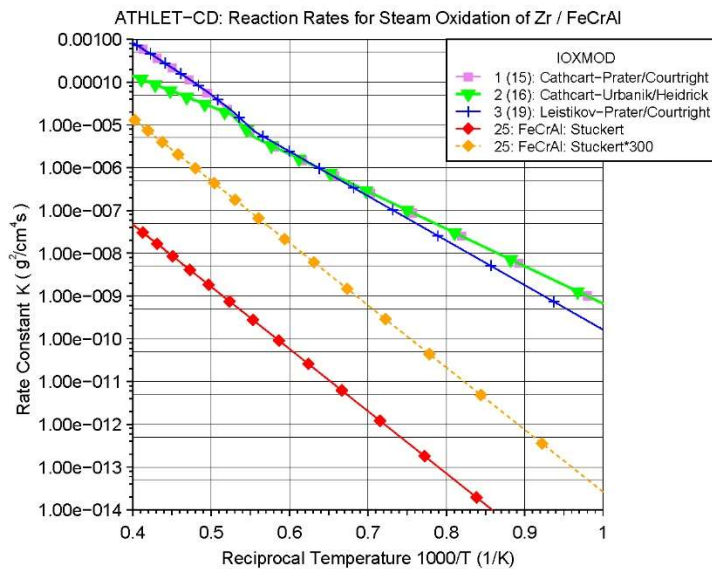


FIG. 13. Comparison of oxidation rates for Zr and FeCrAl in ATHLET-CD.

3.1.3. Main results of QUENCH-19 post-test simulation with ATHLET-CD

The main post-test calculation results for QUENCH-19 are depicted in the Fig. 14 (bundle temperatures) and Fig. 15 (hydrogen release) [8]. The bundle temperatures for inner (ROD1: blue), intermediate (ROD2: red) and outer ring of rods (ROD3: green) are satisfactorily reproduced by the code in comparison with data (black, olive, grey) within the heated length, only for the position above the heated length at 1350 mm height the cladding temperatures were overestimated in comparison to the experiment. Additionally, the comparison shows that there exists a relatively high radial gradient between inner and outer temperatures with a difference up to ≈ 200 K in the measured data (noticeable larger in comparison to QUENCH-15; the reason of this differences are not yet completely clarified [4]) while the simulation yields a flat profile with a difference of at most 50 K.

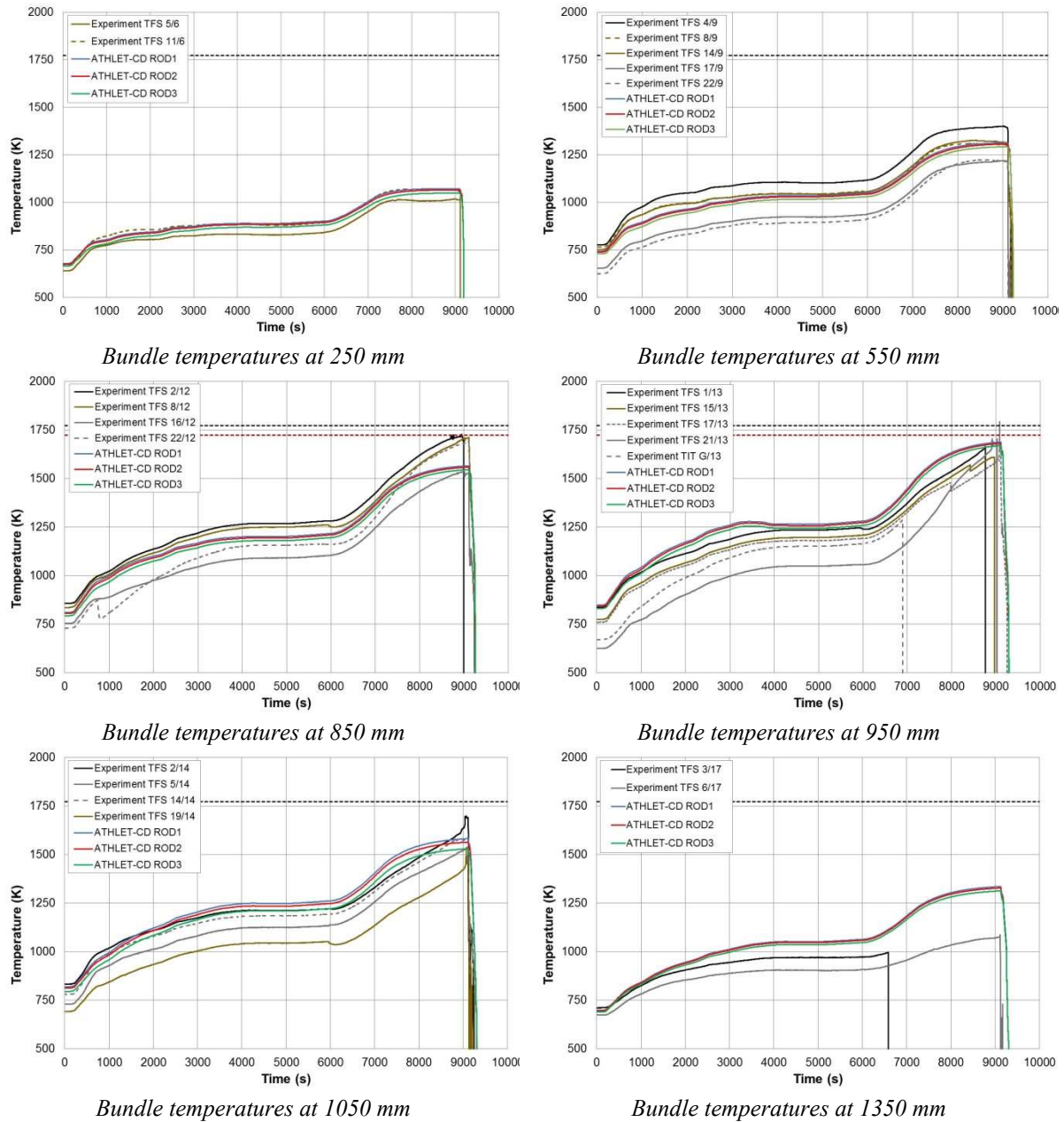


FIG. 14. Measured and simulated cladding temperatures for QUENCH-19.

In agreement with the measurement there is no temperature excursion in the simulation. The peak cladding temperature in the experiment of 1728 K at an elevation of 850 mm is calculated in good concordance with 1685 K at 950 mm height, a deviation of only 43 K. After start of quenching no further temperature increase occurs as shown also for the test. The melting temperature of FeCrAl, which is 1773 K was not reached neither in test nor

in the simulation (horizontal black dashed line) but the videoscope observation of the bundle at the positions of the withdrawn corner rods showed the failure of claddings at the bundle elevations between 850 and 1000 mm. It is assumed that the claddings failed due to melting (central rods), or due to interaction with melted thermocouples (peripheral rods), or by spalling of small annular cladding segments [4].

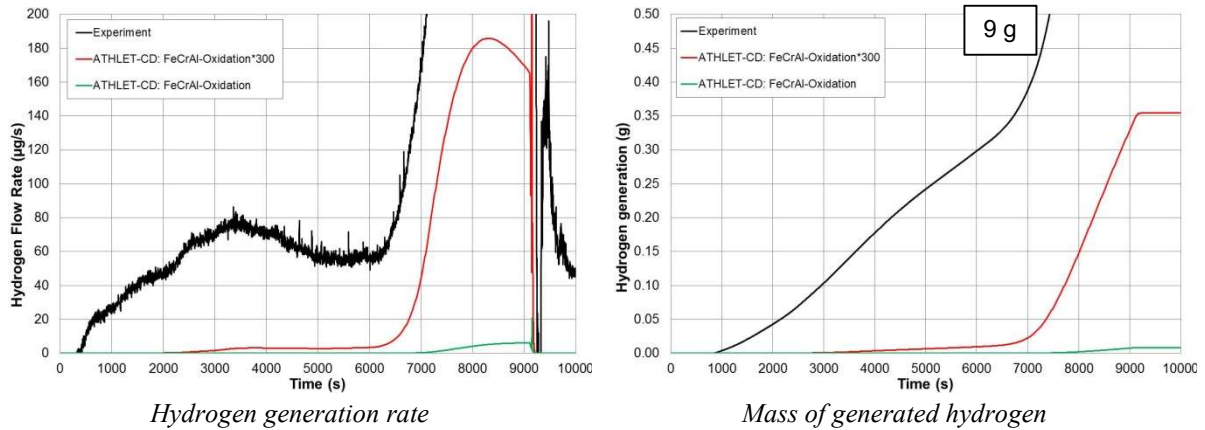


FIG. 15. Hydrogen release for QUENCH-19.

The comparison of hydrogen generation rate and mass of total generated hydrogen (Fig. 15) shows a heavy underestimation of oxidation in the simulation, especially for the reaction rate given by [6], but also with the increased rate (factor 300) as given in [4], with 0.008 g resp. 0.35 g compared to 9 g in the test. The hydrogen production in the test was comparable low up to the time when the maximum temperatures reached a level of $\approx 1400^\circ\text{C}$. Then a sharp increase of hydrogen release rate was observed at about 800 s before reflood. Probable trigger of this event could be the melting of steel thermocouple claddings [4]. This effect was not considered in the post-test calculation; nevertheless, the oxidation modelling for FeCrAl should be improved.

3.2. Simulation with SOCRAT

SOCRAT/V3 code [9] has been adapted for FeCrAl ATF claddings. Due to a lack of experimental data with FeCrAl for validation of thermomechanical model in SOCRAT the calculated time of the FeCrAl claddings burst corresponds to the moment when cladding started to melt, which overestimates the expected time of mechanical failure.

3.2.1. Assumptions and model changes for FeCrAl

The system pressure is 2 bar. The team-argon mixture at the bundle inlet: has the following characteristics: flow rate of Ar 0.003472 kg/s, flow rate of steam 0.00387 kg/s (initial value, decreases with time in accordance with experimental data), temperature 504.7 K (calculated).

The side heat removal in the cooling jackets was chosen according to experimental data with the following parameters: 1) Ar cooling with mass flow rate of 0.00559 kg/s, temperature 296.1 K, pressure 6.25 bar, 2) water cooling with mass flow rate of 0.250 kg/s, temperature 341 K, pressure 6.5 bar. The heat removal from the cooling jacket wall to containment atmosphere occurred by gas convection with heat transfer coefficient $5 \text{ W}/(\text{m}^2 \cdot \text{K})$ at gas temperature 335 K.

The reflood is simulated by water injection from the bundle bottom with flow rate in accordance with experimental data and temperature 296.4 K.

3.2.2. Change of material properties

The basic temperature dependence of zirconia fiber insulation provided in a report for QUENCH-15 experiment was modified to account for supposed water presence in cold regions close to cooling jacket (temperatures 300 and 404 K in Table 2). The heat capacity of zirconia insulation region was not modified and was set in accordance with a two-point time dependence provided in QUENCH-15 report.

TABLE 2. MODIFIED DATA FOR FIBER INSULATION

Temperature, K	300	404	405	673	1373	1673	1923
Heat conductivity, W/(m·K)	0.68	0.68	0.12	0.11	0.14	0.19	0.24

No fiber insulation there is between 1024 and 1300 mm. The basic value of heat conductivity for this region (calculated with account for radiation and convective heat transfer) was increased 3 times to assure the fast decrease of temperature in the experimental data. The values implemented in calculations are shown in Table 3.

TABLE 3. HEAT CONDUCTIVITY ABOVE 1024 MM

Temperature, K	300	500	595	735	885	975	1040	1130	1200
Heat conductivity, W/(m·K)	0.42	0.99	1.56	2.70	3.90	4.95	6.00	7.39	9.00

The density of HfO₂ powder in TC insulation was 1.5 times smaller than that in QUENCH-15 experiment. Therefore, the basic values of density and heat conductivity provided in QUENCH-15 report were decreased 1.5 times.

3.2.3. Applied oxidation model

All FeCrAl alloys are modeled with a correlation based on data for the APMT alloy [10] for temperature range $T \leq 1723$ K:

$$K_1(T) = 0.3041 \cdot \exp(-32850/T), \quad (3)$$

above 1773 K (melting temperature of FeCrAl), the correlation for stainless steel oxidation is used:

$$K_2(T) = 3607 \cdot \exp(-35210/T),$$

where K_1 and K_2 are in $\text{g}^2/(\text{cm}^4\text{s})$. (4)

To assure a transition between these low-temperature and high-temperature oxidation kinetics K_1 and K_2 , a special correlation is implemented for intermediate range of temperatures 1723–1773 K:

$$K_{12}(T) = a \cdot \exp(-b/T), \quad (5)$$

The values of coefficients a and b in (5) are defined by the parameters in correlations (3) and (4):

$$a = a_1 + (a_2 - a_1)(T - 1723)/50, \quad (6)$$

$$b = b_1 + (b_2 - b_1)(T - 1723)/50, \quad (7)$$

where $a_1 = 0.3041$, $a_2 = 3607$, $b_1 = 32850$, $b_2 = 35210$.

The products of oxidation are specified taking into account that the initial metallic components Fe, Al, and Cr are oxidized to FeO, Al₂O₃, and Cr₂O₃ respectively. The weight fractions of Fe, Al, and Cr in alloy are currently fixed at 72%, 6%, and 22%, respectively.

The mass of oxidation products is used for calculating the thermal properties of oxidized FeCrAl. This oxidation model was preliminary validated at a series of 7 separate effect test performed in ORNL [11].

4. MAIN RESULTS OF QUENCH-19 POST-TEST SIMULATION WITH SOCRAT

Figure 16 shows temperature results of in comparison with the experimental results for different bundle elevations. Significant radial temperature gradient observed in experiment was not reproduced by code: for peripheral rods (structure ROD 3) there is noticeable temperature overestimation. Figure 17 shows the modelling results for the integral hydrogen release.

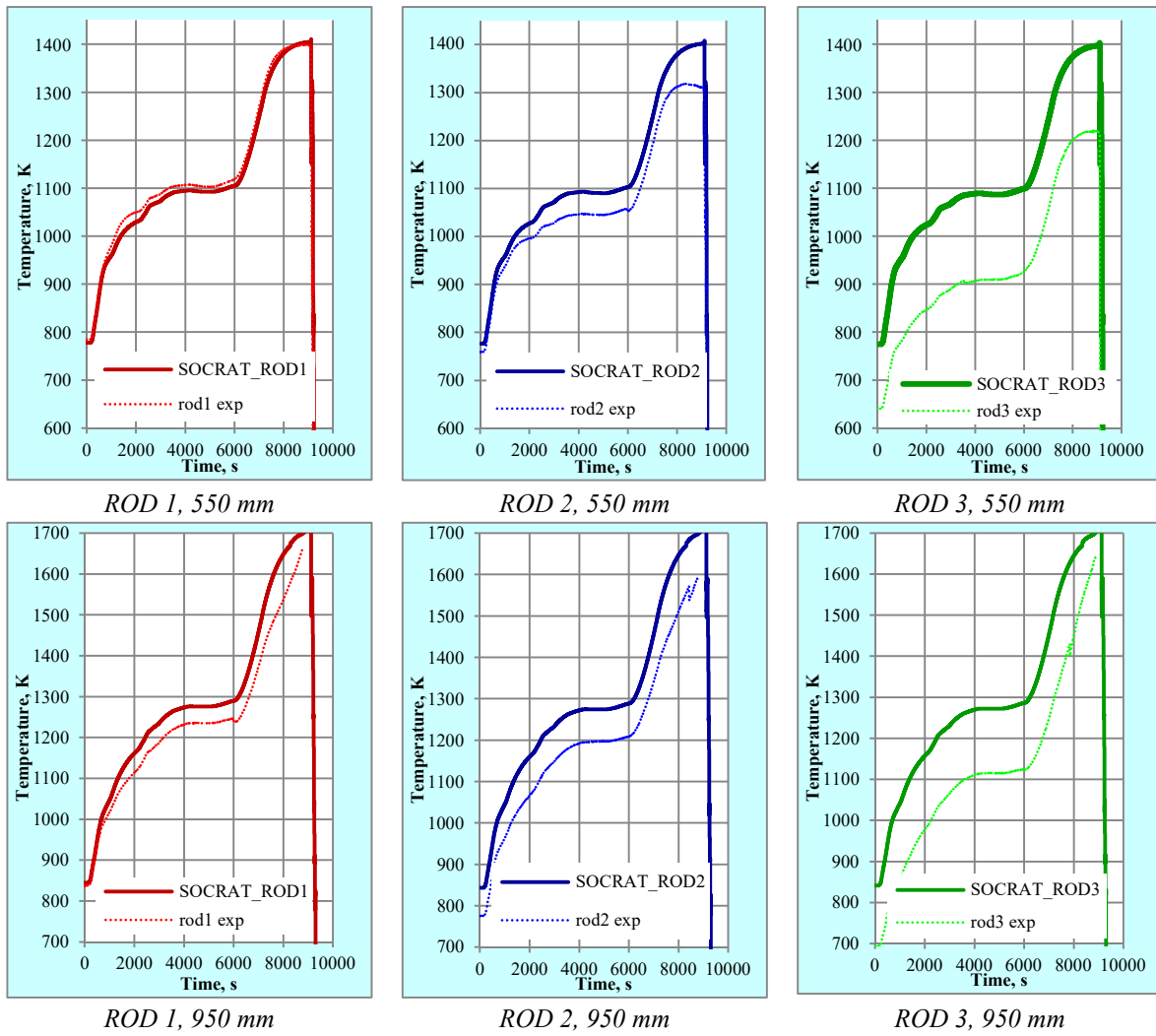


FIG. 16. Cladding temperatures at elevations 550 and 950 mm.

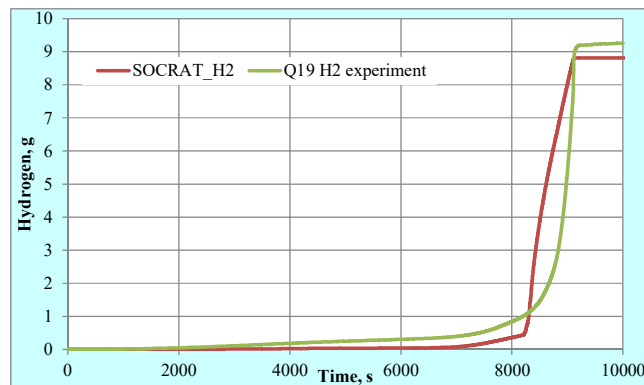


FIG. 17. Comparison of experimental and calculation results for hydrogen release.

5. SUMMARY AND CONCLUSIONS

The QUENCH-19 experiment with bundle containing 24 heated rods with FeCrAl(Y) cladding and 4 FeCrAl(Y) spacer grids as well as 7 KANTHAL APM corner rods and KANTHAL APM shroud was performed at KIT on August 29, 2018 with similar electrical power history as reference test QUENCH-15 (ZIRLO claddings). Not similar conditions were 1) cooler steam-Ar flow, and 2) humid Ar inside the heat insulation for QUENCH-19.

The QUENCH-19 test was performed in four test stages:

- (a) pre-oxidation during about 6000 s (similar to QUENCH-15);
- (b) transient during about 1130 s (similar to QUENCH-15);
- (c) extended period with constant electrical power of 18.32 kW during 1970 s (to extend the temperature increase stage);
- (d) test termination by water flooding with rate of 48 g/s (similar to QUENCH-15).

The peak cladding temperatures during the pre-oxidation stage were about 200 K lower in comparison to QUENCH-15. The radial temperature gradient was noticeable larger in comparison to QUENCH-15. The reasons for these test differences could be the different properties of the bundle materials (lower thermal conductivity and higher heat capacity and thermal expansion of FeCrAl) as well as the different boundary conditions (cooler gas flow, humid heat insulation). Much lower heating rate was measured in comparison to QUENCH-15. A temperature of about 1423 K (1150°C) was reached at the time point as a local melting of QUENCH-15 claddings occurred. No temperature escalation was observed during the extended transient. Maximum cladding temperature measured before reflood was about 1733 K (1460°C). The coping time was about 3200 s (\approx 1200 s for QUENCH-15). Many claddings were damaged at elevations between 850 and 1000 mm: 1) by interaction with melted thermocouples or 2) parts of claddings were spalled (probably due to thermal expansion followed by quench shrinkage). Sharp increase of hydrogen release rate was observed about 800 s before reflood. Probable trigger of this event could be the melting of steel thermocouple claddings. The maximum hydrogen release rate reached before reflood was 280 mg/s (1830 mg/s for QUENCH-15). Total hydrogen production 9.2 g (47.6 g for QUENCH-15).

After the implementation of two approaches for the oxidation kinetics of FeCrAl with the assumption that only Al_2O_3 and no other oxides will be generated, the most recent ATHLET-CD code version has been used for the simulation of the QUENCH-19 experiment. As far as possible the same input data deck and modelling options were used compared to the reference case QUENCH-15, only boundary conditions of the test had been taken from the data file and material data for FeCrAl instead of Zr (given by KIT) and the only considered oxidation product Al_2O_3 instead of ZrO_2 (from [7]) were changed.

The results of the post-test simulations show that ATHLET-CD is able to predict the thermal behaviour of the experiment in good agreement to the measured values, especially within the heated length. Compared to the observed radial temperature profile of up to \approx 200 K in the experiment, which is different to the reference case QUENCH-15 and the reason for this is not clear up to now, ATHLET-CD calculates a flat profile with a difference of only \approx 50 K between inner and outer rods. Different to QUENCH-15 there was no temperature excursion neither in the test nor in the simulation; the temperatures decrease immediately after water injection. The maximum temperature was obtained with high accuracy; there was a small underestimation of only \approx 40 K.

The comparison of the hydrogen production with totally 9 g resulting from the test and less than 1 g for both oxidation approaches in the simulation shows that the oxidation model of FeCrAl in the ATHLET-CD code does not comprise all the effects which contribute to the hydrogen generation in the test. For a detailed evaluation of the calculated hydrogen generation it is necessary to use the final results of the post-test examination of the bundle to know which components account for the total value. Nevertheless, the implementation of the oxidation model for FeCrAl was a first approximation and will be improved.

First validation analyses of the SOCRAT code for FeCrAl applications were performed on the basis of the QUENCH-19. Due to absence of reliable oxidation kinetics of FeCrAl (Y) alloy at high temperatures, results of the modelling have temporarily character.

Both ATHLET-CD and SOCRAT codes able to predict the thermal behavior of the internal bundle rods, however temperatures for the periphery rods were significantly overestimated. The calculated radial temperature gradient was about 50 K, whereas experimental gradient was more than 300 K. The cause of this was the not simulated circumstance of the water penetration into the heat insulation through the leakage at the bundle head.

For simulation of the bundle oxidation, both codes used the correlation established early for the industrial KANTHAL APMT alloy, whereas the test was performed with new B136Y3 alloy developed by ORNL for nuclear applications (FeCrAl alloy with lower Cr content). New experimental data are needed for future correct modelling of the oxidation of the B136Y3 alloy.

ACKNOWLEDGEMENTS

The QUENCH-19 experiment was supported by the KIT programme NUSAFE and partly sponsored by ORNL. The cladding materials and thermocouples were provided by ORNL. The authors thank all colleagues involved in the investigations, particularly M. Steinbrück and M. Große for many useful discussions, J. Moch and U. Peters for bundle preparation, U. Stegmaier for mass spectrometer measurements.

The development and validation of ATHLET-CD are sponsored by the German Federal Ministry for Economic Affairs and Energy (BMWi)

REFERENCES

- [1] STUCKERT, J., STEINBRUECK, M., GROSSE, M., Experimental programme QUENCH at KIT on core degradation during reflooding under LOCA conditions and in the early phase of a severe accident, IAEA-TECDOC-CD-1775 (Nov. 2015) 281–297.
- [2] STUCKERT, J., BIRCHLEY, J., GROßE, M., JAECKEL, B., STEINBRÜCK, M., Experimental and calculation results of the integral reflood test QUENCH-15 with ZIRLO cladding tubes in comparison with results of previous QUENCH tests. Nuclear Engineering and Design **241** (2011) 3224–3233.
- [3] NUCLEAR ENERGY AGENCY (NEA), State-of-the-Art Report on Light Water Reactor Accident-Tolerant Fuels, NEA No. 7317, OECD (2018).
- [4] STUCKERT, J., GROßE, M., LAIER, J., MOCH, J., PETERS, U., STEGMAIER, U., STEINBRÜCK, M., TERRANI, K., “First results of the bundle test QUENCH-19 with FeCrAl claddings”, 24th International Quench Workshop, Karlsruhe, (November 2018).
- [5] AUSTREGESILO, H., et al., “ATHLET-CD 3.2 User’s Manual”, GRS Report, GRS-P-4/Vol. 1, Dec. 2018.
- [6] STUCKERT, J., Mail to GRS from 26.7.2018.
- [7] ACCURATUS, Ceramic Materials and Ceramic Components, 9.10.2018, <https://accuratus.com/alumox.html>.
- [8] HOLLANDS, T., BALS, C., “Pre- and Post-Test Simulations of the ATF Experiment QUENCH-19 with AC2”, 24th International QUENCH Workshop, Karlsruhe, November 2018.
- [9] BOLSHOV, L., STRIZHOV, V., SOCRAT — The System of Codes for Realistic Analysis of Severe Accidents. Proc. of ICAPP’06. Reno, NV USA, June 4–8, 2006.
- [10] UNOCIC, K.A., YAMAMOTO, Y., PINT, B.A., Effect of Al and Cr Content on Air and Steam Oxidation of FeCrAl Alloys and Commercial APMT Alloy, Oxidation of Metals **87** 3–4 (April 2017) 431–441.
ROBB, K.R., HOWELL, M., OTT, L.J., Parametric and Experimentally Informed BWR Severe Accident Analysis Using FeCrAl, ORNL/SPR-2017/373, ORNL, (August 2017).

OXIDATION PERFORMANCE AND FAILURE BEHAVIOUR OF MONOLITHIC AND COATED ATF CLADDINGS UNDER SEVERE ACCIDENT CONDITIONS

C. TANG, M. STEINBRUECK, M. GROSSE

Institute for Applied Materials (IAM-AWP), Karlsruhe Institute of Technology (KIT),
Hermann-von-Helmholtz-Platz 1, 76344 Eggenstein-Leopoldshafen,
Germany

Abstract

Various concepts of ATF claddings with enhanced tolerance to loss of active cooling in nuclear reactor core have been proposed and intensively investigated worldwide. These potential solutions comprise mainly three categories: (1) state-of-the-art zirconium based alloy cladding with high temperature oxidation resistance coatings, (2) new metallic cladding such as FeCrAl alloy and (3) ceramic SiC/SiC composite cladding. These innovative ATF cladding materials have shown excellent or satisfactory performance during design-basis accident conditions. However, their degradation and failure behaviour under simulated severe accident conditions are lacking assessment. In this paper, the oxidation performance and failure behaviour of one type of monolithic ATF cladding (FeCrAl alloys) and two coated Zr alloys (Cr coated and Cr₂AlC coated) in high temperature steam extended to severe accident scenarios are explored. FeCrAl alloys are susceptible to breakaway oxidation (formation of non-protective iron based oxide) at temperatures exceeding 1200°C, depending on heating schedules and chemical compositions. The principal failure mechanisms of metallic (Cr) coated and ceramic (Cr₂AlC) coated Zr alloys are formation of liquid phase via eutectic reaction and cracking, respectively, at high temperatures.

1. INTRODUCTION

Zirconium based alloy fuel claddings used for current light water reactors (LWRs) possess desirable performances during steady state normal operations and design basis accidents. The Fukushima Daiichi Accidents in 2011 highlighted some detrimental performance characteristics of the fuel claddings, i.e. strong heat and hydrogen releases via rapid exothermic zirconium-steam oxidation reaction, during severe accidents and the need to develop advanced accident tolerant fuel (ATF) cladding for enhancing the safety margins of water cooled reactors [1]. One of the crucial performance features of advanced ATF cladding materials is reduced oxidation kinetics in high temperature steam with simultaneously minimized hydrogen generation and enthalpy input [2]. In general, the high temperature oxidation resistance of materials relies on the growth of an external, protective and slow-growing oxide scale. The most common protective oxide scales preventing underlying materials from fast oxidation are Cr₂O₃, Al₂O₃ and SiO₂. Various concepts of enhanced ATF claddings proposed and intensively investigated currently are materials that can form one of those oxide scales during high temperature oxidation [2–4]. These alternative solutions comprise mainly three categories: (1) coated Zr cladding, (2) metallic FeCrAl alloy cladding and (3) ceramic SiC/SiC composite cladding.

In case of coating materials, a variety of metallic and ceramic coatings has been examined. One of the most intensively studied coatings is pure Cr [5]. Oxidation of Cr coatings in steam result in growth of a Cr₂O₃ layer, which possesses good oxidation resistance up to 1200°C. Alumina-forming metallic or ceramic materials, for instance FeCrAl alloys or Ti₂AlC and Cr₂AlC MAX phases, also have been proposed as protective coatings since alumina scale is featured by a much lower growth rate than that of chromia [6]. FeCrAl-based alloys represent a very promising candidate for replacing the Zr-based alloy claddings due to their excellent properties, i.e. excellent high temperature oxidation resistance as well as good formability and mechanical properties [7]. However, majority efforts on characterization and qualification of these enhanced ATF cladding materials are under operational and design basis conditions. So far, only limited studies focused on their degradation and failure behaviour under simulated severe accident conditions. A comprehensive understanding of the oxidation performances and failure mechanisms of these ATF cladding candidates under severe accidents is lacking. In the framework of the QUENCH programme at the Karlsruhe Institute of Technology, in cooperation with international partners, the investigation of the performance of various ATF candidate materials during severe accidents has been established in recent years. Numerous laboratory scale tests from design basis accidents extended to severe scenarios (up to >1750°C in steam) have been performed. In this paper, the oxidation performance and failure behaviour of one type of monolithic ATF cladding (FeCrAl alloys) and two coated Zr alloys (Cr coated and Cr₂AlC coated) in high temperature steam is explored and reported.

2. EXPERIMENTS

The FeCrAl alloys examined in this study consisted of one commercial alloys, Kanthal APM (Fe20.5Cr5.8Al, wt.%), and one model alloy Fe₁₂Cr₅Al (wt.%). The commercial alloy and the mode alloy are in tube and disk shape, respectively. Two types of Cr coated Zr alloys, including physic vapor deposition coated and cold spraying coated, were tested. The thickness of the PVD Cr coating is around 25 μm and of the cold spraying Cr coating is around 30 μm. The Cr₂AlC coatings were synthesized via a two-step approach and more info can be found in [8]. The thickness of the Cr₂AlC coatings was around 6 μm with a 500 nm Cr interlayer as bonding/diffusion barrier.

The majority oxidation experiments were conducted using the so-called BOX furnace with a horizontal corundum tube under normal pressure. The specimen was located at the center of furnace on a corundum crucible sample holder. A Bronkhorst flow controller and gas mixer system was used to define the oxidizing atmospheres. The composition of the off-gas was in-situ analyzed by a mass spectrometer Balzers GAM300. The specimens were oxidized in a flowing argon + steam atmosphere. Argon was used as the carrier gas and as the reference gas for mass spectrometer analysis. Two different kinds of tests were conducted, isothermal tests and transient tests. In the isothermal tests, samples were heated in high purity Ar atmosphere (6N) to the desired temperatures with fixed heating rate 10 K/min. The atmosphere was then switched to 20 l/h Ar and 20 g/h H₂O (≈55 vol.% H₂O) for steam oxidation with different dwell times. Finally, after the isothermal exposure, the specimens were cooled down to room temperature by simultaneously changing the atmosphere back to high purity Ar. In the transient test, the steam was injected at low temperatures, and the specimens were oxidized from low temperature to a pre-defined high temperature with different heating rates; a succeeding isothermal exposure period was applied once reaching the pre-defined temperatures. Few tests were performed using a single-rod quench facility (QUENCH-SR) with a vertical quartz furnace heated by induction coils. After the test, the samples were characterized by X-ray diffraction, scanning electron microscope (SEM), etc.

3. RESULTS

3.1. Monolithic FeCrAl alloys

Figure 1 summarizes the oxidation behaviour of the Kanthal APM alloys during transient test from 500 to 1400°C with subsequent holding for 1 h at 1400°C with two different heating rates. At lower heating rate, 5 K/min, the hydrogen production during the steam exposure was extremely low. Both XRD (Fig. 1(b)) and SEM analysis (Fig. 1c) confirmed that a protective alumina scale established on the surface, inhibiting direct contact of steam with the alloy matrix. However, at the slightly higher heating rate 10 K/min during the ramp period, surprising results were observed. The hydrogen concentration increased abruptly to an extremely high value once the temperature reaching around 1380°C (Fig. 1(a)), two magnitudes higher than at 5 K/min, accompanied by a strong peak. The sample was disintegrated after the test and the final mass gains was around 170 mg/cm² corresponding to 47 wt.%. XRD and SEM results confirmed that the alloy was completely oxidized without alumina scale surviving. These findings reveal that the alloy suffered catastrophic oxidation via rapid growth of non-protective iron based oxide at temperature higher than ≈1380°C. Thus, an adequately thick alumina oxide layer is needed to avoid the occurrence of catastrophic oxidation especially at elevated temperatures for this category of alloys [9].

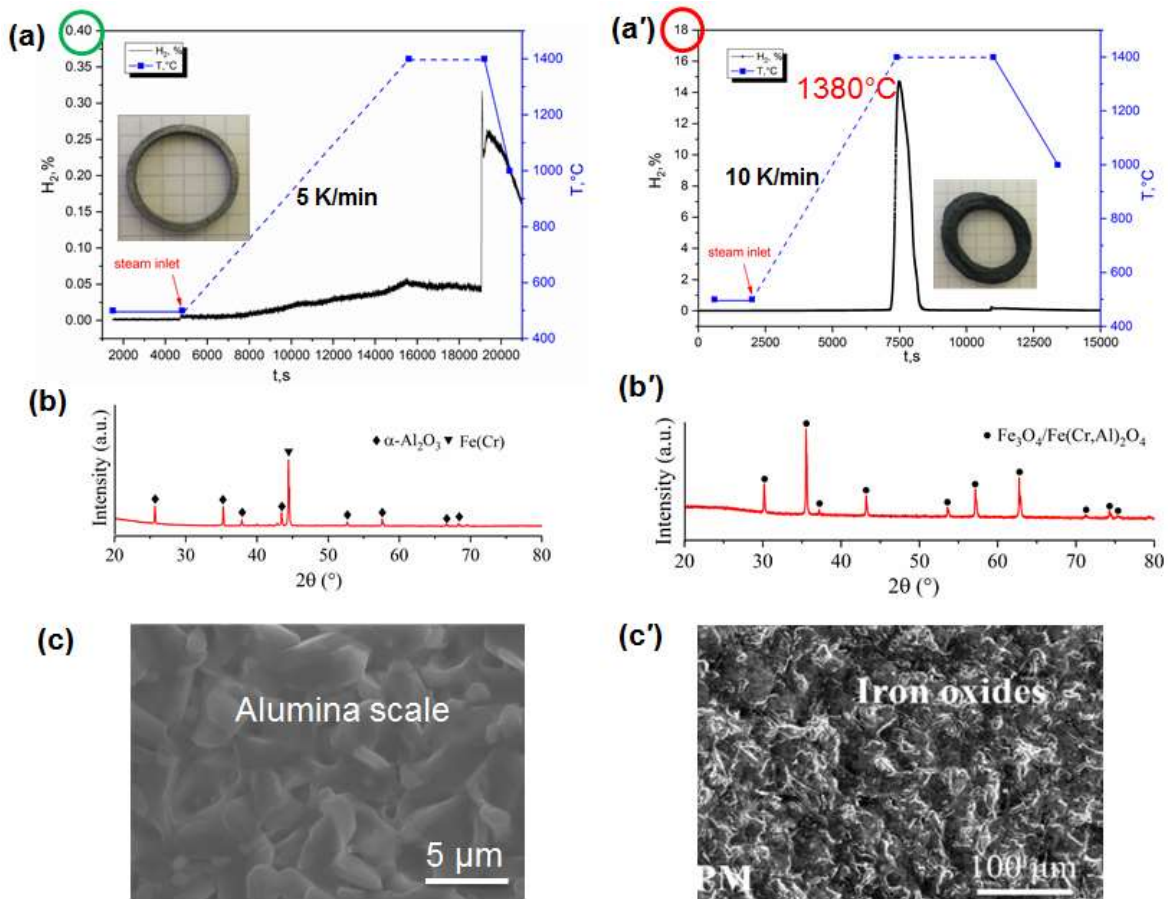


FIG. 1. Oxidation performance of Kanthal APM alloys (Fe20.5Cr5.8Al) during transient test from 500 to 1400°C with subsequent holding for 1 h at 1400°C, left column: 5 K/min heating rate and right column: 10 K/min heating rate. (a) and (a') hydrogen concentration in the off-gas with inserted appearance of the samples after test. (b) and (b') XRD patterns. (c) and (c') SEM images of surface view. Note that alumina scale formed at lower heating rate and breakaway oxidation occurred at higher heating rate.

Since commercial high Cr (≈ 20 wt.%) FeCrAl alloys sustain radiation-induced hardening and embrittlement due to formation of the Cr-rich α' phase under irradiation, relatively low Cr alloys are currently optimized for nuclear application [10]. A low Cr model alloy (Fe12Cr5Al) was further tested and Fig. 2 displays the hydrogen concentration in the off-gas with inserted appearance of the samples during one transient test to 1450°C and one isothermal test at 1200°C. In both tests, a high concentration peak of hydrogen appeared; together with appearance of the samples after test clearly revealed that catastrophic oxidation occurred. The maximum tolerance temperature of the alloy during the transient test was determined as around 1330°C. While, the alloy even cannot form an alumina scale during isothermal oxidation at 1200°C, i.e. here without a pre-oxidation process. The alloys are more susceptible to catastrophic oxidation in high temperature steam considering the absence of a pre-oxidation process. In real accident scenarios, the heating rates in the nuclear core vary from a few K to dozens of K per minute. The response of this alloys under simulated severe accident conditions needs detailed investigations.

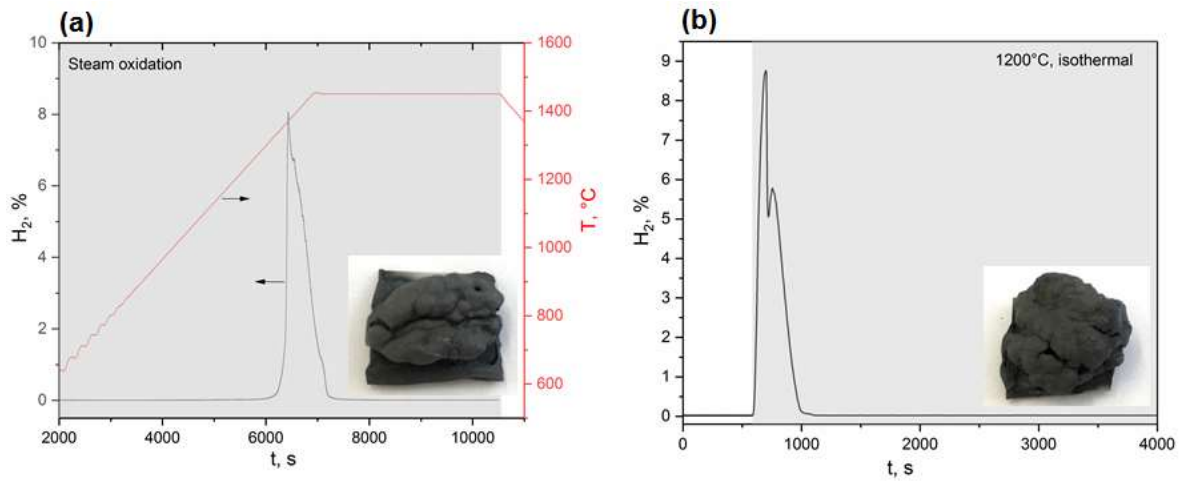


FIG. 2. Hydrogen concentration in the off-gas with inserted appearance of the Fe12Cr5Al samples (a) transient test from 500 to 1400°C at 10 K/min heating rate with subsequent holding for 1 h at 1450°C and (b) isothermal test at 1200°C for 1 h. The grey areas indicating steam oxidation period.

3.2. Coated Zr alloys

3.2.1. Cr coated Zr alloys

Figure 3 shows the cross sectional view of PVD Cr coated Zircaloy-2 after oxidation in steam at 1200°C for 30 min and 1300°C for 5 min, respectively. Under both conditions, a protective Cr₂O₃ grew on the surface and an interdiffusion layer formed at coating/substrate interface. The coating possesses excellent adherence without any sign of cracking and spallation. However, the oxidation rate and the interdiffusion rate both increased significantly with increasing temperature. The oxide scale and interdiffusion layer thicknesses are thicker after oxidation at 1300°C for just 5 min (Fig. 3b) than those at 1200°C for 30 min (Fig. 3a). The diffusion of Cr into the Zr alloy substrate has been proved leading to formation of brittle intermetallic compound (ZrCr₂), which weaken the strength of the alloy substrate [11]. Thus, during low term intermediate temperature (below the Cr-Zr eutectic temperature) scenarios, the failure behaviour due to coating-substrate interdiffusion should be considered.

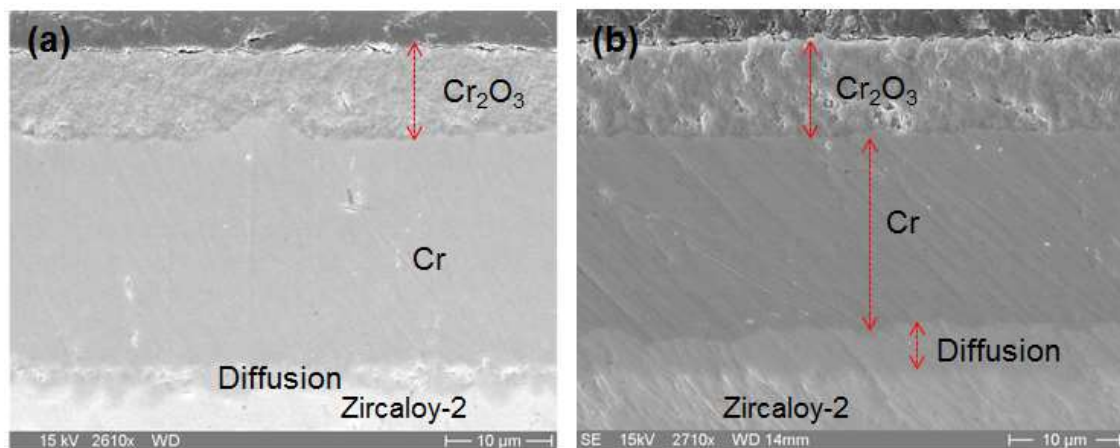


FIG. 3. Cross sectional view of PVD Cr coated Zircaloy-2 after oxidation (a) at 1200°C for 30 min (c) 1300°C for 5 min in steam.

Figure 4 provides hydrogen release rate and surface SEM image of cold spraying Cr coated zircaloy during a transient test up to 1500°C. Obviously, the hydrogen release rate accelerated once the temperature exceeded the eutectic temperature (\approx 1330°C) and a steeply increased hydrogen release was observed at temperatures above approx. 1450°C. Then the hydrogen rate was significantly higher than the hydrogen release rate of the uncoated

reference Zircaloy-4, indicating a much higher oxidation rate after failure of the coatings. Examination of the sample surface clearly showed the formation of liquid protrusions and cracking of the coating, (Fig. 4b).

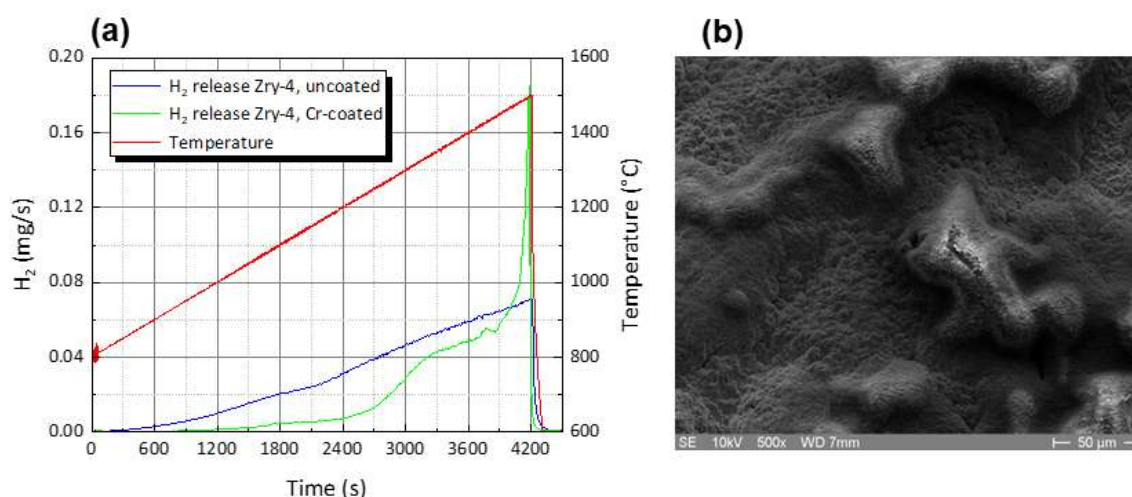


FIG. 4. Transient oxidation tests from 800 to 1500°C in steam with cold spraying Cr-coated and uncoated zirconium (a) hydrogen release rate (b) surface SEM image of coated zirconium after test.

3.2.2. Cr₂AlC coated Zr alloys

Cr₂AlC belongs to a family of layered, ternary compounds known as MAX Phases. It possesses excellent high temperature oxidation resistance and self-healing capability via fast growth of an alumina scale. As can be seen in Fig. 5, a thin and dense alumina layer formed on the surface of the Cr₂AlC coating after oxidation at 1000°C in steam for 1 h, which protects the coating and the substrate from fast oxidation.

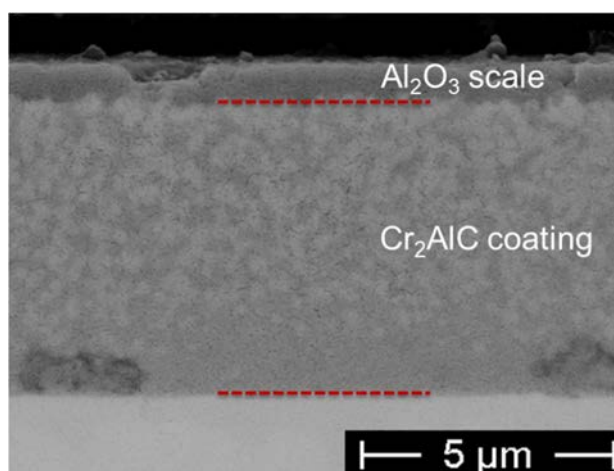


FIG. 5. Cross sectional SEM image of Cr₂AlC coated zirconium after oxidation at 1000°C in steam for 1 h.

Figure 6 shows the hydrogen release rate and cross sectional SEM images of the Cr₂AlC coated and uncoated Zircaloy-4 during transient oxidation tests from 500 to 1400°C in steam. For the coated sample, the hydrogen release rate first increased slowly with the increasing of the oxidation temperature. The slope of the curve changed and became much steeper at temperature \approx 1260°C. The hydrogen release rate of the coated sample then surpassed the uncoated one at around 1300°C. Combined with the cross sectional SEM image, it can be deduced that the coatings cracked, and steam penetrated the unoxidized substrate, as shown in Fig. 6c. The uncoated Zircaloy-4 formed a uniform ZrO₂ layer on top as seen in Fig. 6(b). In comparison, oxidation of the coated sample finally led to the growth of a non-uniform oxide scale and thicker oxide layer was observed beneath the cracks. The thickness of the oxide scale was still much thinner than that on uncoated sample. It is necessary to point out that no liquid

phase was found for the Cr_2AlC coated sample up to 1400°C . The ceramic materials as coating can increase the eutectic reaction temperature between the coating and substrate.

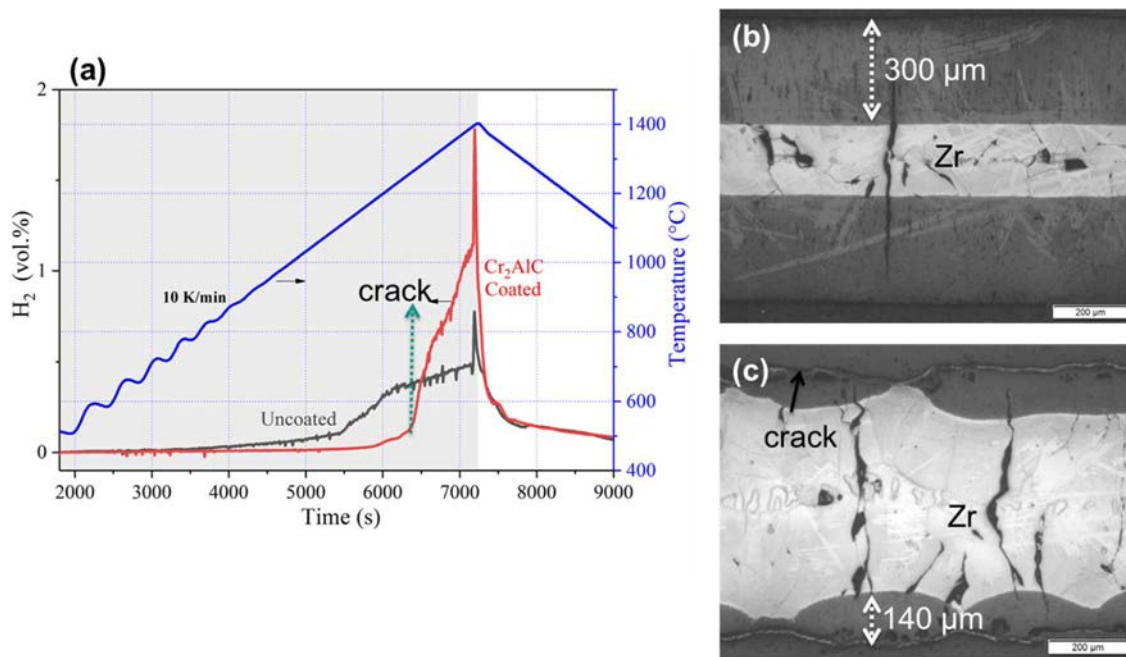


FIG. 6. Transient oxidation tests from 500 to 1400°C in steam with Cr_2AlC coated and uncoated Zircaloy-4 (a) hydrogen release rate, cross sectional SEM image of (b) uncoated and (c) coated zircaloy after test.

4. CONCLUSIONS

The oxidation performance and failure behaviour of one type of monolithic ATF cladding (FeCrAl alloys) and two coated Zr alloys (Cr coated and Cr_2AlC coated) in high temperature steam extended to severe accident scenarios were investigated. Catastrophic oxidation, i.e. rapid and complete consumption of the FeCrAl alloy, can be triggered above 1200°C in case of fast heating during transient tests in steam. The lack of the pre-oxidized alumina scale declines the maximum tolerance temperature of the alloys to high temperature steam. Cr and Cr_2AlC coatings can establish protective Cr_2O_3 and Al_2O_3 scales during high temperature oxidation in steam. Significant inward diffusion of the Cr into the Zr alloy substrate occurred during oxidation at temperatures lower than the Cr-Zr eutectic reaction temperature, which may embrittle the fuel cladding. Formation of liquid phase via eutectic reaction, leading to succeeding fast oxidation rate, dominates the failure feature at temperatures above the Cr-Zr eutectic temperature. The Cr_2AlC ceramic coating formed a protective alumina layer during oxidation, while it cracked more easily at high temperatures. However, no eutectic reaction was found during oxidation up to 1400°C in steam.

ACKNOWLEDGEMENTS

This work was sponsored by the HGF programme NUSAFE at Karlsruhe Institute of Technology. C. Tang appreciates the fellowship supported by the China Scholarship Council (CSC) during his PhD. The authors thank Koroush Shirvan from MIT, USA for providing the cold spraying Cr coated samples and U. Stegmaier and P. Severloh for support during experiments.

REFERENCES

- [1] ZINKLE, S.J., TERRANI, K.A., GEHIN, J.C., OTT, L.J., SNEAD, L.L., Accident tolerant fuels for LWRs: A perspective, *J. Nucl. Mater.* **448** (2014) 374–379.
- [2] TERRANI, K., Accident tolerant fuel cladding development: Promise, status, and challenges, *J. Nucl. Mater.* **501** (2018) 13–30.
- [3] TANG, C., STUEBER, M., SEIFERT, H.J., STEINBRUECK, M., Protective coatings on zirconium based alloys as accident-tolerant fuel (ATF) claddings, *Corros. Rev.* **35** (2017) 141–166.

- [4] BRAGG-SITTON, S., Development of advanced accident-tolerant fuels for commercial LWRs, *Nucl. News*. **53** (2014) 83–91.
- [5] BISCHOFF, J., DELAFOY, C., VAUGLIN, C., BARBERIS, P., ROUBEYRIE, C., PERCHE, D., et al., AREVA NP's enhanced accident-tolerant fuel developments: Focus on Cr-coated M5 cladding, *Nucl. Eng. Technol.* **50** (2018) 223–228.
- [6] TANG, C., GROSSE, M.K., TRTIK, P., STEINBRÜCK, M., STÜBER, M., SEIFERT, H.J., H₂ permeation behavior of Cr₂AlC and Ti₂AlC MAX phase coated Zircaloy-4 by neutron radiography, *Acta Polytech.* **58** (2018) 69–76.
- [7] TANG, C., STEINBRUECK, M., STUEBER, M., GROSSE, M., YU, X., ULRICH, S., et al., Deposition, characterization and high temperature steam oxidation behavior of single-phase Ti₂AlC-coated Zircaloy-4, *Corros. Sci.* **135** (2018) 87–98.
- [8] TANG, C., KLIMENKOV, M., JAENTSCH, U., LEISTE, H., RINKE, M., ULRICH, S., et al., Synthesis and characterization of Ti₂AlC coatings by magnetron sputtering from three elemental targets and ex-situ annealing, *Surf. Coatings Technol.* **309** (2017) 445–455.
- [9] TANG, C., JIANU, A., STEINBRUECK, M., GROSSE, M., WEISENBURGER, A., SEIFERT, H.J., Influence of composition and heating schedules on compatibility of FeCrAl alloys with high temperature steam, *J. Nucl. Mater.* **511** (2018) 496–507.
- [10] DRYEPONDT, S., UNOCIC, K.A., HOELZER, D.T., MASSEY, C.P., PINT, B.A., Development of low-Cr ODS FeCrAl alloys for accident-tolerant fuel cladding, *J. Nucl. Mater.* **501** (2018) 59–71.
- [11] KREJCI, J., SEVECEK, M., KABÁTOVÁ, J., MANOCH, F., KOČÍ, J., CVRČEK, L., et al., Experimental behavior of chromium-based coatings, in: *TopFuel* (2018) 1–14.

FUEL PERFORMANCE CODES APPLIED TO DESIGN BASIS ACCIDENTS (DBA)
AND TO DESIGN EXTENSION CONDITIONS (DEC)

(Session 3)

Chairperson

A. BOULORÉ

France

ASSESSMENT OF HIGH CONDUCTIVITY CERAMIC FUEL CONCEPT UNDER NORMAL AND ACCIDENT CONDITIONS

D.S. GOMES, A. ABE, A.T. SILVA, R.O.R. MUNIZ
Nuclear and Energy Research Institute–IPEN/CNEN, Nuclear Engineering Center–CEN,
Av. Prof. Lineu Prestes 2242, São Paulo, SP, Brazil,

C. GIOVEDI, M.R. MARTINS,
LabRisco, University of São Paulo,
Av. Prof. Mello Moraes 2231, São Paulo, SP, Brazil.

Abstract

After the Fukushima Daiichi accident, the high conductivity ceramic concept fuel has been revisited. The thermal conductivity of uranium dioxide used as nuclear fuel is relatively low, as consequence fuel pellet centerline reaches high temperatures, high fission gas release rate, increase of fuel rod internal pressure reducing the safety thermal margin. Several investigations had been conducted in framework of ATF (Accident Tolerant Fuel) using different additives in ceramic fuel (UO_2) in order to enhance thermal conductivity in uranium dioxide pellets. The increase of the thermal conductivity of fuel can reduce the pellet centerline temperature, consequently less fission gas releasing rate and the low risk of fuel melting, hence improving significantly fuel performance under accident conditions. The beryllium oxide (BeO) has high conductivity among other ceramics and is quite compatible with UO_2 up to 2200°C , at which temperature it forms a eutectic. Moreover, it is compatible with zircaloy cladding, does not react with water, has a good neutronic characteristics (low neutron absorption cross-section, neutron moderation). This work presents a preliminary assessment of high conductivity ceramic concept fuel considering UO_2 - BeO mixed oxide fuel containing 10 wt% of BeO . The FRAPCON and FRAPTRAN fuel performance codes were conveniently adapted to support the evaluation of UO_2 - BeO mixed oxide fuel. The thermal and mechanical properties were modified in the codes for a proper and representative simulation of the fuel performance. The obtained preliminary results show lower fuel centerline temperatures when compared to standard UO_2 fuel, consequently promoting enhancement of safety margins during the operational condition and under LOCA accident scenario.

1. INTRODUCTION

The uranium dioxide has been used as nuclear fuel for pressurized and boiling water reactors (PWR and BWR) for a long time with an outstanding performance. Nonetheless, the research for accident tolerant fuels (ATF) as a consequence of the Fukushima Daiichi accident brought the necessity to improve the performance of nuclear fuels aiming to develop fuels which present enhanced accident tolerance in comparison with the standard and existing UO_2 /zircaloy system widely used by the nuclear industry [1]. Nowadays, a significant effort has been conducted in the cladding material research and investigation in order to accomplish the ATF criteria such as corrosion resistance, good mechanical properties, lower hydrogen generation etc. Additionally, the performance can be improved considering the fuel pellet itself, specially enhancing the thermal conductivity and reducing fission gas release.

The low thermal conductivity of uranium dioxide used as nuclear fuel in PWR induces a high fuel pellet centerline temperature, stores energy consequently reducing the safety thermal margins during steady state irradiation, transients, and under accident scenarios, as for instance loss-of-coolant accident (LOCA). Due to the poor thermal conductivity of UO_2 , the high fuel centerline temperature in the pellet promotes different phenomena such as high fission gas release, steep temperature gradient resulting in high thermal stress, increase of the fuel pellet swelling, plastic deformation, cracking, anticipation of pellet cladding mechanical interaction occurrence, and consequently reduction of operational safety limit. In this sense, the increase of the uranium dioxide thermal conductivity by means of the use of specific additives to the fuel matrix can reduce the fuel centerline temperature, consequently the amount of fission gas release would be lower, less thermal stress, less swelling and deformation allowing high burnup and enabling improved safety due to less stored energy.

In the last decades several investigations have been conducted in order to enhance the thermal conductivity of the fuel pellet and one of the promising techniques is associated to doping the UO_2 pellet with high conductivity additive. The beryllium oxide (BeO) have shown as good candidate due to its high thermal conductivity among oxides, high melting point, low neutron thermal absorption cross section, easily fabricated without significant impacts in the conventional manufacturing process with an acceptable fuel cost. Additionally, to enhancing thermal

conductivity, beryllium oxide presents a large stability and chemical compatibility with uranium at high temperatures as well as some neutron moderation capacity.

In order to perform a preliminary assessment of the effect of the BeO addition to enhance the nuclear fuel behaviour, it was necessary to include the relevant properties, mainly the thermal conductivity into the FRAPCON and FRAPTRAN fuel performance codes.

2. METHODOLOGY

2.1. Modelling Thermal and Mechanical Properties of UO₂ with BeO addition

In the present paper, initially the necessary materials properties to be changed were identified considering the MATPRO (Material Properties Data Library) existing materials properties for fuel pellet correlated directly to temperature and a preliminary literature survey was conducted in order to assess the existing information about Be (beryllium) and BeO (beryllium oxide), especially those related to thermal properties. Moreover, information regarding fabrication process in order to verify the feasible amount of beryllium oxide to be mixed to the UO₂ matrix [2–4]. As begin of assessment it was defined the enhanced fuel pellet with following composition: 10% of BeO and 90% of UO₂ in volume fractions, giving almost 3.10% of BeO in weight percent (wt%).

In order to define the new material properties correlations to be applied in the modified versions of the codes, the first step consists in establish the weight fraction of each fuel pellet component contribution, according to following expressions [5]:

$$\omega_1 = \frac{v_1 \cdot \rho_1}{v_1 \cdot \rho_1 + v_2 \cdot \rho_2} \quad (1)$$

$$\omega_2 = \frac{v_2 \cdot \rho_2}{v_1 \cdot \rho_1 + v_2 \cdot \rho_2} \quad (2)$$

where v_i are the volume fractions, ρ_i are the densities and ω_i are the mass fractions of the two components.

2.1.1. Thermal Conductivity UO₂-BeO

The thermal conductivity of UO₂ pellet usually is a function of burnup, temperature, porosity, theoretical density, and radiation damages due to change in the crystalline network or irradiation defects. The thermal conductivity of UO₂, 8.4 W·m⁻¹·K⁻¹, is significantly lower than that of BeO, 260 W·m⁻¹·K⁻¹, at room temperature. Two type of correlations were considered before implementation in the FRAPCON code, the analytical model proposed by D. Chandramouliand S. T. Revankar [7–9] and experimental correlations [10, 11] presented by HALDEN (Norway) and Nippon Nuclear Fuel Development Co., Ltd (Japan). The thermal conductivity of the UO₂-BeO proposed in this work is a fitting curve of existing data considering a given BeO composition (10%) in the fuel, this fitting curve became function only of temperature according to following expression:

$$K_{UO_2-B} = 3348 T^{-0.928} \quad (3)$$

where K_{UO_2-B} is the UO₂-BeO fuel pellet thermal conductivity in W·m⁻¹·K⁻¹, and T is the temperature in Kelvin unit, the function was implemented in subroutine FTHCON of FRAPCON code.

2.1.2. Specific Heat Capacity

The heat capacity of UO₂-BeO fuel pellet is given by the straightforward result of weight fraction applied to both oxides specific heat capacities UO₂ [13] and BeO [9, 12]:

$$Cp_{UO_2-BeO} = \omega_{UO_2} \times Cp_{UO_2} + \omega_{BeO} \times Cp_{BeO} \quad (4)$$

where:

$$Cp_{BeO} = 0.036 \left(\frac{T-650}{360} \right)^3 - 0.12 \left(\frac{T-650}{360} \right)^2 + 0.2 \left(\frac{T-650}{360} \right) + 1.9 \quad (5)$$

Cp_{UO_2} was considered in equation 2.2-1 from [13].

The function above was implemented in subroutine FCP of FRAPCON code.

2.1.3. Enthalpy

The enthalpy of UO₂-BeO fuel pellet is given by the straightforward result of weight fraction applied to both oxides enthalpies as presented below [7] and the function was implemented in subroutine FENTHL:

$$H_{UO_2-BeO} = \omega_{UO_2} \times H_{UO_2} + \omega_{BeO} \times H_{BeO} \quad (6)$$

$$H_{BeO} = 11.1084 + 7.1245 \cdot 10^{-4} T^2 + \frac{840705}{T} - \frac{53124500}{T^2} - 5453.21 \quad (7)$$

H_{UO_2} was considered in equation 2.2-2 from [13].

2.1.4. Melting Point and Heat of Fusion

The melting temperature of UO₂ pellet is 3113 K and its heat of fusion is 2.74×10^5 J/kg [6, 15]; for UO₂-BeO fuel pellet, these values are 3104 K and 3.19×10^5 J/kg [7], respectively.

2.1.5. Thermal Expansion

Based on the weight fraction presented above, the thermal expansion of the UO₂-BeO fuel pellet is given by the following straightforward expression [7]:

$$\frac{\Delta L}{L}_{UO_2-BeO} = \omega_{UO_2} \times \frac{\Delta L}{L}_{UO_2} + \omega_{BeO} \times \frac{\Delta L}{L}_{BeO} \quad (8)$$

The function was implemented in subroutine FTHEXP of FRAPCON code.

2.1.6. Mechanical Properties

The main mechanical properties for the UO₂-BeO fuel pellet are obtained using volume fraction of each component to calculate following properties: Young modulus, Shear modulus, Poisson coefficient, and strength, as presented below [14]:

$$\rho_{UO_2-BeO} = \omega_{UO_2} \times \rho_{UO_2} + \omega_{BeO} \times \rho_{BeO} \quad (9)$$

$$\nu_{UO_2-BeO} = \omega_{UO_2-BeO} \times \rho_{UO_2-BeO} \quad (10)$$

Then, the mechanical properties for the UO₂-BeO fuel pellet are given by the following straightforward expressions:

$$Y_{UO_2-BeO} = \nu_{UO_2} \times Y_{UO_2} + \nu_{BeO} \times Y_{BeO} \quad (11)$$

$$Shear_{UO_2-BeO} = \nu_{UO_2} \times Shear_{UO_2} + \nu_{BeO} \times Shear_{BeO} \quad (12)$$

$$Poisson_{UO_2-BeO} = \nu_{UO_2} \times Poisson_{UO_2} + \nu_{BeO} \times Poisson_{BeO} \quad (13)$$

2.2. Fuel Performance Codes

The well-known FRAPCON and FRAPTRAN [15] codes, sponsored by the United States Nuclear Regulatory Commission (U.S. NRC) for the licensing of PWR and BWR nuclear power plants, were conveniently modified to support the evaluation of BeO/UO₂ mixed oxide fuel containing 10 wt% of beryllium oxide. The FRAPCON and FRAPTRAN codes have a material data package compilation, namely MATPRO [6], which contains material properties, theoretical and experimental models and correlations considered in the simulation of the fuel performance. The implemented modifications mainly addressed the role of the BeO to enhance the thermal conductivity of the fuel pellet. The modifications of the previously identified subroutines related to UO₂-BeO fuel pellet properties in the fuel performance codes were carried out considering step by step manner in order to assess the contribution of each property to the final fuel global performance. The first modified subroutine was related to the thermal conductivity property, after following by the specific heat, the enthalpy, and finally, the mechanical properties. For each property modification, new versions of the codes were generated and tests were carefully performed. The verification of implemented modification was conducted by means of LOCA experiment (IFA 650-5) performed in HALDEN. It is worthwhile to mention that similar work [7] exist but consider only

FRAPTRAN code modification for UO_2 -BeO as fuel in the LOCA condition, this work considers modification on both codes: FRAPCON and FRAPTRAN to consider the LOCA analysis.

2.3. Fuel Rod Analysis (Test Case: IFA 650-5)

The modified version of the codes (FRAPCON and FRAPTRAN) was evaluated using as test case, the data available in the open literature related to the experiment IFA 650-5 performed in the framework of Halden Reactor Project [16] to study the behaviour of UO_2 /zircaloy fuel rod under LOCA scenario.

The IFA 650-5 test fuel rod was re-fabricated from an irradiated PWR UO_2 /Zircaloy-4 fuel rod. The fuel had a high average burnup of 83 MWd/kgU. The base irradiation of the full-length rod comprised 6 reactor cycles corresponding to about 2000 effective full power days. The properties of the IFA-650.5 fuel rod are summarized in Table 1 below. Initially, steady state condition was simulated using FRAPCON code for UO_2 and UO_2 -BeO.

TABLE 1. FUEL ROD PROPERTIES OF IFA 650-5 TEST FUEL ROD

Fuel type	PWR
Fuel material	UO_2
Fuel pellet diameter (mm)	9.132
Fuel pellet length (mm)	11
Fuel dish depth (mm)	0.28
Fuel dish width (mm)	1.2
Fuel density (% TD)	94.8
Fuel enrichment (w/o %)	3.5
Cladding material	DX ELS0.8b
Cladding outer diameter (mm)	10.735
Cladding wall thickness (mm)	0.721
Fuel rod burnup (MWd/kgU)	83
Fuel rod total length (mm)	480
Fuel rod gap (mm)	0.0805
Fuel Rod plenum volume (cm ³)	15
Fuel rod fill gas	90% Ar +10%He
Fill pressure (MPa)	4.0

2.4. Results and Discussion

The Figs 1, 2 and 3 present the evolution of the fuel centerline temperature, the internal pressure, and the fission gas release as function of burnup for IFA 650-5 considering UO_2 fuel pellet as reference and enhanced fuel UO_2 -BeO pellet. For UO_2 -BeO fuel pellet, the results are shown according to the modified properties into correspondent subroutines.

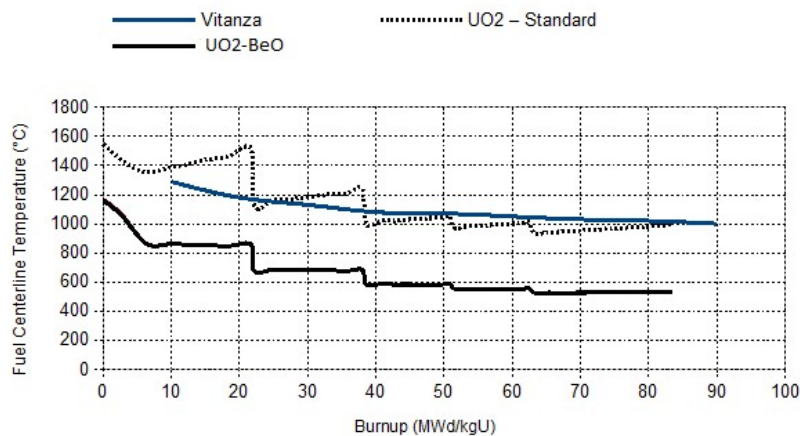


FIG. 1. Fuel centerline temperature for IFA 650-5 as function of burnup for reference UO_2 fuel pellet and UO_2 -BeO fuel pellet using FRAPCON codes (original and modified version) for steady state condition (burnup accumulation).

Figure 1 shows that the fuel centerline temperature is about 500°C lower for UO₂-BeO fuel pellet compared to the reference UO₂ fuel pellet. The figure also shows that the governing property in the fuel pellet behaviour is mainly due to the thermal conductivity; the modification of the other subroutines related to other properties (specific enthalpy, specific heat and mechanical) does not promote significantly changes in the fuel pellet centerline temperature. The result confirms that thermal conductivity plays a very important role in the fuel temperature profile.

The Figure 1 additionally presents the Vitanza threshold [17] curve which is associated to fission gas release rate due to the fuel centerline temperature. As it can be seen from the Vitanza curve, the fission gas release for UO₂-BeO fuel pellet do not exceed the threshold, consequently the dominant phenomena governing the fission gas release process will be athermal up to approximately 40 MWd/kgU.

The evolution of the internal fuel rod pressure as function of burnup for IFA 650-5 presented in Figure 2 show that the internal pressure for the fuel rod with UO₂-BeO fuel pellet is lower than that observed for the reference UO₂ fuel pellet during all the irradiation period, even considering the high burnup reached during the steady state irradiation of the fuel rod.

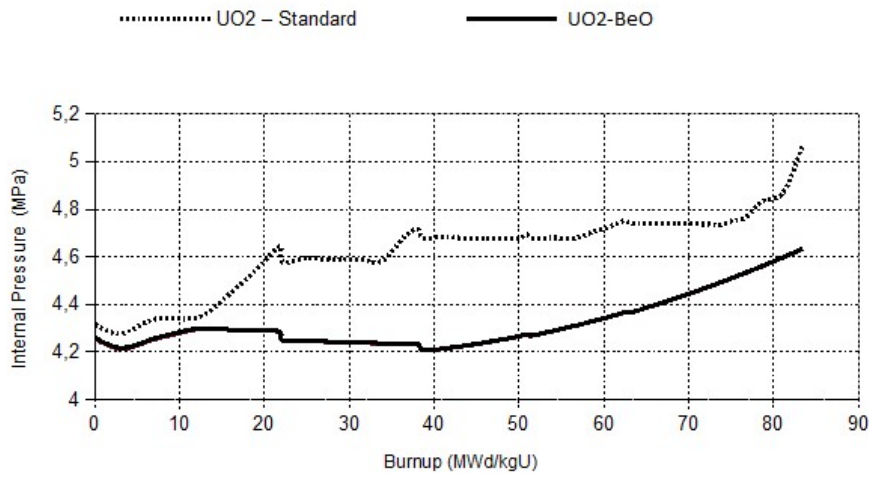


FIG. 2. Internal fuel rod pressure for IFA 650-5 as function of burnup for reference UO₂ fuel pellet and UO₂-BeO fuel pellet using FRAPCON codes (original and modified version) for steady state condition (burnup accumulation).

The evolution of the fission gas release as function of burnup presented in Figure 3 show that the amount of fission gas released by UO₂-BeO fuel pellet is significantly lower than that of the reference UO₂ fuel pellet. Then, the lower temperatures experienced by the UO₂-BeO fuel pellet during the entire irradiation period enable the fuel centerline temperature not to exceed the Vitanza threshold.

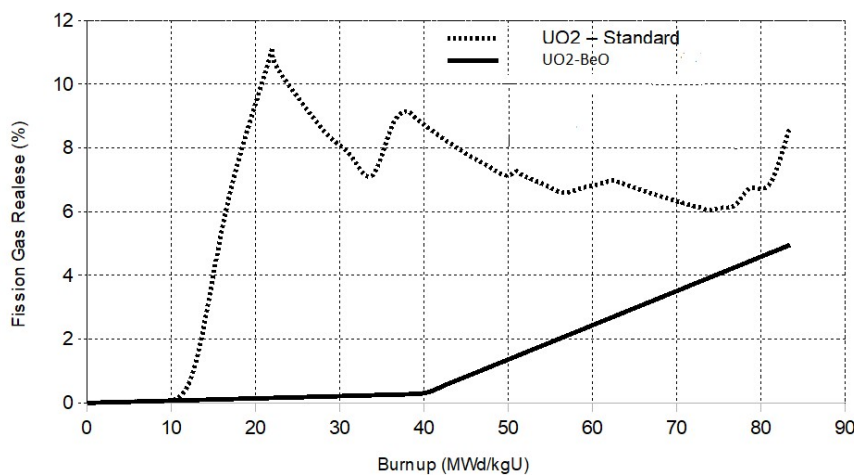


FIG. 3. Fission gas release for IFA 650-5 as function of burnup for reference UO₂ fuel pellet and UO₂-BeO fuel pellet using FRAPCON codes (original and modified versions) for steady state condition (burnup accumulation).

Figure 4 shows the evolution of the internal fuel rod pressure as function of time during the LOCA transient. Initially, this assessment was performed using coupled simulation (FRAPCON and FRAPTRAN), the original version of FRAPCON and FRAPTRAN codes for the reference UO_2 fuel pellet and, for UO_2 -BeO, the modified versions of FRAPCON and FRAPTRAN codes taking into account new properties implementation. Moreover, the steady state condition simulated using modified FRAPCON and original version of FRAPTRAN in order to verify the consistency of FRAPTRAN modification. The curves in the figure show a slight increase of the cladding rupture time for the UO_2 -BeO fuel pellet. The possible reason for a slight improvement shall be associated to temperature boundary condition considered in the FRAPTRAN input, which is conservative assumption considering the previous results (Figure 1) of fuel temperature. Again, it is worthwhile to note the importance of results presented by modified FRAPCON compared to the results obtained from modified FRAPTRAN in order to evaluate the effects of the BeO addition in the global fuel performance during steady state irradiation prior to LOCA scenario.

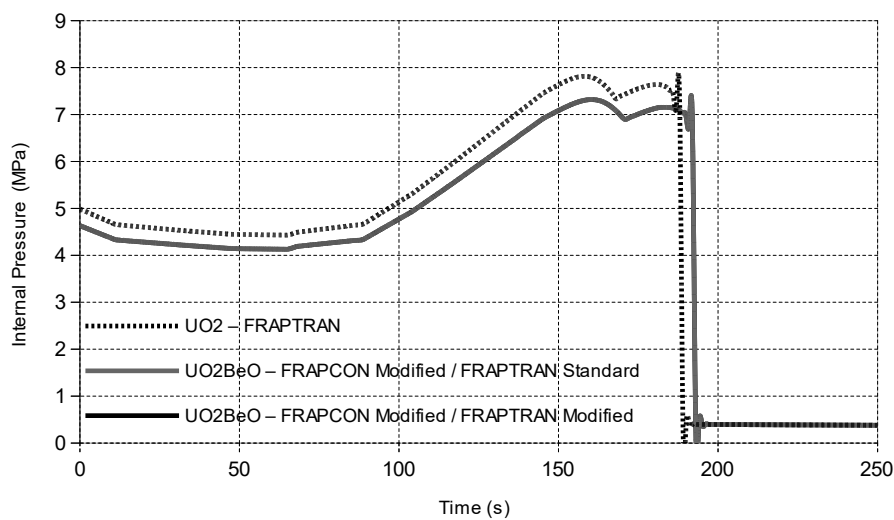


FIG. 4. Internal fuel rod pressure for IFA 650-5 as function of time for reference UO_2 fuel pellet and UO_2 -BeO fuel pellet using FRAPCON-FRAPTRAN codes and the modified versions for LOCA condition.

3. CONCLUSION

All results obtained using modified version of FRAPCON code show an improvement of the parameters directly associated to safety margins, specially the fuel centerline temperature reduction, consequently reduced thermal gradient inside fuel pellet, small amount of fission gas release, lower internal pressure, all effects resulting in the improvement of safety margins during the steady state operational condition. The results of modified FRAPTRAN shown a slight improvement for burst time during the LOCA accident scenario. Some improvement expected for UO_2 -BeO fuel during the LOCA was not clearly achieved mainly due to the assumption of same fuel cladding temperature as boundary condition adopted for both simulations at beginning of transient. Moreover, the future work can address the appropriate cladding temperature profile and the importance of burnup associated to the thermal conductivity degradation and some evaluation of neutronic penalty due to reduction of uranium loading in the UO_2 -BeO fuel pellet.

ACKNOWLEDGMENTS

The authors are grateful to the technical support of AMAZUL, USP and IPEN-CNEN/SP.

REFERENCES

- [1] GOLDNER, F., Development Strategy for Advanced LWR Fuels with Enhanced Accident Tolerance, [http://energy.gov/sites/prod/files/061212%20Goldner%20%20NEAC%20Presentation%20\(FINAL\).pdf](http://energy.gov/sites/prod/files/061212%20Goldner%20%20NEAC%20Presentation%20(FINAL).pdf) (2012).
- [2] NISHIGAKI, S., MAEKAWA, K., Fabrication of BeO- UO_2 Fuel Pellet, *Journal of Nuclear Materials*, **14** (1964) 453-458.

- [3] BEAVER, W.W., THEODORE, J.G., BIELAWSKI, C.A., Effects of Powder Characteristics, Additives and Atmosphere on the Sintering of Sulfate-Derived BeO, *Journal of Nuclear Materials* **14** (1964) 326.
- [4] LI, D.S., GARMESTANI, H., SCHWARTZ, J., Modeling Thermal Conductivity in UO₂ with BeO Additions as a Function of Microstructure, *Journal of Nuclear Materials* **392** (2009) 22.
- [5] SMITH, R. J., Enhanced Thermal Conductivity UO₂-BeO Nuclear Fuel: Neutronic Performance Studies and Economic Analyses, Master Thesis. Texas (2012).
- [6] ALLISON, C.M., et alli., SCDAP/RELAP5/MOD3.1 Code Manual Volume IV: MATPRO - A Library of Materials Properties for Light-Water-Reactor Accident Analysis, NUREG/CR-6150, EGG-2720 Washington (1993).
- [7] CHANDRAMOULI, D., REVANKAR, S.T., Development of Thermal Models and Analysis of UO₂-BeO Fuel during a Loss of Coolant Accident, *International Journal of Nuclear Energy* (2014).
- [8] ZHOU, W., LIU, R., REVANKAR, S.T., UO₂-BeO Composite Fuel Thermal Property and Performance Modeling, *Journal of Energy and Power Engineering* **8** (2014) 7.
- [9] CHANDRAMOULI, D., REVANKAR, S.T., Study of Performances of UO₂-BeO Composted Fuel Using FRAPTRAN, Purdue University School of Nuclear Engineering Report PU/NE-12-16, Purdue University School of Nuclear Engineering (2012).
- [10] ISHIMOTO, S., HIRAI, M., ITO, K., KOREI, Y., Thermal Conductivity of UO₂-BeO Pellet, *Journal of Nuclear Science and Technology* **33** 2 (1996) 134–140.
- [11] MCGRATH, M.A., et. alli., In-reactor Investigation of the composite UO₂-BeO fuel: background, results and perspectives, The Nuclear Materials Conference, Montpellier, France, (2016).
- [12] DOUGLAS, A.C., Thermodynamic Properties of Magnesium Oxide and Beryllium Oxide from 298 to 1200 K, *Journal of Research of the National Bureau of Standards A. Physics and Chemistry* **67A** 4 (1963) 325–329.
- [13] LUSCHER, W.G., GEELHOOD, K.J., Material Properties Correlation: Comparison Between FRAPCON 3.4, FRAPTRAN 1.4 and MATPRO, NUREG/CR-7024, (2010).
- [14] ZHOU, W., and ZHOU, W., Thermophysical and Mechanical Analyses of UO₂-36.4vol % BeO Fuel Pellets with Zircaloy, SiC, and FeCrAl Claddings. *Metals* **8** (2018) 65.
- [15] GEELHOOD, K.J., LUSCHER, W.G., BEYER, C.E., FLANAGAN, M.E., FRAPCON-3.4: A Computer Code for the Calculation of Steady state Thermal mechanical Behavior of Oxide Fuel Rods for High Burnup, U.S.NRC, NUREG/CR-7022, Washington (2011).
- [16] MANNGARD, T., STENGARD, J., Evaluation of the Halden IFA-650 Loss-of- Coolant Accident Experiments 5, 6 and 7, Swedish Radiation Safety Authority, Sweden (2014).
- [17] VITANZA, C., KOLSTAD, E., GRAZIANI, V., Analysis of Fission Gas Release Tests to High Burnup, Proc. ANS Topical Meeting on Light Water Reactor Fuel Performance, Portland, Oregon (1979).

MODELLING OF ACCIDENT SCENARIOS WITH THE FINIX FUEL BEHAVIOUR MODULE

H. LOUKUSA, J. PELTONEN, V. TULKKI
VTT Technical Research Centre of Finland Ltd.
Espoo, Finland

Abstract

The FINIX fuel behaviour module has been under development at VTT for six years for modelling traditional western light water reactor and Russian WWER fuel. The module is designed to be implemented in various other reactor safety analysis tools, such as neutronics and reactor dynamics codes. At VTT, it has been internally coupled with Serpent 2 to provide fuel temperatures for neutronics, and to thermal hydraulics and reactor dynamics codes TRAB1D, TRAB3D and HEXTRAN. FINIX will also be a part of the new VTT reactor analysis framework Kraken, the development of which is currently underway. In such couplings, the fuel temperature distribution is one of the most important parameters passed on to the host code. From the start, FINIX has been able to model the fuel temperature distribution in reactivity insertion accidents (RIA) comparably to established codes such as FRAPTRAN. The irradiated state was typically taken into account with a restart file from FRAPCON. Over the years, additional models have been implemented in the code, and long irradiation periods can now also be modelled with FINIX. The average error in temperature predictions across several Halden irradiations is 6.6%, and FINIX predicts typically 50 to 100 K higher temperatures at the highest temperatures compared to FRAPTRAN. Recently, the ability of FINIX to model loss-of-coolant accidents (LOCA) has been investigated. The main limitation of the current FINIX version is in mechanical modelling, as finite strain deformation cannot be accurately modelled, and the currently implemented failure models are rudimentary. Temperature predictions of FINIX were compared to FRAPTRAN and found to be close to FRAPTRAN until the blowdown phase, at which FINIX overpredicts the temperatures. FINIX LOCA predictions have also been compared to results calculated by FRAPTRAN for the Halden IFA-650.5 LOCA test.

1. INTRODUCTION

The fuel behaviour models in many thermal-hydraulics or neutronics codes are typically based on simple correlations, non-mechanical thermal elements, or even fixed values of temperature. Although they are quick to understand and efficient to solve, such fuel models may be less-than-realistic in, for instance, transient conditions or, in cases where fuel with extended burn-up should be considered.

The FINIX fuel behaviour module has been under development at VTT since 2012 [1], with the latest version published in the beginning of 2019 [2]. The main use of FINIX is in coupling with other core physics codes, and FINIX is to serve as the main fuel model in the upcoming Finnish reactor analysis framework Kraken [3]. The advantages of developing an in-house code are numerous compared to only using codes developed elsewhere. The code is more easily manageable and adapted to different usages. As a self-developed code does not suffer from license limitations, the code is available to academic as well as commercial applications with ease. In addition, code development serves as an interesting project and increases attractiveness of the field for new graduates.

The FINIX code has been designed so that it can be coupled on a source-code level, so that passing input and output files between the codes is not necessary. FINIX includes a collection of built-in functions that can be used for basic setup of the system, and for running the actual simulations, using a fairly high-level syntax. In addition, FINIX has an error message system that can be used to detect beyond-normal operation of the code without aborting programme execution. Because of the direct coupling on a source-code level, FINIX allows for low-level control of its input and output. At VTT, FINIX has already been successfully coupled with the reactor dynamics codes HEXTRAN, TRAB1D and TRAB3D [4] and the Monte Carlo neutronics code Serpent 2 [5].

2. DESCRIPTION OF FINIX

FINIX solves the one dimensional heat equation independently in several axial nodes, with fuel rod internal pressure being equal across these nodes. This approximation is known as the 1.5-dimensional approach and is typically used in fuel performance codes.

The current models are sufficient for simple simulation of reactivity insertion accidents as well as, to some degree, longer irradiation periods. All models necessary for the accurate simulation of loss-of-coolant accidents are not present in FINIX, but in later sections some results calculated by FINIX in these cases are shown. Such

simulations show the current status of FINIX development and serve as guidance to direct future development of the code.

In Table 1, the different FINIX models for physical phenomena and material properties are listed with their respective sources. All FINIX correlations are reported in public sources, and the code contains no proprietary models. It must be noted that not all models are necessary in each coupling, and in coupled application some models should be superseded by the models in the coupled code. For example, the coolant models are not necessary in coupling to thermal hydraulics, and the radial distribution model is not necessary when coupling to neutronics codes.

TABLE 1. SOURCES OF DIFFERENT FINIX MODELS.

FINIX model	Reference
Gap conductance	FRAPTRAN [6], FRAPCON-3.4 [7], FRAPCON-4.0 [8], MATPRO [9]
Cladding heat capacity, thermal conductivity, thermal strain	FRAPTRAN [6]
Cladding Young's modulus, Meyer's hardness, Poisson's ratio	MATPRO [9]
Cladding yield stress	PNNL [10], Shestopalov et al. [11]
Cladding creep	Limbäck and Andersson [12], FRAPCON [8]
Cladding failure model	Simple overstrain criterion
Cladding oxidation	Steady-state: Dyce [13], Kättö [14], FRAPCON [8]; transient: Baker-Just [15]
Cladding oxide heat capacity	NIST-JANAF [16]
Cladding oxide thermal conductivity	MATPRO [9]
Fission gas release	Modified Forsberg-Masih [17, 18], modified SIFGRS [19]
Coolant heat transfer	Dittus-Boelter [20], Jens-Lottes [21]
Coolant properties	Liquid water: IAPWS-IF97 [22]
Radial power distribution	TUBRNP [23]
Pellet heat capacity, thermal conductivity and thermal strain	FRAPTRAN [6], MATPRO [9]
Pellet relocation	FRAPCON [7]
Pellet swelling and densification	FRAPCON [7], MATPRO [9], SIFGRS [19]
Pellet densification	MATPRO [9]
Pellet grain growth	Ainscough [24]

3. VALIDATION

FINIX temperature, FGR and oxidation predictions have been validated against experimental data [25]. At the current development stage, the FINIX temperature predictions are very accurate. On average, FINIX temperature predictions are within 6.6% of experimental data, which corresponds to an average absolute error of 70 K, see Fig. 1. However, high fission gas releases are generally underpredicted, as can be seen from Fig. 2.

Data from Halden tests IFA-515, -677 and -681 has been used in the temperature validation (see Table 2). In IFA-515 rods A1 and B1 and IFA-681 rod 5, the temperature was measured with an expansion thermometer, and this value was compared with the average fuel centreline temperature calculated by FINIX. In the rest of the rods, the data was obtained from thermocouples and the fuel centreline temperature at the axial node containing the thermocouple was used in the comparison. In the fission gas release validation, both Halden results and data from the OECD/NEA IFPE database have been used.

TABLE 2. HALDEN IRRADIATIONS USED IN THE TEMPERATURE VALIDATION OF FINIX.

Rod	Clad type	Burnup at EOL (MWd·kgU ⁻¹)
IFA-515.10 rA1	Zry-2	86.4
IFA-515.10 rB1	Zry-2	95.4
IFA-677.1 r2	Zry-4	29.7
IFA-681 r1	Zry-4	41.1
IFA-681 r5	Zry-4	40

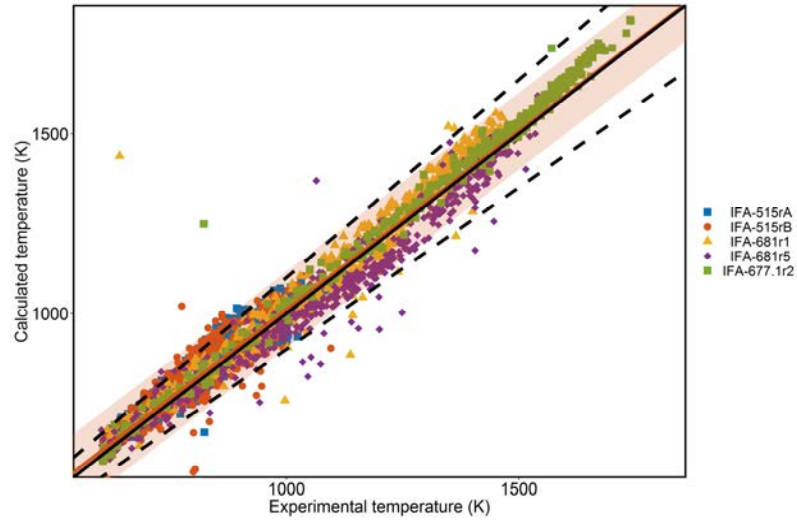


FIG. 1. FINIX steady state temperature predictions compared to experimental data from Halden, where the black diagonal line corresponds to calculated temperature being equal with the measured temperature. The red line is a linear regression line fitted to all of the data, and the red shaded area is the prediction interval. Black dashed lines correspond to 10% deviations from the experimental values.

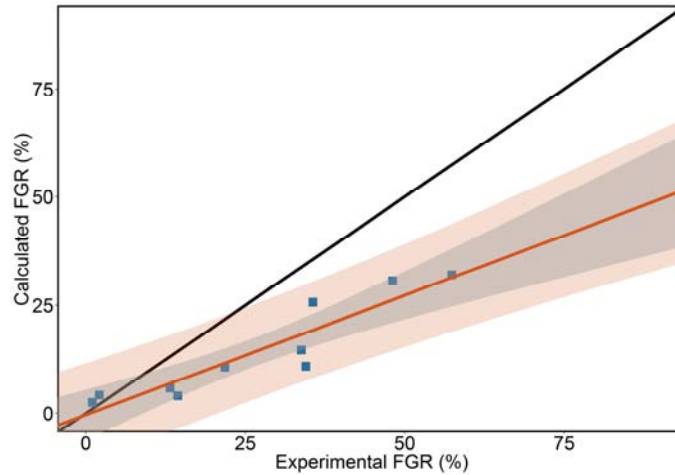


FIG. 2. FINIX FGR predictions compared to experimental data, where the black diagonal line corresponds to calculated FGR being equal with the measured FGR. The red shaded area is the prediction interval, and the darker shade within it the confidence interval of the mean.

4. MODELLING OF REACTIVITY INSERTION ACCIDENTS

From the beginning, the capability of FINIX to model fuel temperature in RIAs has been good [26]. FINIX predictions in RIA cases have been verified against FRAPTRAN, and for the most part the FINIX results are comparable to those calculated with FRAPTRAN. Currently, the main differences between the two codes relate to the pellet thermal expansion in RIAs, cladding mechanical behaviour, rod internal pressure and plenum temperature.

Results from two RIA tests, calculated with both the FINIX and FRAPTRAN codes are shown below. The first results are from the simulation of the CABRI REP-Na3 test, and the other from the BGR RT-8 test. The details of these tests are presented in Table 3.

TABLE 3. RIA VERIFICATION CASES OF FINIX PRESENTED IN THIS ARTICLE.

Base irradiation	Transient reactor	Rod	Rod type	Burnup at EOL (MWd·kgU ⁻¹)	Pulse width (ms)
Gravelines-5	CABRI	Na-3	PWR 17×17	53.8	9.5
Kolskaya	BGR	RT-8	WWER-440	60	3

The pellet cladding gap conductance calculation requires the determination of the effective gap width. The same correlation for the effective gap width is used in both FINIX and in FRAPTRAN. The use of this correlation has been found to yield best results in the temperature validation. The results of the two codes for the gap conductance are also very similar until the power pulse. As the gap reopens in FRAPTRAN but not in FINIX, the FINIX gap conductances also remain higher than the respective values calculated by FRAPTRAN.

The main difference in the mechanical solution regarding the gap width in RIAs is the pellet thermal expansion model. In FRAPTRAN, a special model taking into account the radial expansion due to circumferential strain is present, which increases pellet radial expansion in a RIA. The effect of this model was investigated, and for example in the CABRI REP-Na3 case the gap does not reopen in FRAPTRAN if this model is turned off. The cladding stress and strain behaviours are very similar between FINIX and FRAPTRAN without the RIA pellet thermal expansion model. (see Fig. 3.)

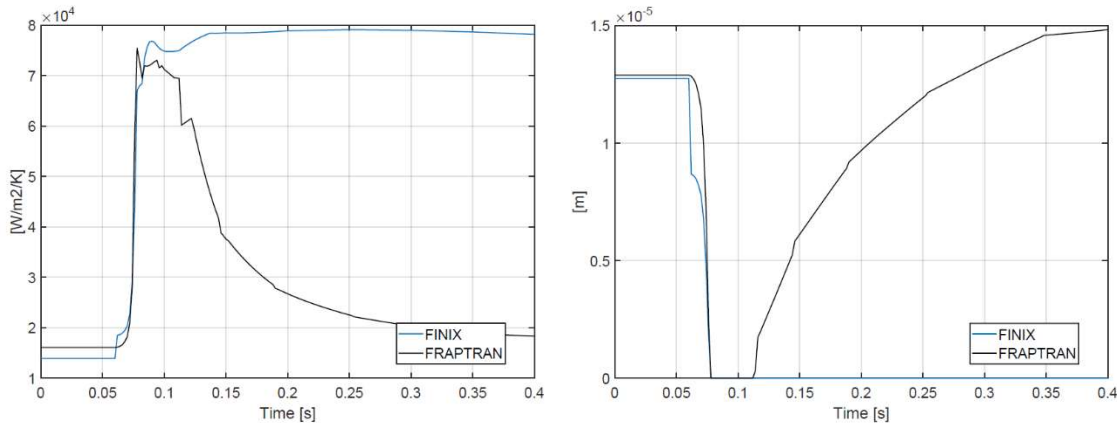


FIG 3. Gap heat transfer coefficient (left) and pellet cladding gap width (right) in the CABRI REP-Na3 case.

The behaviour of the pellet cladding gap is also evident from the cladding hoop stress predictions between the two codes. (see Fig. 4.) As the gap reopens in FRAPTRAN but does not do so in FINIX, the FINIX cladding hoop stress predictions are consistently higher for the remainder of the simulation after the power pulse. The peak of the cladding hoop stress occurs in both codes at the time of the power pulse.

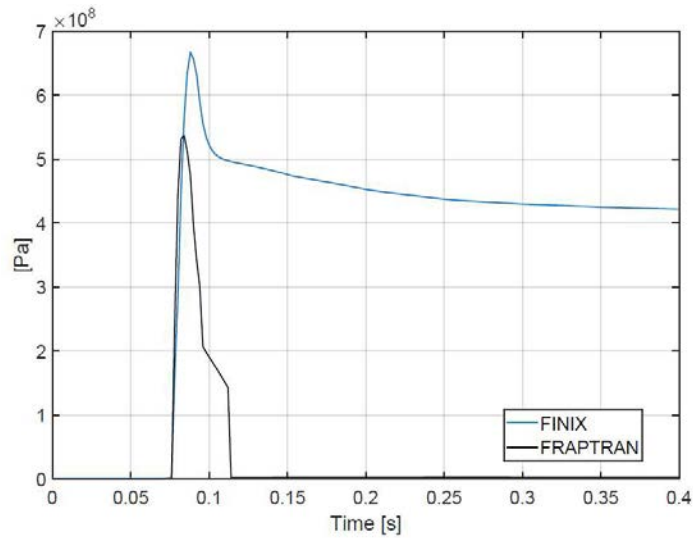


FIG. 4. Cladding hoop stress in the CABRI REP-Na3 case.

The fuel centerline temperatures in RIAs are typically slightly overpredicted in FINIX compared to FRAPTRAN. The Figure 5 shows a very typical result, where the difference in centerline temperature is in the range of 50 to 100 K.

The pellet cladding gap width in the BGR RT-8 case is calculated very similarly in FINIX and FRAPTRAN. As can be seen from the rod internal pressure in Figure 6, the cladding failure occurs at slightly after 0.4 seconds, and this is seen as a bump in the pellet cladding gap width. A similar bump is observed also in FRAPTRAN; however, no cladding failure was observed in FRAPTRAN.

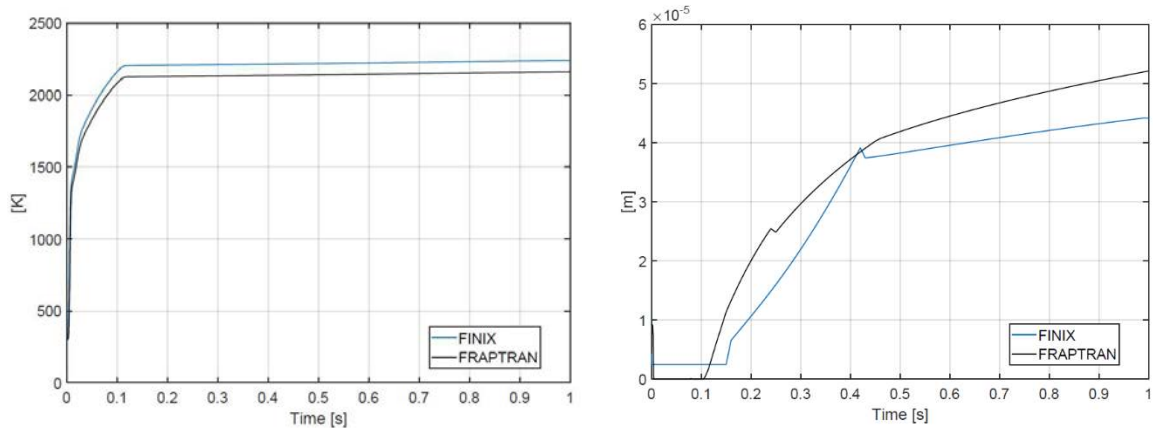


FIG. 5. Fuel centerline temperature (left) and pellet cladding gap width (right) in the BGR RT-8 RIA case.

The pellet surface temperatures between the codes show similar behaviour, although FINIX predicts slightly lower temperatures. The rod internal pressure is first calculated by FINIX to be considerably higher than in FRAPTRAN, and subsequently a cladding failure occurs. The cladding failure is observed from the Figure 6 as the abrupt drop in internal pressure, as the internal pressure is then set to equal the coolant pressure

The moment of rod failure, evident from the rod internal pressure, is also visible in the pellet surface temperature evolution. At the moment of rod failure, the fill gas composition in the rod is adjusted to consist of water vapor, which has a lower thermal conductivity than the initial fill gas helium. This leads to higher pellet surface temperatures after rod failure.

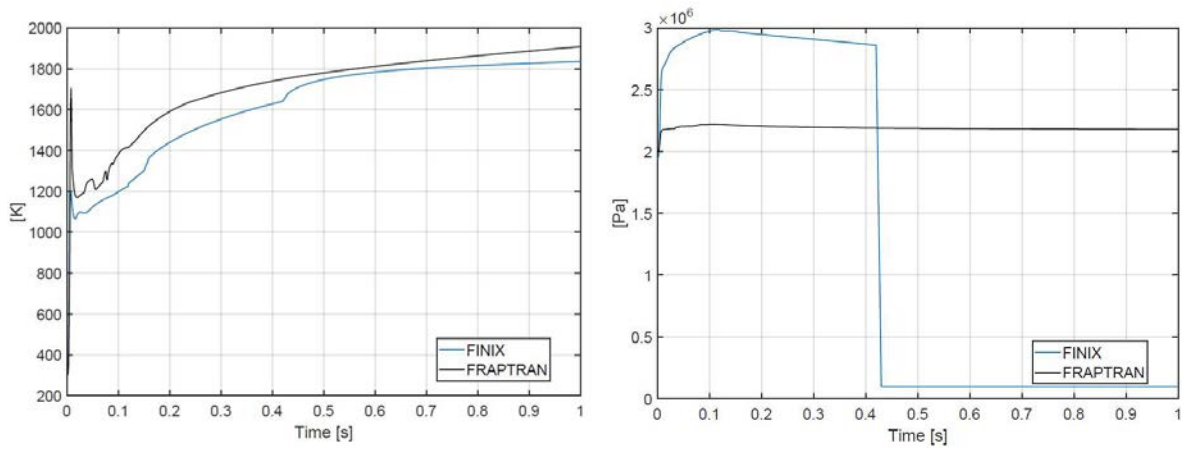


FIG. 6. Pellet surface temperature (left) and rod internal pressure (right) in the BGR RT-8 RIA case.

5. MODELLING OF LOSS-OF-COOLANT ACCIDENTS

FINIX models are limited with regards to modelling LOCAs. For example, FINIX uses the typical infinitesimal strain assumption, which breaks down at finite strains, such as during ballooning in a LOCA. In addition, FINIX cladding failure models are very rudimentary, and currently aid in code convergence rather than prediction of failure time or strain. In an ongoing research project the update of FINIX mechanical modelling is planned.

However, FINIX capabilities with regards to modelling LOCAs were investigated by modelling several Halden LOCA tests from the IFA-650 test series. In the following, some key results calculated for the IFA-650.5 test are shown. The test rod in IFA-650.5 was irradiated up to a burnup of $83 \text{ MWd}\cdot\text{kgU}^{-1}$ in a commercial PWR before the LOCA test at Halden.

The rod internal pressure and cladding hoop stress in FINIX follow similar behaviour than in FRAPTRAN. However, the predictions of FRAPTRAN are peaked higher than those of FINIX, and the failure time in FINIX is slightly later than in FRAPTRAN. The failure time in both figures below (Figs 7(a) and 7(b)) can be seen at the moment where the rod internal pressure drops abruptly to coolant pressure, and when the cladding hoop stress drops to zero.

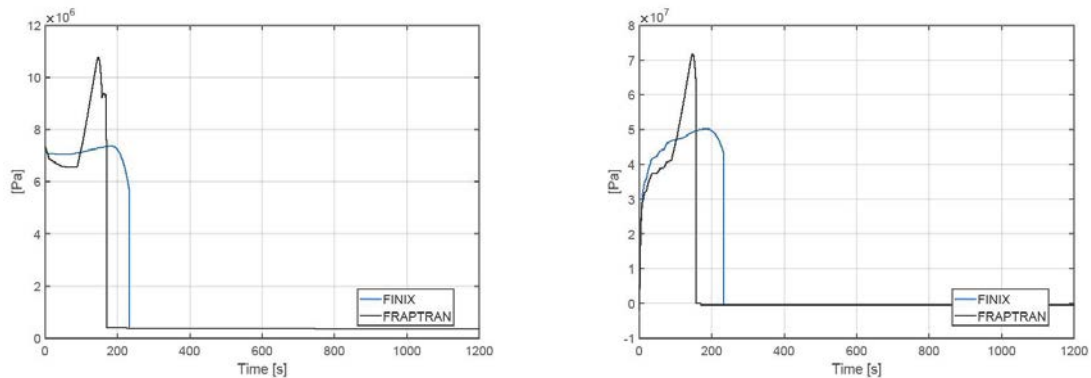


FIG. 7. Rod internal pressure (left) and cladding hoop stress (right) calculated by FINIX compared to FRAPTRAN in the IFA-650.5 LOCA test.

The fuel centerline temperature and pellet cladding gap width were also compared. The gap width in FINIX is calculated to be much larger than in FRAPTRAN. However, even though the difference in Figure 8 is very large, similar behaviour of the gap width is found with FRAPTRAN in other LOCA cases. The large gap width in FINIX also leads to much higher temperatures in FINIX compared to FRAPTRAN. Before the increase in the pellet cladding gap width, the fuel centerline temperatures in FINIX and FRAPTRAN match well.

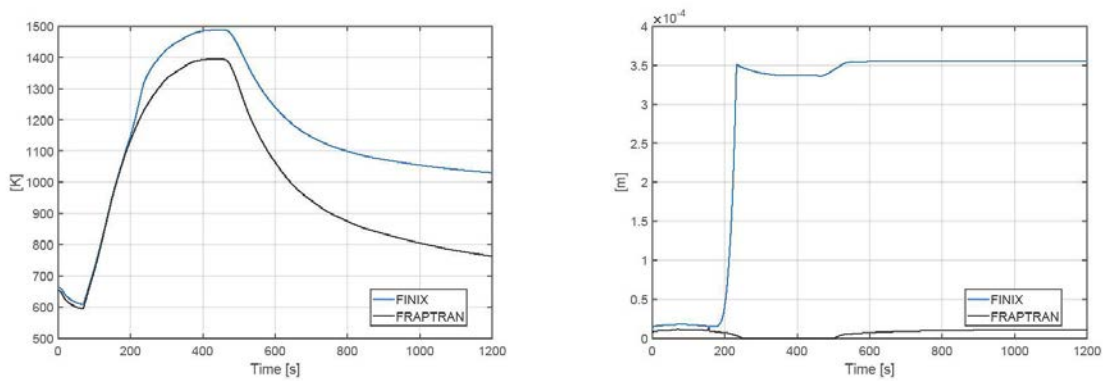


FIG. 8. Fuel centreline temperature (left) and fuel-cladding gap width (right) calculated by FINIX compared to FRAPTRAN in the IFA-650.5 LOCA test.

Cladding elongation was also compared between the two codes, as can be seen from Fig. 9. The reference points for strain differ between the two codes: In FINIX, the reference point of zero strain is the as-fabricated cold state, whereas in FRAPTRAN the reference point is the irradiated cold state. As both codes use a FRAPCON restart file for obtaining the irradiated state parameters, the irradiated state in both codes is the same. The difference in the reference point can be obtained by comparing the as-fabricated cold state parameters to the irradiated state parameters. Correcting for the difference, the cladding elongation results of the two codes are more similar. Before cladding failure, the cladding elongation results perfectly match. After cladding failure, as the failure occurs at a different time and a different strain, the elongation results show the similar behaviour but different absolute values.

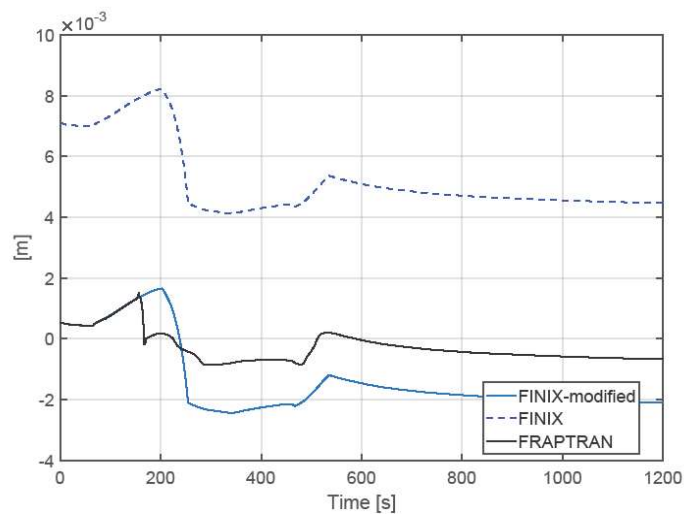


FIG. 9. Cladding elongation in the IFA-650.5 LOCA test with FINIX and FRAPTRAN. The strain reference point used by FINIX is different than in FRAPTRAN, and the solid blue line corresponds to FINIX cladding elongation with the FRAPTRAN reference point.

6. SUMMARY

The FINIX fuel behaviour module has been under development at VTT for several years. Its aim is to provide an easy-to-use fuel performance interface in multiphysics couplings without sacrificing accuracy. The most important parameter to be passed on to other physics solvers is the temperature, which in steady state cases are calculated accurately and in transient scenarios comparably to other, established codes. To be able to perform steady state simulations over long irradiation periods accurately, many of the typical models present in fuel performance codes have been implemented into FINIX, sometimes in some simplified form. The current temperature predictions compared to Halden irradiations are very accurate, with an average relative error of 6.6%.

The FINIX source code in the C programming language is available for OECD/NEA members from the OECD/NEA Data Bank, and the FINIX documentation is available from the VTT research information portal [27].

ACKNOWLEDGEMENTS

FINIX development has been funded by the Finnish Research Programmes on Nuclear Power Plant Safety SAFIR2014 (2011–2014), SAFIR2018 (2015–2018) and SAFIR2022 (2019–2022).

REFERENCES

- [1] IKONEN, T., LOUKUSA, H., SYRJÄLAHTI, E., VALTAVIRTA, V., LEPPÄNEN, J., TULKKI, V., Module for thermomechanical modeling of LWR fuel in multiphysics simulations, *Annals of Nuclear Energy* **84** (2015) 111–121.
- [2] LOUKUSA, H., PELTONEN, J., VALTAVIRTA, V., FINIX - Fuel behavior model and interface for multiphysics applications - Code documentation for version 1.19.1. Technical Report VTT-R-00052-19. VTT Technical Research Centre of Finland Ltd, 2019.
- [3] VALTAVIRTA, V., HOVI, V., LOUKUSA, H., A. RINTALA, SAHLBERG, V., TUOMINEN, R., LEPPÄNEN, J., Kraken - An upcoming Finnish reactor analysis framework, ANS Topical Meeting on Mathematics and Computations, Portland, Oregon, 2019. Abstract submitted.
- [4] IKONEN, T., SYRJÄLAHTI, E., VALTAVIRTA, V., LOUKUSA, H., LEPPÄNEN, J., TULKKI, V., Multiphysics simulation of fast transients with the FINIX fuel behaviour module, *EPJ Nuclear Sciences & Technologies* **2** 37 (2016).
- [5] VALTAVIRTA, V., LEPPÄNEN, J., VIITANEN, T., Coupled neutronics — fuel behavior calculations in steady state using the Serpent 2 Monte Carlo code, *Annals of Nuclear Energy*, **100** (2017) 50–64.
- [6] GEELHOOD, K.J., LUSCHER, W.G., BEYER, C.E., CUTA, J.M., Fraptran 1.4: A computer code for the transient analysis of oxide fuel rods. Technical Report NUREG-CR-7023, Vol. 1, Pacific Northwest National Laboratory, 2011.
- [7] GEELHOOD, K.J., LUSCHER, W.G., BEYER, C.E., Frapcon-3.4: A computer code for the calculation of steady state thermal mechanical behavior of oxide fuel rods for high burnup. Technical Report NUREG-CR-7022, Vol. 1, Pacific Northwest National Laboratory, 2011.
- [8] GEELHOOD, K.J., LUSCHER, W.G., RAYNAUD, P.A., PORTER, I.E. FRAPCON-4.0: A computer code for the calculation of steady-state, thermal mechanical behavior of oxide fuel rods for high burnup. Technical Report PNNL-19418, Pacific Northwest National Laboratory, 2015.
- [9] LUSCHER, W.G., GEELHOOD, K.J., Material property correlations: Comparisons between FRAPCON-3.4, FRAPTRAN 1.4, and MATPRO. Technical Report NUREG-CR-7024, Pacific Northwest National Laboratory, 2011.
- [10] GEELHOOD, K.J., BEYER, C.E., LUSCHER, W.G., PNNL stress/strain correlation for Zircaloy, Technical Report PNNL-17700, Pacific Northwest National Laboratory, 2008.
- [11] SHESTOPALOV, A., LIOUTOV, K., YEGOROVA, L., Adaptation of USNRC’s FRAPTRAN and IRSN’s SCANAIR transient codes and updating of MATPRO package for modeling of LOCA and RIA validation cases with Zr-1%Nb (VVER type) cladding. Technical Report NUREG/IA-0209, US NRC, 2003.
- [12] LIMBÄCK, M., ANDERSSON, T., A Model for Analysis of the Effect of Final Annealing on the In- and Out-of-Reactor Creep Behavior of Zircaloy Cladding, In *Zirconium in the Nuclear Industry* **11** (1996) 448–468.
- [13] MASSIH, A.R., FORSBERG, K., LIMBFICK, M., A model for uniform Zircaloy clad corrosion in pressurized water reactors, *Nuclear Engineering and Design* **154** (1995) 157–168.
- [14] KÄTTÖ, J., Corrosion and its modeling in nuclear reactor fuel cladding. Master’s thesis, Aalto University Department of Energy Technology (2013).
- [15] JUST, L.C., BAKER, L. Jr., Studies of metal-water reactions at high temperatures III. Experimental and theoretical studies of the zirconium-water reaction. Technical Report ANL-6548, Argonne National Laboratory, 1962.
- [16] CHASE, M.W. Jr., NIST-JANAF Thermochemical Tables, Fourth Edition, *J. Phys. Chem. Ref. Data*, Monograph 9. Technical report, NIST, 1998.
- [17] FORSBERG, K., MASSIH, A.R., Diffusion theory of fission gas migration in irradiated nuclear fuel UO₂, *Journal of Nuclear Materials* **135** (1985) 140–148.
- [18] HERMANSSON, P., MASSIH, A.R., An effective method for calculation of diffusive flow in spherical grains, *Journal of Nuclear Materials* **304** (2002) 204–211.
- [19] PASTORE, G., LUZZI, L., DI MARCELLO, V., VAN UFFELEN, P., Physics-based modelling of fission gas swelling and release in UO₂ applied to integral fuel rod analysis, *Nuclear Engineering and Design* **256** (2013) 75–86.
- [20] BOELTER, L.M.K., DITTUS, F.W., Heat Transfer in Automobile Radiators of the Tubular Type, *University of California Publications in Engineering* **2** 13 (1930) 443–461.
- [21] JENS, P.A., LOTTES. W.H., Analysis of Heat Transfer, Burnout, Pressure Drop and DensityData for High-Pressure Water. Technical Report ANL-4627, Argonne National Laboratory, 1951.

- [22] IAPWS. Revised Release on the IAPWS Industrial Formulation 1997 for the Thermodynamic properties of Water and Steam. Technical Report R7-97(2012), IAPWS, 2012.
- [23] LASSMANN, K., O'CARROLL, C., VAN DE LAAR, J., WALKER, C.T., The radial distribution of plutonium in high burnup UO₂ fuels, *Journal of Nuclear Materials* **208** (1994) 223–231.
- [24] AINSCOUGH, J.B., WARE, J.O., Isothermal grain growth kinetics in sintered UO₂ pellets. *Journal of Nuclear Materials* **49** (1973) 117–128.
- [25] LOUKUSA, H., Validation of the FINIX fuel behavior code version 0.13.9. Technical Report VTT-R-06565-13. VTT Technical Research Centre of Finland Ltd, 2013.
- [26] PELTONEN, J., FINIX - Fuel behavior model and interface for multiphysics applications - Validation of version 1.19.1. Technical report VTT-R-00135-19. VTT Technical Research Centre of Finland Ltd, 2019.
- [27] VTT, VTT Research Information Portal.
<http://cris.vtt.fi>.

SAFETY ANALYSIS OF FUEL BEHAVIOUR FOR IMPLEMENTATION LICENSING

H. PAPP
Paks II. Ltd,
Paks, Hungary

K. KULACSY
Hungarian Academy of Sciences, Centre for Energy Research,
Budapest, Hungary

Abstract

Currently four WWER-440 nuclear power plant units operate in Hungary whose service life will expire in 2037. The Paks II. NPP will be built with two new Russian-type WWER-1200 reactors. The Paks II. NPP is currently in the Implementation Licensing stage. According to the Hungarian regulations, the Nuclear Safety Code (NSC) requires the following: "Independent calculations shall be carried out for parameters which are decisive from the safety point of view." The following requirement applies to the depth of the calculations: "The analyses used for the demonstration of safety shall be documented in a such way and to such a depth that they may be repeated, independently reviewed and modified to an extent necessary for the evaluation of modifications throughout the lifetime of the nuclear power plant; furthermore, the extent of conservatism applied and the extent of margins available based on the analysis may be reviewed and re-evaluated." The NSC also prescribes that "For all initiating events included in the design basis or in the extended design basis, the fulfilment of the relevant acceptance criteria shall be demonstrated by deterministic safety analyses." Based on these requirements the fuel behaviour analyses have been performed for normal operation and accident situations.

1. INTRODUCTION

Most of the nuclear power plants in the world are pressurized type; such reactors are currently operating in Paks. Unit 1 and Unit 2 of Paks NPP received 20 years operating license extension until 2032 and 2034. Lifetime of Unit 3 and Unit 4 was extended by HAEA until 2036 and 2037. The Paks II. NPP will be built with two new Russian-type WWER-1200 reactors. From a construction, commissioning and operation point of view, it is important to build units which already have operation experiences in other countries.

The Paks II. NPP is currently in the implementation licensing stage. Nuclear power plants must be licensed with very serious safety requirements. The new units must have the safety systems and technical solutions specific to third generation power plants that will only have the consequences of severe accident events within the power plant.

2. MAIN FEATURES OF WWER-440 AND WWER-1200 ASSEMBLY AND FUEL ROD

The Russian units of 1200 MW electric power are usually given with AES-2006 type indication, where the 2006 Figure refers to the year when the plans of the first block were completed. Such units were built in the Novovoronyez and Leningrad nuclear power plants.

Like most power plant reactors in the world and the current Paks units, the new reactors will also operate with uranium dioxide fuel.

The WWER-440 and WWER-1200 reactors have very similar fuel rods. Both have 7.6 mm outer diameter UO₂ pellets in 9.1 mm outer diameter zirconium tubes. The rods are provided with zirconium plugs at the top and bottom [2] (Table 1).

TABLE 1. MAIN PARAMETERS OF WWER-440 AND WWER-1200 ASSEMBLY

	WWER-440	WWER-1200
Fuel rod length	2600 mm	4033mm
Active length	2480 mm	3730 mm
Pellet outer/inner diameter	7.6/1.2 mm	7.6/1.2 mm
Clad inner/outer diameter	9.1/7.8 mm	9.1/7.8 mm
He gas pressure	6 bar	20 bar
Average linear heat rate	13.8 kW/m	16.7 kW/m
Maximum linear heat rate	32.5 kW/m	42 kW/m
Assembly length	3217 mm	4570 mm
Fuel rod numbers in the assembly	126	312
Control rods	no	18ps

The WWER-1200 reactor core has the same main dimensions as the WWER-1000 core, so the external dimensions of the assemblies are the same. The WWER-1200 assemblies have 534 kg_{UO₂}, which is 7 kg more than the WWER-1000 type. In addition to the 312 pieces fuel rods, 18 control rods are provided. In the WWER-1200 core, assemblies with gadolinium and UO₂ fuel elements are also designed. (Figure 1).

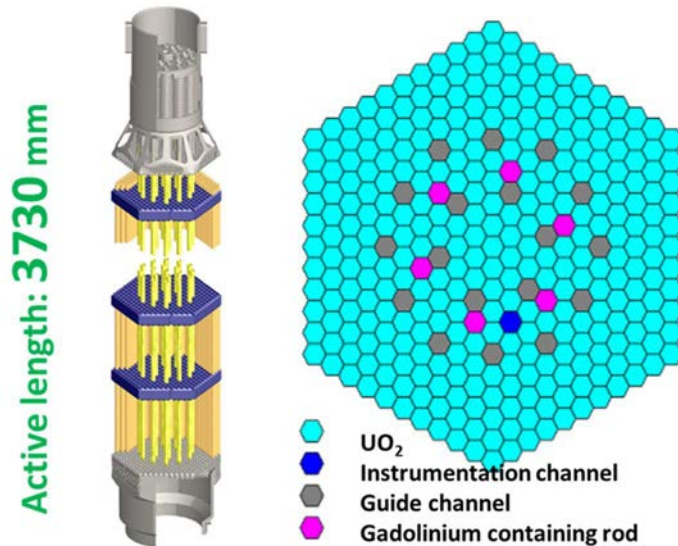


FIG.1. Fuel assembly.

3. REGULATORY BACKGROUND AND REQUIREMENTS

Based on the Hungarian Nuclear Safety Code the “The independent verification of the analyses containing the characteristics of the designs, which are decisive from a safety point of view, shall also be carried out by different calculation methods.”

The following requirement applies to the depth of the calculations: “The analyses used for the demonstration of safety shall be documented in a such way and to such a depth that they may be repeated, independently reviewed and modified to an extent necessary for the evaluation of modifications throughout the lifetime of the nuclear power plant; furthermore, the extent of conservatism applied and the extent of margins available based on the analysis may be reviewed and re-evaluated.”

Based on the above-mentioned requirements as the part of the Implementation Licensing documentation independent safety analyses must be submitted to the Hungarian Atomic Energy Authority. These analyses were carried out by Technical Support Organization experts.

4. SAFETY ANALYSIS FOR LOSS OF COOLANT ACCIDENT

The LOCA calculations were made using the FRAPTRAN code [3] and according to international practice with best estimate models, conservative initial and boundary conditions. The condition of the analyzed fuel rods at the beginning of LOCA were defined based on the results of the FUROM (Fuel Rod Modelling) code [4] calculations.

As a first step, conservative calculations with the FUROM programme were carried out in order to select the rods that behave in the worst way from LOCA point of view. The states of the fuel rods were analyzed in 5 MWd/kgU burnup steps. The highest internal pressure and highest power rods have been defined for UO₂, 5% Gd₂O₃ and 8% Gd₂O₃ rods, as in the highest internal pressure rods the ballooning is the easiest, whereas the highest clad temperatures are reached by the highest power rods at any given burnup.

Finally, the worst state rods have been selected and the LOCA calculations were performed for these rods. (Table 2.)

TABLE 2. SELECTED RODS FOR LOCA CALCULATIONS (BURNUP, PRESSURE AND LHR PARAMETERS ARE AT THE BEGINNING OF THE LOCA) [5]

Rod type	Rod No.	Burnup (MWd/kgU)	Average LHR (kW/m)	Pressure (MPa)
UO ₂	297	0.00	30.1	7.8
	28	19.99	29.1	9.4
	302	34.53	27.4	9.9
	302	54.99	23.8	11.1
	302	65.00	22.8	13.4
UO ₂ +5% Gd ₂ O ₃	194	4.99	14.2	7.2
	194	24.89	19.9	9.5
	194	44.76	19.3	10.4
	194	64.58	11.5	12.4
UO ₂ +8% Gd ₂ O ₃	105	5.00	18.9	7.4
	14	25.26	24.4	10.2
	14	44.96	22.7	10.7
	202	60.01	8.5	10.8

In order to simulate the normal operating irradiation of the rods, the production parameters were adjusted to obtain the highest possible gas emissions. To this end, the gap size and the burnup were maximized (maximum internal radius of the cladding, minimum outer radius of the pellet) and the pressure of the filling gas was also taken as high as possible.

One of the components of the conservatism of thermohydraulic calculations is the choice of axial power profiles: profiles that lead to the highest clad temperature for a given power were selected.

5. CONCLUSIONS

Among the criteria, the maximum temperature of the clad and the fuel, and the maximum oxidation of the clad at both the rod and core level, are far below the criteria under the given thermal hydraulics conditions.

The calculated maximum cladding temperature was 920°C, the maximum local ECR was approx. 3%, the maximum fuel centerline temperature was 1726°C and the maximum cladding strain was below 5%, so no fuel rod failed.

6. NOMENCLATURES

FUROM	Fuel Rod Modelling
FRAPTRAN	A Computer Code for the Transient Analysis of Oxide Fuel Rods
HAEA	Hungarian Atomic Energy Authority
LOCA	Loss of Coolant Accident
NPP	Nuclear Power Plant
NSC	Nuclear Safety Code

REFERENCES

- [1] HÓZER, Z., PÁZMÁNDI T., Új blokkok a paksi atomerőműben, Budapest, Hungary, Nukleon **VII** (2014) 152.
- [2] HÓZER, Z., Az új paksi reaktorok üzemanyag, Fizikai szemle **12** (2015).
- [3] GEELHOOD, K.J., LUSCHER, W.G., CUTA, J.M., PORTER, I.A., “FRAPTRAN-2.0: A Computer Code for the Transient Analysis of Oxide Fuel Rods”, PNNL-19400, Vol.1 Rev2, (2016).
- [4] GADÓ, J., GRIGER, Á., KULACSY, K., The fuel behaviour code FUROM and its high burn-up simulation capabilities, Nuclear Engineering and Design **327** (2018) 274–285.
- [5] KULACSY, K., SOMFAI B., Nagycsőtöréses üzemzavar fűtőelem-viselkedési elemzése (internal report, 2018).

FUEL BEHAVIOUR DURING DBA AND DEC: ANALYTICAL AND EXPERIMENTAL STUDIES FOR DEVELOPMENT OF ATF

A.J. GAIKWAD, A.K. DEO, P. SHARMA, K. OBAIDURRAHMAN, S. BERA
Nuclear Safety Analysis Division (NSAD), NSARG, Atomic Energy Regulatory Board (AERB),
Anushaktinagar, Mumbai 400094,
India

Abstract

Fuel heat-up, fuel degradation in an accident and the resultant fuel failure with release of the fission product (FP) into the primary system during Design Basis Accident (DBA) and Design Extension Conditions (DEC) are the key aspects to demonstrate the safety of the NPPs. Post Fukushima more emphasis is also laid on the development of the Accident Tolerant Fuel Designs (ATFD) to avoid fuel degradation and hydrogen generation. Terms like practically eliminated and ATF, need to be substantiated with physical and analytical evidence. Along with ATF development efforts should also be dedicated in prevention of loss of heat removal and/or quick restoration and lining up of the emergency coolant inventories with in the capabilities/survivability of the ATF. The aspects related to DBA and DEC fuel/core modelling are evolving specially the later one. The expectations, development, is also discussed here along with the comparison of ATF with the existing fuels. The development of ATF may be an iterative process shuffling from nuclear requirements to materials and safety performance while testing out of pile and in-pile. ATF aspect w.r.t reactivity loads is also elaborated for PHWRs. The developments on RIA and high burn-up fuel are also summarised. With improved ATF fuel performance improved MHT design and configuration are also envisaged. It is possible to configure MHT, ECCS and passive safety system in such a manner that the possibility of prolonged loss of cooling is reduced.

1. INTRODUCTION

Fuel heat-up, fuel degradation in an accident and the resultant fuel failure with release of the fission product (FP) into the primary system during Design Basis Accident (DBA) and Design Extension Conditions (DEC) are the key aspects to demonstrate the safety of the NPPs. Post Fukushima more emphasis is also laid on the development of the Accident Tolerant Fuel Designs (ATFD) to avoid fuel degradation and hydrogen generation. Adherent ceramic coatings are being considered to preventing diffusion of oxygen to the fresh metal surface of the cladding to prevent degradation. It is also claimed that the ATFs are tolerant to loss of cooling during accidents, this tolerance needs to be quantified in terms of time and highest temperature which the cladding can tolerate. Ideally the melting point of the clad can be taken as the maximum temperature which an ATF can hold. For zircaloy clad this can be around 1800°C.

The safety in terms of post clad melting consequences also need to be assessed, in terms of the hydrogen which may be released then. DBA domain for zircaloy fuels within 800 to 1200°C. ATFs need to show an improved performance in this temperature range and beyond up to melting of clad. Various operational requirement of fuel in terms of materials aspects including corrosion, fuel fabrication, fuel handling, fuel economy including burn-up need to be assessed.

Terms like practically eliminated and ATF, need to be substantiated with physical and analytical evidence. Along with ATF development efforts should also be dedicated in prevention of loss of heat removal and/or quick restoration and lining up of the emergency coolant inventories with in the capabilities/survivability of the ATF. These aspects are related to the NPP core cooling designs and the generation of the NPPs, which dictates the inherent and engineered safety systems. Confinement of fission products during accidents is also a very important aspects for ATFs.

Analytical and experimental studies are necessary to validate and assess the ATF fuels performance for the DBA and DEC behaviour of fuel pins and fuel assembly. These studies start with clad failure and further degradation on heat-up, based on the type of fuel and core configuration. Various coatings are being considered for ATF cladding on both the sides. Coating on the fuel pellet may also be envisaged to retain the fission products even at high temperature, this may call for sufficient void spaces in the pellet to accommodate the fission products based on the burn-up envisaged. These materials also have to with stand very high temperature so the choices will be limited.

2. DBA AND DEC FUEL/CORE MODELLING ASPECTS

Lumping of several fuel assemblies in the reactor core modelling and the corresponding realistic simulation of heat transfer phenomena including radiation modelling play an important role in DBA/DEC predictions. Also the fuel models face challenges in modelling of the deformed, non-cool-able geometries of the overheated fuel and the hot/deformed primary system attained during the DEC core disassembly. Certain assumptions are made to close the fuel as well as primary system models. These modelling limitations and assumptions mandate more research, as experimental evidences and the detailed models are still evolving as more claims are made on the performance of ATF. The safety analysis codes need to be updated for the particular ATF design being envisaged/tested and included in the design of the NPP. The updating of the codes will require the performance details based on physical and analytical studies. On the fuel failure resistance aspect the creep behaviour of the cladding is very important. The coating also should not allow penetration/diffusion of oxygen and hydrogen into the base metal of the cladding.

Typical fuel bundle for PHWR is as shown in Figure 4. Temperature predictions after channel voiding using 2-D transverse cross sectional model (COMSOL) and a lumped code (RELAP/SCDAP5) are shown in Figures 5 and 6 for voided channel. Two different modelling approach has been used for lumped parameter code calculation. For the first case, view factor between bundle and PT is calculated assuming two concentric cylinder with inner cylinder circumscribing fuel bundle. While in the second case, effective view factor between fuel various pins in a bundle and PT is calculated using Monte-Carlo simulation and further used for the temperature prediction. When the view factors are calculated using an approximate geometry, the lumped code under-predicts the temperature values. However, it can be noted that steady state temperature predictions of lumped code closely matches with 2-D model predictions when appropriate view factors are used in the analysis.

Fuel modelling for DBAs and DECs are different, in case of DBAs a conservative approach is followed i.e. peak clad temperature is important parameter to compare with the acceptance criteria. However, for DEC analysis, Severe Accident Management Guidelines (SAMG), source term estimation etc., a realistic modelling approach is required as the conservative assumption may lead to misleading results. In the DEC analysis, core/fuel modelling is divided in to various zones based on the relative power to the fuel assemblies with an appropriate lumping as shown in Figure 1. Further accident management actions and their timings are important in SAMGs. The release of FPs based on the fuel temperature predicted decide the dose (which may be one of acceptance criteria) for DBAs, DEC.

Typical fuel temperature variation during first phase (till moderator boil-off) of LOCA initiated DEC-B event is as shown in Figure 2. Nodalization of fuel in core for PWR is shown in Fig. 3(a). PWR core is divided into five ring type regions by grouping similarly powered fuel assemblies together for vertical core disassembly. Whereas PHWR horizontal core channels are clubbed for core disassembly dictated by moderator boil off in the Calandria Vessel. Fuel temperature for a PWR DEC behaviour is shown in Figure 3(b). Temperature starts increasing when the water inventory in RPV starts depleting and on exhaustion of ECCS passive systems. The fuel behaviour depicted in Figs 2 and 3(b) will change based on the ATF characteristics and design as and when they are deployed. Some ATFs may lead to delay in fuel failure which can altogether stop the accident progression if innovative active and passive means for heat removal are restored with this period.

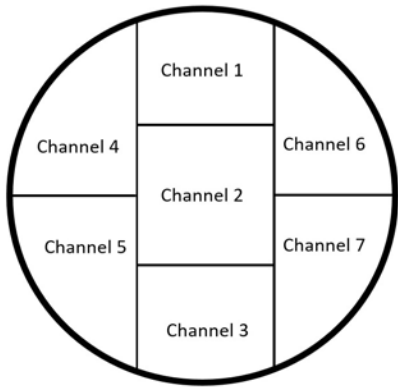


FIG. 1. Core lumping based on elevation.

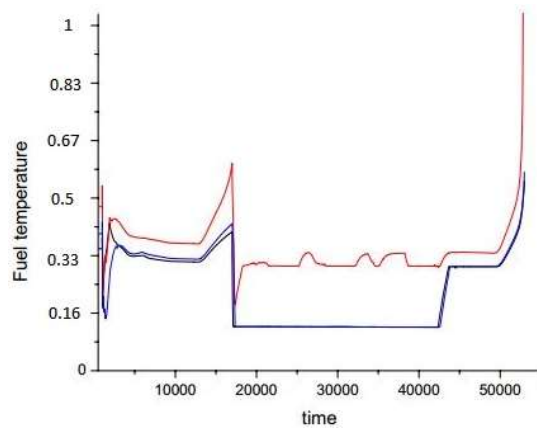


FIG. 2. Variation of Fuel Temperature of Three Axial Nodes of top Channel 1st Phase.

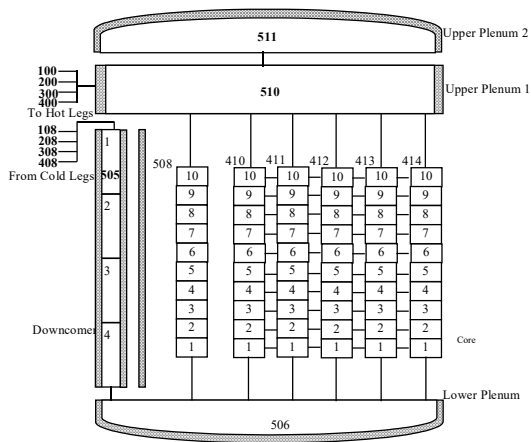


FIG. 3a. Fuel temperature for a typical PWR.

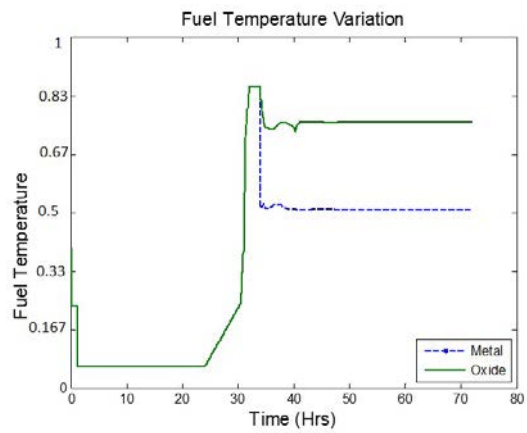


FIG. 3b. Fuel temperature for a typical PWR.

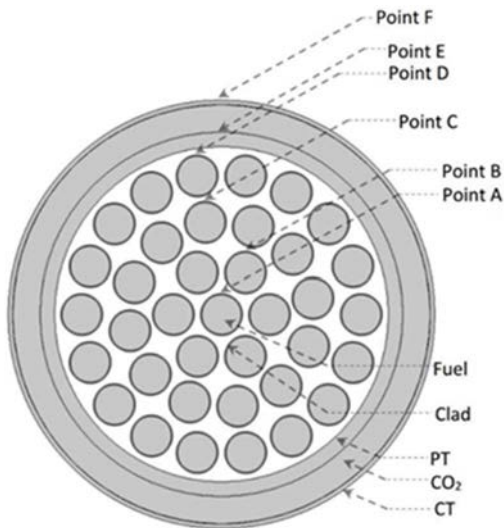


FIG. 4. Typical 37 pin fuel bundle for PHWR.

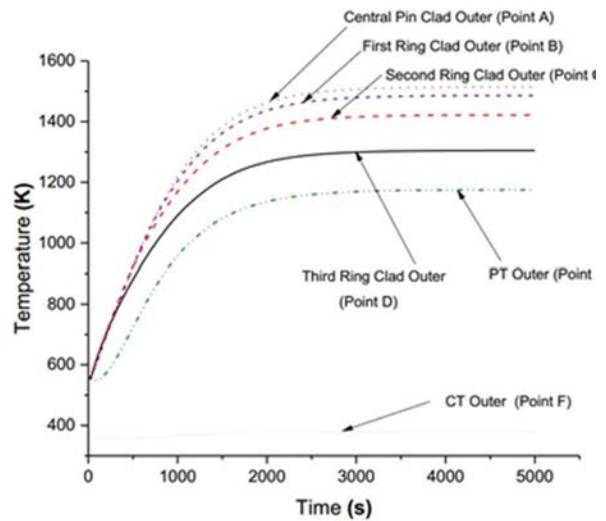
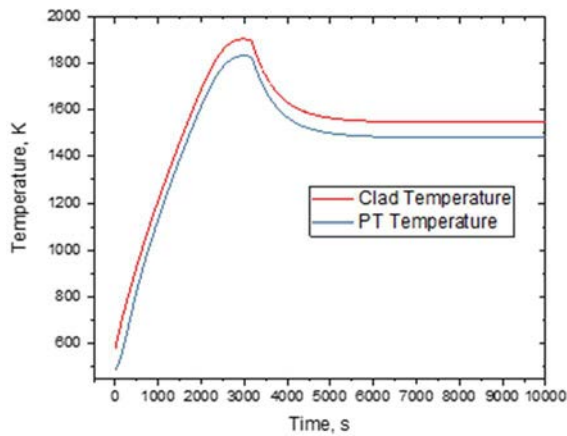
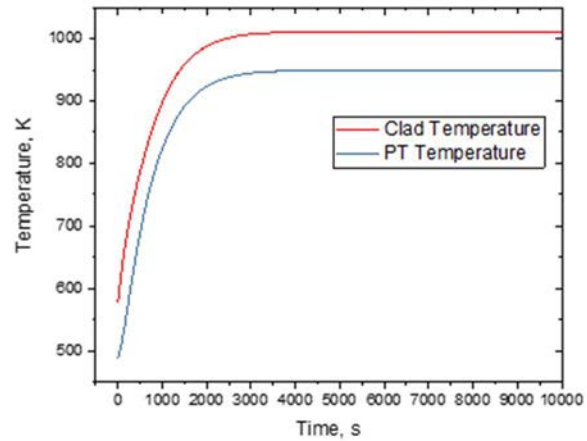


FIG. 5. Temperature variation after channel voiding using COMSOL.



(a) View factor based on Monte-Carlo Simulation



(b) View factor based on outer bundle

FIG. 6. Lumped code temperature predictions.

3. ATF FUEL DESIGN/STUDIES AND COMPARISON WITH EXISTING FUEL

Modelling of detailed fuel behaviour involves multi physics in terms of nuclear, physical and chemical interactions. Fuel behaviour analysis gets inputs from various codes such as neutronics code, system thermal hydraulics codes, at times coupled reactor physics and thermal hydraulics codes analysis is necessary along with structural aspect for DEC scenarios. Both in-house developed and internationally available code are used for analysis.

While designing/studying ATF the following aspects also should be considered:

- Nuclear Properties: Load on reactivity i.e. reduction in excess reactivity/burn-up, swelling;
- Physical and Metallurgical behaviour of clad and coating, adherence, uniformity;
- Chemical Integrations mainly corrosion with coolant and other core materials;
- Heat transfer characteristics: modes of HTC on cladding surface;
- Initial oxidation thickness of clad and variation during transient;
- Variation of gap conductance during transient & PCMI;
- Pressure difference across cladding, has bearing on clad burst fuel failure;
- Avoiding hydrogen and heat generation due to Zr–water reaction: This is an additional heat source to the cladding, and hydrogen produced by the reaction can be absorbed by the cladding and the mechanical properties of the cladding may be degrade further;
- Cladding deformation, pin holes, ductility and creep behaviour, ballooning or geometrical distortions of fuel assemblies may degrade the cooling. In the case of a large pressure difference across the cladding, such as in a large break LOCA, cladding burst can occur. Avoiding clad burst will improve safety and DEC performance;
- Power distribution in fuel element can generate additional loads/stress;
- Fission gas release: In the course of the accident, due to the fuel temperature rise, a large fraction of the fission gas accumulated in the fuel matrix will be released to the gap and the internal pressure will increase. During DEC, even non volatiles/refractories may get released depending on the fuel temperatures reached.

The comprehensive comparison of the expectation from the ATF w.r.t existing zircaloy is summarized in Table 1.

TABLE 1. COMPARISON OF ATF WITH EXISTING FUEL.

Requirements	Existing zircaloy fuel (ZF)	Expectation from Accident Tolerant Fuel (ATF)
Design	Caters to AOO & DBA	Caters to AOO, DBA & DEC
Nuclear	Neutron economy, fuel cycle length	May not Preserves neutron economy
AOO	Heat Transfer Characteristics (HTC): LHR, clad temperature (coolant boiling & plant efficiency), Corrosion i.e. compatibility with coolant & pellet (prolonged durations). Ease of Fabrication Nuclear Characteristics Fuel Handling	Similar/Enhanced HTC: Does not hamper Normal operations & AOO performance. Higher corrosion resistance, more compatible with coolant & fuel. Fabrication may be more involved May involve certain reactivity burden New material may not have desired Nu Pro Fuel Handling, Adherence of coating, tribology studies, anticipated loads
DBA	Burst Criteria and pin-hole development. ECCS Acceptance Criteria Fuel Failures (none/acceptable based on criteria) Poor performance beyond pin hole development & further heat-up Rewetting Diffusion of Hydrogen & Oxygen Hydrogen Generation	Similar/Enhanced burst characteristics avoids pin-hole development. Similar/Enhanced behaviour beyond 1200 C No Fuel Failures expected even beyond 1200 C Similar/Enhanced resistant to pin hole development & further degradation beyond 1200 C Stable in Rewetting with no failures Resistant to diffusion of Hydrogen & Oxygen Resistant to Hydrogen Generation
DEC	Diffusion of Hydrogen, Oxygen and Hydrogen Generation Similar Enhanced clad ductility and creep properties Retaining coolable fuel configuration Fission Products Releases	Resistant to diffusion of Hydrogen, Oxygen and resistant to Hydrogen Generation Similar/Enhanced clad ductility and creep properties Ability to retaining coolable fuel configuration Resistant to Fission Products Releases
DEC MHT-core Design Aspects	Core disassembly & fuel degradation Post Core-disassembly Cooling	ATF can survive higher temperatures, the core-MHT structures also need to sustain these high temperature to retain cool-able geometries and avoid core disassembly Post fuel degradation and core-disassembly need to be amenable to cooling. It should not lead to sudden & high amount of hydrogen generation
Pellet	FP release Swelling & Cracking PCMI Internal Pressure in the clad Ease of Fabrication	Less FP releases Accommodate swelling for high burn-ups Resistant to PCMI with various coatings Less pressurization expected even at HiBurn New materials development
MHT Design & Configuration	Loss of cooling	Resistant to loss of cooling for prolong periods. Based on the PHT configuration and the ECCS design, Natural Circulation, Power supply Reliability.

With improved ATF fuel performance improved MHT design and configuration are also envisaged. It is possible to configure MHT, ECCS and passive safety system in such a manner that the possibility of prolonged loss of cooling is reduced. Studies were carried out on a four loop channel type natural circulation boiling water reactor where it was possible to configure the MHT, ECCS in such a manner that even a large LOCA without SCRAM did not lead to any temperature rise for a prolonged period. The details are not published here to limit the text.

4. ESTIMATION OF REACTIVITY LOAD IN PHWR FOR VARIOUS ATF COATINGS

ATF for PHWR700 can be developed through coating of the clad on both the sides of the cladding tube. The coating materials add reactivity load on the core due to the absorption of neutron corresponding to the coating thickness. Impact on the full core reactivity due to coating of various materials has been studied to arrive at possible candidate coating material for the natural uranium fuelled PHWR. Based on the analysis, the coating materials are classified into three categories (as shown in Table 2) w.r.t. reactivity loads: best suitable (with small reactivity load 0 to -5 mk), may be acceptable (with medium reactivity load -5 mk to -10 mk) and not suitable (with large reactivity load more than -10 mk). The reactivity load for both side coating thickness of 10 μm , 20 μm , 30 μm and 40 μm are used for estimating the reactivity load for potential 24 number of zircaloy based ATF clad coating materials for PHWR700 (Figs 7–10).

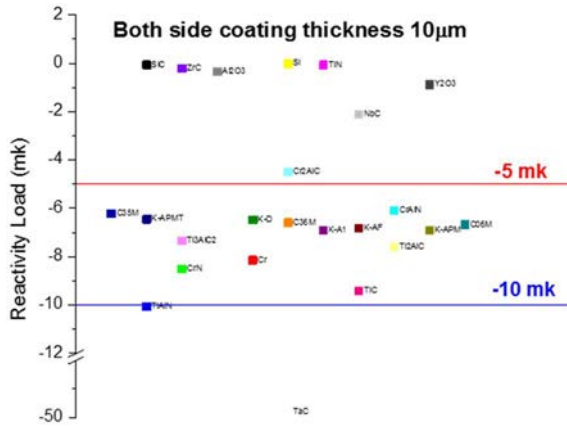


FIG. 7. Coating thickness 10 μm .

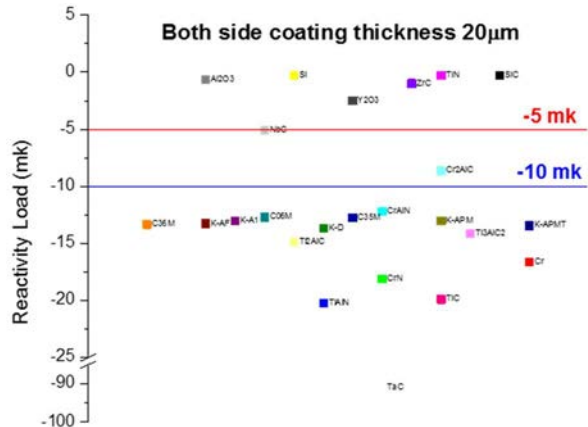


FIG. 8. Coating thickness 20 μm .

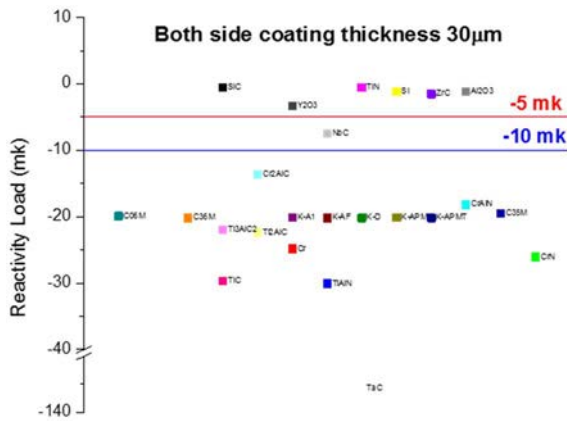


FIG. 9. Coating thickness 30 μm .

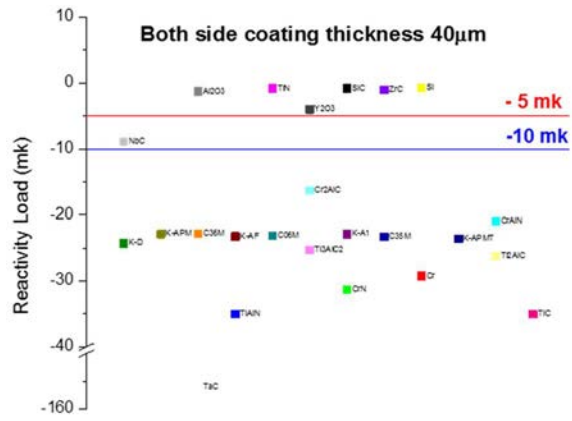


FIG. 10. Coating thickness 40 μm .

TABLE 2. CATEGORISATION OF COATING MATERIAL BASED OF NEUTRON ECONOMY

Coating Thickness μm	Category	Material
10	Best suitable	SiC, ZrC, Al ₂ O ₃ , Si, TiN, NbC, Y ₂ O ₃ , Cr ₂ AlC
	May be acceptable	C35M, Kanthal-APMT, Kanthal-D, CrAlN, C36M, C06M, Kanthal-A1, Kanthal-AF, Ti ₃ AlC ₂ , CrN, Cr, TiC, Tr ₂ AlC, TiAlN
	Not suitable	TaC
20	Best suitable	SiC, ZrC, Al ₂ O ₃ , Si, TiN, NbC, Y ₂ O ₃
	May be acceptable	Cr ₂ AlC
	Not suitable	C35M, Kanthal-APMT, Kanthal-D, CrAlN, C36M, C06M, Kanthal-A1, Kanthal-AF, Ti ₃ AlC ₂ , CrN, Cr, TiC, Tr ₂ AlC, TiAlN, TaC
30	Best suitable	SiC, ZrC, Al ₂ O ₃ , Si, TiN, Y ₂ O ₃
	May be acceptable	NbC
	Not suitable	Cr ₂ AlC, C35M, Kanthal-APMT, Kanthal-D, CrAlN, C36M, C06M, Kanthal-A1, Kanthal-AF, Ti ₃ AlC ₂ , CrN, Cr, TiC, Tr ₂ AlC, TiAlN, TaC
40	Best suitable	SiC, ZrC, Al ₂ O ₃ , Si, TiN, Y ₂ O ₃
	May be acceptable	NbC
	Not suitable	Cr ₂ AlC, C35M, Kanthal-APMT, Kanthal-D, CrAlN, C36M, C06M, Kanthal-A1, Kanthal-AF, Ti ₃ AlC ₂ , CrN, Cr, TiC, Tr ₂ AlC, TiAlN, TaC

Fuel behaviour analysis for accident conditions can be grouped into the three types of transients:

- Power excursion accident: When a large reactivity spike is inserted by a very fast ejection of a rod control, a power excursion occurs. Since the time duration of the accident is quite short, fuel behaviour is determined by how much energy is generated in the fuel during the short period in the local region. Therefore, one of the acceptance criteria for this accident is usually defined as the maximum adiabatic enthalpy per unit mass added to the fuel element;
- Power cooling mismatch accident: Mismatch of heat generation and heat removal may cause DNB, and the cladding temperature may rise suddenly due to the small heat removal capability of transition boiling or film boiling. Safety criteria for this type of accident are usually defined by the cladding temperature, the number of rods entering DNB and the amount of cladding oxidation. Flow rate and flow distribution is an important aspect;
- Decrease of reactor cooling inventory: A loss of coolant accident (LOCA) is caused by the loss of integrity of the primary circuit or its associated pipes and devices. Safety criteria for this type of accident are usually defined by cladding temperature and amount of cladding oxidation.

5. EXISTING EXPERIMENTAL STUDIES ON FUEL RIA BEHAVIOUR

Reactivity initiated accidents (RIA) leads to increase in reactor power, thermal as well as mechanical load in fuel elements thereof. Nuclear design should ensure that the power pulse width and height are manageable with combination of inherent feedbacks as well engineered safety features [1]. RIA simulation tests have been performed on fresh un-irradiated fuel rods, using pulse reactors in various countries. To generate matrix of RIA response of rods, simulation tests have been conducted on about 140 pre-irradiated light water reactor fuel rods in six different power pulse reactors.

The results of these experiments though added significant value to the overall knowledge base on RIA fuel behaviour, direct application of the results from the pulse irradiation tests to power reactors is difficult due to difference in the test conditions and the conditions of the fuel pellet in test rodlets. The results have brought out that PCMI and energy deposition as a possible failure mechanism. Evolving trend for increasing the fuel burn up has also been assessed with regard to RIA failure. In general, fuel burn-up aggravates the mechanical loading of the cladding, while corrosion, or better the hydrogen absorbed in the cladding as a consequence of corrosion, may under some conditions make the cladding brittle and more susceptible to failure. Experiments have also shown

that corrosion impairs the fuel resistance for RIA transient occurring at cold conditions, though there is no evidence of important embrittlement effects at hot conditions, unless the cladding was degraded by oxide spalling.

The cladding failure limit for RIA is based on the NRC standard review plan, which suggests a maximum radially averaged fuel enthalpy of 170 cal/g for BWRs and the DNB criterion for PWRs. Though In Japan, the threshold of PCMI failure in terms of enthalpy increase (cal/g UO₂) has been determined in terms of burn-up (GWd/t). Acceptable Incremental enthalpy increase is 110 Cal/g upto 25 GWD/t BU of fuel. This limit reduced to 40 Cal/g at burnup of the range 60GWD/t [2] as shown in Table 3.

TABLE 3. PCMI FAILURE THRESHOLD IN JAPAN

Burn-up (GWd/t)	Enthalpy Increase (cal/g UO ₂)
< 25	110
25–40	85
40–65	50
65–75	40

ATF concepts include modifying the fuel, coatings on clad, new clad materials etc. Different types of coated zircaloy claddings, Molybdenum (alloy) cladding coated with Zr or FeCrAl, different variants of FeCrAl (solid tube), SiC-SiC composite, MAX phase (example Ti₃SiC₂) and various types of layered claddings are being tested by various organizations (Table 4) [3–16]. In house, experimental studies on Cr coated Zircaloy-4 claddings are being carried out.

TABLE 4. COMPARISON OF COATING MATERIAL BASED ON MECHANICAL PERFORMANCE

ATF	Coating	Advantage	Limitations
Zircaloy cladding coatings	SiC	Thermal Characteristics	Limiting Temperature 650°C, not as good as SiC cladding
	Ti ₃ AlC ₂ , Ti ₃ SiC ₂	High MP, K, favorable material properties	Oxidation limited to 1450°C, 1000°C
	Coating required on both the side, Quality of coating, Adherence, Uniformity, etc		
Hybrid	Si Ceramic Metal Composite	Sustains high Temperatures, High Strength, Hard CMC with Zry-4	Hydrogen diffusion, development of bonding techniques between SiC & Zry-4
New cladding	SiC	Sustains high Temperatures, High Strength, Compatible with UO ₂	Requires large pellet clad gap, Joining techniques to be developed
Engineered Steels & Advanced Zr-alloys are being developed & have a long way to go			

To develop the burst criterion for zircaloy-clad tubes used in Indian PHWRs, experimental clad burst facilities were developed. A generalized correlation for the burst stress using the present and previous experimental data has been developed. The effect of pressure-rise during the clad tube heating prior to bursting is incorporated in the burst criterion model developed. The effect of anisotropic parameters has been considered. Predictions from the developed criterion model have been found in good agreement with experimental results. Facilities were further developed to study the Influence of Hydrogen Content on Burst Characteristics of Zircaloy-4 Cladding.

The development of ATF may be an iterative process shuffling from nuclear requirements to materials and safety performance while testing out of pile and in-pile. The nuclear criteria in terms of the neutron economy may be the starting point for the non-enriched/enriched fuel NPPs. The LWRs also cannot afford much reactivity loads to the clad coatings as it will affect the cycle length and cost. It is advisable to carry out major portion of testing and elimination in out of pile tests. This may include testing at the elevated temperatures in steam environment with pre and post adherence tribology studies to meet all the fuel handling and the safety expectations/requirements. Certain material like grapheme may be more promising but the development and deployment of these materials may be difficult and costly also.

6. CONCLUSIONS

The ATF development has gained importance especially after Fukushima. Aspects such as fuel design, fuel coating, fuel coating stability, diffusion of O₂ and H₂ through coating, corrosion, for delaying/avoiding fuel failures are being explored. The next step is related to studies on out of pile and in-pile for fuel heat-up, fuel degradation and minimal release of the fission products (FPs) for future deployment. After this the fuel design and safety analysis code will be updated to account for the ATFs. Along with the code capabilities, also the modelling/lumping aspects related to DBA and DEC fuel/core modelling play wide role in estimating the fuel temperature. The development of ATF may be an iterative process shuffling from nuclear requirements to materials and safety performance while testing out of pile and in-pile. Reactivity loads and neutron economy which affects the fuel cycle costs/duration, are also major concerns in the development of ATF especially for heavy water reactors.

REFERENCES

- [1] JERNKVIST, L., MASSIH, A., Nuclear fuel behaviour under reactivity-initiated accident (RIA) condition: State-of-the-art report (2010).
- [2] BECK, W., et. al, Nuclear Fuel Safety Criteria Technical Review, (2012).
- [3] ALLEN, T., BUSBY, J., et. al, "Materials challenges for nuclear systems," Elsevier.
- [4] CHENG, B., KIM, Y., et. al, "Improving accident tolerance of nuclear fuel with coated Mo-alloy cladding," Elsevier.
- [5] M. K.-N. E. and Technology and undefined, "Research and development methodology for practical use of accident tolerant fuel in light water reactors," Elsevier (2016).
- [6] ZINKLE, S., TERRANI, K., et. al, "Accident tolerant fuels for LWRs: A perspective," Elsevier.
- [7] RAMANATHAN, L.V., Scope for High Temperature Coatings in the Nuclear Field, (2016).
- [8] VAN NIEUWENHOVE, R., "Overview of ATF research..." EERA workshop on Materials resistant to extreme conditions for future energy systems, Kyiv, Ukraine (2017).
- [9] BISCHOFF, J., BLANPAIN, P., et. al, Development of fuels with enhanced accident tolerance (2016).
- [10] BACZYNSKI, J., High temperature steam oxidation of titanium-coated Zircaloy-2 and Titanium-Zirconium Alloys (2014).
- [11] IDARRAGA-TRUJILLO, I., LE FLEM, M., BRACHET, J., LE SAUX, M., Assessment at CEA of coated nuclear fuel cladding for LWRs with increased margins in LOCA and beyond LOCA conditions.
- [12] INTERNATIONAL ATOMIC ENERGY AGENCY, Technical Meeting on Accident Tolerant Fuel Concepts for Light Water Reactors 2014 : ORNL, "Accident tolerant fuel concepts for light water reactors" : proceedings of a technical meeting held at ORNL, United States of America, 13-16 October 2014. .
- [13] KIM, H., KIM, I., etal, High temperature oxidation behavior of Cr-coated zirconium alloy.
- [14] BRAGG-SITTON, S., "Overview of international activities in accident tolerant fuel development for light water reactors", Presentation given at the IAEA technical working group on fuel performance and technology, Vienna, Austria (2014) 24–25.
- [15] PINT, B.A., TERRANI, K.A., et. al, Material Selection for Accident Tolerant Fuel Cladding, Metallurgical and Materials Transactions E, vol. 2 3 (Sep.2015) 190–196.
- [16] BARRETT, K., BRAGG-SITTON, S., Advanced LWR nuclear fuel cladding system development trade-off study (2012).

AN INTRODUCTION TO A MULTIDIMENSIONAL REACTOR SIMULATION ENVIRONMENT WITH THE CAPABILITY OF ADVANCED MODELLING OF NUCLEAR FUEL UNDER ACCIDENT CONDITIONS

R. VADI, K. SEPANLOO

Nuclear Science and Technology Research Institute (NSTRI),
Tehran, Islamic Republic of Iran

Abstract

In this paper, a Simulation Environment (SE) is introduced which has the capability of performing comprehensive and accurate analysis of different types of nuclear reactors and behaviour of their fuel under various steady-state and accident conditions. The SE currently consists of three main novel codes, a CFD-based, multidimensional code which works in transient and steady states for both single and two-phase flows and two separate neutronic codes. First code solves the point kinetics equations with multi-group delayed neutron precursors using four different methods. The second code solves multidimensional multi-group diffusion equations in transient and steady states and isotropic or anisotropic forms. Using the finite volume method for spatial discretization has provided considerable flexibility regarding geometry and boundary conditions, so that the most sophisticated details of fuels geometry such as spacer grids could be modelled accurately. The most important innovations incorporated into this SE are "simultaneous solution" approach which is a novel method for coupling the neutronic and thermohydraulic analyses based on the use of the point-implicit solver, "multi-region porous media" model which is an improvement over the original model by modifying the method of resistance coefficients evaluation and the approach by which this model is applied to the core of nuclear reactor and an introduction to the "improved SIDK", a temporal discretization method for accident analysis which has been obtained by combining the key feature of the original method that is decoupling of the prompt and delayed neutron equations with the separated solution approach of the point-implicit solver. The advantages provided by the mentioned innovations are partially indicated by presenting some practical examples and to demonstrate the accident modelling capabilities of this novel SE some relevant results associated with the case studies on TRR are presented and discussed which includes analyses of two DBAs i.e. RIA and LOCA.

1. INTRODUCTION

"Insatiable growth in energy consumption has increased the demands on the rate and efficiency of nuclear power production systems [1]. It means higher discharge burnup, longer operation cycles and transient regimes. In order to fulfil these demanding criteria, the technology incorporated into the design of these systems has to improve constantly, especially with regard to geometry optimization, so that the conventional one dimensional numerical methodologies are losing their function as reliable and accurate tools for both design purposes and safety assessment" [2, 31].

"Accordingly, Advanced Modelling and Simulation Office (AMSO) of the US Department of Energy introduced the concept of 'predictive simulation' in 2008 for the first time [2]. The purpose of this concept is to remove or minimize the use of empirical correlations (mathematical based methods) to develop reactor simulation tools by incorporating the first-principles effects of the governing physics and transcending them to the traditional "engineering" scale [1]. AMSO has initiated two parallel programmes [3, 4] to develop a new generation of integrated modelling and safety software according to this concept. Similar efforts have been implemented in the European Union and other countries as well [5–8]. This article is an introduction to a reactor simulation environment, developed within the framework of the corresponding author's Ph.D. dissertation, as an absolutely independent academic effort, which pursues the same objective" [9–11].

Structure of the SE which currently consists of three main codes is presented in Section 2 along with a brief review of the primary and secondary numerical models and treatments incorporated in the development process, in addition to the algorithms of these codes in the combined form for coupled thermohydraulic neutronic analyses of nuclear reactors. In Section 3, some of the most noteworthy innovations associated with the SE are briefly introduced along with a few selective outputs which indicate the practical advantages provided by these innovations. Lastly, in order to demonstrate the accident modelling capabilities of the SE, selective outputs of simulation associated with two DBAs, i.e. LOCA [9] and RIA [11] on TRR (Tehran Research Reactor) are presented in Section 4. General conclusions on the matters discussed in this paper are presented in Section 5.

2. STRUCTURE OF THE SIMULATION ENVIRONMENT

The SE currently consists of three main codes which have been programmed from scratch. A CFD-based code that solves the transient and steady states thermohydraulic sets of conservation equations (including the Navier-Stokes equations for momentum balance) in two and three dimensions, for both single and two-phase flows. “Table 1 gives a brief review of numerical methods and special treatments incorporated into the new CFD code along with the references in which they are explained. Many subtle modifications are applied to the original methods mentioned in the table. These modifications are mainly focused on two points; reducing computational resources required and applying these methods to an unstructured and hybrid mesh grid. The most noteworthy modifications are:

- Improving method of applying the least-square scheme for gradients evaluation;
- Modifying the PISO scheme for pressure-velocity coupling;
- Using geometric-based method for AMG accelerator instead of mathematic-based one” [10].

Further information has been presented in Ref. [9].

TABLE 1. BRIEF REVIEW OF NUMERICAL METHODS AND SPECIAL TREATMENTS INCORPORATED INTO THE CFD CODE

Title	Applied method		
Spatial discretization method	Finite volume [12]		
Temporal discretization method	Direct kinetic [1]		
	HOBD [13]		
Solver approach	Point-implicit solver [14]		
Turbulence model	Simple	General	Standard k-ε [15]
		Wall modelling	Standard wall-function [15]
	Advanced	General	Realizable k-ε [16]
		Wall modelling	Enhanced wall-treatment [17]
Linearization shape function	Second-order linear function [12]		
Method of evaluation of dependant variables on faces of a numerical cell	Convection terms (except for pressure term in the momentum equations)		Second-order upwind [18]
	Diffusion terms		Central-difference [19]
Pressure interpolation scheme (including the momentum equations)	Natural-convection dominated problems		Body force weighted [20]
	Other problems		Central-difference [19]
Gradients evaluation method	Least squares cell-based [21]		
Gradient (slope) limiter	Differential type [22]		
Pressure-velocity coupling scheme (pressure-correction equation)	Steady state problems		SIMPLE [23]
	Time-dependant problems		PISO [24]
Under-relaxation method	Variables (explicit) relaxation scheme [12]		
Solution accelerator	Algebraic Multi-Grid (AMG) with V-cycle recursive procedure [25]		
solution method of Linear Algebraic Equations (LAE) set	LU decomposition with partial implicit pivoting [26]		
General multiphase model	Drift flux (Mixture) model [27]		
	Two-flow (Eulerian) model [27]		
wall boiling models in the context of the Eulerian multiphase model	Sub-cooled boiling regime		RPI nucleate boiling [28]
	Departed nucleate boiling regime		Extended RPI [29]

The second code solves the point kinetics set of neutronic differential equations with up to six groups of delayed neutron precursors using three different numerical methods i.e. Runge-Kutta method of order 4, an open-integral method of order 5 and the Gear method and one semi-analytical method i.e. the Spectral method [9]. Among these four prominent methods, the last one revealed to be the best for coupling with the CFD-code based on the criterion that "It works with longest possible time-step while it keeps accuracy and stability of the solution". Further information could be found in Ref. [9].

The third code solves transient and steady states sets of multi-group neutron diffusion equations in one to three dimensions and isotropic or anisotropic forms. Table 2 presents a brief survey of numerical models incorporated into the diffusion code along with the references in which they are explained. Note that the general secondary numerical methods and treatments, which are similar to ones mentioned in Table 1, are omitted from Table 2.

TABLE 2. BRIEF REVIEW OF NUMERICAL MODELS INCORPORATED INTO THE DIFFUSION CODE

Title	Applied method
Spatial discretization method	Finite volume [12]
Temporal discretization method	Direct kinetic [1]
	HOBD [13]
	Original SIDK [1]
	Improved SIDK of first order and second order
Solver approach	Point-implicit solver [14]

The solution algorithms of these codes are represented in Fig. 1 and 2 in the combined form for coupled thermohydraulic neutronic analyses of nuclear reactors.

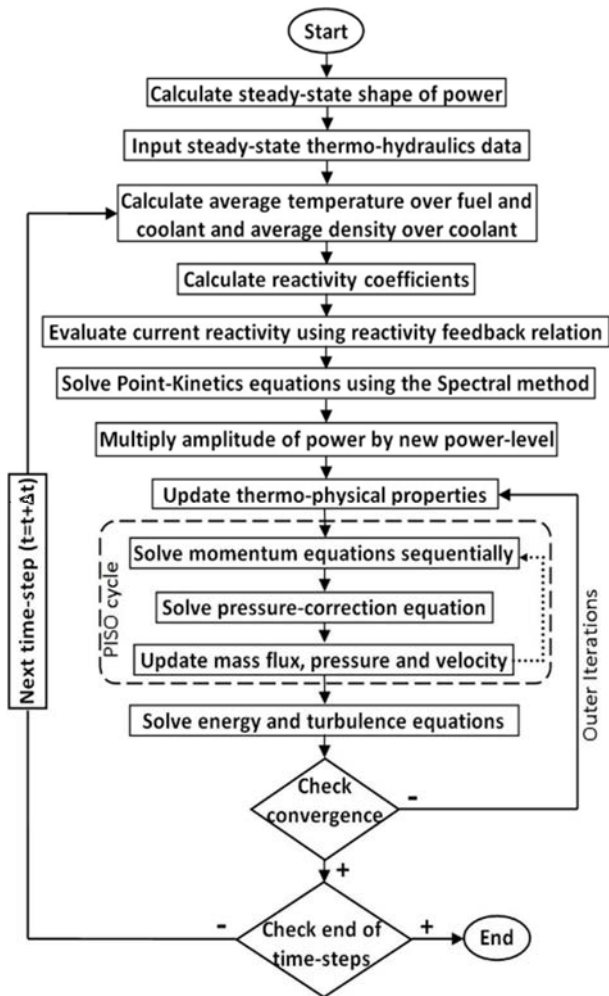


FIG.1. Coupled algorithm of point-kinetic and CFD codes.

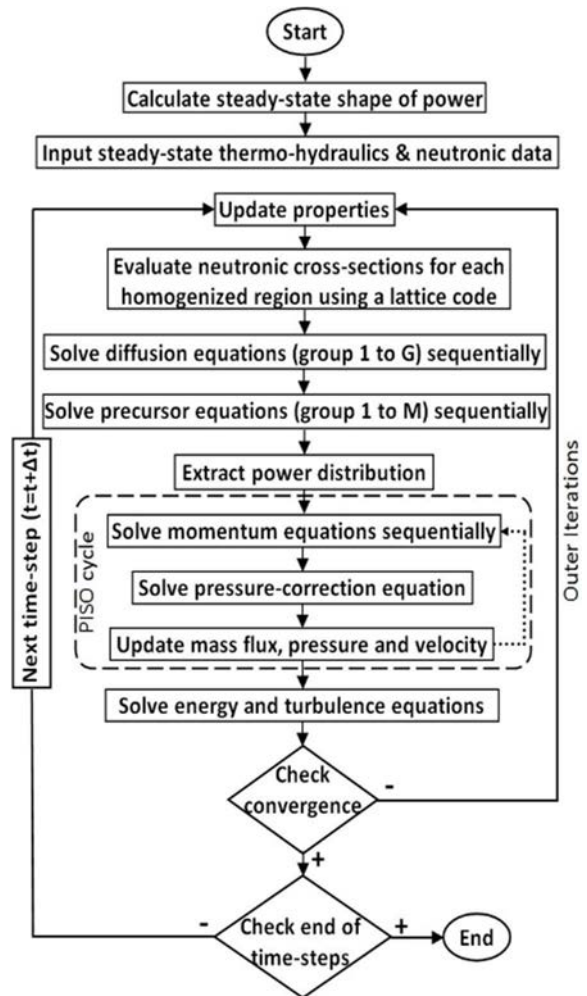


FIG.2. Coupled algorithm of diffusion and CFD codes.

3. A BRIEF REVIEW OF THE INNOVATIONS INCORPORATED INTO THE SIMULATION ENVIRONMENT.

In this section some of the most noteworthy innovations associated with the SE are briefly introduced along with a few selective outputs for the cases which are not going to be covered in the next section and indicate the practical advantages provided by the innovations.

Most important innovation is named "simultaneous solution" which is a novel approach for coupling the neutronic and thermohydraulic analyses. In the conventional method for this purpose, as represented in Fig. 3, each analysis is conducted separately and then it is attempted to close the gap between them and exchange feedbacks. This task is usually accomplished by employing a complicated and costly platform. However, in the methodology introduced in this study, i.e. the simultaneous solution approach, the "point-implicit" solver is used whereby all steps of solving the neutronic and thermohydraulic equations along with all steps of computing and exchanging feedbacks are transferred into the numerical iteration cycle of this solver as depicted in Fig. 1 and 2. Therefore, three iteration cycles of the conventional method (see Fig. 3) reduce to one and consequently, computational cost reduces significantly. More importantly, the step of using platforms and the associated problems is fundamentally removed which is very crucial. Furthermore, flexibility of the conventional method with regard to mesh grid, time step and the basic method applied to the both analyses is completely preserved and even, improved.

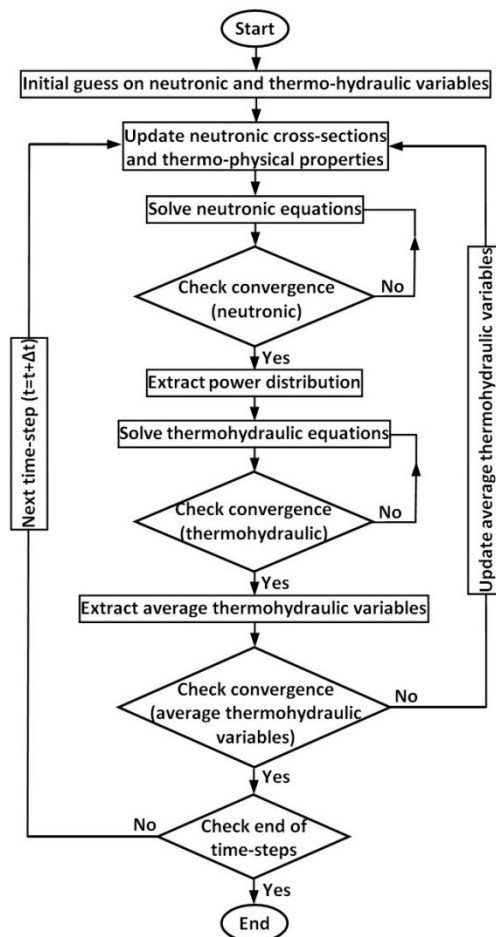


FIG.3. Typical algorithm for conducting the conventional neutronic-thermohydraulic coupled analysis.

Although, the new generation of advanced modelling codes (similar to the CFD and diffusion codes devolved for the SE introduced in this study) are highly flexible to the details of geometry of solution domain and this domain could be directly modelled up to its smallest details, but the computational cost of conducting a large-scale simulation such as the whole core of a power nuclear reactor is way beyond the level of numerical resources which is normally available to an average researcher. As a result, transcending the application of these coded to the

traditional "engineering" scale is an inevitable part of all programmes indicated in Section 1 [2]. Employing the porous media model is one of the widely regarded approaches to achieve this goal [10]. However, in the conventional method of applying this model to the CFD codes, the whole reactor core simplifies to a single porous medium and also, the resistance coefficients that are essential to use this model are constant values. These conditions impose significant errors and restrict the applications of the model to the cases like accident analysis and simulation of pure natural convection in an accurate manner for which mass flow rate changes during the solution or it is basically unknown. In the "multi-region porous media" model developed and incorporated into the SE, the procedure for calculating the coefficients is modified by introducing a practical algorithm. Using this algorithm will result in obtaining each coefficient as a function of mass flow rate. Furthermore, the method of applying these coefficients to the reactor core is modified by dividing the core into several porous media, each of which comprises a single fuel assembly and then the data on the boundaries of each porous medium are extracted during the solution and applied as boundary conditions to the detailed model of fuel assembly to retrieve the detailed information regarding the fuel behaviour under any sort of conditions. Full information regarding this new model is available in Ref. [10]. Here, some selective outputs obtained by employing the multi-region porous media model for a research reactor (whole pool of TRR) and a power reactor (whole core of BNPP) are presented in Fig. 4 and 5, respectively.

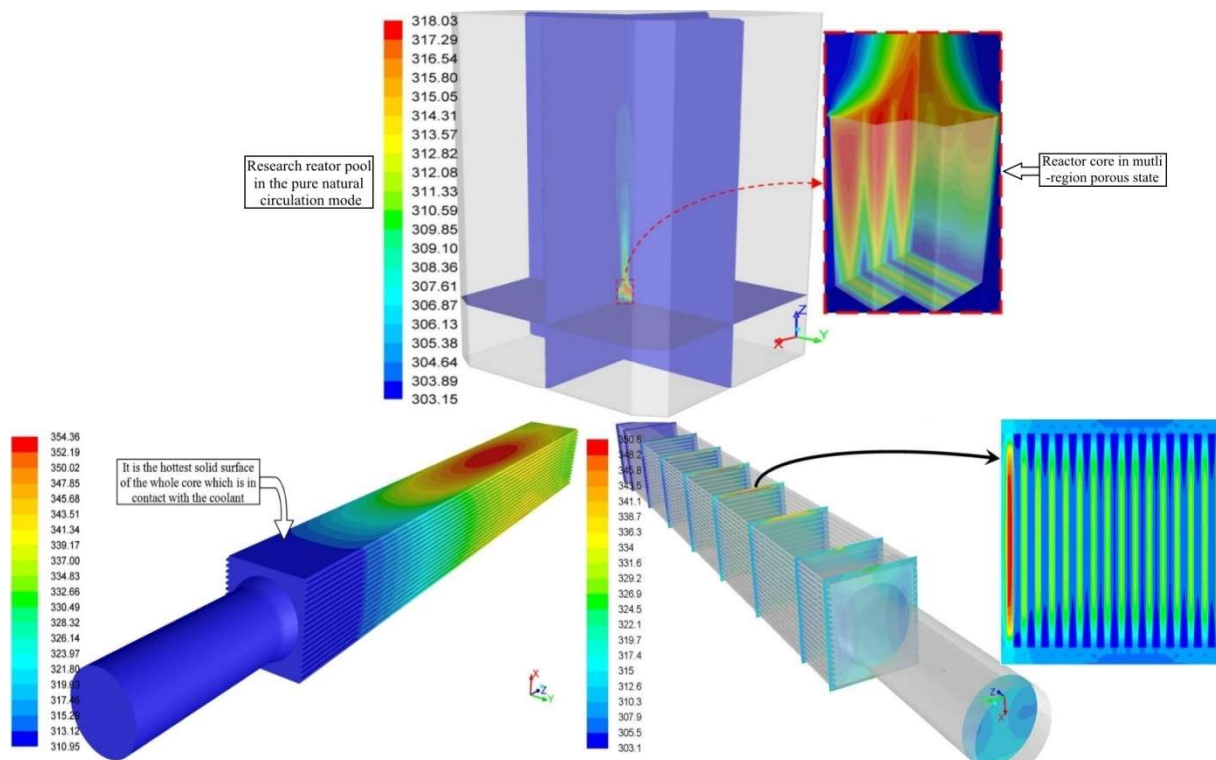


FIG.4. An example of the multi-region porous media model application to TRR (temperature in Kelvin) [9, 10].

"Semi-Implicit Direct Kinetic (SIDK) is an innovative method for temporal discretization of neutronic equations proposed by J. Banfield [1]. The key approximation of SIDK method is to substitute a time-averaged quantity for fission source term in the delayed neutron differential equations. Hence, these equations are decoupled from prompt neutron equations and an explicit analytical representation of precursor concentrations is obtained which lead to significant reduction in the computational cost. Since, fission source is not known in a time-step, the original study suggested using the constant quantity pertaining to the previous time-step for this purpose and reduction in the size of time-step was proposed to lessen the imposed errors. However, this remedy notably diminishes the main advantage of SIDK method. In the Improved SIDK method incorporated into the SE, the key feature of the point-implicit solver [14] which is the separated solution of the governing equations is employed to mitigate the mentioned drawbacks. Accordingly, the SIDK's analytical relations are inserted into the numerical iteration cycle of the point-implicit solver as independent explicit steps, while the quantity of fission source is not constant but it is being updated, according to a modified formulation, using the most recent values of neutron

group fluxes. This remedy has resulted in attaining a much more accurate estimation of the time-averaged fission source term in the current time-step, while significant portion of the computational costs reduction has been retained. Here, some selective outputs obtained by employing Improved SIDK method for the LRA transient benchmark problem [30] are presented in Fig. 6 and 7". Further information could be found in Ref. [31].

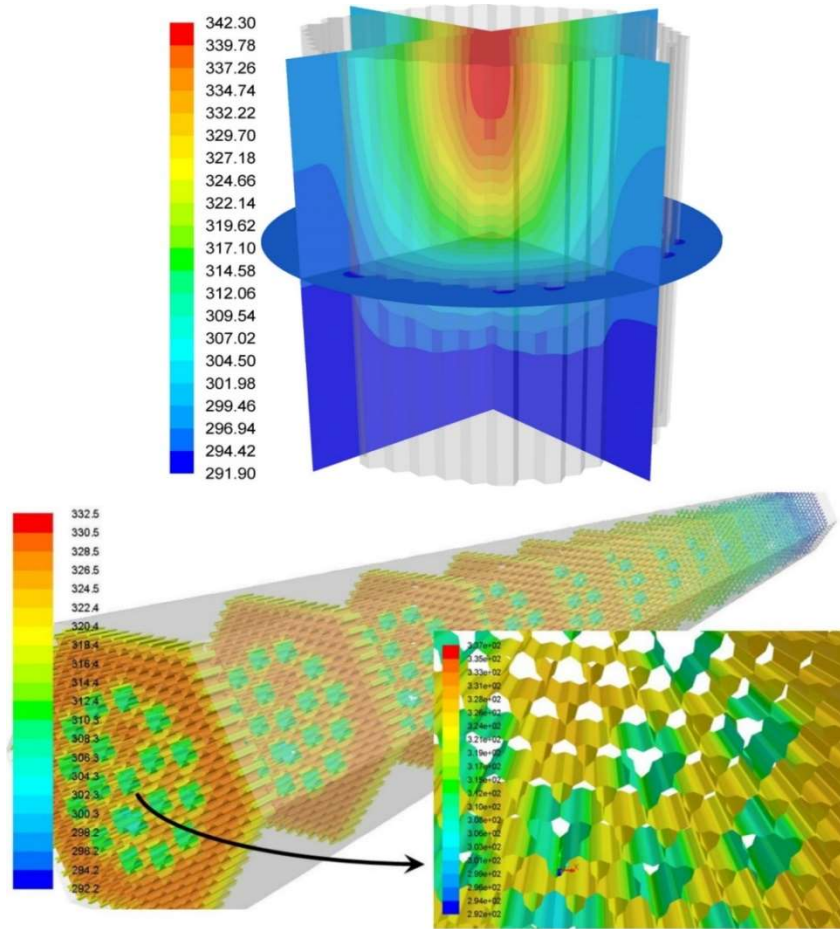


FIG.5. An example of the multi-region porous media model application to BNPP (temperature in Kelvin).

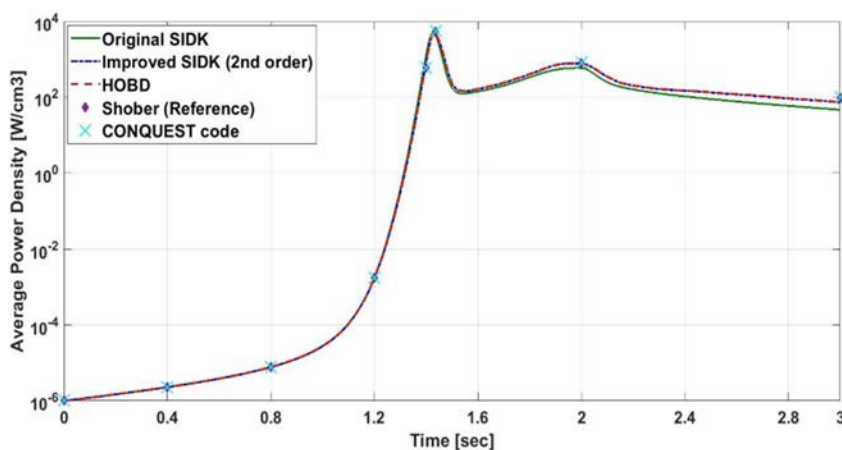


FIG.6. Variations of average power density of the BWR core versus time for LRA problem. (Reproduced courtesy of Springer [31]).

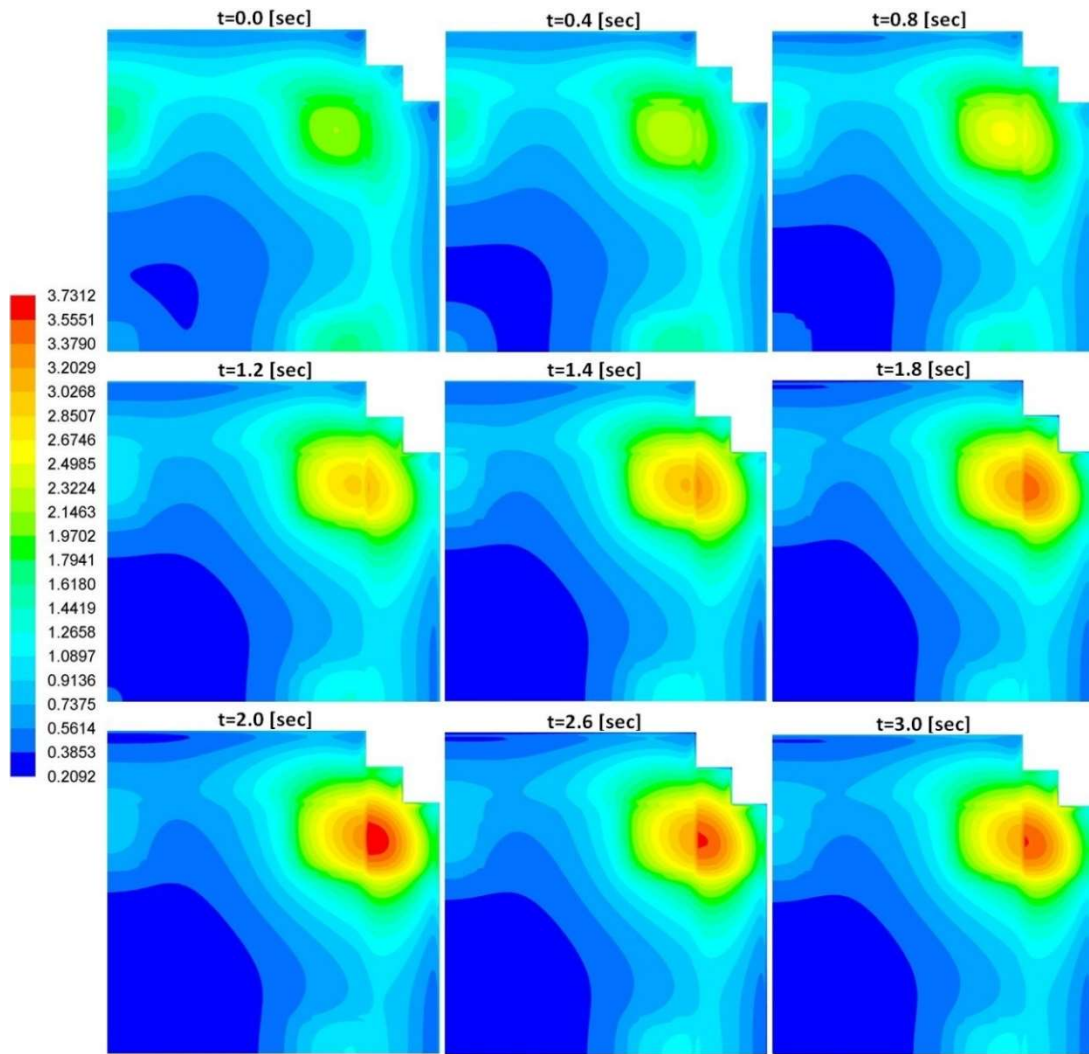


FIG. 7. Temporal sequence of normalized contours of power density distribution on the central cross-section of the BWR core associated with LRA problem during the accident using the improved SIDK method (Reproduced courtesy of Springer [31]).

4. CASE STUDIES ON TRR

In order to demonstrate the accident modelling capabilities of the SE, selective outputs associated with simulation of two DBAs, i.e. RIA and LOCA in TRR, which is a pool-type material test research reactor, are presented in this section. A brief review of the relevant specifications of TRR is presented in Table 3 [9].

TABLE 3. SPECIFICATIONS AND MAIN OPERATING CONDITIONS OF TRR [9].

Title	Design specifications	
Thermal power	5 MW	
Fuel type and materials	MTR, LEU 20%, U ₃ O ₈ -Al (Meat), Al (Clad)	
Fuel assembly dimensions	7.6×8.01×87.8 cm	
Each location cross sectional dimensions	7.71×8.1 cm	
Grid plate locations for fuel assemblies	9×6	
No. of fuel plates in standard fuel assembly	19	
Coolant material/Operating pressure	Light water/0.171 MPa	
Cooling method	-Operational condition	-Forced flow primary loop
	-Full shutdown condition	-Natural circulation
Primary coolant flow rate	500 m ³ /h	

Both accidents have been modelled using the algorithm delineated in Fig. 1. The LOCA in TRR involves the flow reversal phenomenon which characterizes as a sophisticated transition from fully-turbulent forced convection flow regime to pure passive natural circulation combined with limited reactivity insertion due to thermohydraulic feedbacks. On the other hand, the large positive reactivity induced in the case of RIA demanded to modify the conventional reactivity feedback formulation in framework of the point-kinetics method, especially with regard to the void generation effects in the two-phase flow realm. All details and information concerning the RIA and LOCA modelling could be found in Ref. [11] and [9] respectively. Here, two major outputs of the RIA and LOCA modelling are represented in Fig. 8 and 9 respectively, in order to focus on a very crucial point.

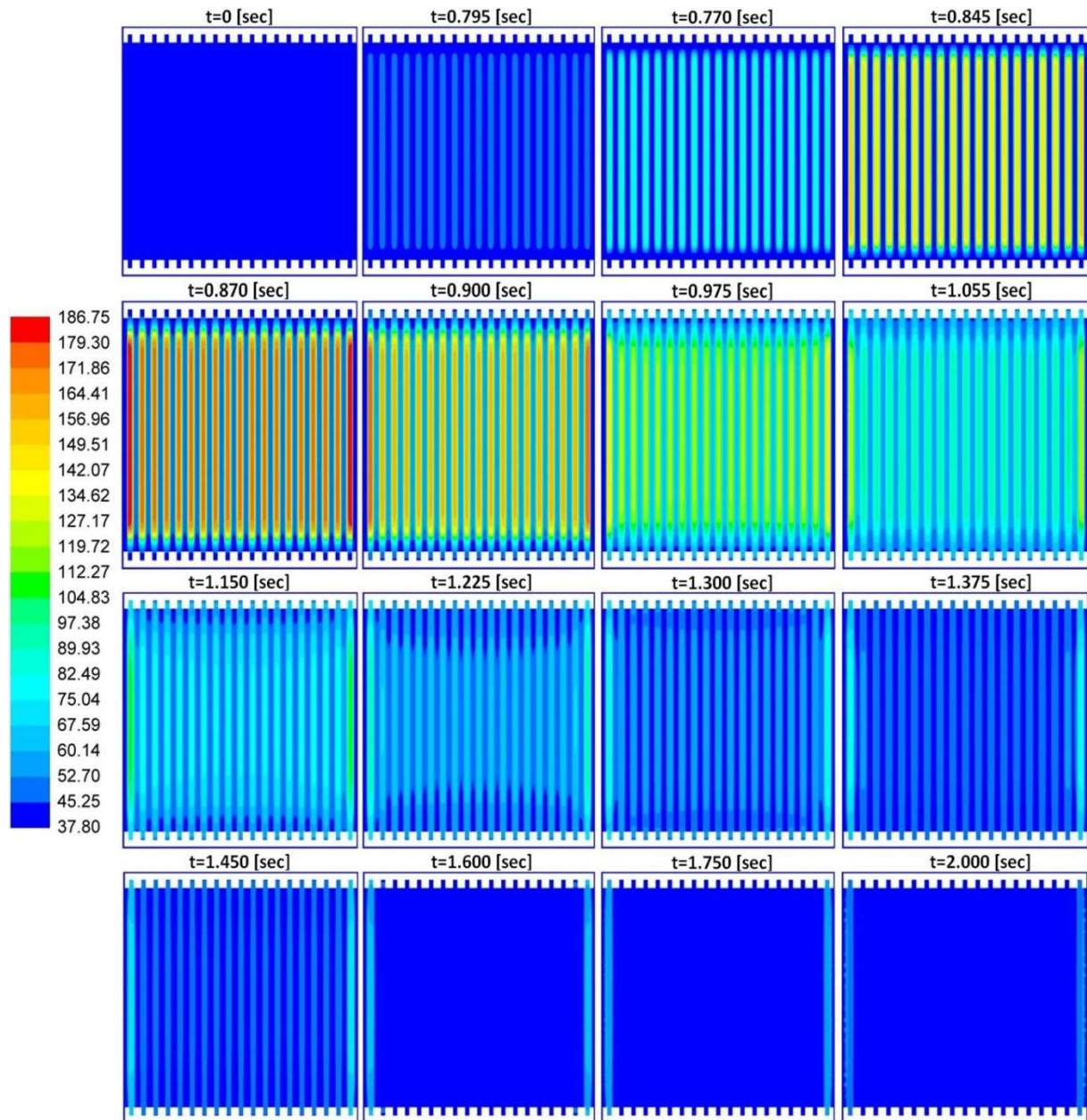
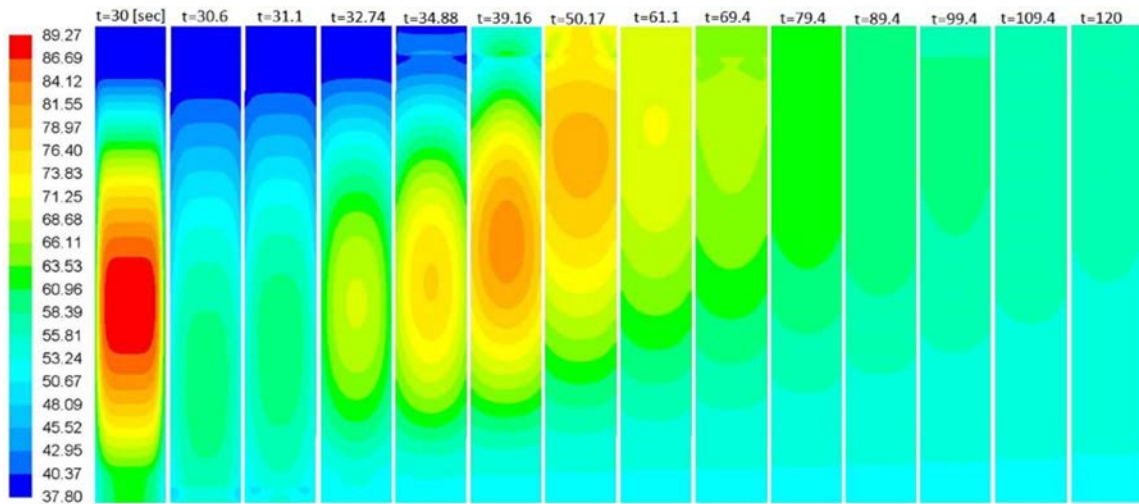
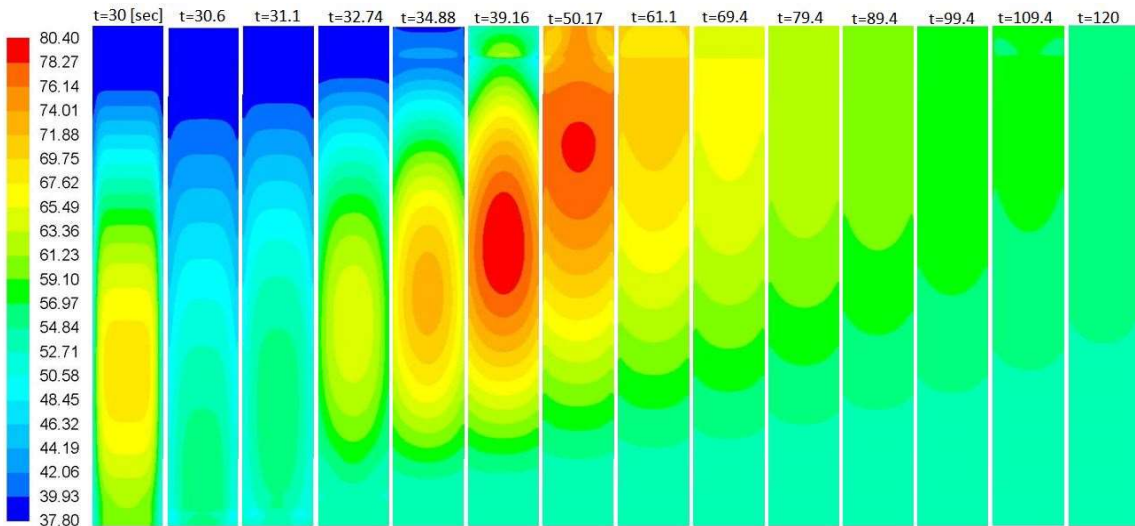


FIG. 8. Temporal sequence of temperature distribution contours (in $^{\circ}\text{C}$) on the virtual cross-section that cuts through the centre of FA perpendicular to the fuel plates for RIA (Reproduced courtesy of Elsevier [11]).

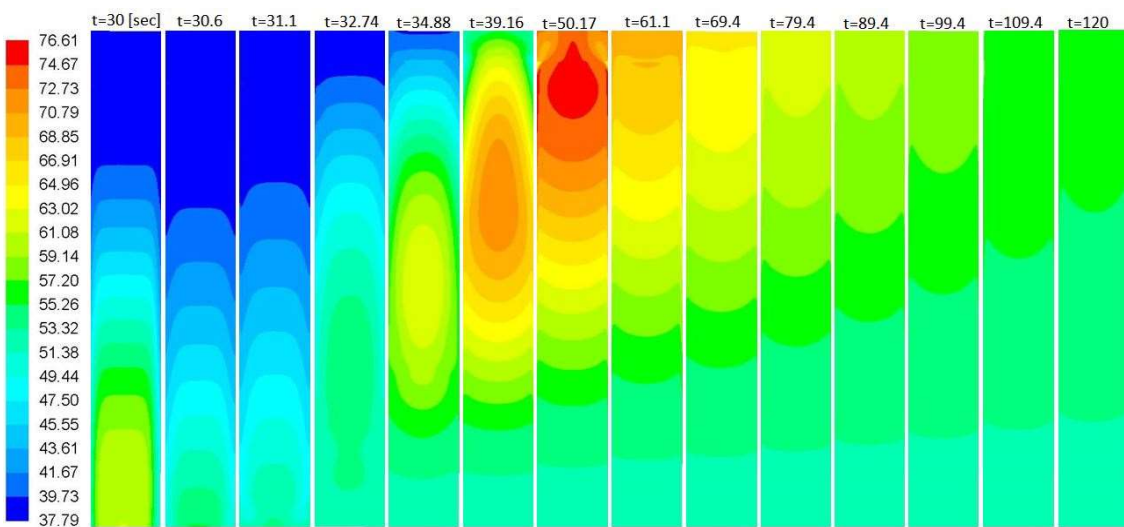
These three dimensional and detailed oriented outputs clearly indicate that the most vulnerable position of the reactor core to effects of both accidents is on the outer side of the two fuel plates located in the outermost of the fuel assembly. In all cases, the pressure loss in the side passage is higher than the central one, as well.



(a) $X=0$ [mm] (on the surface of fuel plate)



(b) $X=0.2$ [mm] (in the boundary layer region)



(c) $X=0.675$ [mm] (in the free stream region)

FIG. 9. Temporal sequence of temperature distribution contours (in $^{\circ}\text{C}$) of coolant on three virtual sections parallel to the fuel plate in the hot channel for the LOCA [9] (X refers to distance from the fuel plate) (Reproduced courtesy of Elsevier [9]).

The detailed results have also revealed that the reason for this vulnerability is 27% mass distribution imbalance between the central and side passages due to very narrow diameter designated for the side passage (2.1 mm). Furthermore, 15% reduction in this diameter, halfway through the grid plate which apparently designed to avoid the possibility of reversal flow formation at outlet of the passages [11] has clearly intensified the mass imbalance issue. Accordingly, we repeated the simulation on the solution domain for which the mentioned reduction in diameter was removed and then the total diameter is increased by only 9% (to the utmost safe extent) [11]. The combined effects of these two adjustments resulted in more than 44% reduction in the amount of mass imbalance at a very reasonable cost while the flow velocity calculated at outlet of the modified side passage has been high enough to avoid any possibility of flow reversal occurrence [11].

This practical example profoundly demonstrates that how the detailed-oriented data and the consequent significant physical insight provided by the new generation of codes developed based on the "predictive simulation" concept could be used to specify the vulnerable positions of the reactor core under any accident conditions and recognize the associated reasons whereby it provides the opportunity to achieve an accurate estimation of the effects of various possible modifications, in order to select an optimized solution which could resolve or mitigate the consequences of accidents in an informed manner. The crucial fact is that this essential virtue could not be achieved using the conventional one-dimensional, mathematical-based codes such as the PARET or Relap 5, simply because they could not include the required geometric details and also the empirical correlations incorporated into them have many recognized restrictions [2].

5. CONCLUSIONS

In this paper, a novel SE developed based on the "predictive simulation" concept was introduced. Structure of the SE which currently consists of three main codes was described and algorithms of these codes in the combined form for coupled thermohydraulic-neutronic analyses of nuclear reactors were presented. Then, some of the most noteworthy innovations associated with the SE were briefly explained using a few selective outputs which indicate the practical advantages provided by these innovations. Lastly, in order to demonstrate the accident modelling capabilities of the SE, selective outputs of simulation associated with two DBAs, i.e. LOCA and RIA on TRR were presented and discussed. The varied and diverse results represented in this paper indicated the capability of the SE in performing comprehensive and accurate analysis of different types of nuclear reactors (including MTR, VVER and BWR) and behaviour of their fuel under various steady-state and accident conditions. However, the most noteworthy conclusion might be drawn from the practical examples mentioned in Sec. 4 which demonstrated how the detail-oriented, three-dimensional outputs provided by the SE on the real geometry of the reactor instead of the homogenized one used by the conventional one-dimensional codes led to specifying the vulnerable positions of the reactor core to the accident, discovering its causes and thereby proposing informed and optimized modifications to mitigate the consequences of the accident.

6. NOMENCLATURES

SE	Simulation Environment
CFD	Computational Fluid Dynamics
SIDK	Semi-Implicit Direct Kinetic
TRR	Tehran Research Reactor
DBA	Design Basis Accident
LOCA	Loss of Coolant Accident
RIA	Reactivity Insertion Accident
AMSO	Advanced Modelling and Simulation Office
MTR	Material Test Reactor
BWR	Boling Water Reactor
BNPP	Bushehr Nuclear Power-Plant
AMG	Algebraic Multi-Grid
PISO	Pressure-Implicit with Splitting of Operators
FA	Fuel Assembly

ACKNOWLEDGEMENTS

This article has been prepared based on the researches conducted in the Ph.D. dissertation of the corresponding author and it has been entirely funded by the authors. This personal study has no connection with any governmental or non-governmental entities.

REFERENCES

- [1] BANFIELD, J.E., "Semi-implicit direct kinetics methodology for deterministic, time-dependent, and fine-energy neutron transport solutions", Ph.D. diss., University of Tennessee, Knoxville, 2013. http://trace.tennessee.edu/utk_graddiss/1694.
- [2] AMSO, Advanced Modelling and Simulation Office. [Online] the USA DOE/NE (December 17, 2014) <http://energy.gov/ne/nuclear-reactor-technologies/advanced-modeling-simulation>.
- [3] NEAMS, Nuclear Energy Advanced Modelling and Simulation programme. [Online] the USA DOE/NE (December 17, 2014) <http://neams.ne.anl.gov>.
- [4] CASL, The Consortium for Advanced Simulation of Light Water Reactors. [Online] the USA (December 17, 2014) <http://www.casl.gov>.
- [5] F-BRIDGE, Framework of Basic Research for Innovative Fuel Design for GEn IV systems project, [Online] the European Union. (December 17, 2014) <http://www.f-bridge.eu>.
- [6] SMART project, Integrated Modular Advanced Reactor project. [Online] Korea Atomic Energy Research Institute (December 17, 2014) <https://www.kaeri.re.kr>.
- [7] IVNET, Innovative and Viable Nuclear Energy Technology Development project. [Online] Research Group for Thermal and Fuel Energy. Japan Atomic Energy Agency (December 17, 2014) nsec.jaea.go.jp.
- [8] ASRC, Advanced Science Research Centre. Sector of Nuclear Science Research (SNSR). [Online] Japan Atomic Energy Agency (December 17, 2014) asrc.jaea.go.jp.
- [9] VADI, R., SEPANLOO, K., Investigation of a LOCA in a typical MTR by a novel best-estimate code, *Progress in Nuclear Energy* **86** (2016) 141–161.
- [10] VADI, R., SEPANLOO, K., An improved porous media model for nuclear reactor analysis, *Nuclear Science and Techniques* **27** (1) (2016) 1–24.
- [11] VADI, R., SEPANLOO, K., Reassessment of the generic assumptions applied to the conventional analysis of the reactivity insertion accident in the MTRs using a novel coupled code, *Progress in Nuclear Energy* **93** (2016) 96–115.
- [12] LEVEQUE, R.J., *Finite Volume Methods for Hyperbolic Problems*, Cambridge University Press, UK, 2004.
- [13] GINESTAR, D., High-order backward discretization of the neutron diffusion equation. *Ann. Nucl. Energy* **25** (3) (1998) 47–64.
- [14] CHORIN, A. J., Numerical solution of Navier-Stokes equations, *Mathematics of Computation* **22** (1968) 745–762.
- [15] LAUNDER, B. E., SPALDING, D. B., *Lectures in Mathematical Models of Turbulence*, Academic Press, London, England, 1972.
- [16] SHIH, T. H., LIOU, W. W., SHABBIR, A., YANG, Z., ZHU, J., A New k- ϵ Eddy-Viscosity Model for High Reynolds Number Turbulent Flows - Model Development and Validation, *Computers Fluids* **24** (3) (1995) 227–238.
- [17] CHEN, H. C., PATEL, V. C., Near-Wall Turbulence Models for Complex Flows Including Separation, *AIAA Journal* **26** (6) (1988) 641-648.
- [18] BARTH, T.J., JESPERSEN, D., The design and application of upwind schemes on unstructured meshes, Technical Report AIAA-89-0366, AIAA 27th Aerospace Sciences Meeting, Reno, Nevada, 1989.
- [19] LEONARD, B.P., The ULTIMATE conservative difference scheme applied to unsteady one dimensional advection, *Comp. Methods Appl. Mech. Eng* **88** (1991) 17–74.
- [20] PATANKAR, S.V., *Numerical Heat Transfer and Fluid Flow*, Hemisphere, Washington, DC, 1980.
- [21] ANDERSON, W., BONHUS, D.L., An Implicit Upwind Algorithm for Computing Turbulent Flows on Unstructured Grids, *Computers Fluids* **23** (1994) 1–21.
- [22] WANG, Z.J., A Fast Nested Multi-grid Viscous Flow Solver for Adaptive Cartesian/Quad Grids, *International Journal for Numerical Methods in Fluids* **33** (2000) 657-680.
- [23] RHIE, C.M., CHOW, W.L., Numerical Study of the Turbulent Flow past an Airfoil with Trailing Edge Separation, *AIAA Journal* **21** (1983) 1525–1532.
- [24] ISSA, R. I., Solution of Implicitly Discretized Fluid Flow Equations by Operator Splitting, *Journal of Computational Physics* **62** (1986) 40–65.

- [25] HUTCHINSON, B.R., RAITHBY, G. D., A Multi-grid Method Based on the Additive Correction Strategy, *Numerical Heat Transfer* **9** (1986) 511–537.
- [26] PRESS, W.H., TEUKOLSKY, S.A., VETTERLING, W.T., FLANNERY, B.P., “Numerical Recipes in C”, Cambridge University Press, UK, 2th edition (1992).
- [27] FERZIEGER, J.L., PERIC, M., “Computational Methods for Fluid Dynamics”, Springer-Verlag, Heidelberg. 1996.
- [28] KURUL, N., PODOWSKI, M.Z., “On the modelling of multidimensional effects in boiling channels”, In Proceedings of the 27th National Heat Transfer Conference, Minneapolis, Minnesota, USA. 1991.
- [29] HOYER, N., Calculation of dryout and post-dryout heat transfer for tube geometry, *International Journal of Multiphase Flow* **24** (1998) 319–334.
- [30] COMPUTATIONAL BENCHMARK COMMITTEE OF THE MATHEMATICS AND COMPUTATION DIVISION OF THE AMERICAN NUCLEAR SOCIETY, National energy software centre: benchmark problem book, Technical Report, ANL-7416, supplement 3, Argonne, Illinois, USA, 1985.
- [31] VADI, R., SEPANLOO, K., An improved semi-implicit direct kinetics method for transient analysis of nuclear reactors, *Nuclear Science and Techniques* **30** 11 (2019) 162.

SIMULATION OF IFA650.5 EXPERIMENT USING THE FULLY COUPLED SPACE-FRAPTRAN CODE SYSTEM

H.C. KIM

Nuclear Fuel Safety Research Division,
Korea Atomic Energy Research Institute,
989-111, Daedeok-daero, Yuseong-gu, Daejeon, 34057,
Republic of Korea

S.W. LEE, K.D. KIM

Thermal Hydraulics and Severe Accident Research Division,
Korea Atomic Energy Research Institute,
989-111, Daedeok-daero, Yuseong-gu, Daejeon, 34057,
Republic of Korea

Abstract

A system analysis code, SPACE was coupled with a fuel transient analysis code, FRAPTRAN using a dynamic link library (DLL) scheme. In this coupling scheme, FRAPTRAN handles the heat conduction model including fuel deformation of single fuel rod and, SPACE deals with the calculation of all hydraulic cells and heat structures except for the fuel rod coupled with FRAPTRAN. This coupled code has been developed for coping with the change of auditing requirements for the emergency core cooling system (ECCS). To couple SPACE with FRAPTRAN, coupling scheme was proposed and coupling variables were defined. For reflood phase, new boundary conditions for FRAPTRAN calculated by SPACE have been developed in the view. In this work, IFA-650.5 experiments, which was a LOCA (loss of coolant accident) test without reflood phase using a high burnup fuel in order to validate the SPACE-FRAPTRAN coupled code. From the simulation results of SPACE-FRAPTRAN coupled system against Halden IFA-650.5 test, the cladding and heater temperatures predicted by code agreed well with experimental data. In addition, it was revealed that the most important factor for the cladding and heater temperature in the IFA-650 test is the surface-to-surface radiation heat flux and the fuel model had little effects on them. Therefore, it is required that surface-to-surface radiation enclosure model should be simulated appropriately for the Halden IFA-650 test to predict the proper behaviour of the cladding temperature.

1. INTRODUCTION

SPACE [1] is a system analysis code for design and safety analysis of nuclear power plants (NPPs), developed by Korea Hydro and Nuclear Power (KHNP), Korea Atomic Energy Research Institute (KAERI), Korea Electric Power Corporation Engineering and Construction (KEPCO-E&C), and Korea Electric Power Corporation Nuclear Fuel (KEPCO-NF). SPACE is equipped with thermal hydraulic analysis models, heat structures analysis models including fuel behaviour analysis model, trip and control systems etc. However, the fuel deformation model of SPACE is not a delicate mechanistic model but is similar to that of RELAP5 [2] based on NUREG-0630 model [3] developed in the early 1980s. Recently, revision of acceptance criteria for emergency core cooling system (ECCS) has been proposed by Korea Institute of Nuclear Safety (KINS) in Korea [4]. In the revised criteria, it is required to consider the improvement in our understanding of zirconium alloy cladding fuel behaviour during a LOCA transient. For example, the fuel rod undergoes exothermic high temperature oxidation, cladding burst, thermo mechanical deformation of cladding, and fuel fragmentation, relocation, and dispersion (FFRD) during loss of coolant accident (LOCA). Therefore, to simulate proper fuel behaviour during LOCA, the system code should incorporate transient fuel models in view of the best-estimated calculation. FRAPTRAN [5] developed by U.S. Nuclear Regulatory Commission (NRC) is equipped with considerably delicate fuel model but limited thermal hydraulics model compared with SPACE. Therefore, to compensate for the weakness and preserve the analyzing capability of both codes, a linkage function between the two codes using the features of the Dynamic Link Library (DLL) has been developed. In this coupling scheme, FRAPTRAN deals with heat conduction including fuel deformation of single fuel rod and SPACE takes charge of the calculation of all hydraulic cells and heat structures except the fuel rod coupled with FRAPTRAN. It is observed that the output of FRAPCON [6], which calculates the steady state fuel characteristic related with fuel burnup, is incorporated to generate the initial condition for the input of FRAPTRAN.

In this work, IFA-650.5 experiment [7], which was a LOCA (loss of coolant accident) test without reflow phase using a high burnup fuel in order to validate the SPACE-FRAPTRAN coupled code. From the simulation results of SPACE-FRAPTRAN coupled system against Halden IFA-650.5 test, the cladding and heater temperatures predicted by code agreed well with experimental data. In addition, it was revealed that the most important factor for the cladding and heater temperature in the IFA-650 test is the surface-to-surface radiation heat flux and the fuel model had little effects on them. Therefore, it is required that surface-to-surface radiation enclosure model should be simulated appropriately for the Halden IFA-650 test to predict the proper behaviour of the cladding temperature.

2. DEVELOPMENT OF SPACE-FRAPTRAN COUPLED CODE SYSTEM

2.1. The coupling algorithm

In SPACE-FRAPTRAN coupling calculation, SPACE is a master programme and FRAPTRAN is coupled with SPACE as a dynamic link library (DLL). Figure 1 shows the overview of the linkage between SPACE and FRAPTRAN. FRAPTRAN DLL named as “M-TRAN” is called by SPACE and data transfer from SPACE to FRAPTRAN is conducted through the functions name by “SET_”. Afterwards, FRAPTRAN calculates heat conduction including fuel deformation and returns the heat flux, surface temperature, and outer diameter to SPACE through “GET_” functions. Functions with a prefix “CALL_” are the functions that call the subroutines in FRAPTRAN such as “CALL_SFRAPTRAN” for initialization and “CALL_CRANK6” for time advancement during transient. If required, the FRAPCON output file can be used for burnup fuel simulation.

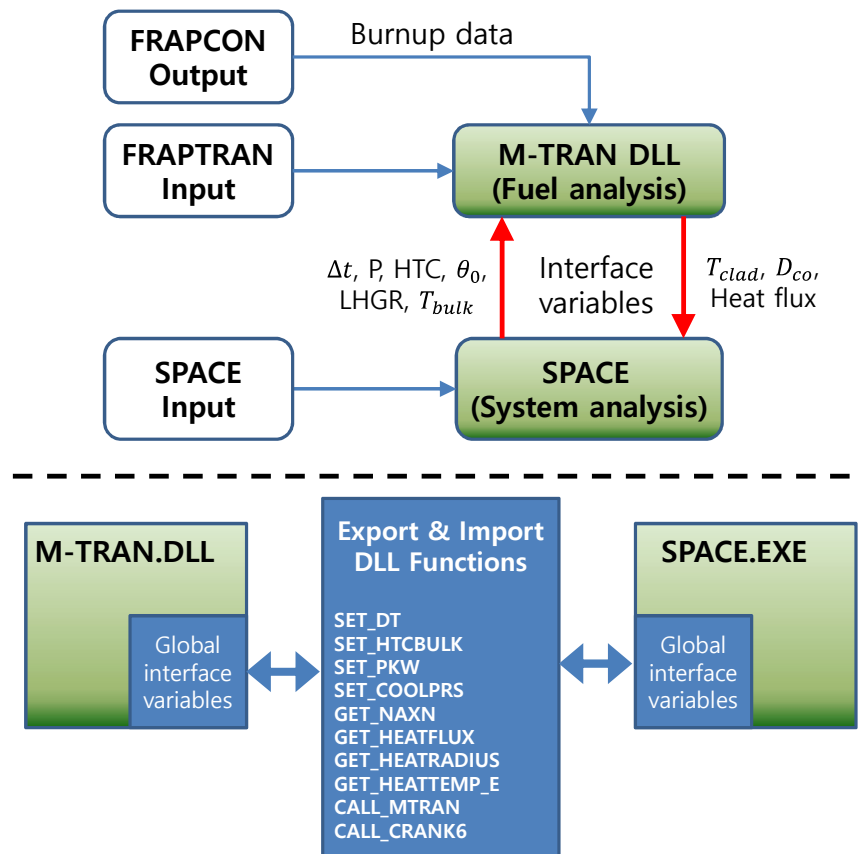


FIG. 1. Overview of SPACE-FRAPTRAN coupling scheme.

To couple SPACE/FRAPTRAN code system, coupling methodology should be defined because each code system already was used and validated with their own methodology. As shown in Figure 2, we proposed coupling methodology of two codes for steady state and transient maintaining each calculation flow and I/O (Input/Output) system.

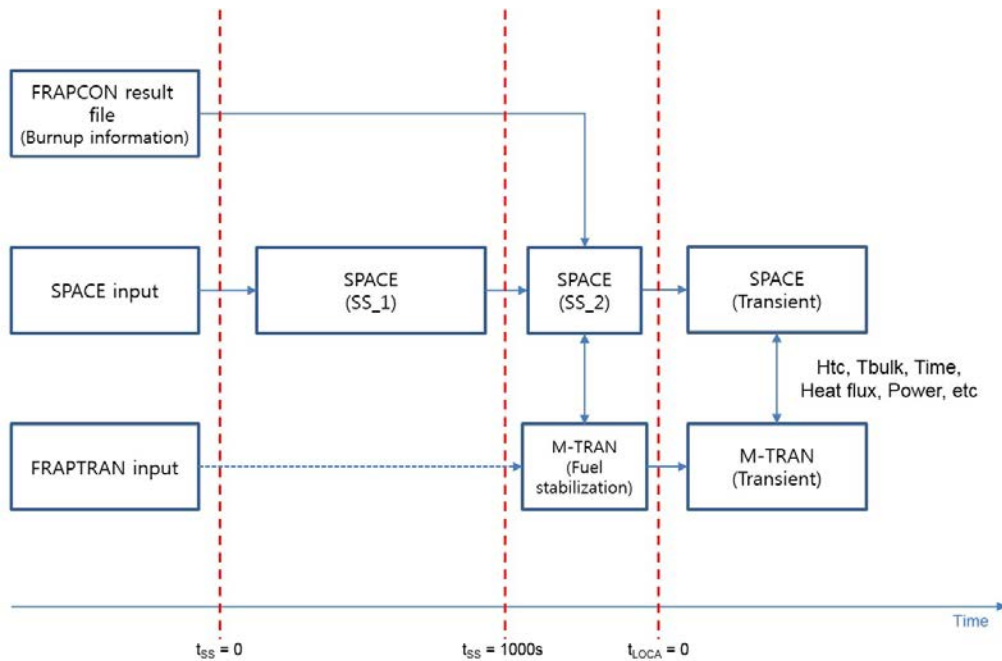


FIG. 2. Calculation sequence of SPACE-FRAPTRAN.

At the beginning of fully coupled calculation, SPACE performs steady state calculation with input file of SPACE. For this calculation, SPACE employs its heat structure instead of fuel rod. We call the 1st SS (steady state) calculation which performs null transient calculation without FRAPCON/FRAPTRAN. Once SPACE completes the 1st SS, it calls M-TRAN which is modularized FRAPTRAN to be implemented as DLL. For the first calling, M-TRAN initiates input variables and stores FRAPCON result file to apply burnup dependent variables. The M-TRAN starts fuel stabilization which increase power gradually to stabilize fuel thermo mechanical behaviour. We call the 2nd SS for fuel stabilization. Once fuel stabilization is completed, fully coupled SPACE/FRAPTRAN is ready to start transient calculation for LOCA.

2.2. Coupling variables

For coupling calculation, several interface variables have been defined. First, the interface variables from SPACE to FRAPTRAN are as follows: 1) total heat transfer coefficient (HTC), which is a simple summation of all HTCs; 2) temporary heat flux, which is based on previous wall temperature and current HTCs; 3) linear heat generation rate (LHGR); 4) coolant pressure of each cell. Among these variables, total HTC and temporary heat flux are used for boundary condition of heat conduction in FRAPTRAN. The LHGR is also provided as a heat source of the heat conduction model in FRAPTRAN. In addition, the coolant pressure is essential for fuel deformation model. Second, the interface variables from FRAPTRAN to SPACE are as follows: 1) surface heat flux; 2) fuel center and clad outer surface temperatures; 3) clad outer diameter. In SPACE, surface heat flux, clad surface temperature, and clad outer diameter are used for calculating the energy conservation equations, wall HTCs, and fluid deformation, respectively. The fluid deformation model deals with time dependent flow area and physical models related with hydraulic diameter. Table 1 shows the summary of interface variables for the SPACE-FRAPTRAN coupling method. Currently, the time increment for temporal advance is determined by SPACE and provided for FRAPTRAN.

TABLE 1. COUPLING VARIABLES FOR SPACE-FRAPTRAN

Calling module	Variable name	Content
M-TRAN	Time increment	Size of Time step
	Power	Linear Heat Generation Rate (LHGR)
	CoolPress	Coolant pressure
	Htc	Heat transfer coefficient of cladding surface
	Tbulk	Coolant T
SPACE	Outdia	Cladding outer diameter (incl. oxide thickness)
	Heatflux	Cladding heat flux
	Tsurf	Cladding surface T

2.3. Coupling of convection model for reflood phase

In coupled calculation, heat conduction inside the fuel rod and convection at the fuel rod surface are solved using FRAPTRAN and SPACE, respectively. The boundary condition at the right surface in heat conduction equation of FRAPTRAN.

It is observed that only one HTC and fluid temperature are used to solve the heat conduction equation in FRAPTRAN. However, various HTCs and fluid temperatures exist in SPACE because SPACE deals with three-field (droplet, vapour and liquid) conservation equations and thus, it is required that a representative HTC and bulk fluid temperature should be provided by SPACE. Therefore, HTCs and fluid temperatures could be averaged for over current time step at each axial position with a type of weighting factors but every averaging method exhibits certain weak points in that singular point exists. To overcome the shortcomings, we modified the boundary condition of the heat conduction equation for coupled calculation as follows [8]:

$$\theta^{n+1} = \theta_0 + h_{tot}(T_w^{n+1} - T_w^n) = AT_w^{n+1} + B \quad (1)$$

$$T_w^{n+1} = \frac{B + h_{tot}T_w^n - \theta_0}{h_{tot} - A} \quad (2)$$

where θ^{n+1} is current heat flux, θ_0 is a heat flux based on new HTCs and previous surface temperature, h_{tot} is a total HTC, T_w^{n+1} is surface temperature in current time step, T_w^n is surface temperature in previous time step, A and B are constant based on thermal properties.

Eq. (1) represents new boundary conditions for FRAPTRAN thermal calculation to obtain current surface temperature. Therefore, temporary heat flux, θ_0 and total HTC, h_{tot} is added to the interface variables for the coupling of SPACE-FRAPTRAN.

3. SIMULATION OF IFA-650.5 EXPERIMENT

3.1. Thermal hydraulic modelling for space

An overall layout of SPACE modelling for IFA-650.5 [7] is presented in Figure 3. As for the fluid system, the inlet flow from TFBC (Temporal Face Boundary Condition) of C100 enters lower plenum (C110) and is spilt into two channels for fuel rod and heater through cross flow (C115). Both channels are mixed at the top of upper plenum (C160) and finally exit to the outlet TFBC (C300) via the outlet pipeline (C200). Active fuel region and heater region are divided into 9 axial nodes. Flow and pressure boundary condition are applied to inlet and outlet TFBC, respectively. Blowdown valve to simulate the LOCA and spray injection are modelled as TFBC-999 and TFBC-555, respectively. For the heat structures, there are three heat structure components to simulate a fuel rod (H130), electric heater (H140) and pressure flask (H150), respectively. It was pointed out that the radiation heat transfer played a very important role in behaviour of the cladding temperature in IFA-650 test [9], therefore, a radiation enclosure model is applied into the facing surface of the fuel rod, heater and flask. A convective heat transfer condition is applied to the outer surface of the flask and, the heat transfer coefficient and bulk fluid

temperature are assumed to be $3000 \text{ W/m}^2\cdot\text{K}$ and 235°C which is the coolant temperature of heavy water in Halden reactor. A schematic diagram of the test rig for SPACE is presented in Figure 2.

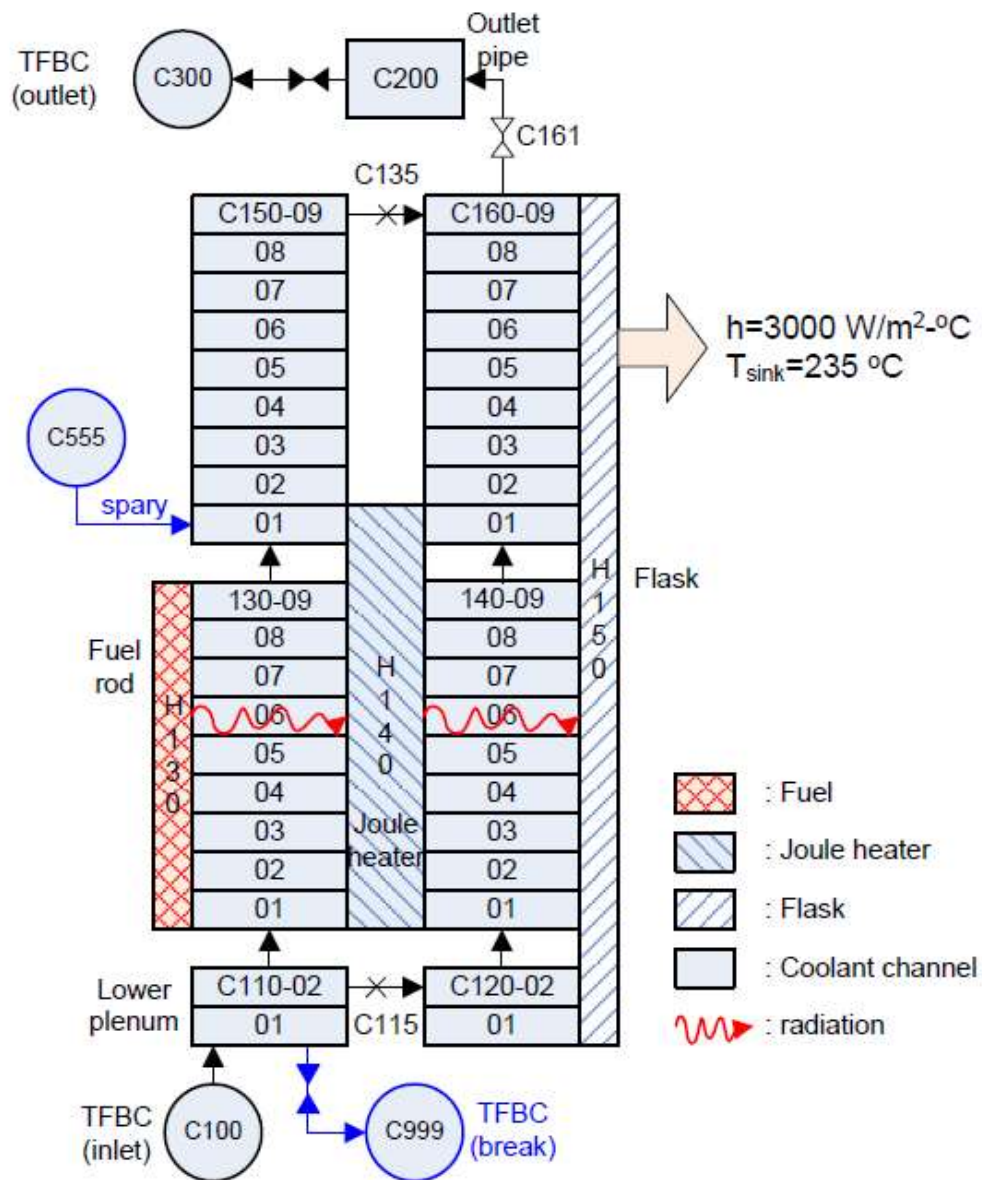


FIG. 3. SPACE Nodalization for test rig.

3.2. Fuel modelling for FRAPTRAN

The father rod is a UO_2 rod with a SRA Zircaloy-4 cladding, irradiated during six annual cycles up to 83 MWd/kgU (rod average) under moderate power conditions (average liner heat rate used without taking into account the gamma power generated in the coolant: 375, 280, 220, 200, 180, and 180 W/cm). At the end of the irradiation on the tested part of the rod, the corrosion layer thickness measured are mean $65 \mu\text{m}$ and maximum $80 \mu\text{m}$. The measured hydrogen content is around 650 ppm. Fig. 4 shows the calculation results for the base irradiation of IFA-650.5. Table 2 shows fuel rod information of IFA-650.5. This experiment was performed using an IFA-650 device, and the HWR report presents the experiment.

TABLE 2. FUEL ROD INFORMATION OF IFA-650.5

Item	IFA-650.5
Active length (mm)	480
Rod diameter (mm)	10.73
Pellet diameter (mm)	9.144
Pellet height (mm)	11.0
Pellet dish depth (mm)	0.28
Pellet outer surface roughness (mm)	0.002
Cladding type	Zry-4
Cladding inner surface roughness (mm)	0.0005
Cladding thickness (mm)	0.712
Number of coils in spring	20
Spring height (mm)	28.1
Total plenum volume (m ³)	1.5×10 ⁻⁵
Fill pressure (bar, RT)	40
Gas composition	He 10% Ar 90%
Number of axial node	9

For the simulation, the following assumptions were made:

- The plenum temperature was set as TOA plus 5.6 K;
- The initial free volume is 15 cm³.

To simulate the transient behaviour, a FRAPTRAN input is generated as follows: Burnup file required (FRAPCON file); gap gas, 95 % Ar; 5%He/ 40 bar at Room Temperature; simulation time, 0 to 500 s (time step, 0.01 s); HT oxidation, C-P model; deformation, Balon2 model.

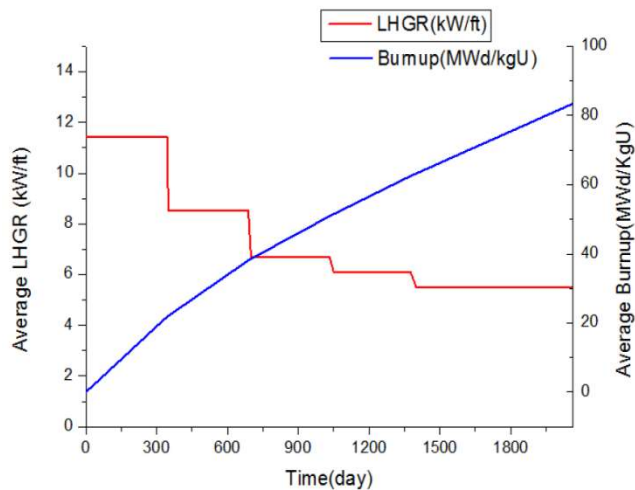


FIG. 4. Power and burnup history of IFA-650.5 rod.

4. SIMULATION RESULTS

4.1. Clad and Heater Temperature

Comparison of clad and heater temperature between coupled code and experiment are shown in Figure 5. As shown in the figure, clad and heater temperature show a very good agreement with the experimental results. This good agreement resulted from not the fuel deformation model but the radiation enclosure model. Figure 6 is a simulation results of SPACE standalone calculation in which the fuel deformation model was not used but the same radiation enclosure model as that of coupled calculation was applied. Comparing Figure 5 and Figure 6, it is found that there is little difference between the simulation results. Therefore, it can be induced that the fuel deformation model has little effect on the clad temperature in IFA-650 tests. Figure 7 shows a comparison of predicted and experimental rod internal pressure. Fuel clad was ruptured at 155 s in the simulation and at 178 s in the experiment. As shown in Figure 8, only the coupled code calculates hoop strain of each axial node because heat structure of SPACE cannot take into account fuel deformation. Hoop strain at node 4 where rupture occurs is the highest. After the rupture, the rod internal pressure decreased very slowly in the experiment, whereas predicted one drastically fell off to the level of coolant pressure. This discrepancy is caused by high content of hydrogen in the clad. Due to the high content of hydrogen, the clad became brittle and the rupture area was very small. Finally, the rod internal pressure decreased slowly due to a small rupture area.

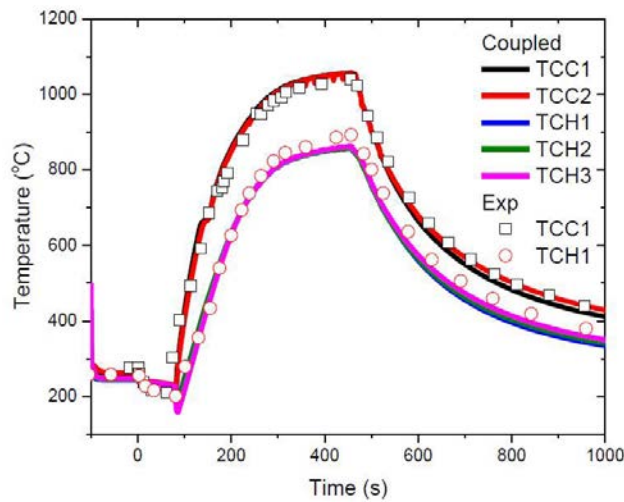


FIG. 5. Clad and heater temperature (coupled).

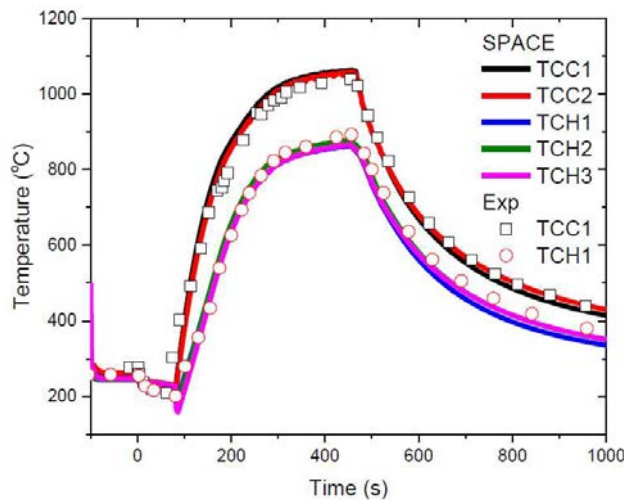


FIG. 6. Clad and heater temperature (SPACE standalone).

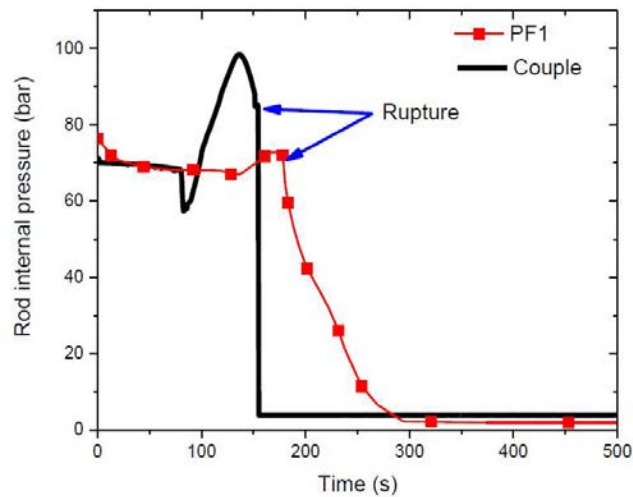


FIG. 7. Rod internal pressure.

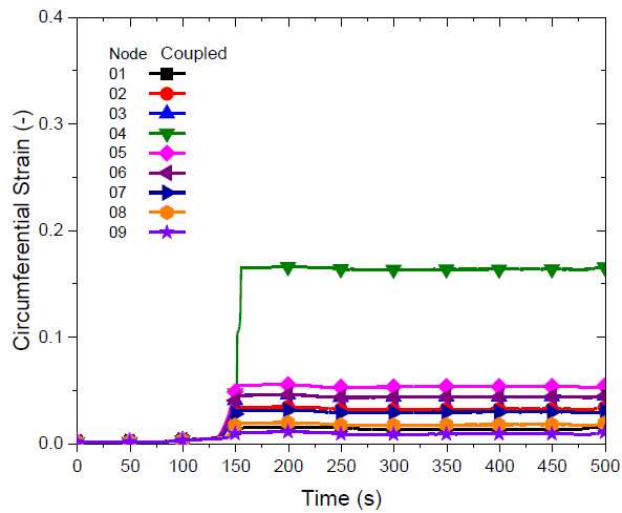


FIG. 8 Hoop strain calculated by the coupled code.

5. CONCLUSIONS

SPACE/FRPATRAN fully coupled code system has been developed to take into account fuel behaviour for safety analysis. The coupling algorithm and sequence were proposed to maintain own methodology of each code. To overcome various HTC and fluid temperature in SPACE, new coupling variables were proposed. In order to validate the SPACE/FRAPTRAN code system, IFA-650.5 experiment was simulated. From the simulation results of SPACE-FRAPTRAN coupled system against Halden IFA-650.5 test, the cladding and heater temperatures predicted by code agreed well with experimental data. In addition, it was revealed that the most important factor for the cladding and heater temperature in the IFA-650 test is the surface-to-surface radiation heat flux and the fuel model had little effects on them. Therefore, it is required that surface-to-surface radiation enclosure model should be simulated appropriately for the Halden IFA-650 test to predict the proper behaviour of the cladding temperature.

REFERENCES

- [1] HA, S.J., et al., Development of the SPACE Code for Nuclear Power Plants, *Nuclear Engineering and Technology* **43** (2011) 45–62.
- [2] RELAP5/MOD3.3., Code Manual Volume I: Code Structure, System Models, and Solution Methods, NUREG/CR-5535/Rev P4-Vol I, Information Systems Laboratories, Inc., Oct. 2010.
- [3] POWERS, D.A., et al., Cladding Swelling and Rupture Models for LOCA Analysis, NUREG-0630, U. S. Nuclear Regulatory Commission, April 1980.
- [4] BANG, Y.S., et al., Technical Basis for the Revision of ECCS Acceptance Criteria of Domestic PWR Plants, KINS/RR-1686, Korea Institute of Nuclear Safety, 2017.
- [5] GEELHOOD, K.J., et al., FRAPCON-4.0: A Computer Code for the Calculation of Steady-State, Thermal mechanical behavior of oxide fuel rods for high burnup, PNNL-19418, Vol. 1, 2015.
- [6] GEELHOOD, K.J., et al., FRAPTRAN-2.0: A Computer Code for the transient analysis of oxide fuel rods, PNNL-19400. Vol.1 Rev.2 (2016).
- [7] KEKKONEN, L., LOCA Testing at HALDEN; The PWR Experiment IFA-650.5, HWR-839, OECD HALDEN Reactor Project, Jan. 2007.
- [8] LEE, S.W., et al., Coupled Calculation of SPACE and FRAPTRAN, Transactions of the Korean Nuclear Society Spring Meeting, Jeju, Republic of Korea, May 17–18, 2018.
- [9] CHOI, T.S., Code Assessment against IFA-650 LOCA Tests, S06NX08-F-1-TR-041 Rev.0, KEPSCO-NF, July 2016.

THERMO MECHANICAL PERFORMANCE OF TRISO COATED FUEL PARTICLE USED IN HIGH TEMPERATURE GAS COOLED REACTOR

S. LIU, Y. ZHOU, P. CHEN, W. LI, S. GAO, H. PANG, C. TANG, X. QIU
Nuclear Power Institute of China,
Science and Technology on Reactor System Design Technology Laboratory,
Chengdu 610200, China

Abstract

Three dimensional characterized unit was used for TRISO particle with UN as the kernel to analyze the influence of PyC layers and internal pressure on the thermal mechanical performance of TRISO coated fuel particles by using the multi physics coupling software COMSOL. The influence of operation conditions including steady state and reactivity introduced accident (RIA) conditions on the thermal mechanical performance of TRISO particle was conducted. The results indicate that the structure integrity of SiC layer was maintained but the IPyC layer was failed in steady state condition. Thermal expansion is a dominant factor resulting in the loss of structure integrity of the TRISO coated fuel particle under RIA condition.

1. INTRODUCTION

TRISO coated fuel particles are the key parts of Fully Ceramic Microencapsulated (FCM) accident tolerant fuel (ATF). As the pellets of FCM fuel, TRISO particles are designed by three buffer layers which can provide more barriers for the released fission gas under reactivity introduced accident conditions. Since FCM fuel pellets still have about 50% NITE-SiC matrix, in order to increase uranium loading with reasonable ^{235}U enrichment to achieve approximated cycle length compared with LWRs fuels, uranium mononitride (UN) with high uranium density has become a research hotspot of kernel fuel in TRISO coated fuel particles [1]. For the FCM fuel, the diameter of kernel fuel in TRISO coated fuel particles is usually 500–800 μm ; the thickness of buffer layer which can absorb fission fragment, release irradiation damage of other layers, accommodate kernel swelling and contain fission gas is usually 50–100 μm ; the typical thickness of IPyC, SiC and OPyC layers are 30, 40 and 30 μm , respectively. The main function of SiC layer is the pressure bearing boundary and the barrier preventing the diffusion of fission products. Based on the neutron economy analysis [2], when the TRISO particles loading volume ration reaches 50% and the diameter of kernel fuel reaches about 800 μm , the FCM fuel with 19% enrichment UN kernel could reach the comparative core power and lifetime in contrast with LWRs with UO_2 fuels.

A 3D thermal mechanical coupling model was developed for TRISO coated fuel particle with UN as the kernel by using the multi physics coupling software COMSOL in this study. Performance analysis of the TRISO coated fuel particle with typical design parameters was conducted under steady state and reactivity introduced accident (RIA) conditions, which is useful for further optimizing the FCM fuel design.

2. MATERIAL PHYSICAL AND BEHAVIOUR MODELS

2.1. Material physical properties

The thermal conductivity of UN (K_{UN}) is the function of burn-up (Bu), temperature (T) and porosity (p) [3], and thermal expansion coefficient (α_{UN}) and specific heat ($C_{p,UN}$) are as follows [4]:

$$K_{UN} = 1.37T^{0.361} \frac{1-p}{1+p} (1 - 0.025Bu) \quad (1)$$

$$\alpha_{UN} = 7.096 \times 10^{-6} + 1.409 \times 10^{-9}T \quad (2)$$

$$C_{p,UN} = 205.3834 \left(\frac{365.7}{T}\right)^2 \frac{\exp\left(\frac{365.7}{T}\right)}{\left(\exp\left(\frac{365.7}{T}\right) - 1\right)^2} + 0.0381T + 1.061 \times 10^{12}T^{-2} \exp\left(-\frac{18081}{T}\right) \quad (3)$$

The elastic modulus of the PyC layer is isotropic which can be written as follows [5]:

$$E_{buffer} = 11.06(1 + 0.23\Phi) \cdot (0.9560275 + 0.00015T) \quad (4)$$

The elastic modulus of the PyC layer is anisotropic, and can be calculated by the following equation [5]:

$$E_{PyC} = 25.5 \left(0.384 + 0.000324 \rho_{PyC} \right) \cdot (1 + 0.23 \Phi) (0.9560275 + 0.00015T) \quad (5)$$

The elastic modulus, thermal conductivity and thermal expansion coefficient of SiC layer are achieved by the following equations [5, 6]:

$$E_{SiC} = 460 - 0.04 T \exp\left(-\frac{962}{T}\right) \quad (6)$$

$$K_{SiC} = \frac{17885}{T} + 2 \quad (7)$$

$$\alpha_{SiC} = \begin{cases} -1.8276 + \frac{0.0178}{T} - 1.5544 \times 10^{-5} T^2 + 4.5246 \times 10^{-9} T^3, & T < 1273K \\ 5.0, & T \geq 1273K \end{cases} \quad (8)$$

where, Φ is the fast neutron fluence, and ρ is the density.

The basic thermal mechanical physical properties of each part in TRISO coated fuel particle are listed in Table 1.

TABLE 1. BASIC THERMAL MECHANICAL PROPERTIES OF THE RELATIVE MATERIALS [7-9]

Material	Density ($\text{kg}\cdot\text{m}^{-3}$)	Poisson ratio	Thermal conductivity	Thermal expansion coefficient	Specific heat	Weibull modulus
UN kernel	13760	0.32	—	—	—	—
Buffer layer	1000	0.23	0.5	5.7×10^{-6}	720	—
IPyC layer	1900	0.23	4.0	5.7×10^{-6}	720	9.5
SiC layer	3200	0.13	—	—	620	6.0
OPyC layer	1900	0.23	4.0	5.7×10^{-6}	720	9.5

2.2. Mechanical behaviour model

The irradiation swelling relation of UN kernel is expressed by the following equation [10]:

$$\frac{\Delta V}{V} = 4.6473 \times 10^{-11} T^{3.12} \text{Bu}^{0.83} \quad (9)$$

where, ΔV and V are the volume change by the swelling and the initial volume, respectively.

The irradiation deformation of PyC layer has significant effects on the mechanical properties of TRISO particles and the choices of computation relations between them are various. In this study, the relations of radial and hoop irradiation strain of PyC layers are expressed by the following equations, respectively [11].

$$\dot{\varepsilon}_r = 0.181 \Phi^2 - 1.066 \Phi \quad (10)$$

$$\dot{\varepsilon}_\theta = 0.140 \Phi^2 - 1.324 \Phi \quad (11)$$

where, $\dot{\varepsilon}_r$ and $\dot{\varepsilon}_\theta$ are the radial and hoop irradiation strain, respectively.

There is a saturation value when the irradiation deformation of PyC layer increase as the fast neutron fluence increase. PyC layer would be considered as failed when the fast neutron fluence reaches $8.14 \times 10^{25} \text{m}^{-2}$, and there would be no more irradiation deformation [11]. The irradiation deformation change of buffer layer is written as follows [12]:

$$\dot{\varepsilon}_r = \dot{\varepsilon}_\theta = -0.176 \exp(-1.75 \Phi) \quad (12)$$

where, $\dot{\varepsilon}_r$ and $\dot{\varepsilon}_\theta$ are the radial and hoop irradiation strain, respectively. Meanwhile, since irradiation creep is the significant mechanism of stress relaxation, irradiation creep models of PyC and buffer layer are considered in this study as well [12].

2.3. Fission gas release model

The fission gas (Xe, Kr and He) release was modeled by two mechanisms, the recoil release and the diffusion release. These two mechanisms would cause the release of Xe and Kr, but the release of He will be only considered coming from diffusion release mechanism. The total release fission gas will be the sum of recoil and diffusion release. The recoil release will be the predominant mechanism at low temperature and its portion of fission gas can be calculated from the following empirical equation [13]:

$$f = \frac{1}{2} \frac{S}{V} \alpha \quad (13)$$

where f is the portion of Xe and Kr; S is the superficial area of fuel particle in m^2 ; V is the volume of fuel particle in m^3 and α is the mean recoil range of fission gas atoms in m. The mean recoil range of Xe and Kr is 3.98 μm and 5.68 μm , respectively.

The main mechanism of fission gas release at high temperature is diffusion release and Booth classical diffusion model was employed in this study to compute the final release fission gas of loose pyrolytic carbon and gap through diffusion mechanism. The grain of UN was considered as the ideal sphere of 20 μm in diameter which means the solving equation can be simplified as one dimensional form. The effective diffusion coefficient of fission gas atoms within the fuel grains can be set from the following empirical relation [5]:

$$D_g = 6.66454 \times 10^{-8} \exp(-19164/T) \quad (14)$$

where D_g is the effective diffusion coefficient of fission gas atoms within the fuel grains in $\text{m}^2 \cdot \text{s}^{-1}$.

2.4. Fuel particle failure probability model

SiC layer is the main barrier preventing the release of radioactivity and is also the main pressure bearing structure layer. The pressure vessel failure probability of SiC layer can be computed through equation (13) based on the Weibull distribution theory [5].

$$\Psi = 1 - \exp\left(-\int_V \left(\frac{\sigma_p}{\sigma_0}\right)^m dV\right) \quad (15)$$

where, Ψ is the failure probability; σ_p is the stress in MPa and the principal stress is employed to compute; m is the irradiated Weibull modulus of SiC layer and $m = 6$; σ_0 is Weibull parameter and $\sigma_0 = 9.64 \text{ MPa} \cdot \text{m}^{1/2}$.

Besides, heat transfer across gaps between buffer layer and IPyC layer and internal pressure are also considered in this study.

3. MODEL VERIFICATION AND APPLICATION

3.1. Performance analysis under steady conditions

The thermal power density of TRISO particles used in LWRs is higher compared with the typical TRISO particles used in high temperature gas cooled reactor. The particle power was set as 0.5 W; the maximum fast neutron fluency and burn-up were $18 \times 10^{25} \text{ m}^{-2}$ and 19% respectively and the simulation time was 1200 Effective Full Power Days (EFPDs). The structure size of TRISO particle was set as follows: diameter of UN kernel was 800 μm , thickness of buffer, IPyC, SiC and OPyC layers were 100 μm , 30 μm , 40 μm and 30 μm respectively. The outside temperature of fuel particles was set at 1073 K as the boundary condition. The defect on SiC layer was set in the model to analyze the effect of fabrication defect on the performance of TRISO particle. The fabrication defect and model boundary condition were showed in Fig. 1.

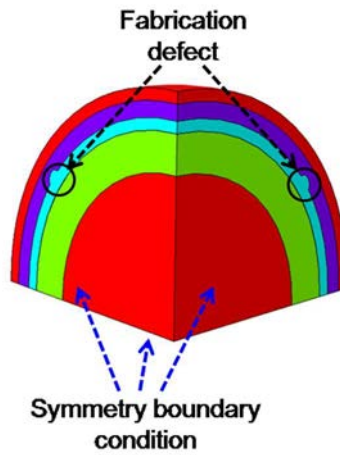


FIG. 1. Schematic diagram of TRISO particle characteristic unit used in this work.

Figure 2 shows the variation of average radius at inner surface of buffer layer, IPyC layer and the gap width with the increase of fast neutron fluence when computed the irradiation deformation of PyC layer. At the beginning of operation, the radius of buffer layer would decrease rapidly due to the irradiation deformation while the radius of IPyC would increase at the same time which caused the gaps between them. The buffer layer shrink because of the densification of buffer layer, which was similar with the UO_2 pellet. The shrinkage of IPyC layer was saturated when the neutron flux reached at about $13 \times 10^{25} \text{ n/m}^2$, which was good agreement with the literature [14]. After the increasing of gap size between buffer and IPyC layer, due to the irradiation creep and the expansion caused by the radial irradiation deformation of IPyC layer, the radius of IPyC layer would start to decrease again until the irradiation deformation reached saturation. The radius of buffer layer would start to increase as the irradiation swelling of UN kernel. The maximum width of gaps would reach about $23 \mu\text{m}$, the large gap was bad for the heat transfer efficiency at the internal fuel particles.

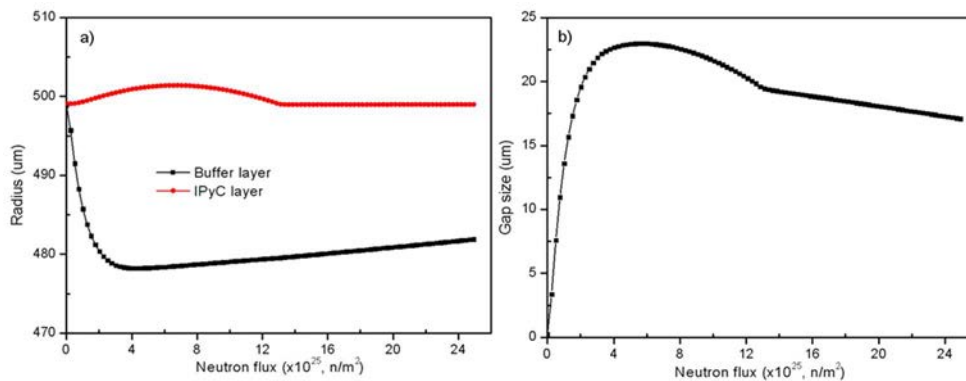


FIG. 2. Variation of a) buffer and IPyC layer radius and b) gap size between buffer and IPyC layers.

The radial temperature distribution of fuel particles for different fast neutron fluence is shown in Figure 3. Before the appearance of gaps, the internal fuel particles existed high temperature gradient which mainly due to the low thermal conductivity of buffer layer. Since gaps would form between IPyC layer and buffer layer in later period, fission gas would accumulate in the gaps and buffer layer which would dramatically decrease the thermal conductivity efficiency of internal fuel particles. And there was up to 200 K temperature difference between buffer layer and IPyC layer. The maximum temperature of UN kernel was about 1250 K when the neutron flux reached $25 \times 10^{25} \text{ n/m}^2$ which was lower than the melting point of UN ceramics. The gap between buffer and IPyC layer offered the space which can contain the fission gas, and the amount of fission and internal pressure in the gap was calculated.

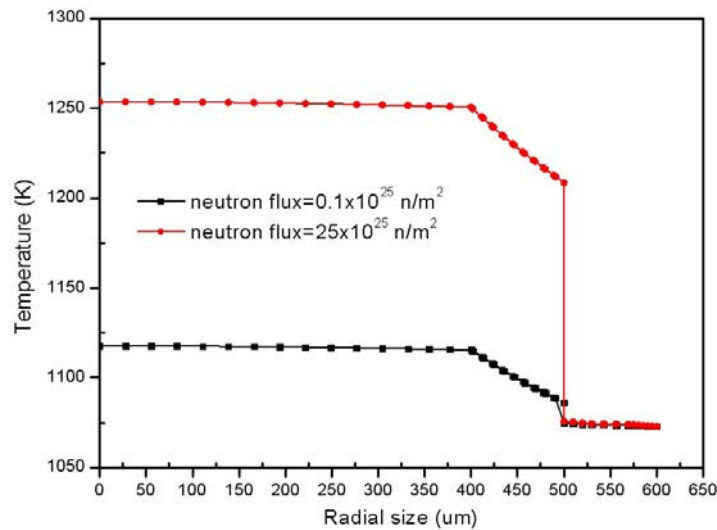


FIG.3. Temperature distribution of TRISO particle along radial direction.

Figure 4 shows the variation of fission gas release and internal pressure with the fast neutron fluence. The release of fission gas and internal pressure were approximately linear increasing as fast neutron fluence increased. Since there is no CO release in UN kernel, gas production and internal pressure were much smaller compared with TRISO particle with UO₂ kernel. When burn-up reached 19% FIMA, the internal pressure was only 1.78 MPa which conformed to the literature [14]. Compared with TRISO particles used in high temperature gas cooled reactor, internal pressure makes less contribution to the pressure vessel failure probability of SiC layer. The stress state and structure integrity of SiC layer are mainly influenced by the irradiation deformation of PyC layer.

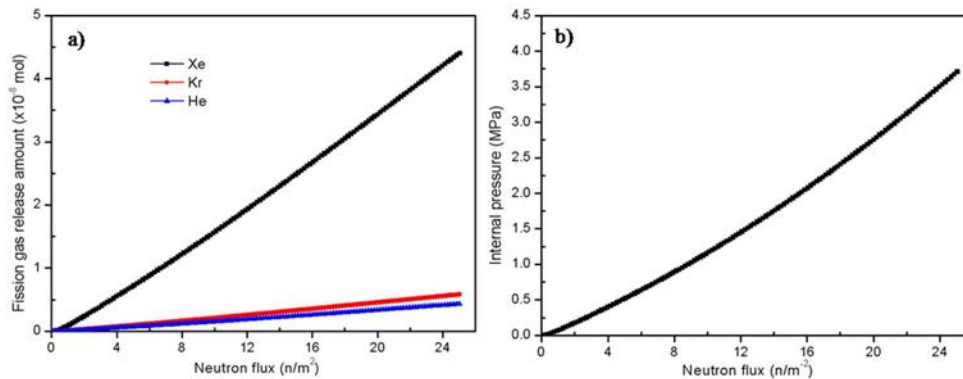


FIG.4. Variation of a) fission gas release and b) internal pressure of TRISO particle with neutron flux.

Figure 5 plots the variation of average hoop stress at inner surface of PyC and SiC layers with fast neutron fluence. At the beginning of operation, the radial and hoop shrinkage of IPyC and OPyC layers would squeeze SiC layer which caused the increase of normal stress at hoop direction of SiC layer while tensile stress at hoop direction would be applied on PyC layer which was a big threat to the structure integrity of PyC layer. With PyC layer gradually change to rapid expansion at radial direction, the stress state of PyC layer at hoop direction changed to pressure stress. Instead, pressure stress changed rapidly to tensile stress of SiC layer at hoop direction. Oversize tensile stress might cause the pressure vessel failure probability of SiC layer and lost the barrier prevent fission production leaking. With the irradiation deformation reached saturation, hoop stress of each layer would progress to low stress which meant the irradiation deformation of PyC layer had great influence on the structure integrity of fuel particle.

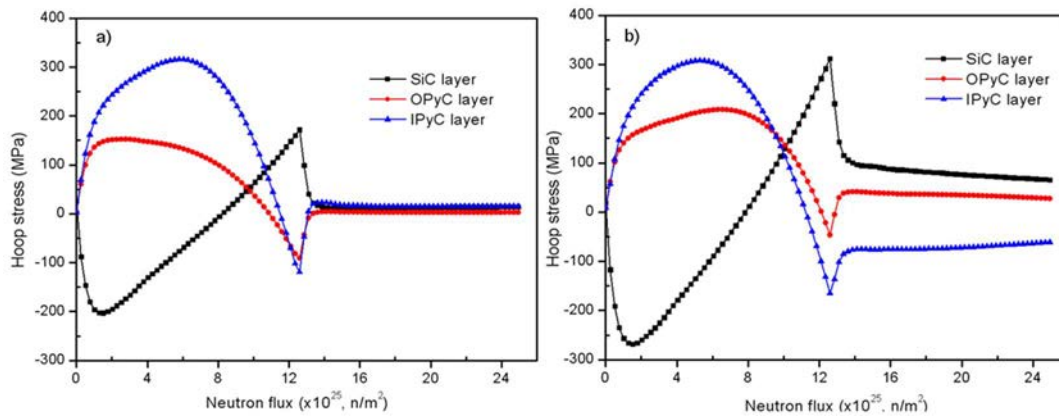


FIG. 5. Variation of hoop stress at inner surface of PyC and SiC layers with neutron flux, a) non defect surface, b) surface with defect.

SiC layer is the main pressure bearing structure and safety barrier of inner parts of fuel particle. The failure of SiC layer would have significant influence on the structure integrity of fuel particle. SiC is brittle material which can use Weibull distribution model to compute its random failure probability and results is shown in Figure 6. When Eq. 15 was employed to compute the irradiation deformation of IPyC layer, it would occur failure earlier with higher probability. In fact, failed IPyC layer has great influence on the structure integrity of SiC layer and it is essential to conduct more experiments and theoretical studies on the specified SiC layer alone which is also a part of further investigations.

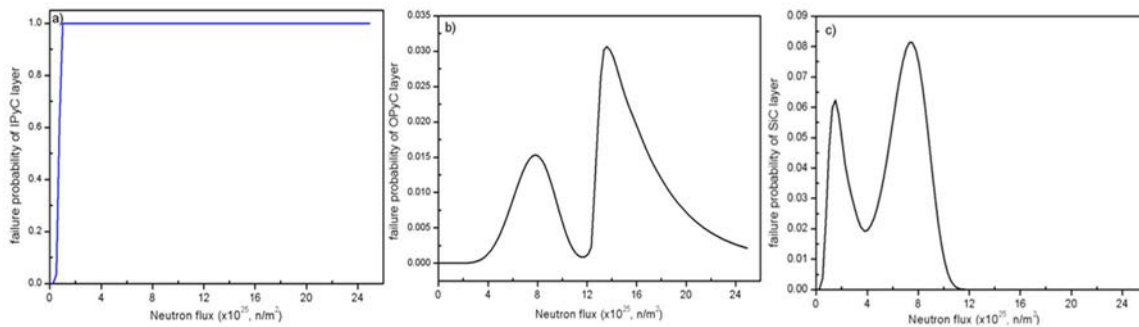


FIG. 6. Failure probability of the coated layers, a) IPyC layer, b) OPyC layer and c) SiC layer.

3.2. Performance analysis under RIA conditions

In order to analysis the performance of TRISO coated particle fuel under RIA condition, rod ejection accident needs to be considered under hot shut down condition where reactivity is great caused by deep control rods. Assume reactor operated at full power for 900 EFPD under thermal work condition and then turned into zero power maintaining 10 EFPD. After that, rod ejection accident happened with high reactivity which would cause the particle power of fuel assembly hottest area increasing to 30 times of rated power (15 W) and then decreasing to zero power rapidly. Assume the time of this duration was 5 s. Finally, the reactor was shut down emergently.

The fuel particle central temperature variation of time was shown in Figure 7. Due to the appearance of gaps, the central temperature increased rapidly and then stabilized gradually. The rod ejection accident happened at zero power thermal work condition caused power increased and decrease rapidly at very short time so as the corresponding central temperature. The highest temperature of UN kernel would reach 2200 K which was not enough to cause fuel melting. In addition, the thermal shock caused by temperature rapid increasing would cause great thermal expansion deformation which would cause the rapid contact between buffer layer and IPyC layer.

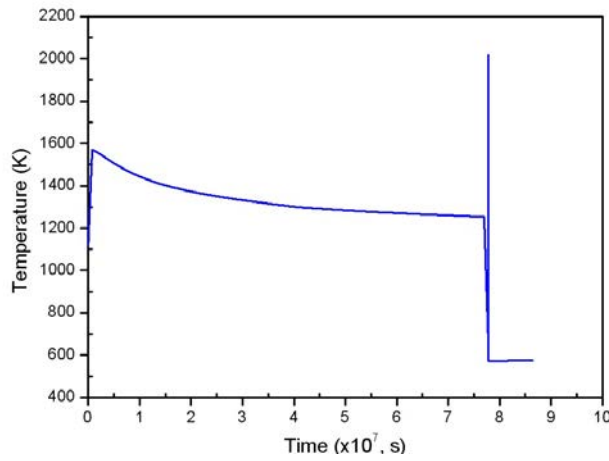


FIG. 7. Variation of kernel temperature with time under RIA condition.

Figure 8 plots the average hoop stress at inner of PyC and SiC layers variation of time which shows PyC and SiC layers had huge stress shock caused by contract pressure and formed great tensile stress in a moment. PyC and SiC layers might crack and lead structure failure. Therefore, thermal expansion is the dominant factor causing structure failure of fuel particle under RIA condition.

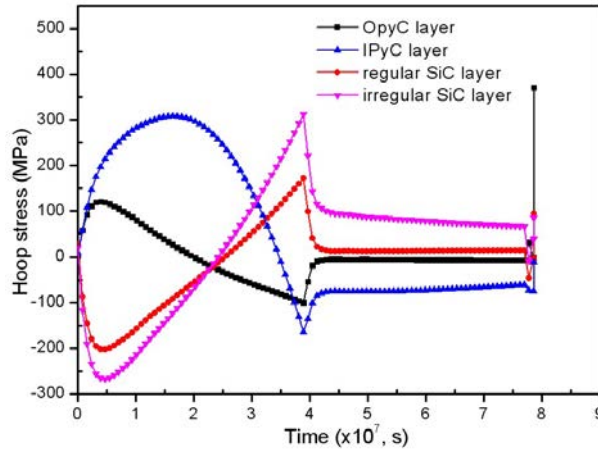


FIG. 8. Hoop stress of PyC and SiC layers under RIA condition.

4. CONCLUSIONS

A computation model which is able to analysis the irradiation performance of TRISO coated fuel particle was developed by using the multi physics coupling software COMSOL in this study and the main results are as follows:

A three dimensional thermal mechanical coupling model was developed for TRISO coated fuel particle with UN as the kernel which considered the physical properties and behaviour of materials. Under steady condition, buffer and IPyC layers would separate and the gaps between them would affect the thermal conductivity efficiency. The internal pressure caused by fission gas have little influence on the structure integrity of SiC layer while the complicated irradiation deformation behaviour has a great influence on the stress of PyC and SiC layers. IPyC layer have biggish structure failure risk while SiC layer can maintain the integrity of structure. Under RIA condition, drastic thermal expansion would cause each layer contact and form great tensile stress which is the dominant factor causing structure failure of TRISO coated fuel particle.

5. NOMENCLATURES

RIA	Reactivity introduced accident
FCM	Fully ceramic microencapsulated
ATF	Accident tolerant fuel
TRISO	Tri-isotropic
UN	Uranium mononitride
Buffer	porous pyrolytic carbon
IpyC	Inner dense pyrolytic carbon
SiC	Silicon carbide
OpyC	Outer dense pyrolytic carbon

REFERENCES

- [1] TERRANI, K.A., SNEAD, L.L., CEHIN, J.C., Fully ceramic microencapsulated fuels for LWRs. Transactions of the American Nuclear Society **106** (2012) 107.
- [2] MANCHANG, L., DAN, W., Neutronic feasibility analysis of fully ceramic microencapsulated fuel for commercial PWRs, TOPFUEL2016. USA: Boise, 2016.
- [3] ROSS, S.R., MATTHEWS, R.B., Thermal conductivity correlation for uranium nitride fuel between 10 and 1923 K. Journal of Nuclear materials **151** (1988) 317.
- [4] HAYES, S.L., THOMAS, J.K., Material property correlation for uranium mono nitride, I: Physique properties. Journal of Nuclear materials **171** (1990) 270.
- [5] MILLER, G.K., PETTI, D.A., PARFUM theory and model basis report, INL/EXT-08-14497, USA: INL, 2009.
- [6] SNEAD, L.L., NOZAWA, T., Handbook of SiC properties for fuel performance modeling. Journal of Nuclear materials **371** (2007) 377.
- [7] COLLIN, B.P. Modeling and analysis of FCM UN TRISO fuel using the PARFUM code, INL/EXT-13-30193, USA: INL, 2013.
- [8] HAYES, S.L., THOMAS, J.K., Material property correlations for uranium mono nitride, II: Mechanical properties. Journal of Nuclear materials **171** (1990) 288.
- [9] HALES, J.D., Williamson, R.L., Multidimensional multi physics simulation of TRISO particle fuel. Journal of Nuclear materials **443** (2013) 543.
- [10] GENK, M.S., ROSS, S.B., "Uranium nitride fuel swelling and thermal conductivity correlations", Transactions of the Fourth Symposium on Space Nuclear Power system. USA: Albuquerque (1987) 313-317.
- [11] DEMANGE, P., MARIAN, J., TRISO fuel element thermo mechanical performance modeling for the hybrid LIFE engine with Pu fuel blanket. Journal of Nuclear materials **405** (2010) 155.
- [12] PETTI, D., MATEIN, P., Development of improved models and designs for coated-particle gas reactor fuels, INL//EXT-05-02615, USA: INL, 2004.
- [13] BESMANN, T.M., FERBER, M.K., Fission product release and survivability of UN-kernel LWR TRISO fuel. Journal of Nuclear materials **448** (2014) 419.
- [14] SCHAPPEL, D., TERRANI, K., POWERS, J., Thermo mechanical analysis of fully ceramic microencapsulated fuel during in-pile operation, Top Fuel 2016, Boise, ID, September 11-15, 2016.
- [15] COLLIN, B.P., Modeling and analysis of UN TRISO fuel for LWR application using the PARFUME code. Journal of Nuclear materials **451** (2014) 77.

MAIN RESULTS OF THE CRP ACTOF

(Session 4)

Chairperson

T.LIU
China

REACTIVITY INITIATED ACCIDENT ASSESSMENT FOR ATF CLADDING MATERIALS

C. GIOVEDI, M.R. MARTINS

LabRisco, University of São Paulo,

Av. Prof. Mello Moraes 2231, 05508-030, São Paulo, SP, Brazil,

A. ABE, R. REIS, A.T. SILVA

Nuclear Engineering Center — CEN, Nuclear and Energy Research Institute - IPEN/CNEN,

Av. Prof. Lineu Prestes 2242, 05508-000, São Paulo, SP, Brazil.

Abstract

Following the experience that came from the Fukushima Daiichi accident, one possible way of reducing risk in a nuclear power plant operation would be the replacement of the existing fuel rod cladding material (based on zirconium alloys) by other materials which could fulfill the requirements of the accident tolerant fuel (ATF) concept. In this sense, ATF should be able to keep the current fuel system performance under normal operation conditions; moreover, it should present superior performance than the existing conventional fuel system (zirconium based alloys and uranium dioxide) under accident conditions. The most challenging and bounding accident scenarios for nuclear fuel systems in Pressurized Water Reactors (PWR) are Loss of Coolant Accident (LOCA) and Reactivity Initiated Accident (RIA), which are postulated accidents. This work addresses the performance of ATF using iron based alloys as cladding material under RIA conditions. The evaluation is carried out using modified versions of the coupled system FRAPCON/FRAPTRAN. These codes were modified to include the material properties (thermal, mechanical, and physics) of an iron based alloy, specifically FeCrAl alloy. The analysis is performed using data available in the open literature related to experiments using conventional PWR fuel system (zirconium based alloys and uranium dioxide). The results obtained using the modified code versions are compared to those of the actual existing fuel system based on Zircaloy-4 cladding using the original versions of the fuel performance codes (FRAPCON/FRAPTRAN).

1. INTRODUCTION

Accident Tolerant Fuels (ATF) have been studied after the Fukushima Daiichi accident in order to improve the nuclear safety under steady state irradiation and accident scenarios. The most challenge scenarios to be studied are those related to postulated accidents, specifically LOCA and RIA. In this sense, in the framework of the ATF programme, it is necessary to evaluate the performance under postulated accident scenarios of different cladding materials which could be applied to replace the zirconium based alloys currently used. The cladding materials that present higher potentiality to this are iron based alloys such as iron-chromium-aluminum (FeCrAl), and ceramic materials such as silicon carbide (SiC).

There are two accident scenarios of particular interest considering inadvertent insertion of reactivity in nuclear power reactors: the control rod ejection accident in Pressurized Water Reactors (PWR), and the control rod drop accident in Boiling Water Reactors (BWR). These are design basis accidents, which may result in serious consequences if they were not accounted properly in the design of the reactor and related safety systems. The cause of accident is related to mechanical failure of a control rod mechanism housing and the primary coolant pressure ejects a control rod assembly completely out of the core. The main consequence of the control rod ejection is a rapid positive reactivity insertion, which shall occur within about 0.1 s in the worst possible scenario. The fuel rod behaviour during a RIA is mostly influenced by characteristics of the power pulse (amplitude and pulse width), coolant condition (pressure, temperature and flow rate), level of fuel burnup (degree of hydrogen pickup, cladding corrosion, internal fuel pressure), and fuel rod design (cladding thickness, pellet geometry and initial fill pressure). The rapid power excursion (0.1 s) leads to nearly adiabatic heating of the fuel pellets, which immediately deform by solid thermal expansion and depending of burnup degree, the amount of gaseous fission products retained in the fuel will contribute more to the solid pellet deformation. Due to pellet expansion the pellet cladding gap is reduced or closed leading to pellet cladding mechanical interaction (PCMI) with significant mechanical loading on the cladding tube [1].

Fuel performance codes are good tools to be applied to assess the behaviour of different materials under irradiation; however, the conventional fuel codes need to be modified to introduce the properties of the materials, which are being studied.

The FRAPTRAN code has two models to predict cladding failure, first failure model is related to RIA event, where deformation is due to pellet cladding mechanical interaction and at relatively low temperature (< 700 K), where PCMI is the driving force for cladding deformation, the model considers basically uniform plastic elongation from irradiated cladding as function of temperature and hydrogen concentration. The second failure model is applicable to LOCA events where deformation is relatively high due to gas overpressure and the temperature of the cladding (> 700 K) [2].

This paper presents some preliminary results obtained using modified versions of the FRAPCON-FRAPTRAN codes containing the properties related to the FeCrAl alloy to simulate the fuel behaviour under steady state and RIA conditions.

2. METHODOLOGY

2.1. FeCrAl alloy

FeCrAl alloy presents better properties compared to zirconium based alloys specifically concerning to the oxidation rates which are of 1 to 3 orders of magnitude lower [3]. Data from literature [3] based on computational simulations also indicate that FeCrAl alloy maintains acceptable thermo mechanical properties, and fuel-clad interactions under PWR conditions. The thermal, mechanical e physical properties of FeCrAl were obtained from literature [3] and used to modify the fuel performance codes.

2.2. Fuel performance code modification

The basis for the code modification applied to study the steady state irradiation was the FRAPCON-3.4 code [4], and for RIA evaluation the FRAPTRAN-1.5 [2]. The main subroutines related to the cladding in the codes modified to introduce the properties in MATPRO [5] of FeCrAl alloy were: CELMOD, CORROS, CREEPR, CSHEAR, and CTHCON. The material properties concerning to each of these subroutines are: CELMOD defines the correlation for the cladding Young's modulus; CORROS is related to the cladding waterside corrosion; CREEPR; CSHEAR calculates shear modulus of cladding based on type and conditions; and CTHCON defines the correlation for the cladding thermal conductivity.

2.3. Test case

The test case applied to compare the fuel performance of Zircaloy-4 and FeCrAl alloy was the HBO-5, which data are available in the FRAPCON-3.5 assessment [6]. This case is part of a large scale RIA experiment carried out at NSRR reactor by JAERI (Japan Atomic Energy Research Institute). The NSRR facility has a TRIGA type reactor, which can generate significantly narrow power pulses, the RIA simulation tests on pre-irradiated fuel segment (test rod) employ a capsule with stagnant water. The HBO-5 fuel rod was refabricated from a standard 17×17 PWR fuel rod with uranium dioxide fuel pellet that was irradiated under steady state condition at OHI#1 reactor comprising a period of about 1360 days until an average burnup of 44 GWd/MTU. After this, the full-length fuel rod was refabricated and submitted to the test under RIA conditions. The HBO-5 fuel rod experienced failure at 0.2113 s.

The input for both codes were prepared following strictly according to the recommendations presented in the assessment volume as presented in Table 1.

TABLE 1. HBO-5 FUEL ROD MAIN CHARACTERISTICS AND BOUNDARY CONDITIONS

Characteristic/boundary condition	PWR
Fuel material	UO ₂
Fuel pellet outer diameter (mm)	8.05
Fuel pellet height (mm)	9
Fuel density (% TD)	95
Fuel enrichment (w/o %)	3.2
Cladding outer diameter (mm)	9.5
Cladding inner diameter (mm)	8.22
Cladding wall thickness (mm)	0.64
Fuel-cladding diametral gap (μm)	170
Fill rod pressure (MPa)	3.23
Coolant temperature (°C)	310
Coolant pressure (MPa)	15.5

The average power history and the rod average burnup as function of the irradiation time are presented in Figs 1 and 2, respectively.

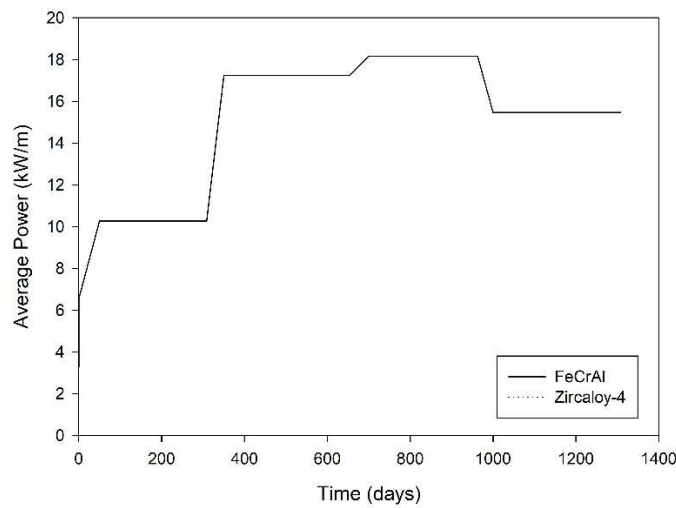


FIG. 1. Average power history for HBO-5 test case.

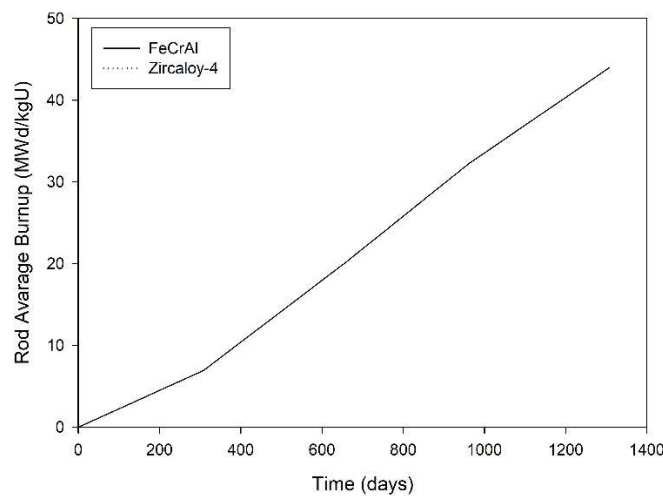


FIG. 2. Rod average burnup as function of irradiation time for HBO-5 test case.

3. RESULTS AND DISCUSSION

The main results obtained comparing the performance of Zircaloy-4 and FeCrAl alloy as cladding under steady state irradiation for the HBO-5 fuel rod are presented in Figures 3 to 7.

Figure 3 shows that FeCrAl fuel rod presents fuel centreline temperatures higher than Zircaloy-4 fuel rod. This occurs due to the higher thermal expansion of the FeCrAl. Then, the gap thickness is larger, as shown in Figure 4, and, consequently, the fuel temperature reaches higher values.

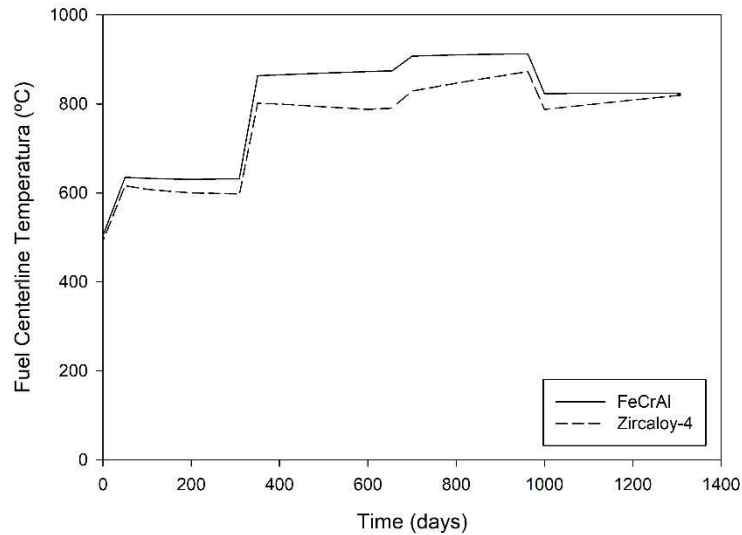


FIG.3. Fuel centerline temperature evolution under steady state irradiation as function of time for HBO-5 test case considering as cladding: Zircaloy-4, and FeCrAl alloy.

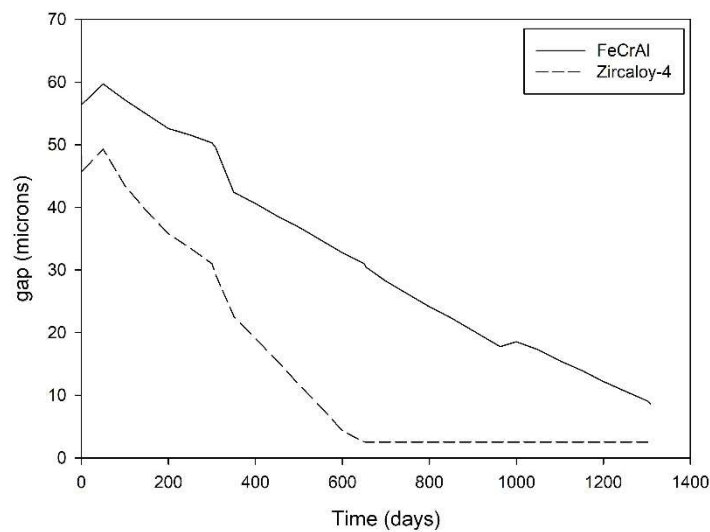


FIG.4. Gap thickness evolution under steady state irradiation as function of time for HBO-5 test case considering as cladding: Zircaloy-4, and FeCrAl alloy.

Also, it can be observed in Figure 5 that FeCrAl fuel rod presents a lower plenum pressure compared to the Zircaloy-4 fuel rod due to the higher internal free volume available that is a result of the higher thermal expansion of the FeCrAl alloy.

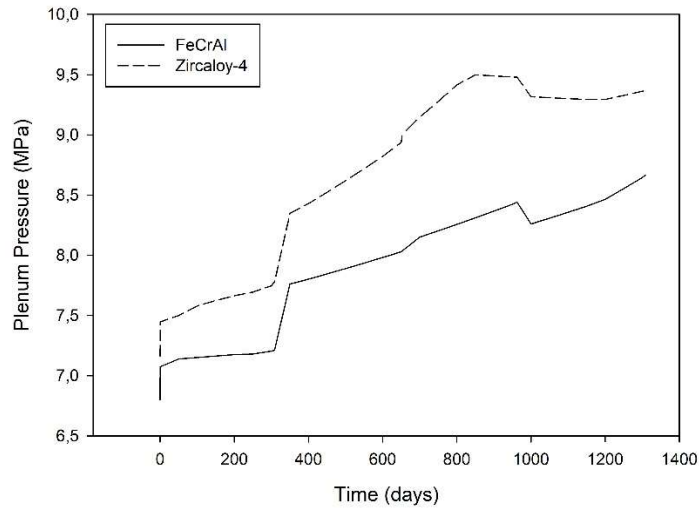


FIG.5. Plenum pressure evolution under steady state irradiation as function of time for HBO-5 test case considering as cladding: Zircaloy-4, and FeCrAl alloy.

Due to the gap closure around 600 irradiation days observed for the Zircaloy-4 fuel rod, the cladding hoop stress, as shown in Fig. 6, changes from a compressive to a tensile state. This is not observed for the FeCrAl fuel rod because the gap remains open during all the irradiation time, also, as a consequence of the higher thermal expansion compared to Zircaloy-4.

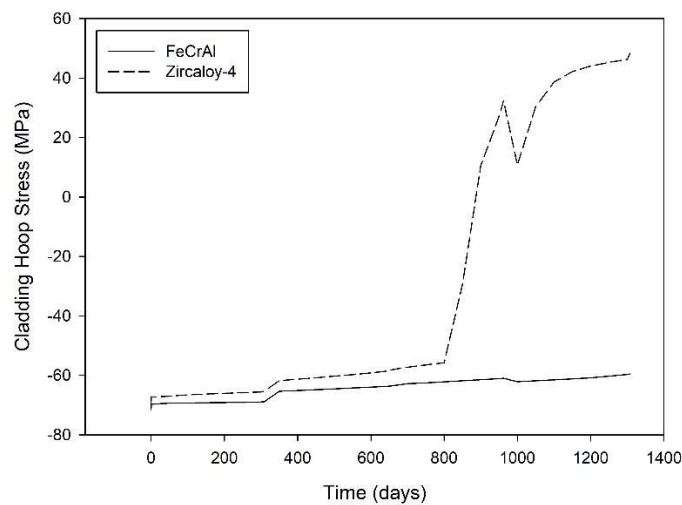


FIG.6. Cladding hoop stress evolution under steady state irradiation as function of time for HBO-5 test case considering as cladding: Zircaloy-4, and FeCrAl alloy.

Regarding to the fission gas release, Figure 5 shows that the behaviour is exactly the same for both studied materials. This shows that the differences observed in the fuel centerline temperatures are not enough to affect the fission gas release behaviour for both studied materials.

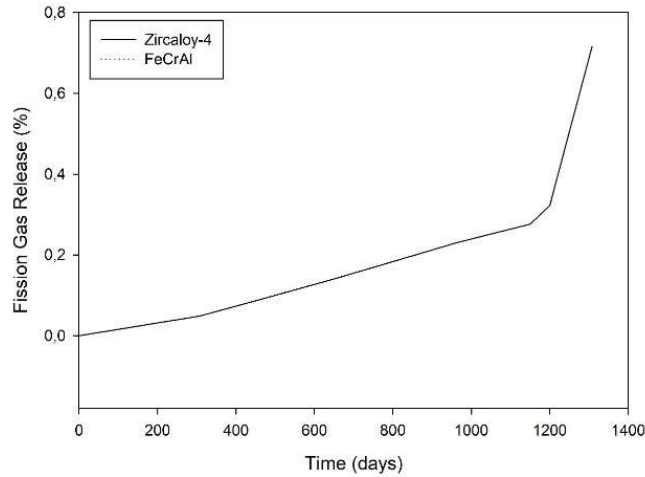


FIG.7. Fission gas release evolution under steady state irradiation as function of time for HBO-5 test case considering as cladding: Zircaloy-4, and FeCrAl alloy.

After steady state irradiation, the RIA condition was simulated using FRAPTRAN code in order to reproduce the experimental test for the HBO-5 fuel rod. Figure 8 presents the cladding hoop stress after RIA, considering that the RIA starts at time equal to 0. It can be observed that the Zircaloy-4 fuel rod experiences failure 0.21 s after starting the RIA, result that is very similar to that observed in the experiment. This confirms that the simulation was appropriately carried out. The same simulation was performed under RIA conditions using the transient code modified considering FeCrAl as cladding material. And, in these preliminary results the FeCrAl fuel rod experiences failure at a time very close to that observed for Zircaloy-4 due to the fact that the failure criterion adopted in the FRAPTRAN code for Zircaloy-4 cannot be appropriate to evaluate the FeCrAl fuel rod behaviour under RIA conditions.

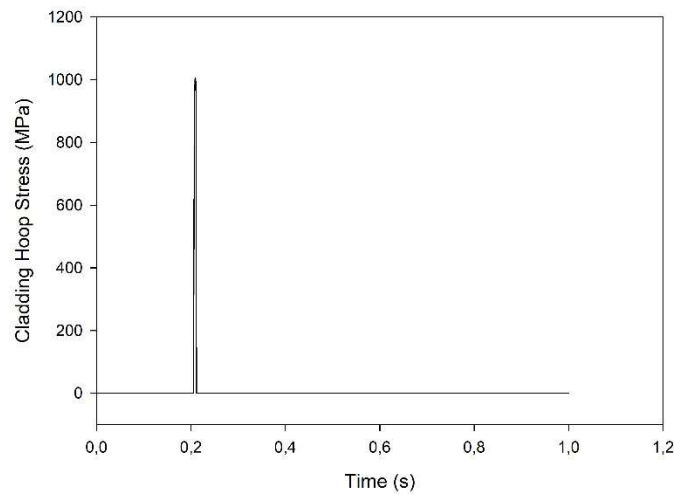


FIG.8. Cladding hoop stress after RIA ($t=0$) for HBO-5 test case.

4. CONCLUSIONS

The obtained results for the HBO-5 test case indicate that under steady state irradiation FeCrAl present a good performance compared to Zircaloy-4 showing: higher fuel temperatures (about 100°C), lower internal pressure, open gap during all the irradiation time, and lower cladding hoop stress.

The simulations carried out to under the RIA scenario reproduced exactly the experimental result registered for the studied test case, occurring the failure of the fuel rod at the same time verified in the experiment.

Although the results of simulation obtained in the steady state condition have shown differences, mainly in the fuel gap parameter, the fuel rod test case failure at similar time in the transient simulation, consequently it is necessary to evaluate and establish a better and consistent failure criterion for FeCrAl cladding.

The strain-based failure criterion used in the original code version for Zircaloy-4 considers the effects of hydride content and temperature [7]. In this sense, it is necessary to carry out experiments in order to obtain data to better predict the cladding failure for FeCrAl behaviour under RIA conditions.

5. NOMENCLATURES

ATF	Accident Tolerant Fuel
BWR	Boiling Water Reactor
FeCrAl	Iron-Chromium-Aluminum alloy
HBO-5	Experimental test case
LOCA	Loss-of-Coolant Accident
PCMI	Pellet Cladding Mechanical Interaction
PWR	Pressurized Water Reactor
RIA	Reactivity Initiated Accident
SiC	Silicon Carbide

ACKNOWLEDGEMENTS

The authors are grateful to the technical support of USP and IPEN-CNEN/SP, and to the financial support of IAEA to attend the Technical Meeting.

REFERENCES

- [1] RASHID, Y.R., ZANGARI, A.J., LIN, C.L., Modeling of PCI Under Steady State and Transient Operating Conditions, IAEA Technical Committee Meeting on Water Reactor Fuel Element Computer Modeling in Steady State, Transient and Accident Conditions, IAEA-659/IWGFPT/32 Preston England, (1988) 91.
- [2] GEELHOOD, K.J., LUSCHER, W.G., CUTA, J.M., FRAPTRAN- 1.5: A Computer Code for the Transient Analysis of Oxide Fuel Rods, PNNL-19400, 1, Rev.1 (2014).
- [3] GAMBLE, K.A., BARANI, T., PIZZOCRI, D., HALES, J.D., TERRANI, K.A., PASTORE, G., An Investigation of FeCrAl Cladding Behavior Under Normal Operating and Loss of Coolant Conditions, *Journal of Nuclear Materials* **491** (2017) 55.
- [4] GEELHOOD, K.J., LUSCHER, W.G., BEYER, C.E., FLANAGAN, M.E., FRAPCON-3.4: A Computer Code for the Calculation of Steady state Thermal mechanical Behavior of Oxide Fuel Rods for High Burnup, U.S.NRC, NUREG/CR-7022, Washington (2011).
- [5] ALLISON, C.M., BERNA, G.A., CHAMBERS, R., CORYELL, E.W., DAVIS, K.L., HAGRMAN, D.L., et al., SCDAP/RELAP5/MOD3.1 Code Manual Volume IV: MATPRO—A Library of Materials Properties for Light-Water-Reactor Accident Analysis, NUREG/CR-6150, EGG-2720, Washington (1993).
- [6] GEELHOOD, K.J., LUSCHER, W.G., FRAPCON-3.5: Integral Assessment, PNNL-19418, 2, Rev.1 (2014).
- [7] NEA/CSNI/R (2010) 1, Nuclear Fuel Behaviour under Reactive Initiated Accident (RIA) Conditions, OCDE (2010) 179.

ROUND ROBIN EXERCISE OF THE CANDIDATE ATF CLADDING MATERIALS WITHIN THE ACTOF PROJECT

M. ŠEVEČEK, J. KREJČÍ, A. CHALUPOVÁ, J. KABÁTOVÁ, F. MANOCH, J. KOČÍ, L. CVRČEK
Czech Technical University in Prague/UJP Praha,
Prague, Czech Republic,

C. TANG, M. STEINBRÜCK, M. GROSSE
Institute for Applied Materials, Karlsruhe Institute of Technology,
Karlsruhe, Germany,

S. PENTTILÄ, J.-M. AUTIO, J. LYDMAN, A. TOIVONEN
VTT Materials for Power Engineering, Technical Research Centre of Finland,
Espoo, Finland,

B. SARTOWSKA, W. STAROSTA, L. WALIŚ, A. KRZEŚNIAK, E. PAŃCZYK, P. KALBARCZYK, K.
KULISA, J. SMOLIK, J. MIZERACKI
Institute of Nuclear Chemistry and Technology,
Warsaw, Poland,

Z. HÓZER, T. NOVOTNY, E. PEREZNÉ FERÓ, A. PINTÉR CSORDÁS, M. HORVÁTH, P. SZABÓ
Hungarian Academy of Sciences, KFKI Atomic Energy Research Institute,
Budapest, Hungary,

C. GIOVEDI
University of São Paulo,
São Paulo, Brazil,

P. XU
Westinghouse Electric Company,
Hopkins, SC, USA.

Abstract

The paper presents a summary of the round robin test activity organized within the IAEA ACTOF project. The test conditions and sample matrix were finalized during fall 2017, production and transportation of samples started in Q1 2018 and the tests have been performed during the past 14 months. Two fundamental experimental tests related to normal operating conditions and accidental conditions of LWRs were defined: High temperature steam oxidation and Long term corrosion tests. Originally, four laboratories/institutes joined the round robin exercise — CTU in Prague, KIT, VTT, and INCT. Later, also MTA EK joined the activity. Westinghouse Electric Company provided Zircaloy-2 substrate. Two institutes applied their protective coatings on the Zircaloy-2 substrate by PVD methods (CTU — pure Cr coating and INCT — ZrSi-Cr coating). KIT applied MAX phase coating on Zircaloy-4 substrate. Additionally, AISI 348 steel provided by USP, Brazil was tested. The geometry of the samples varied based on the needs of particular institutes. Long term corrosion tests were performed by three laboratories in PWR and WWR chemistry for at least 63 cumulative days. High temperature steam oxidation tests were performed by four institutes at three pre-defined conditions. Participants performed pre- and post-characterization of the materials based on their standard procedures and available techniques. The paper summarizes motivation, plans, sample matrix, materials, testing conditions and preliminary results including lessons learnt and recommendations for future joint projects.

1. INTRODUCTION

One of the key joint actions planned within the IAEA Coordinated Research Project on “Analysis of Options and Experimental Examination of Fuels for Water cooled Reactors with Increased Accident Tolerance (ACTOF)” was the round robin test (RRT) for cladding materials that are considered as Accident Tolerant Fuel (ATF) cladding candidates. The tested cladding materials include three coated cladding concepts and AISI stainless steel. There were two fundamental tests defined — high temperature steam oxidation test and long term corrosion test in prototypical LWR conditions. The participants of the RRT are: Czech Technical University/UJP Praha (CTU),

Karlsruhe Institute of Technology (KIT), Institute of Nuclear Chemistry and Technology (INCT), VTT Technical Research Centre of Finland (VTT), University of São Paulo (USP) and Hungarian Academy of Sciences Centre for Energy Research (MTA EK). The RRT can be subdivided into three sub-activities:

- ATF cladding sample production;
- Long term corrosion test in WWER or PWR chemistry;
- High temperature oxidation.

The involvement of the parties in particular tasks of the RRT activity is summarized in Table 1.

TABLE 1. INVOLVEMENT OF PARTICIPANTS IN THE RRT

	CTU	KIT	INCT	VTT	USP	MTA EK
Sample production	X	X	X	—	X	—
Long term corrosion	X	—	X	X	—	—
High temperature oxidation	X	X	—	X	—	X

As can be seen in Table 1, there were four different types of ATF cladding samples produced by four institutes. Three institutes performed long term corrosion tests in PWR or WWER chemistry and four institutes performed high temperature oxidation testing.

2. SAMPLE PRODUCTION

Traditional Zr-based cladding materials were used as substrates (Zry-2, Zry-4 and E110) and three different coatings were deposited on their surfaces using physical vapour deposition methods (PVD). Originally, standard Zry-2 LK3 alloy was chosen as the substrate for all tests with two predefined geometries shown in Fig. 1. Due to time and other limitations, it was decided to use also Zry-4 substrate provided by KIT and E110 substrate provided by UJP Praha and change the sample geometry based on the requirements of particular participants (due to size limitations in furnaces, to allow for mechanical testing or single-sided oxidation etc.).

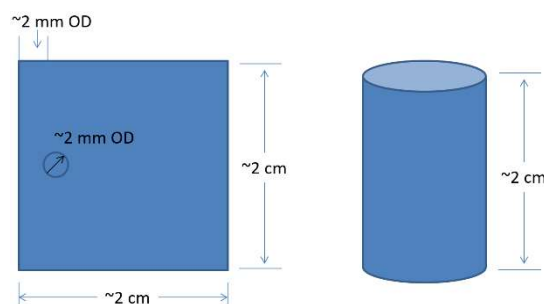


FIG. 1. The geometry of samples for RRT as originally defined.

The coatings deposited by PVD methods are: pure Cr (CTU), ZrSi-Cr (INCT) and Cr/Cr₂AlC/Cr (KIT). Additionally, AISI 348 stainless steel provided by USP was tested. Their fabrication and specifications are described further.

2.1. Cr PVD coated Zr-based alloys

Zr-based samples were Cr coated in two batches using unbalanced magnetron sputtering (UBM) in the Hauzer Flexicoat 850 industrial system. It is a multi purpose device flexible for numerous applications. Depending on the type, it can utilize a combination of different deposition technologies such as sputtering, HIPIMS, PACVD and other. For the purposes of this work, UBM was used. It is a special type of sputtering with extended and increased plasma density using coils in an unbalanced closed magnetic field. The images of the system, deposition

chamber and rotating sample holders with Cr target are shown in Figure 2. More details about the methods used and coating parameters can be found in [1–5].



FIG. 2. Images of the Hauser Flexicoat 850 at CTU in Prague. Overview of the system (left); Deposition chamber (centre); Rotating sample holders with Cr target in the back (right) (Reproduced courtesy of Elsevier [16]).

The coatings were deposited in a metal mode using the gas flow 90 sccm Ar (99.999 %) for about 18 hours. The thickness of the coatings was measured with a Calotest (CSM, Switzerland) and was found to be $28 \pm 0.1 \mu\text{m}$ in the first batch and $16 \pm 0.1 \mu\text{m}$ in the second batch.

2.2. ZrSi-Cr PVD coated Zry-2

ZrSi-Cr coated samples were produced at the Institute for Sustainable Technologies ITS (Radom, Poland). Balzers system shown in Fig. 3 was used. The system contains three magnetron plasma sources, three power and control panels. It allows to deposit materials from separate targets and to obtain multi elemental coatings [6].

Two magnetrons with separate, flat, circular targets were used. One was made of ZrSi_2 and the second of pure Cr. The resulting composition of the coatings as confirmed by XRD is $\text{— Zr}_{40}\text{Si}_{24}\text{Cr}_{36}$ and its thickness is about 2.5 microns.

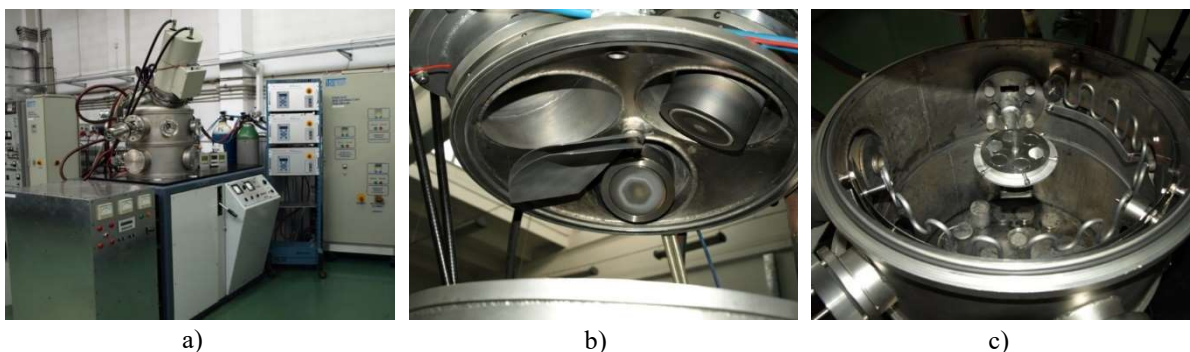


FIG. 3. Balzers system facility: a) general view, b) position of flat, circular magnetrons, c) chamber overview.

2.3. Cr/Cr₂AlC/Cr (MAX phase) PVD coated Zry-4

A research group at KIT investigates the deposition of Ti_2AlC , Cr_2AlC and Zr_2AlC MAX phases on Zircaloy-4 by a PVD. Pre-tests have shown that the Cr_2AlC MAX phases are the most promising with respect to their high temperature oxidation behaviour. The coatings were synthesized via a two-step process, i.e. first deposited by magnetron sputtering and subsequently thermally annealed in pure argon. The as-deposited coatings were deposited using laboratory PVD equipment (Leybold Z 550 coater). Three high purity cylindrical elemental plates of chromium (Cr: 99.95%, FHR Anlagenbau GmbH), graphite (C: 99.95%, Schunk Kohlenstofftechnik GmbH) and aluminium (Al: 99.95%, FHR Anlagenbau GmbH) are used as targets for magnetron sputtering process. Figure 4 shows the schematic representation of the design of the as-deposited coatings on Zircaloy-4 substrates and the arrangement of the targets and substrates during deposition.

After deposition, the coated Zircaloy-4 specimens were ex-situ annealed in pure argon (99.9999%) at atmospheric pressure using a commercial thermal balance (NETZSCH STA-449 F3 Jupiter) to facilitate the growth of MAX phases by solid reaction of the nanoscale elemental multilayers. The isothermal holding time was 10 min

at annealing temperature 550°C. Cr₂AlC MAX phase was successfully obtained while no significant interdiffusion between the Cr and Cr₂AlC layer has been confirmed at such conditions [7, 8].

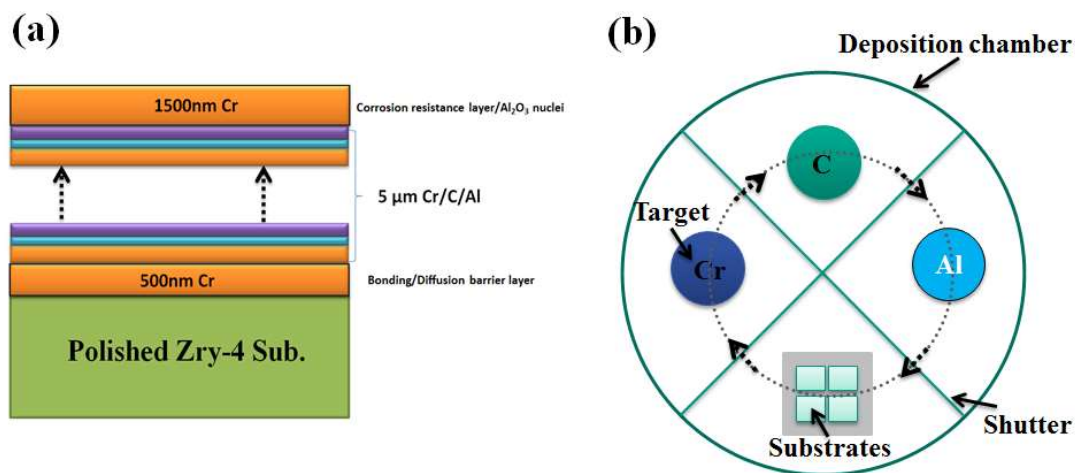


FIG. 4. Schematic representation of (a) the design of the as-deposited coatings on Zircaloy-4 substrates, and (b) arrangement of the targets and substrates during deposition.

2.4. AISI 348 SS

USP produced austenitic stainless steel AISI 348 samples within the RRT joint activity. There were two different geometries of austenitic stainless steel (AISI 348) samples supplied: tubes and plates. The composition and properties of both materials were the same:

- Chemical composition: Fe-balance, C-0.055%, Mn-1.70%, P-0.017%, S-0.003%, Si-0.41%, Cr-17.5%, Ni-11%, Nb-0.85%, N-0.0018%, Co-0.021%, Ta<0.005%, B-0.0008%;
- Micro-hardness: 150–200 HV;
- Surface roughness: $\leq 0.7 \mu\text{m Ra}$;
- Mechanical properties at 20°C: tensile strength — 640 MPa, yield strength — 330 MPa, elongation of a 50 mm specimen — 47%;
- Mechanical properties at 370°C: tensile strength — 455 MPa, yield strength — 260 MPa, elongation of a 50 mm specimen — 26%;
- Non-metallic inclusions (ASTM E45, Table 1 [9]): ≤ 1 ;
- Niobium carbides evaluation (ASTM E407 [10]): continuous non-stabilized areas < than 0.05 mm of equivalent diameter;
- Intergranular corrosion (ASTM A262, Practice A [11]): material does not present intergranular cracks (magnification in the range 5x to 20x).

Plate samples were prepared from AISI 348 bars with a diameter of 22 mm. After machining, each plate sample was polished, identified and cleaned. Tubular samples were prepared by cutting long tubes of AISI 348 tubes with a diameter of 9.8 mm and a thickness of 0.6 mm.

3. EXPERIMENTAL

3.1. Long term corrosion

The long term corrosion tests were done in two prototypical LWR chemistries — PWR (VTT, INCT) and WWER (CTU) at 360°C. The period of 21 days was defined with a goal of three minimal periods (63 cumulative days). Destructive testing was performed after 63 days but if there was enough material available, the tests continued for a longer time. The long term corrosion tests performed by the participants are summarized in Table 1.

TABLE 1. LONG TERM CORROSION TESTS ORGANIZED WITHIN THE RRT PERFORMED BY INDIVIDUAL PARTICIPANTS

	CTU — Czech Republic	VTT — Finland	INCT — Poland
Cladding material	Long term corrosion (WVER chemistry)	Long term corrosion (PWR chemistry)	Long term corrosion (PWR chemistry)
AISI348	164 days	63 days	63 days
Zry-2/Zry-2	164 days	63 days	63 days
Cr coated Zry-2	164 days	63 days	63 days
MAX phase coated Zry-4	147 days	63 days	63 days
ZrSi-Cr coated Zry-2	101 days	16.5 days	63 days
Cr coated E110	164 days	—	—

The experimental procedures vary depending on the available setups and standard procedures used at the institutes. For example, CTU/UJP uses 360°C, 19.4 MPa, 4 dm³ static autoclave, VTT used standard operational PWR parameters at 360°C with recirculation loop and online chemistry control whereas INCT used 360°C, 19.5 MPa, 1 dm³ static autoclave.

The samples were characterized before, during and after testing by non-destructive as well as destructive methods. The characterization techniques include visual inspections, XRD, SEM, metallography, weight changes and hydrogen and oxygen pickup measurements.

3.2. High temperature steam oxidation

Four participants performed high temperature (HT) oxidation tests. The three predefined conditions are:

- Flowing steam 1100°C, 60 minutes;
- Flowing steam 1200°C, 30 minutes;
- Flowing steam 1300°C, 5 minutes.

These parameters were defined based on estimates taking into account the standard DBA fuel safety criteria for Zr-based cladding materials such as 17% ECR limit calculated using the Baker-Just correlation [12]. Additionally, previous experience with testing of ATF cladding materials was used to estimate potential additional margins provided by the near-term ATF concepts tested and to determine reasonably long testing periods for all samples [13]. Some of the participants decided to perform more tests if larger quantities of samples were available. The summary of tested samples by particular institutes is shown in Table 2.

TABLE 2. STEAM OXIDATION TESTS PERFORMED BY INDIVIDUAL PARTICIPANTS

	CTU — Czech Republic	VTT — Finland	KIT — Germany	MTA EK — Hungary
Cladding material	HT steam oxidation - 1100,60'; 1200,30'; 1300°C,5'	HT steam oxidation - 1100,60'; 1200,30'; 1300°C,5'	HT steam oxidation - 1100,60'; 1200,30'; 1300°C,5'	HT steam oxidation - 1100,60'; 1100,180'; 1200,30';1200,45'; 1200°C,60'
AISI348	X	X	X	—
Zry-4 ref.	—	X	X	—
Cr coated Zry-2	X	X	X	—
MAX phase coated Zry-4	X	X	X	—
ZrSi-Cr coated Zry-2	—	—	X	—
E110 ref.	X	—	—	X
Cr coated E110	X	—	—	X

The experimental procedures vary depending on the experimental setup used. For example, the heating rates, steam flow rates, quench parameters, temperature measurements or sample holders are setup-dependent which might slightly affect the results. In addition, different experimental setups are able to measure different parameters such as hydrogen production or online weight changes. For example, only KIT was able to measure hydrogen generation and on the other hand, only CTU and MTA EK performed post-quench mechanical testing.

The samples were characterized before and after testing. The characterization techniques include visual inspections, XRD, SEM, microhardness, metallography, ring compression tests, hydrogen production, weight changes or hydrogen absorption measurements.

4. RESULTS

4.1. Long term corrosion

The results of the long term corrosion test show the expected corrosion behaviour of Zr-based alloy. This confirms that applied setups and procedures are valid and acceptable. Additionally, the data measured on Zr-based alloys serve as a baseline for comparison with ATF candidate materials.

The results summarized in Figure 5 indicate drastic weight loss in the case of the MAX phase coated sample suggesting dissolutions and spallation of the coating for both WWER and PWR chemistry. The weight loss/spallation is slightly slower in WWER chemistry but still extreme. Since spallation was observed for this sample, the weight change is not fully representative parameter in this case. It should be noted residuals of coating system remained on the Zr substrate even after the drastic weight loss. This suggests that some parts of the coating system are stable in LWR conditions.

ZrSi-Cr coating shows comparable corrosion kinetics to uncoated samples. It should be noted that with the more complex systems, both weight loss and gain happen during the test. This was the case for ZrSi-Cr as well as MAX phase coating. In the case of ZrSi-Cr coating, a high concentration of Si-based ions was found in the autoclave after the tests. This confirms that weight gain evaluation standardly used for Zr-based alloys might not be a suitable parameter for advanced materials. Additionally, the ZrSi-Cr PVD coated samples show very high hydrogen pickup.

Both, AISI 348 and Cr coated samples show extremely low weight gains. However, hydrogen concentration inside the Cr-coated is comparable to uncoated material suggesting higher H-pickup fraction. Figure 5 shows the weight gains of the samples tested in WWER chemistry up to 164 days as a function of exposure time. The detail of the weight gains of the Cr-coated samples is shown in Fig. 6 as well. Data measured on three samples as well as their average are shown. The scattering is due to extremely low weight gains where slight uncertainty in measurement results in higher scatter. But the absolute values are generally very low.

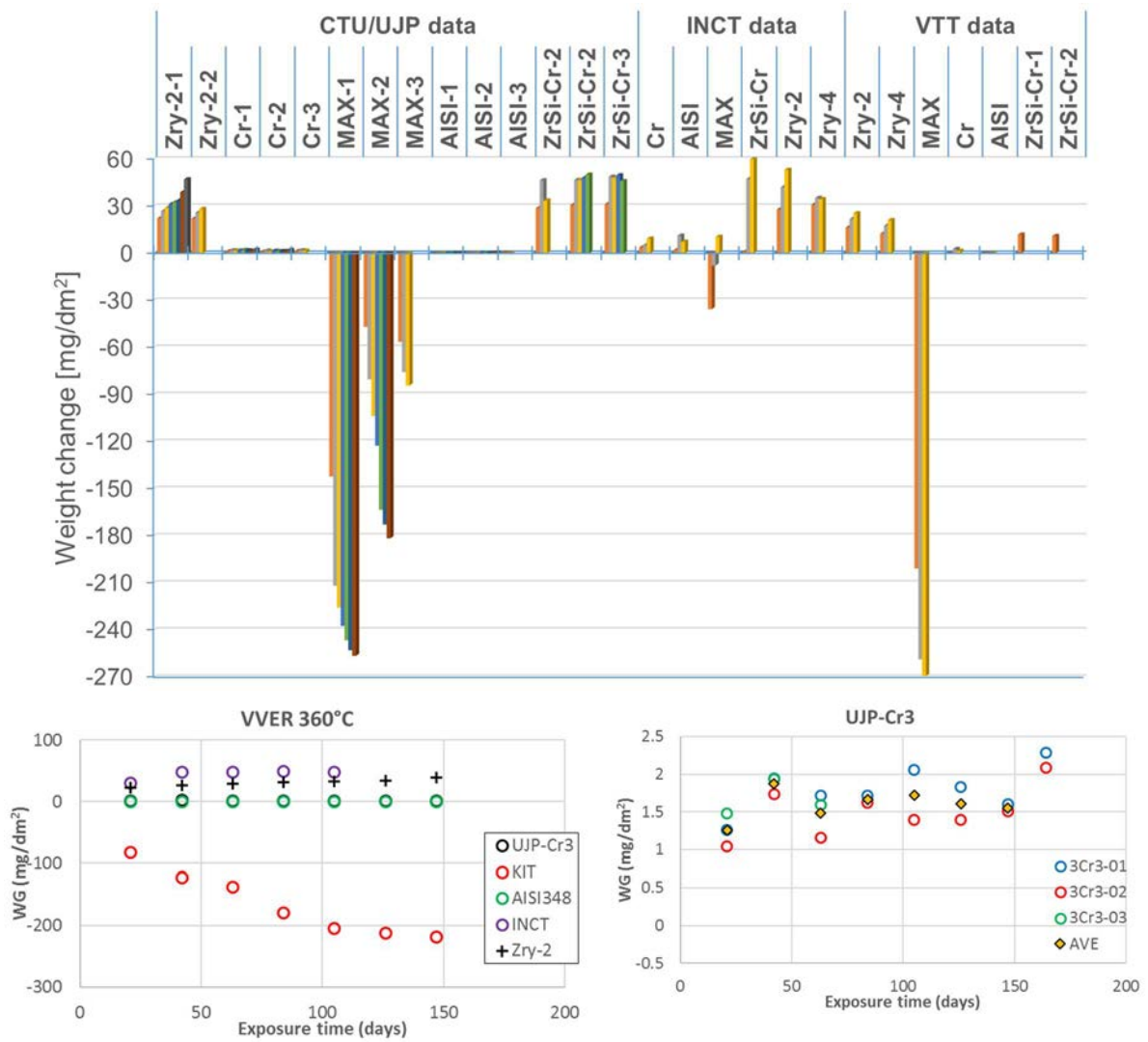


FIG. 5. Results of the weight gains from the corrosion test in WWER water chemistry. Top — summary of all WGs measured; Bottom left — summary of weight gains measured in WWER chemistry; Bottom right — detail of the weight gain for Cr-coated samples.

High resolution SEM micrographs of Cr-coated samples during the long term corrosion test are presented in Figure 6. Micrographs show the top view of the columnar structure of the Cr coating during the corrosion test. The grains are tightly coupled to each other with an average diameter of about 1 micron. The grains were clear and smooth on the as-received material. Small oxide particles cover the pyramidal grains as the surface oxidizes.

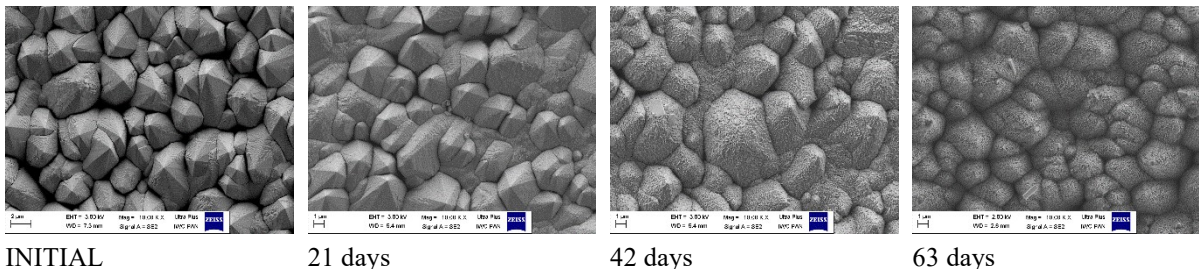


FIG. 6. SEM micrographs — top view of the Cr-coated Zry-2 during the corrosion test in PWR chemistry (as-received, 21 days, 42 days, 63 days).

To summarize, AISI 348 and Cr-coated ATF cladding materials seem to be very promising from the perspective of normal operation. They might provide also other benefits during normal operation such as improved wear resistance or improved creep behaviour. Nevertheless, unresolved issues such as hydrogen pickup still remain.

4.2. High temperature oxidation

The weight gains of the oxidized samples as a function of calculated weight gains using Cathcart-Pawel correlation [14] as measured at UJP Praha is shown in Figure 7. The results show a reduction of the weight gains for all of the tested samples in comparison with uncoated Zr-based cladding materials.

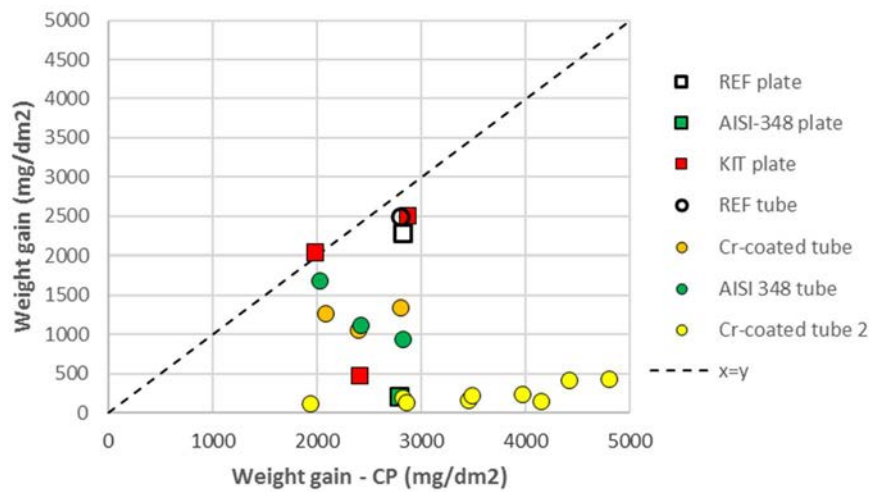


FIG. 7. Experimentally measured weight gains in relation with calculated weight gain using Cathcart-Pawel correlation (valid for most Zr-based alloys).

Additionally, the weight gains are directly linked with the oxidation kinetics for Zr-based alloys and the weight gain reduction suggests lower hydrogen production and limitations of the exothermic HT reaction with steam as well. These are the main required properties of ATF cladding materials.

However, the weight gain evaluation was established for Zr-based alloys and does not fully cover the cladding performance during accidental conditions. The oxidation testing needs to be accompanied by mechanical testing to quantify the accidental tolerance. Similarly, to long term corrosion tests, some of the samples showed extensive oxide and material spallation (e.g. AISI 348). For that reason, the weight change is a summation of oxidation weight gains and spallation (weight loss). The weight gain is from this perspective not a representative parameter for oxidation kinetics evaluation.

When evaluating the oxidation kinetics based on the hydrogen production measured during the tests, the results differ. The results of integral hydrogen production during the three predefined tests are shown in Figure 8. It can be seen that for example, the Cr-coated samples produce very low hydrogen which was suggested also by the low values of weight gain shown in Figure 7. On the other hand, the AISI 348 samples produce more hydrogen than uncoated Zr-based alloys but its weight gain is low.

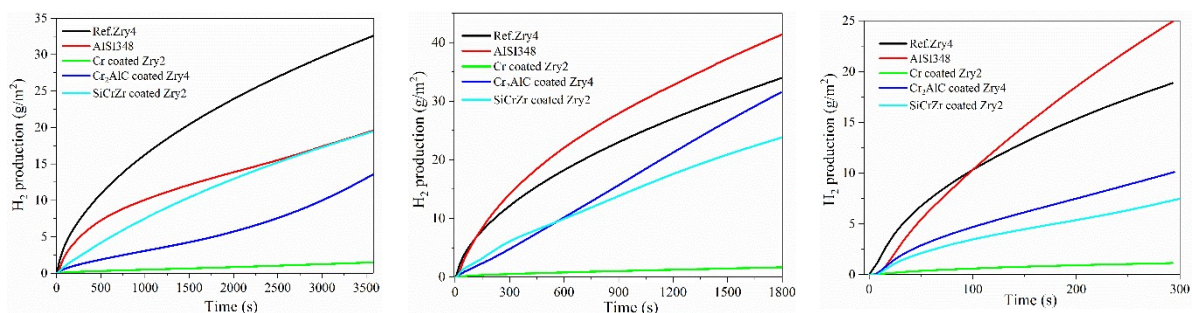


FIG. 8. Integral hydrogen production for 1100°C, 60min; 1200°C, 30min and 1300°C, 5min steam oxidation tests.

4.2.1. AISI 348 SPP 3, 1300°C, 5 min

The characterization of the AISI 348 sample after the steam oxidation test at 1300°C for 5 minutes shown in Figs 9 and 10 was done by VTT. The SE and BSE images shown in Figure 9 present the outer oxide layer on the top and the inner oxide layer. The bulk alloy can be seen on the bottom. The outer oxide layer is porous and partly loosened as a result of sample preparation. The inner oxide layer has large cracks. The thickness of the whole oxide layer varied from 520 µm to 1050 µm.

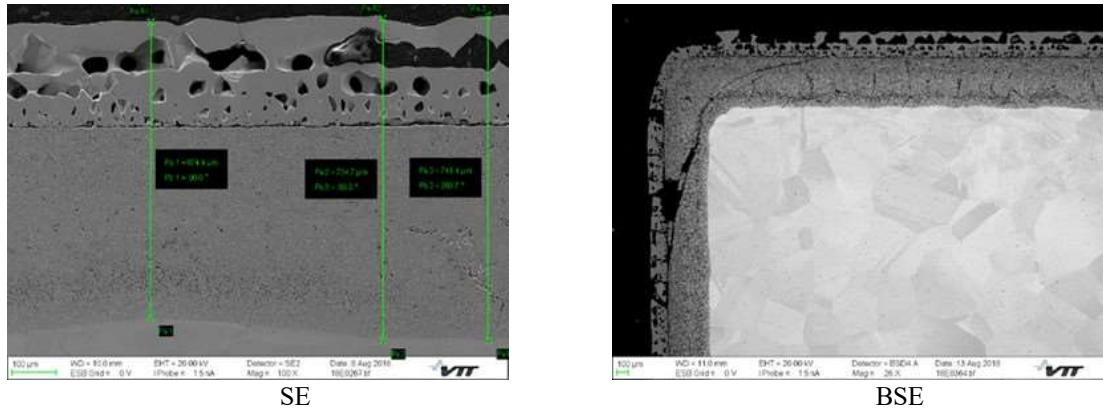


FIG. 9. SE and BSE images of the AISI 348 sample after exposure at 1300°C / 5 min.

SEM-EDS maps of O, Si, Cr, Mn, Fe and Ni are shown in Figure 10 where the detail of the outer and inner oxide layer is on the left side. The outer layer contains mainly Fe with some Mn and the inner layer Fe, Mn, Cr and Ni. The Fe content in the outer oxide layer has slightly increased when the test temperature has been increased. The results of hydrogen production shown in Figure 8 together with the post-characterization prove that Fe-oxides formed on this sample are not protective, spall off and do not enhance the oxidation resistance. This is in contrast with other advanced steels such as FeCrAl that form protective chromia and alumina scales at high temperature and considerably enhance the oxidation resistance [15]. Therefore, the HT oxidation resistance of the AISI 348 is limited and does not enhance the accidental tolerance in severe accidental conditions.

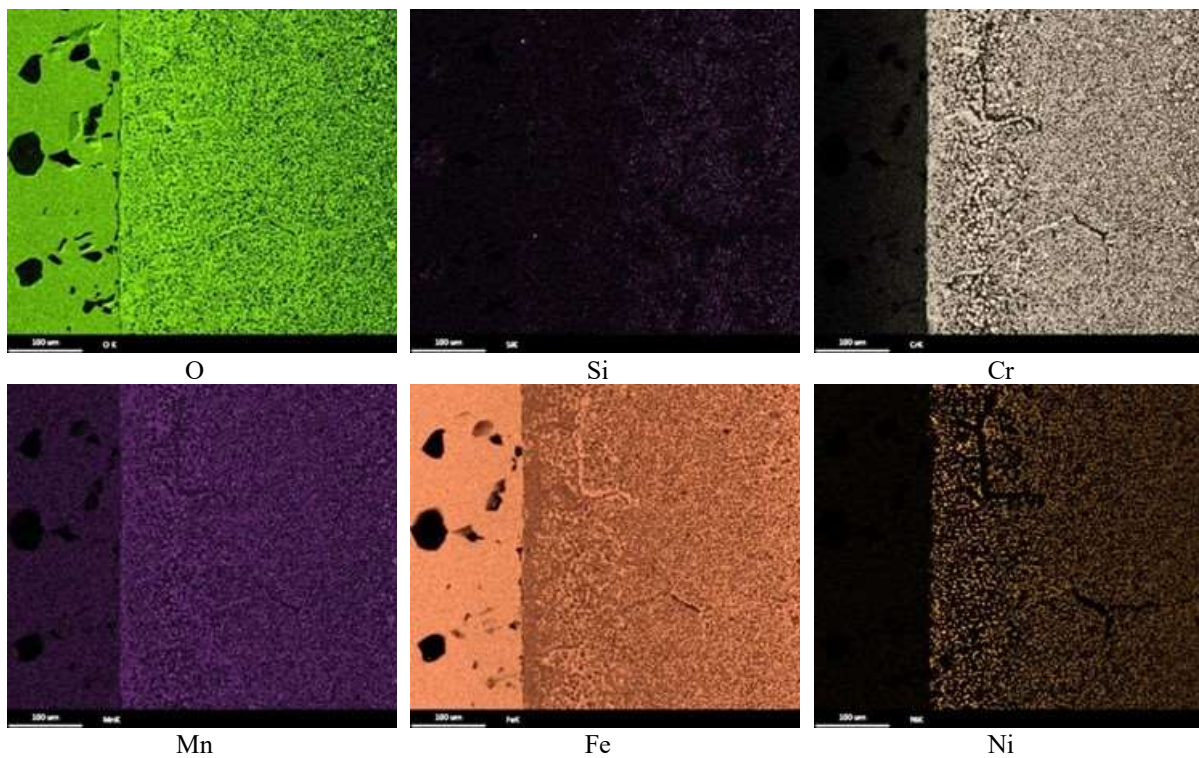


FIG. 10. SEM-EDS maps of AISI 348 SS after exposure at 1300°C / 5min showing the distribution of O, Si, Cr, Mn, Fe and Ni. The outer oxide layer is on the left side, the inner oxide layer in the middle and the bulk is on the right side outside the images.

4.2.2. Cr-coated Zr1%Nb, 1200°C, 60 min

Some of the participants performed also more extensive testing of ATF candidate samples than originally required. It includes for example also testing of samples in air atmosphere simulating severe accidental conditions. The Cr PVD coated samples oxidized in air show higher weight gains (approx. 2.2 times) than Cr-coated samples oxidised in steam at the same temperature and for the same time. The surface of the samples became dark (Figure 11), but not as dark as after oxidation in steam. Zirconium uncoated samples under similar conditions show about 10 x higher weight gains. This behaviour shows that the Cr coated samples are protective also in severe accidents with air ingress that is another proven benefit of Cr coated materials.



FIG. 11. Cr-coated IAEA-01 specimen in the quartz boat before (left) and after oxidation (right) in air at 1200°C for 3600 s.

The close view of the Cr coated tube surface showed (Figs 12 and 13) that after oxidation in air a non-uniform structure was developed. The kinetics of the oxidation in air needs to be further studied but the results obtained within this activity suggest the protective nature of Cr coatings in air as well as in steam.

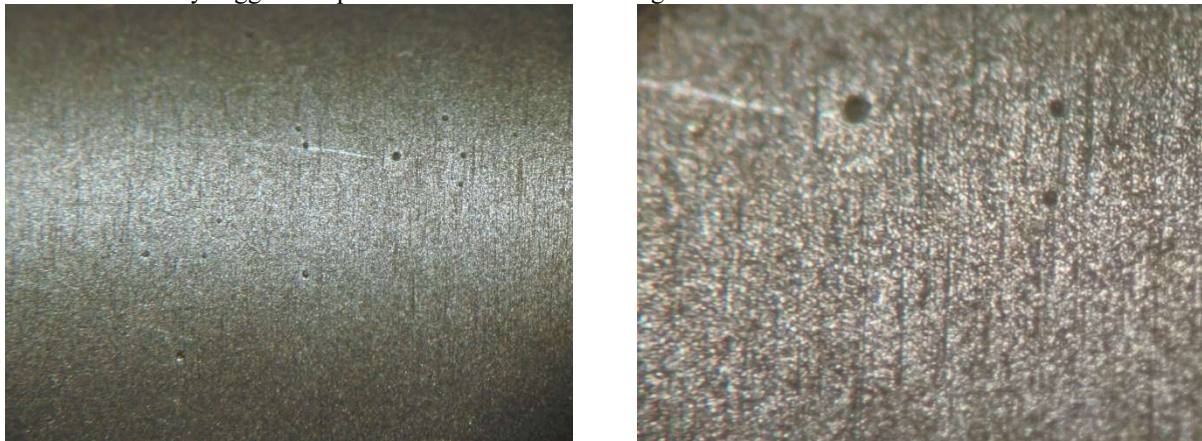


FIG. 12. Surface of the Cr-coated sample in as-received conditions.

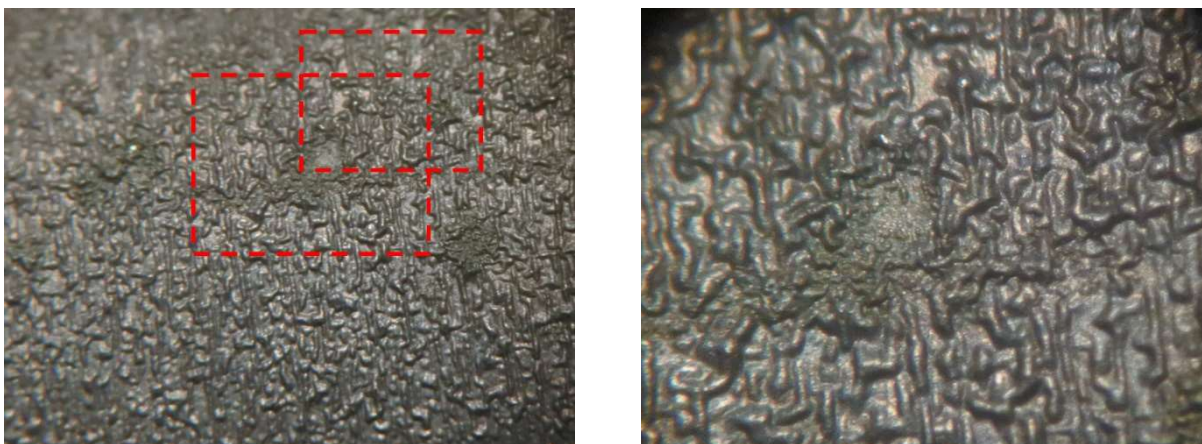


FIG. 13. Surface of the Cr-coated sample IAEA-01 after oxidation in air (1200°C, 3600 s).

5. CONCLUSION

An experimental programme has been carried out with four types of ATF candidate cladding samples. Four institutes produced their ATF candidate samples — Cr PVD coated Zr alloys, MAX phase PVD coated Zr alloys, ZrSi-Cr PVD coated Zr alloys and AISI 348 SS. Two fundamental tests were defined — high temperature oxidation and long term corrosion. Three participants performed long term corrosion testing for minimal 63 days period in PWR or WWER chemistry. Four participants performed oxidation tests in steam and air atmosphere between 1100°C and 1300°C including characterization and mechanical testing.

When evaluating the performance of tested samples, it can be seen that ZrSi-Cr coated samples show higher weight gains and extremely high hydrogen pickup during long term corrosion test compared to uncoated samples. Spallation and dissolution of MAX phase coated samples was observed in PWR as well as WWER chemistry during long term corrosion tests. These two concepts are therefore not feasible for further development from the perspective of normal operation.

AISI 348 SS, as well as Cr, coated samples show low weight gains and acceptable corrosion performance in both WWER and PWR chemistries. The hydrogen pickup of Cr-coated samples should be, however, further studied. In the accidental conditions, the AISI 348 performs much worse than Cr coated samples and also worse than uncoated reference samples at extreme severe accidental conditions. AISI 348 does not form protective oxides at HT and shows rapid oxidation with excessive hydrogen production. It can be concluded that only Cr-coated cladding satisfies the requirements of ATF cladding materials when evaluating the four studied ATF concepts.

Additionally, it was found that standard methods (e.g. weight gain evaluation) might not be fully representative for the evaluation and testing of new materials that differ from Zr-based alloys. The testing and industry standards related to handling, cleaning as well as testing are not fully developed for these new materials and new unexpected issues might appear in future.

It should be noted that not all activities originally planned were finished due to the limited time of the ACTOF project. The activity was initiated during the second half of the project and there were several delays caused by transport and regulatory issues, unavailability of required materials or funding. Despite the problems encountered during the RRT activity, there was a high number of valuable data produced by all participants. The RRT activity can be considered as very successful from the perspective of the involved parties as well as the community. The full report presented in the ACTOF TECDOC will include all the details about the production, testing methods and results that were produced within this RRT activity.

REFERENCES

- [1] KREJCI, J., SEVECEK, M., CVRCEK, L., Development of Chromium and Chromium Nitride Coated Cladding for VVER Reactors, 2017 WRFPM.
- [2] KREJČÍ, J., et al., Experimental behavior of chromium-based coatings, *Top Fuel 2018 - React. Fuel Perform.*, vol. 2018, 9.–4.10 2018, p. 13.
- [3] KRAUSOVÁ, A., TŮMA, L., NOVÁK, M., CVRČEK, L., KREJČÍ, J., MACÁK, J., Chromium Coating as a Surface Protection of Zirconium Alloys, *Koroze Ochr. Mater.* **61** 5 (Dec. 2017) 169–172.
- [4] HORNÍK, J., KRUM, S., TONDL, D., PUCHNIN, M., SACHR, P., CVRČEK, L., Multilayer coatings Ti/TiN, Cr/CrN and W/WN deposited by magnetron sputtering for improvement of adhesion to base materials, *Acta Polytech.* **55** 6 (Dec. 2015) 388–392.
- [5] KREJČÍ, J., ŠEVEČEK, M., CVRCEK, L., KABÁTOVÁ, J., MANOCH, F., "Chromium and Chromium Nitride Coated Cladding for Nuclear Reactor Fuel", in *Proceedings of the 20th International Corrosion Congress, EUROCORR 2017, Prague, Czech Republic (2017)*.
- [6] STAROSTA, W., SEMINA, V.K., SMOLIK, J., WALÍŠ, L., RYDZEWSKI, M., SARTOWSKA, B., Studies on magnetron-sputtered zirconium-silicide coatings deposited on zirconium alloy for the enhancement of their high temperature oxidation resistance, *Nukleonika* **63** 3 (Sep. 2018) 73–79.
- [7] TANG, C., et al., Synthesis and characterization of Ti₂AlC coatings by magnetron sputtering from three elemental targets and ex-situ annealing, *Surf. Coat. Technol.* **309** (Jan. 2017) 445–455.
- [8] TANG, C., et al., Deposition, characterization and high temperature steam oxidation behavior of single-phase Ti₂AlC-coated Zircaloy-4, *Corros. Sci.*, 135 (May 2018) 87–98.
- [9] ASTM E45-18A, Standard Test Methods for Determining the Inclusion Content of Steel, 10.1520/E0045-18A, ASTM International, West Conshohocken, PA (2018).
- [10] ASTM E407-07(2015) E1, Standard Practice for Microetching Metals and Alloys, ASTM International, West Conshohocken, PA (2015).

- [11] ASTM A262-15, Standard Practices for Detecting Susceptibility to Intergranular Attack in Austenitic Stainless Steels, ASTM International, West Conshohocken, PA (2015).
- [12] BAKER, L., JUST, L., Technical Report ANL-6548, Argonne Natl. Lab., 1962.
- [13] ŠEVEČEK, M., et al., Development of Cr cold spray-coated fuel cladding with enhanced accident tolerance, Nucl. Eng. Technol. **50** 2 (Mar. 2018) 229–236.
- [14] PAWEL, R.E., CATHCART, J.V., McKEE, R.A., The Kinetics of Oxidation of Zircaloy-4 in Steam at High Temperatures, J. Electrochem. Soc. **126** 7 (Jan. 1979) 1105–1111.
- [15] REBAK, R.B., TERRANI, K.A., FAWCETT, R.M., FeCrAl Alloys for Accident Tolerant Fuel Cladding in Light Water Reactors, p. V06BT06A009, (Jul. 2016).
- [16] KREJČÍ, J., et al. Development and testing of multicomponent fuel cladding with enhanced accidental performance. Nuclear Engineering and Technology (2019).

INTRODUCTION OF ATF DEVELOPMENT AND MAIN RESULTS OF THE CRP ON ACTOF OF KAERI

C.H. SHIN, H.C. KIM, Y.S. YANG
Nuclear Fuel Safety Research Division,
Korea Atomic Energy Research Institute,
111, Daedeok-daero 989 beon-gil, Yuseong-gu, Daejeon, 34057,
Republic of Korea

Abstract

As a candidate of the accident tolerant fuel (ATF) in the KAERI, the microcell UO_2 pellet and the surface modified cladding with coating are being developed as the near term technology. The microcell UO_2 pellet is to enhance the fission product retention and to increase thermal conductivity. The surface modified cladding is based on the coating technology on the conventional Zirconium alloy cladding. It is to enhance the oxidation and deformation resistance of the fuel cladding. In the IAEA-CRP ACTOF, the research objectives and anticipated outcomes of KAERI were the development and implementation in the FRAPCON/FRAPTRAN code of ATF models for the coated cladding and metallic microcell UO_2 pellet of KAERI. In order to evaluate the mechanical behaviours of the ATF cladding under the normal operation conditions, a new analytical module, FRACAS-CT, was developed based on the thick-wall theory to consider the multi-layered structure of the coated cladding. The FRACAS-CT model was verified by comparison with an equivalent finite element model. And the module was implemented into FRAPCON code with consideration of creep and stress relaxation behaviours of the multi-layered cladding. The implemented FRACAS-CT can simulate the mechanical response and fuel performance of the multi-layered ATF cladding. The preliminary analysis of the fuel performance for the KAERI's ATF concept was summarized. The major material properties of ATF such as the thermal conductivity and thermal expansion of the pellet and the corrosion behaviour of the CrAl-coated cladding were modified based on out-of-pile test results. The differences compared to a conventional UO_2 -Zircaloy fuel was assessed. From the FRAPCON results under the normal operation condition, ATF shows a significant advantage in the reduction of the fuel centreline temperature, cladding oxidation thickness, fission gas release, and so on, because of the increased thermal conductivity of the metallic microcell pellet and the oxidation resistance of the CrAl-coated cladding.

1. INTRODUCTION

After Fukushima Daiichi Nuclear Plant accident, the R&D has been conducted to improve the safety of the nuclear fuel under the accident conditions. The accident tolerant fuel (ATF) is used as a representative expression of the safety-enhanced nuclear fuel. The DOE-Programme suggested that the goal of accident tolerant fuel should have a similar or better performance under normal operation conditions and during design basis accidents, as well as in beyond design basis accidents compared to a conventional nuclear fuel [1, 2]

In Republic of Korea, the development of the accident tolerant fuel is classified into near term application technology and long term development technology. As a near term technology, the microcell UO_2 pellet with metal or ceramic materials and the surface modified claddings with coating technology are being developed. The microcell UO_2 pellet is to enhance the fission product retention and to increase thermal conductivity. The surface modified cladding is based on the coating technology on the conventional Zr alloy cladding. It is to enhance the oxidation and deformation resistance of the fuel cladding [3].

In the IAEA-CRP ACTOF, the research objectives and anticipated outcomes of KAERI were the development and implementation into the FRAPCON/FRAPTRAN code of accident tolerant fuel (ATF) models for the Cr-coated cladding and the metallic microcell pellet, model validation using data from the out-of-pile experiment. In this paper, the main results of the research conducted by KAERI in IAEA CRP ACTOF is summarized.

2. DEVELOPMENT OF ATF IN KAERI

2.1. Fuel Pellet and Cladding for ATF

KAERI has been developing Cr-alloy coated cladding and metal microcell UO_2 pellets as one of the candidates of for ATF. As the coating material, CrAl or FeCrAl was coated on the zircaloy base cladding by Arc ion plating or a 3D laser coating technique as shown in Figure 1. Various tests were conducted to evaluate the coated cladding performance such as the corrosion, oxidation, creep, wear, and so on [4].

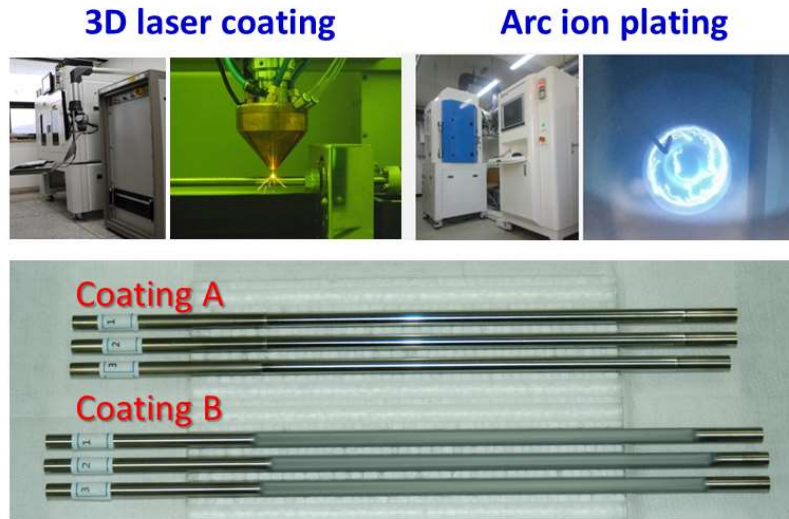


FIG. 1. Manufacturing techniques and samples for surface modified zircaloy cladding [4].

As the ATF pellet, ceramic and metallic microcell UO_2 pellets are being developed as shown in Figure 2. The enhanced pellet thermal conductivity is the distinct feature of a metallic microcell UO_2 pellet to effectively decrease the fuel temperature. The out-of-pile tests were performed to evaluate the thermo physical properties, such as the thermal conductivity, the linear thermal expansion, steam oxidation, and so on [5].

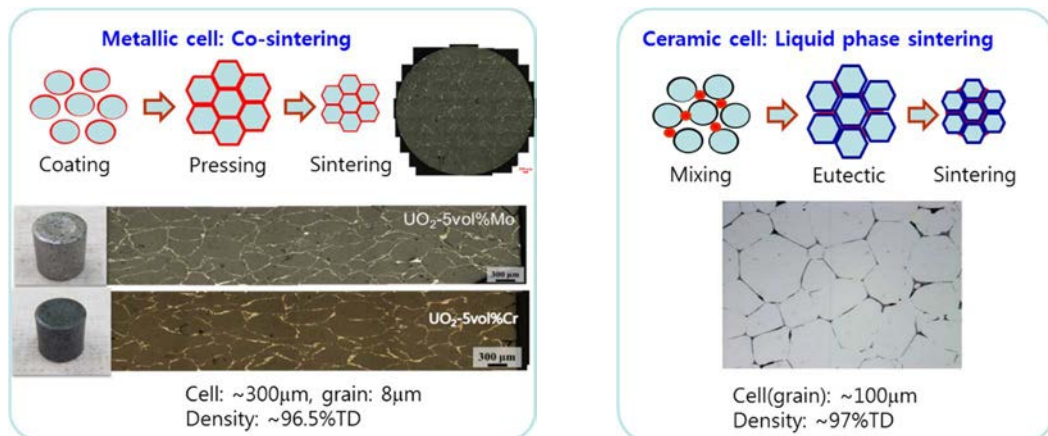


FIG. 2. Fabrication process and micro structure of the metallic and ceramic microcell UO_2 pellet (Reproduced courtesy of Elsevier [3]).

2.2. Performance Analysis for ATF

A comparative performance analysis of the cores having different ATF fuel assemblies was performed to show the effects of the new ATF fuels on the performances of the cores such cycle length, discharge burnup, and reactivity coefficients. The candidate ATF fuel rods includes the UO_2 -Mo, UO_2 -Cr, UO_2 - SiO_2 - TiO_2 microcell pellets with zircaloy cladding coated with or without Cr layer. The reference core using UO_2 fuel rods was designed with the design data for the OPR1000 which is Korean standard reactor such that the core has 480 EFPDs cycle

length. The cores using Cr-coated zircaloy cladding have a slightly reduced cycle length, but the cores using metallic microcell pellets have more reduced cycle length because of the higher neutron absorption by metal composition and reduced loading amount of UO_2 .

For the fuel performance code, some material properties from the out-of-pile test were modified in FRAPCON code. Increased thermal conductivity of a metallic microcell pellet was modified as function of temperature for the fresh fuel condition. For the ATF cladding, the corrosion, oxidation, and hydrogen pick-up model was modified based on the out-of-pile test. ATF performance results are compared to UO_2 and zircaloy reference fuel. A mechanical behaviour model for multi-layer structure analysis of coated cladding was developed and verified, as an effort of developing ATF performance model.

Safety of ATF for the DBA and BDBA was evaluated using MARS, RELAP5 and SCDAP codes, comparing ATF micro-cell pellet and CrAl-coated claddings to the reference fuel, UO_2 pellet and zircaloy cladding. The target reactor was OPR1000 and selected accident type was LBLOCA, SBLOCA plus addition failure, and so on.

3. ESTIMATION OF FUEL PERFORMANCE FOR ATF

3.1. Development of Mechanical Model for Multi-layered Cladding for FRAPCON

The fuel performance code FRAPCON have FRACAS-I model for the small displacement deformation of the cladding based on the thin-wall theory. The analysis is performed to determine cladding stresses and strains [6]. However this model based on the thin-wall cannot use for the multi-layered cladding such as a coated cladding. In order to evaluate the mechanical behaviour of the ATF cladding under the normal operation conditions, a new analytical module, FRACAS-CT, was developed based on the thick-wall theory to consider the multi-layered structure of the coated cladding. The FRACAS-CT module was implemented into FRAPCON code for consideration of creep and stress relaxation behaviours of the multi-layered cladding [7]. This module can model the cladding consisting of 2- or 3-layers like the coated cladding, assign properties to each layer, and calculate the stresses and strains for each layer of the coated cladding. To maintain the input structure of the original FRAPCON, the FRACAS-CT module was added as one of mechanical model option, “mechan = 3”.

To verify the implemented module, the power condition was set to have a simple power history, and the coating material was set to be identical to the substrate, Zr cladding. For code verification, the gap thickness behaviour was compared in Figure 3. The calculated results of the gap thickness at top, center and bottom axial node were highly consistent, which is reasonable because material properties and inelastic model used for the FRACAS-CT are equal with ones of the original FRAPCON.

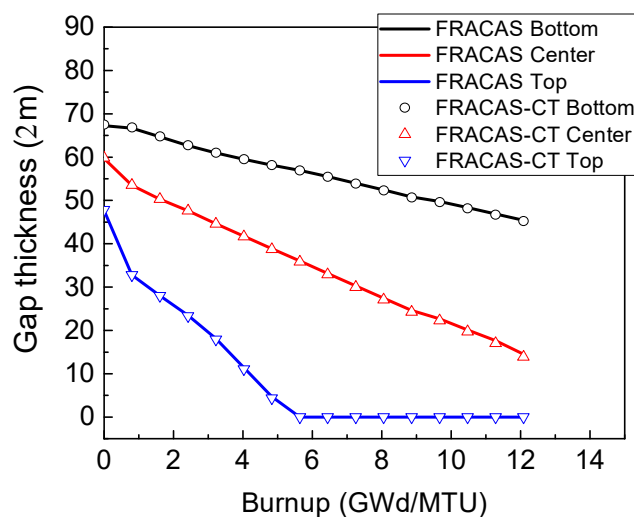


FIG. 3. Comparison of the gap thickness behaviours for the verification of FRACAS-CT in FRAPCON (Reproduced courtesy of Taylor and Francis [7]).

3.2. Fuel Performance Analysis under Normal Operation Condition

The preliminary analysis of the fuel performance for the KAERI's ATF concept was conducted under the normal operation condition in ACTOF. The thermal conductivity model for metallic microcell pellet and the corrosion model for CrAl-alloy as coating material was modified based on out-of-pile test results as shown in Figure 4. For the simple comparison, the simple power history and the cosine axial power profile were applied as shown in Figure 5.

The thermal conductivity of the metallic microcell UO_2 pellet was improved about twice as compared with that of the conventional UO_2 pellet. Therefore, it is expected to show a great benefit in the temperature of the pellet. The fuel centreline temperature and average fuel temperature was shown in Figure 6. At the peak power node, the centreline temperature was reduced from 220 to 340 K and the average fuel temperature was lowered by about 100 K.

The rod internal pressure was reduced by decreasing the temperature of the pellet as shown in Figure 7. In the low burnup region, the internal void gap volume of rod was maintained relatively large due to the reduced deformation amount of the pellet. In the high burnup region, the fission gas will be partially released into the rod gap region. When the FRAPFGR model was applied, the amount of fission gas release was reduced for ATF, which can be expected due to the decrease in the temperature of the fuel pellet. In this analysis condition, the rod internal pressure was predicted to decrease by 20% at the end of life.

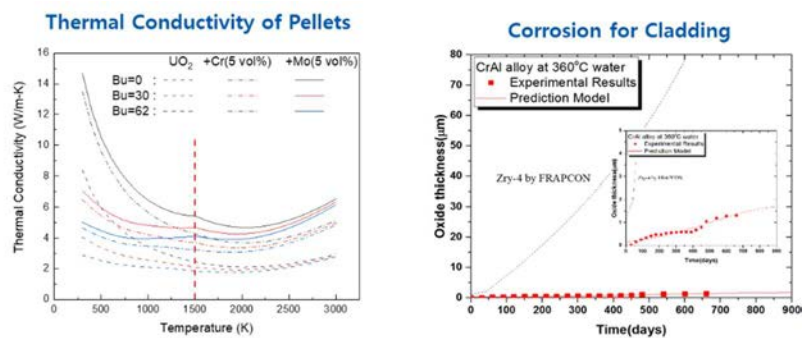


FIG. 4. The thermal conductivity model of metallic microcell UO_2 pellet and the corrosion model for CrAl-alloy as coating material.

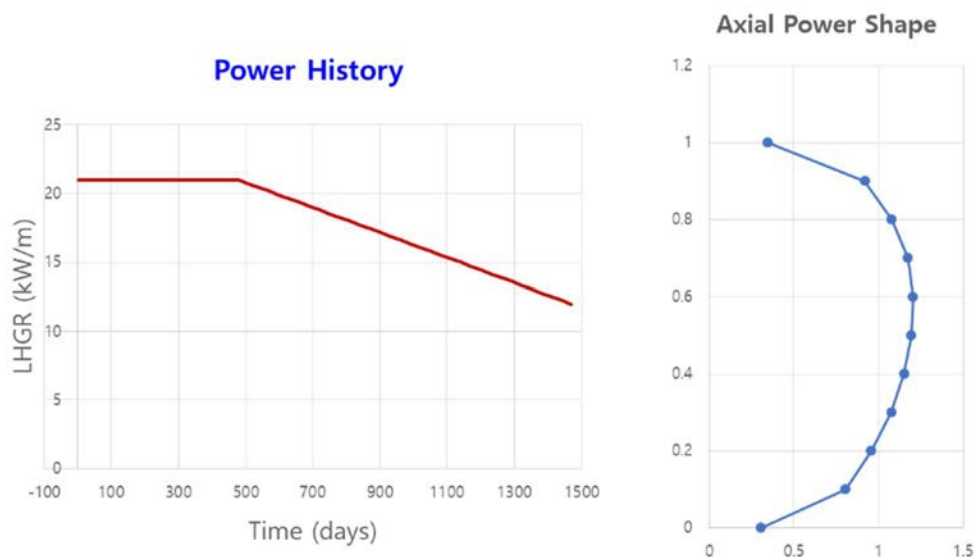


FIG. 5. The power history and the axial power profile to analysis ATF performance.

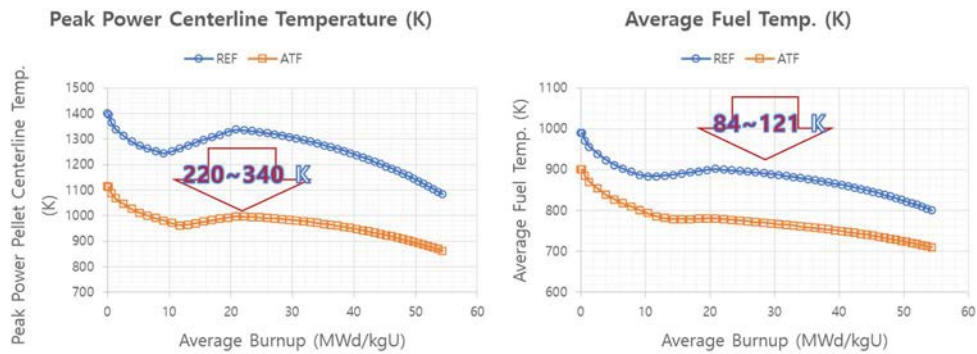


FIG.6. The fuel centreline temperature at the peak power node and average fuel temperature.

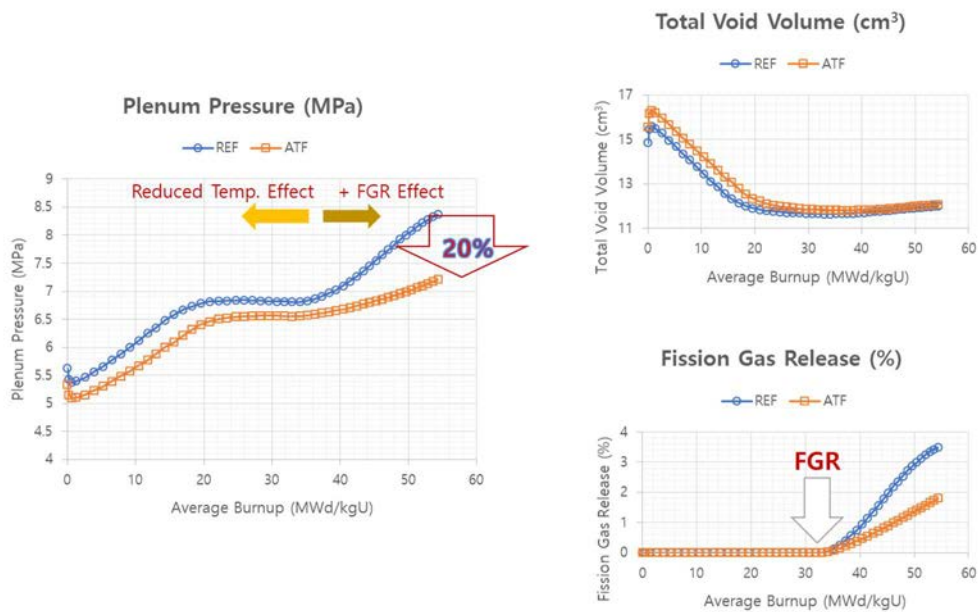


FIG. 7. The behaviour of the fuel rod internal pressure, the total void volume and the fission gas release.

4. CONCLUSIONS

In the IAEA-CRP ACTOF, the research objectives and anticipated outcomes of KAERI were the development and implementation in the FRAPCON/FRAPTRAN code of ATF models for Cr-coated cladding and metallic microcell pellet, model validation using data from the out-of-pile experiment. In the ACTOF, the work done of KAERI is as follows.

"In order to evaluate the mechanical behaviour of the ATF cladding under the normal operation conditions, a new analytical module, FRACAS-CT, was developed based on the thick-wall theory to consider the multi-layered structure of the coated cladding. The FRACAS-CT model was verified by comparison with an equivalent finite element model. And the module was implemented into FRAPCON code with consideration of creep and stress relaxation behaviour of the multi-layered cladding. The implemented FRACAS-CT can simulate the mechanical response and fuel performance of the multi-layered ATF cladding" [7]

The preliminary analysis of the fuel performance for the KAERI's ATF concept was summarized. The major material properties of ATF such as the thermal conductivity and thermal expansion of the pellet and the corrosion behaviour of the CrAl-alloy coated cladding were modified based on out-of-pile test results. The differences compared to a conventional UO₂-Zircaloy fuel was assessed. From the FRAPCON results under the normal operation condition, ATF shows a significant advantage in the reduction of the fuel centreline temperature,

cladding oxidation thickness, fission gas release, and so on, because of the increased thermal conductivity of the metallic microcell pellet and the oxidation resistance of the CrAl-alloy coated cladding.

ACKNOWLEDGEMENTS

This work was supported by the IAEA CRP ACTOF and the National Research Foundation of KOREA (NRF) grant funded by the government (MSIT: Ministry of Science and ICT) (NRF-2017M2A8A5015064)

REFERENCES

- [1] BRAGG-SITTON, S.M., et al., Advanced Fuel Campaign: Enhanced LWR Accident Tolerant Fuel Performance Matrix, INL/EXT-13-000264, Feb., (2014)
- [2] CARMACK, J., GOLDNER, F., BRAGG-SITTON, S.M., SNEAD, L.L., Overview of the U.S. DOE Accident Tolerant Fuel Development Programme, TopFuel 2013, Charlotte, North Carolina, U.S., Sept., (2013)
- [3] KIM, H.G., YANG, J.H., KIM W.J., KOO, Y.H., Development Status of Accident-Tolerant Fuel for Light Water Reactors in Korea, Nuclear Engineering and Technology **48** (2016) 1–15.
- [4] KIM, H.G., KIM, I.H., JUNG, Y.-I., PARK, D.-J., PARK, J.-H., YANG, J.-H., KOO, Y.H., Progress of Surface Modified ZR Cladding Development for ATF at KAERI, 2017 Water Reactor Fuel Performance Meeting, Jeju, Republic of Korea, Sep., (2017).
- [5] KIM, D.J., KIM, K.S., KIM, D.S., OH, J.S., KIM, J.H., YANG, J.H., and KOO, Y.H., Development status of microcell UO₂ pellet for accident-tolerant fuel, Nuclear Engineering and Technology, **50**, 253–258, (2018).
- [6] GEELHOOD, K.J., LUSCHER, W.G., RAYNAUD, P.A., and PORTER, I.E. FRAPCON-4.0: A Computer Code for the Calculation of Steady-State, Thermal mechanical Behaviour of Oxide Fuel Rods for High Burnup, PNNL-19418. Vol.1 Rev.2, (2015)
- [7] KIM, D.H., KIM, H.C., SHIN, C.H., KIM, H.S., Development of FRACAS-CT Module with FRAPCON4.0P01 for Simulation of Mechanical behaviors for Accident Tolerant Fuel Cladding in a Reactor, Journal of Nuclear Science and Technology **56** (2019) 671-683.

MODELLING OF TRADITIONAL UO₂ AND ADVANCED ATF FUELS BEHAVIOUR IN
INTEGRAL SEVERE ACCIDENT (SA) CODES

(Session 5)

Chairperson

J. STUCKERT

Germany

STATUS OF ATF MODELLING AND APPLICATION WITH ATHLET-CD

T. HOLLANDS, L. LOVASZ, C. BALS

Gesellschaft für Anlagen und Reaktorsicherheit (GRS) gGmbH,
Garching, Germany

Abstract

To investigate the cladding material FeCrAl which is one option of Accident Tolerant Fuel (ATF), the bundle experiment QUENCH-19 was performed at Karlsruhe Institute of Technology (KIT). ATF claddings could be used as one option to reduce e.g. the thermal impact by oxidation and to increase time margins for accident management measures. On the other hand, the neutron absorption is higher and the melting temperature is lower of FeCrAl compared to Zry based claddings. The test QUENCH-19 was accompanied by post test analyses at GRS with the AC² module ATHLET-CD. The experiment QUENCH-19 was conducted similarly to the experiment QUENCH-15 for comparing the oxidation behaviour of FeCrAl and Zry at high temperatures. In contrast to test QUENCH-15, which showed a sharp escalation after start of quenching resulting in temperatures up to $\approx 1900^{\circ}\text{C}$, no escalation occurred during QUENCH-19 and peak cladding temperatures of only $\approx 1450^{\circ}\text{C}$ were reached. For the post test simulations an oxidation correlation for KANTHAL APMT was available and also a second approach derived from an OECD/NEA report. Both approaches were implemented in ATHLET-CD with the assumption that only Al_2O_3 was generated but no other oxides. Compared to Zry oxidation both approaches give orders of magnitude lower oxidation rates and are only valid for one special composition, while different materials were used in the experiment. In general, the results of the post test simulation show good agreement of the thermal behaviour. While the maximum temperature well reproduced an underestimation of only app. 50°C , the radial temperature profile was significantly underestimated by $150\text{--}200^{\circ}\text{C}$ compared to the measured data. The comparison of the hydrogen production of in total 9 g in the test and less than 1 g for both oxidation approaches in the simulation shows that the oxidation model for FeCrAl in the code has to be improved. For a detailed evaluation of the calculated hydrogen generation the post test examination of the bundle is necessary to know which components contribute to the total value.

1. INTRODUCTION

Zirconium based claddings have been widely used all over the world for decades due to its good mechanical, corrosion resistant and low neutron absorption properties at around operational temperatures. At higher temperatures, however, the zirconium becomes more reactive, in case of a nuclear accident most likely with the steam around it. The oxidation of zirconium by the surrounding steam unfortunately has several negative effects. The oxidation itself is an exothermic process, which can accelerate the heat-up of the core significantly. This has a high safety relevance, because it reduces the time available to mitigate or avoid the transition to a severe accident. As a product of oxidation ZrO_2 is formed, which degrades the mechanical properties of cladding. Also, large amounts of hydrogen are generated, which can lead to. These negative characteristics at higher temperatures give the nuclear community reasons and motivation to develop improved, more accident tolerant cladding material.

Research and development on accident tolerant fuel (ATF) and cladding (ATC) material began already before the accident at the Fukushima Daiichi nuclear power plant, but this event highlighted the importance of the development of such a new material. The new material should have significantly slower oxidation kinetics compared to the Zr-based alloys that are used in a typical light water reactor. This should reduce the hydrogen generation rate and slow down the core heat up after core uncovering [1]. One of the most promising accident tolerant cladding materials under investigation is FeCrAl. This material has at 1200°C an oxidation rate which is 1000 times smaller than a typical Zirconium based material.

The objective of the QUENCH experimental programme [2] at the Karlsruhe Institute of Technology (KIT) has been the investigation of oxidation characteristics of different fuel claddings during different accident scenarios for more than 20 years. So far 19 experiments were conducted successfully, using fuel rod simulators that were electrically heated. During the QUENCH-19 experiment the behaviour of FeCrAl cladding material was investigated and compared to reference experiment QUENCH-15, where the behaviour of ZIRLO material was tested.

ATHLET-CD has been used many times for pre- and post test calculations to support the QUENCH experimental programme. The simulation of oxidation processes is very complex; oxidation models were developed and validated over the years with a strong cooperation with KIT to be able to predict the fuel cladding behaviour during a nuclear accident. Most of these models were, however, developed for the oxidation of

zirconium based claddings. New materials require adjustments and improvements also in the existing models. The results of the QUENCH-19 experiment helped to develop the first version of FeCrAl oxidation model for ATHLET-CD.

This paper presents the main findings of the QUENCH-19 experiment and shows the applicability of the newly implemented correlations for FeCrAl material compared to the old oxidation models.

2. CONDUCT AND FIRST RESULTS OF THE QUENCH-19 EXPERIMENT [3]

“The QUENCH-19 bundle experiment was conducted at KIT on 29th August 2018. It was performed in cooperation with the Oak Ridge National Laboratory (ORNL) and was supported by the KIT programme NUSAFE. The test objective was the comparison of FeCrAl and ZIRLO claddings under similar configuration and similar boundary conditions as the previous QUENCH-15 experiment [3].

Different to QUENCH-15, the new test QUENCH-19 had FeCrAl (Y) claddings and 4 FeCrAl (Y) spacer grids as well as 8 KANTHAL APM corner rods and a KANTHAL APM shroud. For both tests the PWR-typical bundle consisted of 24 heated rods and 8 corner rods inside a shroud, which was insulated by ZrO₂ fiber and surrounded by an Inconel cooling jacket (Fig. 1).

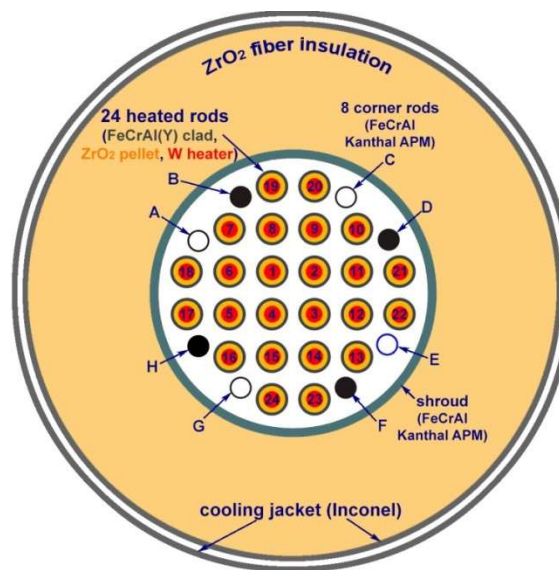


Fig.1. Cross section of test bundle QUENCH-19 (arrangement the same as for QUENCH-15).

To get the same temperature conditions as for the QUENCH-15 test similar gas flow conditions were adopted (Fig. 2) and the same stepwise increase of electrical power was used up to a value of 18.12 kW (Fig. 3).

In spite of these very similar boundary conditions there was a significant difference in the bundle heating already during the pre-oxidation period. Fig. 3 shows that there was a $\approx 200^\circ\text{C}$ lower temperature plateau for the QUENCH-19 test. After reaching the maximum power value there was a strong escalation of the peak cladding temperature up to $\approx 1900^\circ\text{C}$ during QUENCH-15, but only a slow increase of maximum values for QUENCH-19. Therefore, the power was kept constant for about 2000 s until a peak cladding temperature of $\approx 1455^\circ\text{C}$ was reached. The reflood was initiated at ≈ 9100 s; at the same time the electrical power was reduced to 4.1 kW which was kept during the reflood. A temperature excursion was not observed.

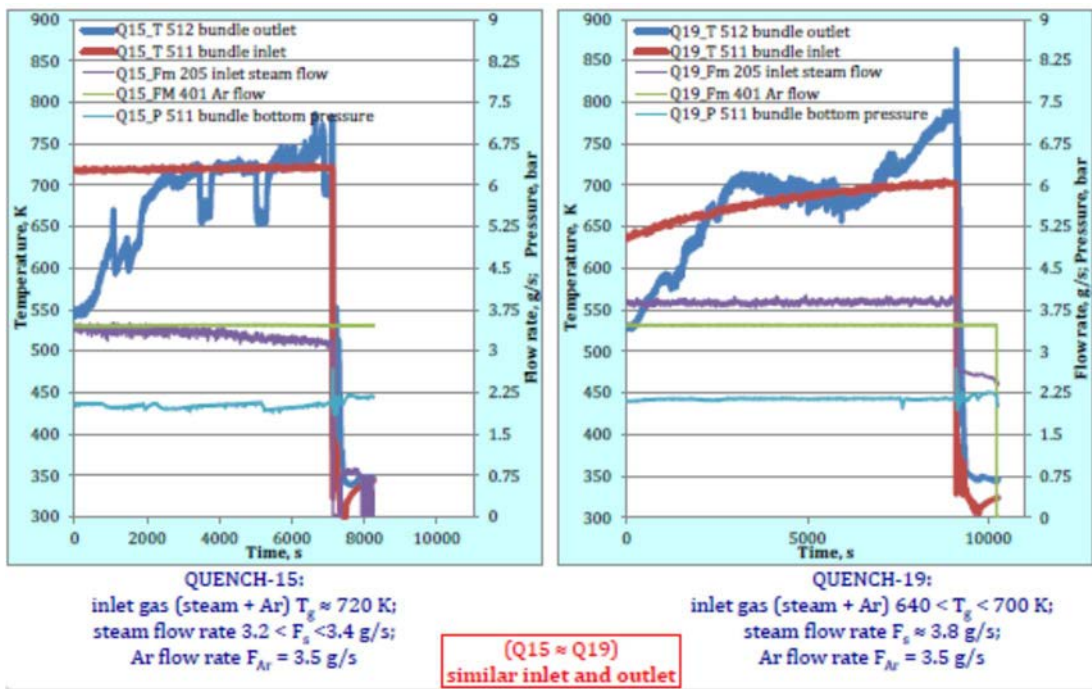


FIG.2. Steam and argon flow rates of QUENCH-15 and QUENCH-19 [3].

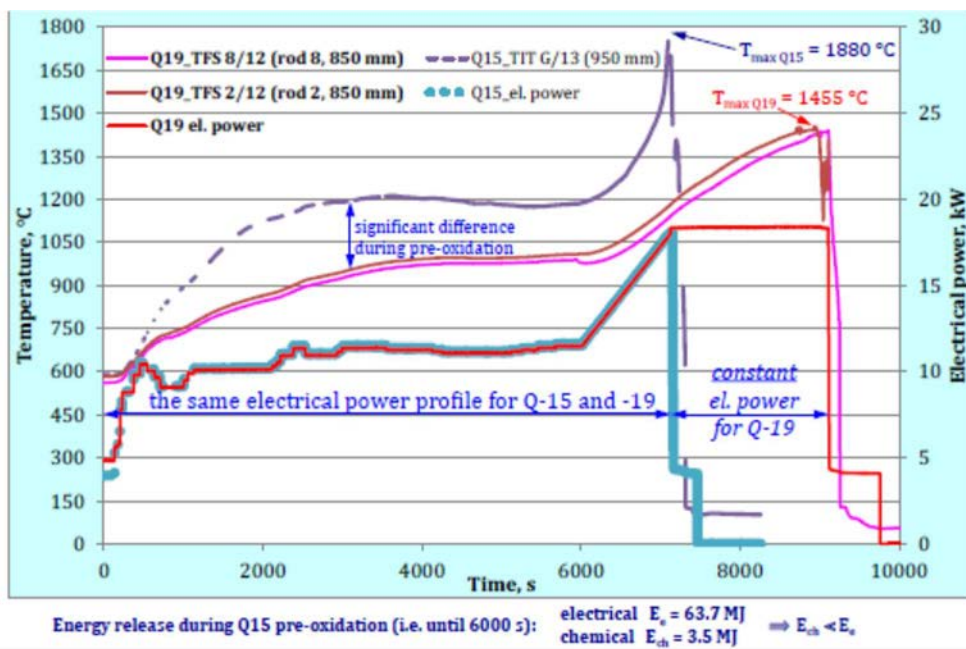


FIG.3. Comparison of QUENCH-15 and QUENCH-19 [3].

The total hydrogen release during the whole test was 9.2 g compared to 47.6 g in the QUENCH-15 test with a much shorter period of high electrical power. While during pre-oxidation a very small release rate resulted in only 0.3 g hydrogen mass a sharp increase of hydrogen release rate was observed after the peak cladding temperature exceeded 1400°C.” [4]

3. POST TEST CALCULATIONS AND COMPARISON

3.1. Description of the code ATHLET-CD

"ATHLET-CD (Analysis of THERmal-hydraulics of LEaks and Transients with Core Degradation) [5] describes the reactor coolant system thermal hydraulic response during severe accidents, including core damage progression as well as fission product and aerosol behaviour, to calculate the source term for containment analyses, and to evaluate accident management measures. It is developed by GRS in cooperation with IKE, University of Stuttgart. ATHLET-CD includes also the aerosol and fission product transport code SAFT and as a part of the system code AC2 it is coupled with COCOSYS for modelling thermal-hydraulics and fission product behaviour in the containment.

The code structure is highly modular to include a manifold spectrum of models and to offer an optimum basis for further development. ATHLET-CD contains the original ATHLET models for comprehensive simulation of the thermal-hydraulics in the reactor coolant system. The ATHLET code comprises a thermo-fluid-dynamic module, a heat transfer and heat conduction module, a neutron kinetics module, a general control simulation module, and a general-purpose solver of differential equation systems called FEBE. The thermo-fluid-dynamic module is based on a six-equation model, with fully separated balance equations for liquid and vapor, complemented by mass conservation equations for up to 5 different non-condensable gases and by a boron tracking model. Alternatively, a five-equation model, with a mixture momentum equation and a full-range drift-flux formulation for the calculation of the relative velocity between phases is also available. Specific models for pumps, valves, separators, mixture level tracking, critical flow etc. are also included in ATHLET.

The rod module ECORE consists of models for fuel rods, absorber rods (AgInCd and B4C) and for the fuel assemblies including BWR canisters and absorbers. It describes mechanical rod behaviour (ballooning), Zr-alloy and B4C oxidation (Arrhenius-type rate equations), Zr-UO₂ dissolution and melting of metallic and ceramic components. Melt relocation (candling) is simulated by rivulets with constant velocity and cross-section, starting from the node of rod failure. The models allow oxidation, freezing, re-melting, re-freezing and melt accumulation due to blockage formation. Feedback to the thermal-hydraulics considers steam starvation and blockage formation. Besides convective heat transfer, energy can be exchanged by radiation amongst fuel rods and to surrounding core structures.

The release of fission products is modeled by rate equations or by a diffusion model within the module FIPREM. The transport and retention of fission products and aerosols in the reactor coolant system are simulated by the module SAFT. For the simulation of debris bed a specific model MEWA can be applied, with its own thermal hydraulic equation system, coupled to the ATHLET fluid-dynamics on the outer boundaries of the debris bed. The transition of the simulation of the core zones from ECORE to MEWA depends on the degree of degradation in the zone. Finally, the code also comprises late phase models for core slumping, melt pool behaviour in the lower plenum and vessel failure within the module AIDA.

The code validation is based on integral tests and separate effect tests, as proposed by the CSNI validation matrices, and covers thermal-hydraulics, bundle degradation as well as release and transport of fission products and aerosols. They include out-of-pile bundle experiments performed in the CORA and in the QUENCH facility as well as in-pile experiments performed in the PHÉBUS or in the LOFT facility. The TMI-2 accident is used to assess the code for reactor applications. " [4]

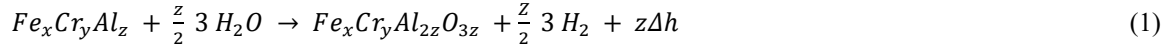
3.2. Model changes for simulating oxidation of FeCrAl with ATHLET-CD

Two types of changes were needed to enable a post test calculation of the QUENCH-19 experiment. First the input deck for the simulation of the QUENCH-15 experiment had to be adjusted slightly. The material properties of the zirconium cladding had to be replaced by the material properties of the FeCrAl cladding. The used material properties were given by KIT for the Kanthal APM material with a composition of 69% Fe, 21.6% Cr, 4.9% Al (+ 4.5% others). It is assumed that due to the oxidation only Al₂O₃ is produced. The used material properties [6, 7] are summarized in Table 1.

TABLE 1. USED MATERIAL PROPERTIES

Material Property	FeCrAl	Al ₂ O ₃
Density (kg/m ³)	7.1×10 ³	3.9×10 ³
Thermal conductivity (W/mK)	11 (323 K) → 35 (1673 K)	35
Specific Heat (J/kg K)	460 (293 K) → 800 (1673 K)	880

Code changes were also necessary in ATHLET-CD to compute the different oxidation kinetics of the ATF material. The oxidation of the chosen ATF material is governed by the following chemical reaction [8]:



where:

Δh is energy release during oxidation = 9.3×10^5 J/mol = 9.32×10^6 J/kg_{FeCrAl};
 x, y, z is composition of FeCrAl molar masses of $x=1.307$, $y=0.404$ and $z=0.215$

A parabolic law was used to determine the oxidation rate that was derived from the analytical solution of the diffusion equation, similarly to the method for the oxidation of Zirconium:

$$dW^2 = K dt \rightarrow \frac{dW}{dt} = \frac{K}{2W} \quad (2)$$

where:

W $m_{ox}/(surface\ area)$ in (kg/m²);
 m_{ox} is mass of the resulting oxide (Al₂O₃);
 K is reaction rate in (kg²/m⁴s);
 dt is time step (s).

The reaction rate is determined by the following Arrhenius equation:

$$K = A \cdot \exp(-B/RT) \cdot g(p_s) \quad (3)$$

where:

R is the gas constant (8.314 J/molK);
 T is cladding temperature (K);
 $g(p_s)$ reduction factor to consider steam starvation ($0 \leq g(p_s) \leq 1$);
 A, B are rate constants as given by KIT for KANTHAL APMT [6]: $A = 3.1$ kg²/m⁴s, $B = 2.78519 \times 10^5$ J/mol.

3.3. Main findings of QUENCH-19 post test simulations

Altogether three post test simulations were performed, and their results were compared to the experimental data. All of the simulations were based on the input deck for QUENCH-15 experiment, which represents the heated part of the QUENCH facility with 10 axial nodes and three concentric rings. The innermost part (ROD1) contains four heated rods, the second ring (ROD2) consists of eight heated rods, while the outermost ring (ROD3) has 12 heated rods. Five spacer grids, 8 corner rods and the shroud insulation with ZrO₂ are also taken into account. Besides the heated part of the facility, steam/ argon flows and the water quenching are simulated. A more detailed description of the used input is given in [9]. All the inputs use the material constants of Table 1 for the cladding. Differences are caused by the oxidation models. One simulation used the oxidation kinetic defined by constants given by KIT for KANTHAL APMT [6] (Kanthal), the other used the same constants, but the reaction rate was multiplied by 300 (Kanthal*300) derived from [1], and the last simulation used the oxidation kinetic model by Cathcart/Prater/Courtright [5] for zirconium (Zr).

The results of the three simulations and experimental data are depicted in Figs 4–7. Figs 4 and 5 show the evolution of temperatures in the innermost part of the bundle (ROD1) at elevation 550 mm and 950 mm, respectively. It is clearly visible, as expected, that at lower temperatures the change of the oxidation model doesn't influence the simulation results, as visible at lower elevation in Fig.4. The bundle temperatures are satisfactorily

reproduced by ATHLET-CD with the newly implemented ATF oxidation models also at higher temperatures and elevations, there is no significant temperature escalation visible. The simulation with the standard oxidation model for Zr-based cladding resulted however in much higher maximal temperatures due to the extensive heat generation during oxidation (Fig. 5.)

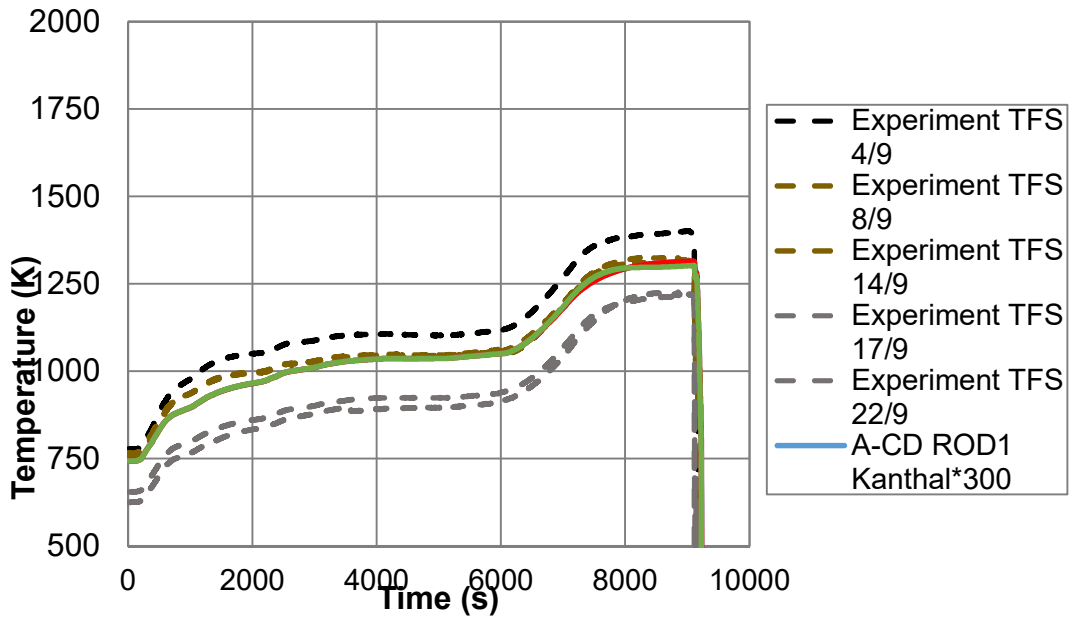


FIG.4. Evolution of temperatures in experiment and in the different simulations at elevation 550 mm.

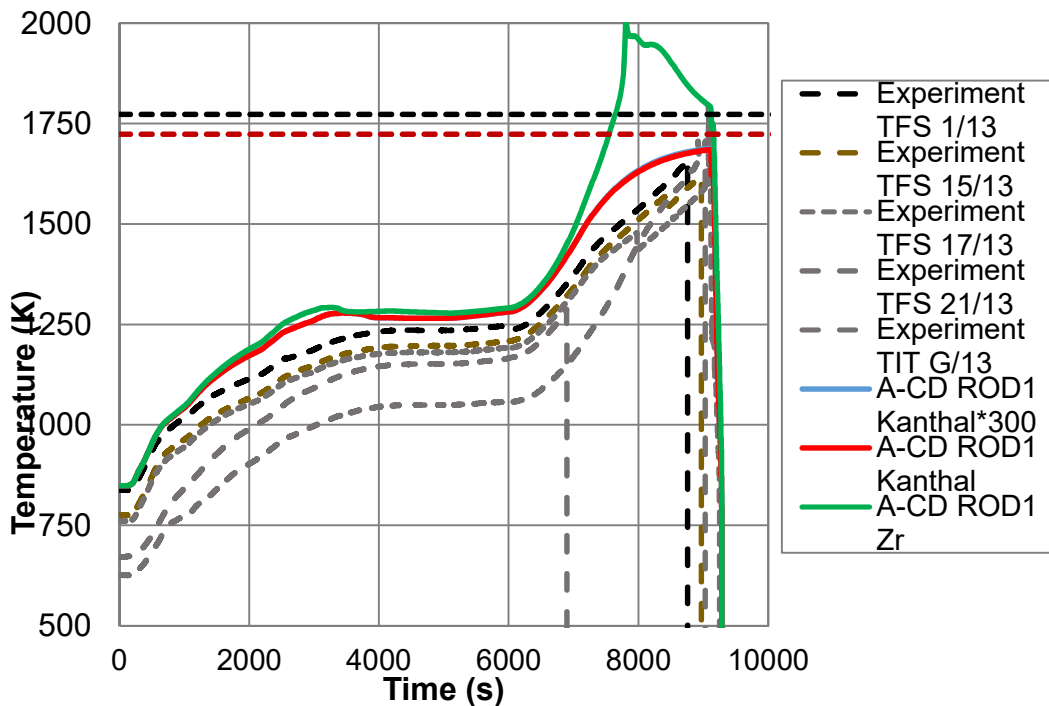


FIG.5. Evolution of temperatures in experiment and in the different simulations at elevation 950 mm.

Figure 6 depicts the temperature evolution at different horizontal positions of a simulation at elevation 850 mm. The comparison shows that there is a relatively high radial gradient between internal and external temperatures with a difference of up to $\approx 200^{\circ}\text{C}$ in the measured data (significantly larger than QUENCH-15; the reason for these differences is not yet fully clarified [3]), while all the simulations result in a flat profile with a

maximum difference of 50°C. The final report of the experiment could clarify the reasons for such a large horizontal temperature gradient.

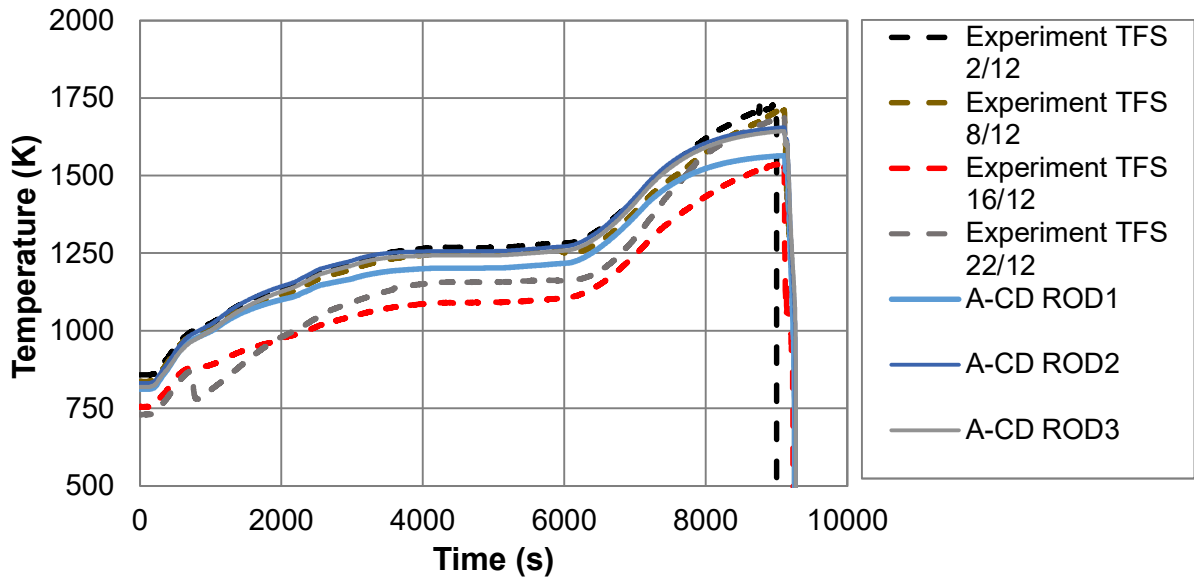


FIG.6. Temperature evolution at different horizontal positions at elevation 850 mm (Kanthal).

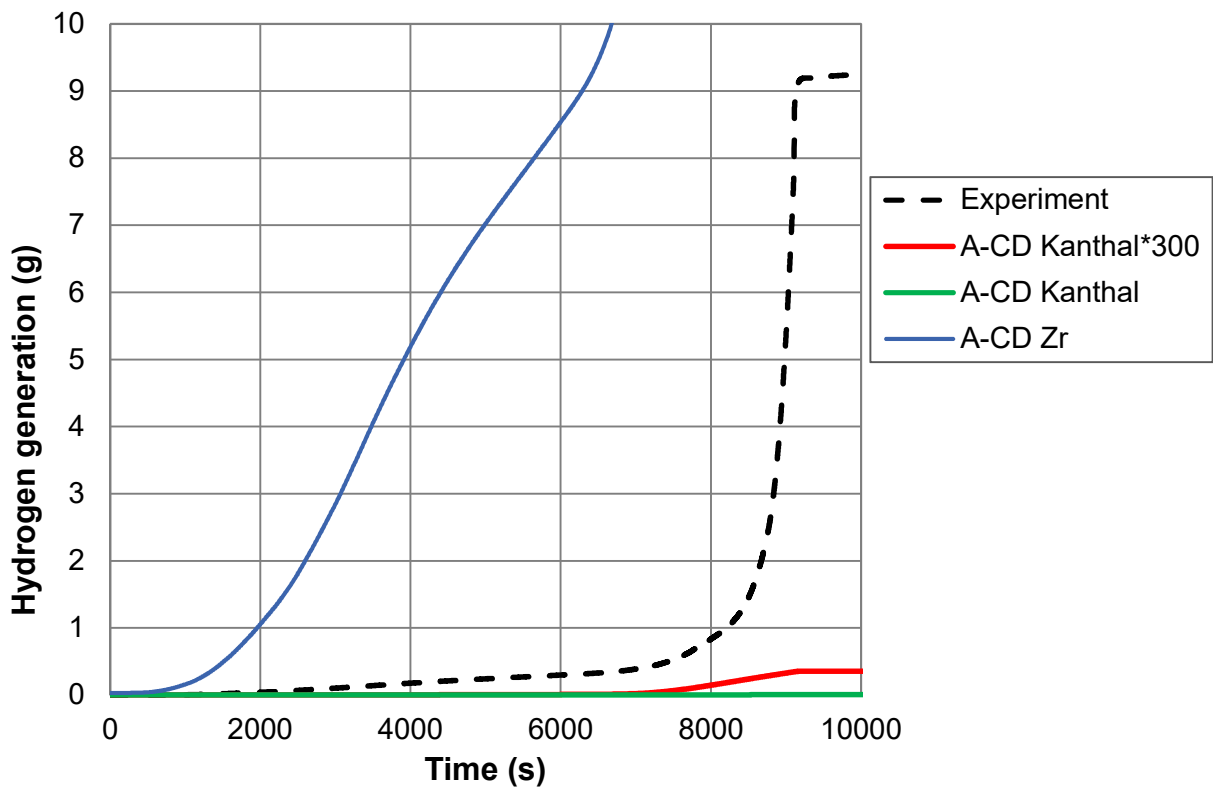


FIG.7. Total hydrogen generated.

The total generated mass of hydrogen (Fig.7) shows a significant underestimation of oxidation in the simulations, in particular with the reaction rate given by [6] (Kanthal), but also the Kanthal*300 underestimated the generated hydrogen mass, with 0.008 g and 0.35 g respectively, compared to 9 g in the experiment. The hydrogen generation in the experiment was comparably low until the maximum temperatures was reached ($\approx 1400^{\circ}\text{C}$). A sharp increase in the hydrogen release was observed at approximately 800 s before the quenching.

One possible trigger for this event could be the failure and melting of the cladding of the steel thermocouples [3]. This was not considered in the post test calculations.

4. SUMMARY AND CONCLUSIONS

In order to be able to more accurately simulate accident scenarios in nuclear power plants that are loaded with accident tolerant materials, changes to the oxidation model were implemented in the code ATHLET-CD. The extended models were tested on the QUENCH-19 experiment by comparing them with test data as well as the simulation results with the previous modelling. The simulations showed that the oxidation models have a big effect on the temperature evolution of the fuel cladding and therefore also on the whole accident scenario. The newly implemented correlations for the oxidation of FeCrAl material deliver more reasonable results than the correlations for Zr-based claddings, but their accuracy and applicability have to be further improved. GRS is plans to further improve the oxidation models of ATF material in ATHLET-CD.

ACKNOWLEDGEMENTS

The development and validation of ATHLET-CD are sponsored by the German Federal Ministry for Economic Affairs and Energy (BMWi) based on decisions of the German Bundestag.

REFERENCES

- [1] NUCLEAR ENERGY AGENCY (NEA): State-of-the-Art Report on Light Water Reactor Accident-Tolerant Fuels, NEA No. 7317, OECD 2018.
- [2] STUCKERT, J., et al.: Experimental programme QUENCH at KIT on core degradation during reflooding under LOCA conditions and in the early phase of a severe accident, IAEA-TECDOC-CD-1775, Nov. 2015.
- [3] STUCKERT, J., et al.: First results of the bundle test QUENCH-19 with FeCrAl claddings, 24th International Quench Workshop, Karlsruhe, November 2018.
- [4] BALS, C., et al.: POST TEST SIMULATION OF QUENCH TEST 19 WITH ATHLET-CD, IAEA TECDOC, CRP ACTOF, (to be published).
- [5] AUSTREGESILO, H., et al., ATHLET-CD 3.2 User's Manual, GRS Report, GRS-P-4/Vol. 1, Dec. 2018.
- [6] STUCKERT, J., KIT, Mail from 26.7.2018.
- [7] ACCURATUS, Ceramic Materials and Ceramic Components, 9.10.2018, <https://accuratus.com/alumox.html>.
- [8] US DOE: Handbook on the Material Properties of FeCrAl Alloys for Nuclear Power Production Applications, ORNL/TM-2017/186.
- [9] BALS, C., et al., Post test calculation of QUENCH-15 with ATHLET-CD, 15th International Quench Workshop, Karlsruhe, November 2009.

ADVANCED LOCA SAFETY CRITERIA: IMPLEMENTATION IN MECHANISTIC FUEL PERFORMANCE CODES AND APPLICATIONS

M.S. VESHCHUNOV
International Atomic Energy Agency,
Vienna International Centre,
PO Box 100, 1400 Vienna,
Austria

A.V. BOLDYREV, V.E. SHESTAK
Nuclear Safety Institute (IBRAE),
Russian Academy of Sciences,
52, B. Tulkaya, Moscow, 115191,
Russian Federation

Abstract

The advanced Chung-Kassner criteria on capability of fuel rods to withstand thermal shock during LOCA reflooding and to withstand post-quench fuel handling, as well as complementary cladding embrittlement criteria of KAERI and KIT, are compared with the traditional LOCA safety criterion related to 17% ECR oxidation. The advanced criteria were implemented in the thermo mechanical code SVECHA/QUENCH (S/Q) and successfully applied to predicting the fuel rod failure behaviour in a postulated LOCA scenario and in high temperature (1400°C) pre-oxidation and quenching tests performed with fresh and irradiated fuel rod simulators. Extension of the advanced criteria to coated Zr alloy claddings is discussed.

1. INTRODUCTION

In accordance with the IAEA Safety Standards [1] developed on the basis of international consensus by revision of the Safety Guide No. NS-G-1.12 [2], to ensure that the structural integrity of the fuel rods is preserved the following design limit should be defined and justified: the total oxidation of the cladding should remain below limits such that the cladding can still withstand accident induced loadings (e.g. in the quenching phase of a loss of coolant accident). Such limit should be determined by experiments that take into account pre-transient in-reactor cladding oxidation and transient oxidation (outer side oxidation and possibly inner side oxidation), pre-transient and transient hydrogen absorption, as well as chemical interactions between fuel pellets and cladding material (§3.73b of [1]).

In addition to the thermal shock failure characteristics of zircaloy cladding during quenching, fuel rods should be designed to withstand loadings resulting from post-transient fuel assembly handling, storage and transport to a reprocessing or disposal facility (§3.73e of [1]). Following this requirement of the Safety Standards, one must evaluate the impact and load-deflection properties of cladding that has been subjected to postulated LOCA transients.

The existing regulatory LOCA safety criteria accepted in many countries establish the 1477 K (1204°C) peak cladding temperature and 17% equivalent cladding reacted (ECR) maximum oxidation, calculated as function of oxidation temperature and square root of time based on the Baker-Just correlation (see, e.g. [3]), with some modifications in different countries. The purpose of these criteria, regarding maximum cladding temperature and total oxidation, is to ensure that the cladding shall remain sufficiently ductile so that it does not shatter into pieces during and after the quench phase of the LOCA transient.

In some countries (e.g. Japan) the current LOCA criterion on fuel safety is based on the failure threshold value determined in the integral thermal shock tests. In other countries, although most of the attention is focused on the events of the first few minutes after a postulated major cooling line break, the long term maintenance of cooling would be equally important [4]. In particular, the U.S. Atomic Energy Commission (AEC) promulgated Criterion 3 of the Interim Acceptance Criteria for ECCS for LWR [5] which states that: "The clad temperature transient is terminated at a time when the core geometry is still amenable to cooling, and before the cladding is so embrittled as to fail during or after quenching."

2. CLADDING CAPABILITY TO WITHSTAND THERMAL SHOCK

The thermal shock failure properties of Zircaloy-4 cladding have been investigated for tubes oxidized at controlled temperatures for various times and bottom flooded with water, or in a more advanced tests, ruptured in steam under transient-heating conditions, oxidized at controlled temperatures and bottom flooded [3, 6]. The failure map based on the ECR parameter and the oxidation temperature in steam, Fig. 1, typically shows that no failures occurred for specimens oxidized to 17% of the total cladding thickness, based on the ECR parameter, and temperatures to 1477 K, which are the present oxidation limits in the acceptance criteria for emergency-core-cooling systems in LWRs. Open and closed symbols in Fig. 1 respectively denote the specimens which survived and failed after a cold-water injection followed after a high temperature oxidation. However, these observations highlighted a rather high conservatism of the currently accepted criterion. For instance, it was deduced in [6, 7] that the critical ECR which is defined as the minimum point where a cladding fails, lies between 20% and 30%.

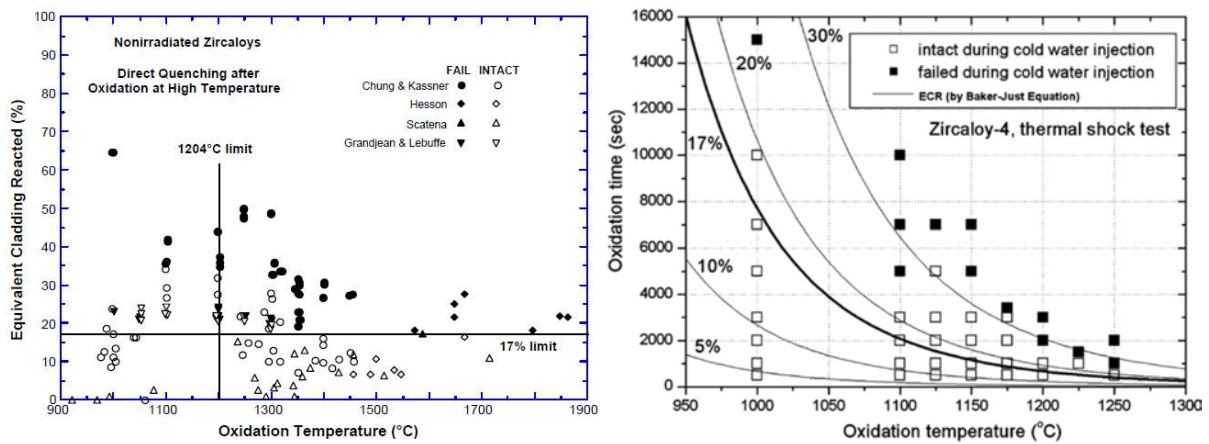


FIG. 1. Failure boundary of zircaloy cladding tubes after oxidation at high temperature and direct quenching from peak oxidation temperature (left panel from [3] and [6]; right panel reproduced courtesy of Elsevier [7]).

To overcome this problem of the traditional ECR criterion, Chung and Kassner performed detailed analysis of their own and former test results [6]. In these tests the mechanical response of zircaloy cladding under thermal shock conditions typical for hypothetical LOCA situations in LWRs has been evaluated. Various failure maps for fracture of the cladding by thermal shock were developed relative to the maximum oxidation temperature and various time dependent oxidation parameters. The best correlation of the thermal shock failure data was obtained relative to the thickness of the ductile β -phase layer; i.e. cladding in which the thickness of the β -phase, with ≤ 0.9 wt % oxygen, exceeded 0.1 mm remained intact irrespective of the specimen thickness, oxidation temperature and total oxygen content of the cladding, Fig. 2.

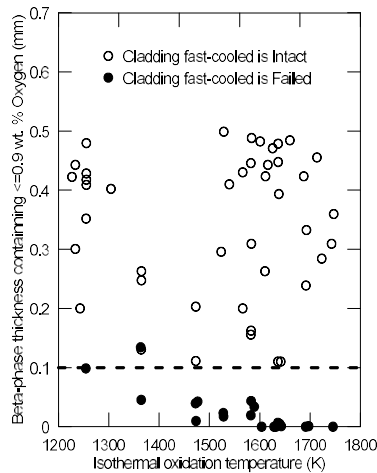


FIG. 2. Failure map for Zircaloy-4 cladding by thermal shock relative to the wall thickness with ≤ 0.9 wt% oxygen after isothermal oxidation and flooding with water at the oxidation temperature (from [6]).

Comparison of Figs. 1 and 2 shows that a high conservatism of the traditional 17% ECR criterion, that notably underestimates a cladding capability to withstand thermal shock during LOCA reflooding, is essentially reduced in the advanced Chung-Kassner criterion eventually formulated in [6] as:

- **Capability to withstand thermal shock during LOCA reflooding:** calculated thickness of the cladding with ≤ 0.9 wt % oxygen should be greater than 0.1 mm.

In particular, it was noted in [6] that the absorbed hydrogen (analyzed by an inert-gas fusion technique) had a minimal effect relative to that of oxygen on the thermal shock behaviour, assuming that the rapid cooling rate below the Leidenfrost temperature suppresses hydride precipitation. This conclusion was confirmed in more recent KAERI tests of J.H. Kim et al. [7]. In those tests, to simulate LOCA conditions specimens were oxidized in a flowing steam at a desired temperature and time. To simulate the transient, the specimens were cooled at an intermediate temperature of 700°C for 100 s after being oxidized, and then quenched.

In the failure map obtained in these tests, Fig. 3, dotted lines correspond to different oxidation levels in terms of ECR; closed (open) symbols represent failed (intact) claddings during the water quench. Post test absorbed hydrogen content in the oxidized cladding was measured by a gas analysis method and represented by solid lines in Fig. 3. This diagram shows that the effect of the absorbed hydrogen (up to 700 wppm) on the failure behaviour during quenching of the Zircaloy-4 cladding was low, i.e. it practically did not influence the failure criterion in terms of ECR.

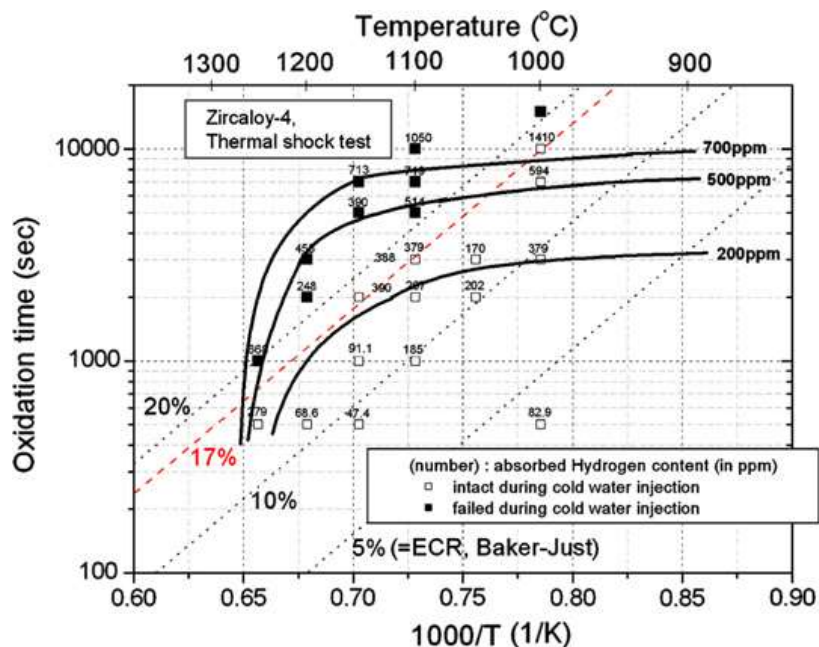


FIG. 3. Changes of the material properties of the fuel cladding with the oxidation temperature and time, depending on absorbed hydrogen content (< 700 wppm) (Reproduced courtesy of Elsevier [7]).

A similar conclusion was derived in the JAERI tests [8], also for pre-hydrated claddings, showing that the influence of pre-hydrating, up to 600 ppm, is negligible on the thermal-shock fracture threshold under the unrestrained condition, whereas the effect is more remarkable in the case of restrained test rods.

Furthermore, the oxygen content inside the prior β -layer was additionally determined after oxidation and quenching in the tests [7], Fig. 4. These data were not correlated with the thermal shock failure data; however, they were further used for interpretation of cladding post-quench embrittlement, see Section 3 below.

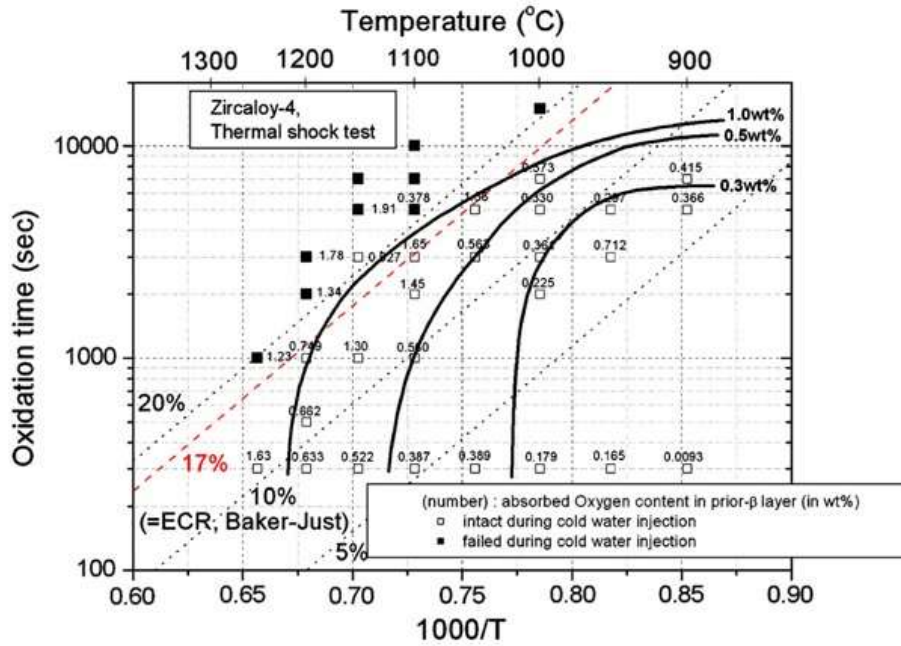


FIG. 4. Changes of the material properties of the fuel cladding with the oxidation temperature and time, depending on oxygen content inside the prior β -layer (Reproduced courtesy of Elsevier [7]).

3. CLADDING POST-QUENCH EMBRITTLEMENT

In order to justify the fuel rod capacity to withstand loadings resulting from post-transient fuel assembly handling, storage and transport (following the requirement, §3.73e, of the IAEA Safety Standards [1]), one must evaluate the impact and load-deflection properties of cladding that has been subjected to postulated LOCA transients.

In particular, critical fracture loads under conditions of impact, tension, and diametral compression were determined in [6] as functions of the degree of oxidation of the material and microstructure produced by cooling through the temperature range of $\beta \rightarrow \alpha$ phase transformation at different rates. Quantitative correlations were established between the failure-impact energy and the diametral-compression properties for cladding from the integral tube-burst/thermal-shock tests. As with the thermal shock failure characteristics, the best correlation of the room-temperature impact and diametral-compression properties was obtained relative to the thickness of the transformed β -phase layer with a maximum oxygen content. The results indicated that zircaloy cladding that could survive an impact energy of 0.3 J at 300 K after rupture, oxidation in steam and cool-down would also withstand either diametral deflections to the point of cladding-pellet contact or deflections of ≈ 3 mm before fragmentation occurs, provided the thickness of the β -phase layer containing ≤ 0.7 wt% oxygen is ≥ 0.3 mm irrespective of the wall thickness produced by ballooning and rupture of the cladding and the maximum oxidation temperature, Fig. 5. These results also showed that for a given thickness and a given oxygen content in transformed-beta layer, hydrogen at concentrations up to ≈ 2000 wppm would not cause a significant change in the room-temperature failure-impact behaviour.

On this base, the following embrittlement criterion was formulated by Chung and Kassner [6]:

- **Capability to withstand fuel handling, transport and storage:** calculated thickness of the cladding with ≤ 0.7 wt % oxygen should be greater than **0.3 mm**.

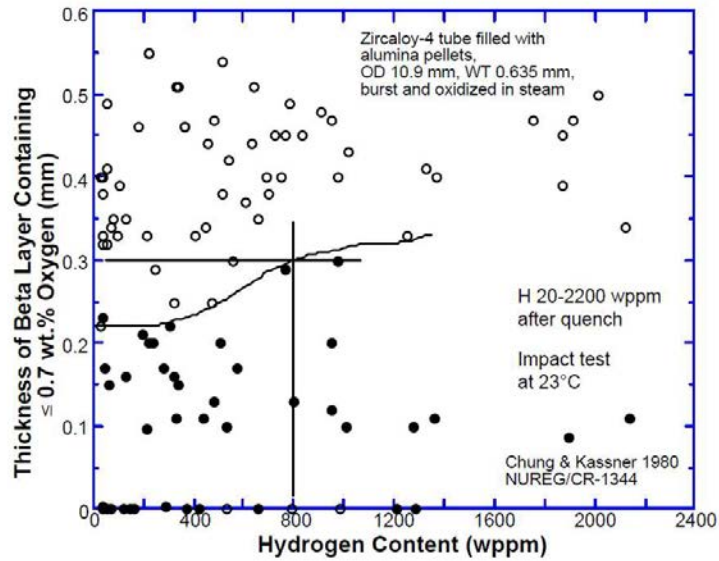


FIG. 5. Impact failure map as function of hydrogen content and thickness of the β -layer containing ≤ 0.7 wt.% oxygen; Zircaloy-4 tube burst, oxidized, slow-cooled and quenched (from [3, 6]).

A similar result was confirmed later in the KAERI [9] tests, which evidenced that after the simulated LOCA the cladding lost its ductility abruptly when the prior β -layer decreased below the threshold metal thickness of 0.3 mm, Fig. 6.

In the subsequent KAERI tests [7] (briefly described above in Section 2) at the same LOCA simulation facility, the ductility of the oxidized cladding was evaluated by mechanical tests such as ring compression test and 3-point bend test at room temperature after the LOCA test. The absorbed energy during the mechanical test was accurately determined as the area under the load–displacement curve and showed an abrupt decrease with the loss of the cladding ductility. As a result of such studies the empirical failure diagram of the Zircaloy-4 cladding was constructed in [7], Fig. 7.

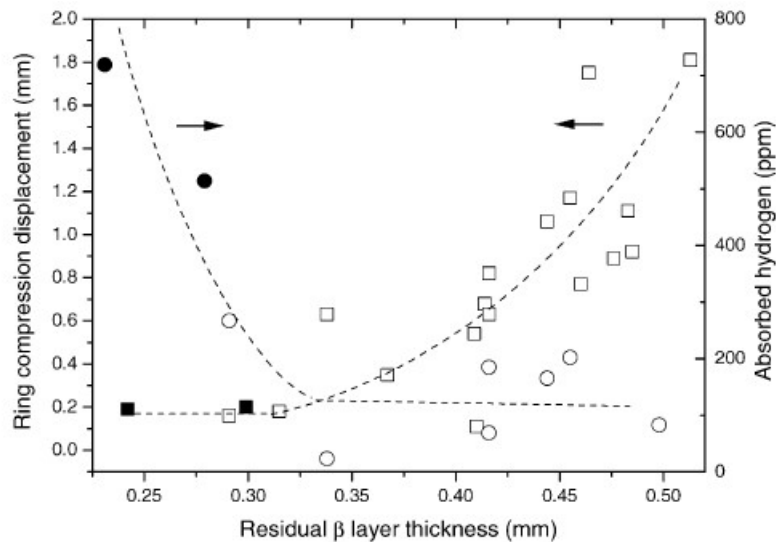


FIG. 6. Comparison of the microstructural parameters presenting the ring-compression ductility and absorbed hydrogen content vs. residual β -layer thickness. An open symbol represents a specimen that survived and a closed symbol a specimen that failed during the water quenching (Reproduced courtesy of Elsevier [9]).

“Brittle failure at a thermal shock” (red region in Fig. 7) indicates that the cladding is too brittle to withstand a thermal stress during a water quenching. ‘Brittle fracture at the mechanical test’ (green region in Fig. 7) means that although the cladding at first survived the water quenching, it has already lost its mechanical ductility so that it could be failed during a handling, such as refuelling or transporting the fuel bundles to the spent fuel storage. ‘Ductile bending’ (blue region in Fig. 7) means that the cladding can assure its mechanical ductility after a thermal shock.

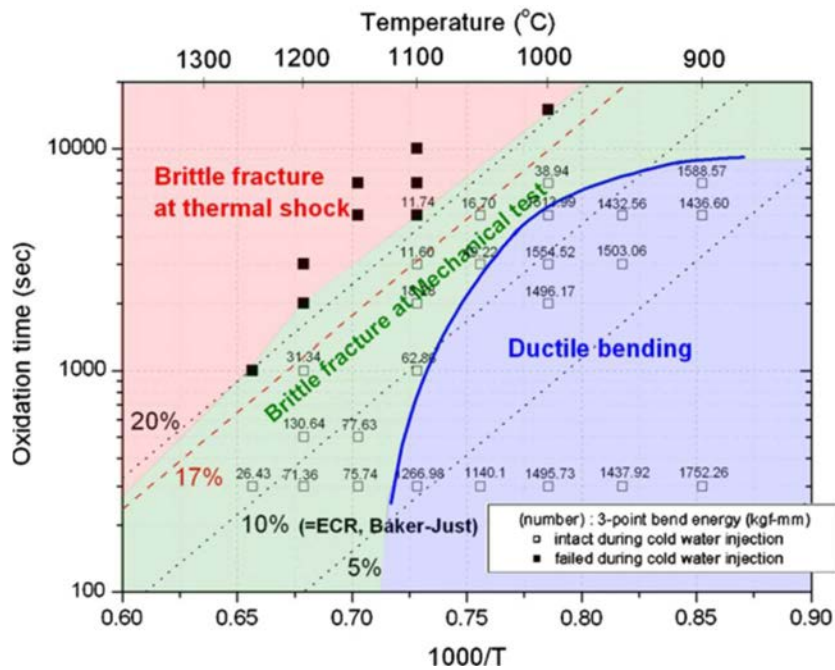


FIG. 7. Failure map of Zircaloy-4 claddings at different oxidation temperatures and times (Reproduced courtesy of Elsevier [7]).

By superposition of Figs 4 and 7, one can see that the brittle-ductile transition curve (blue line in Fig. 7) practically coincides with the curve in Fig. 4 corresponding to the oxygen content in the prior β -layer of 0.5 wt%.

This conclusion is also confirmed by the measurements of 3-point bending moment with respect to the oxygen content inside beta layer presented in Fig. 8 (reproducing data from [7]). In this figure, it is clearly seen that the absorbed energy of ductile and brittle cladding can be easily distinguished by the value of 1468 ± 153 kgf-mm and 47 ± 35 kgf-mm, where ductile and brittle claddings could be separated by the vertical dashed line of ≈ 0.5 wt% of oxygen content inside the prior beta layer, regardless of test temperature and time.

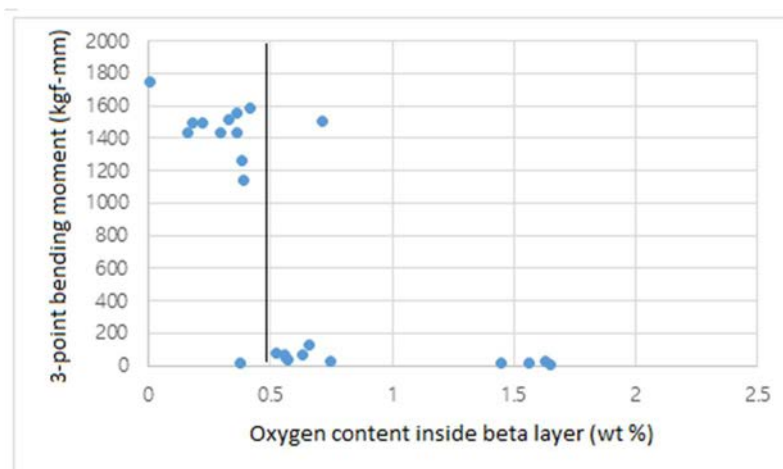


FIG. 8. Plot of 3-point bending moment with respect to the oxygen content inside beta layer (by courtesy of J.H. Kim with KAERI permission).

These important observations allowed the authors of [7] deriving a conclusion:

- When the absorbed oxygen content in the prior β -layer was **less than 0.5 wt%**, the cladding maintained its **mechanical ductility after the LOCA test**.

This conclusion can be considered as a new embrittlement criterion for Zry-4 claddings being complementary to the Chung-Kassner criterion on capability to withstand fuel handling, considering that the latter criterion was consistent with the results of the earlier KAERI tests [9] at the same test facility (see above). As shown in Fig. 3, the cladding post test hydrogen content did not exceed 700 wppm, this value determines the applicability range of the KAERI criterion. The observed weak dependence of the new criterion on the hydrogen content in this range (as seen from comparison of Figs. 3 and 4) well correlates with the similar conclusion regarding the weak dependence of the second Chung-Kassner criterion on the absorbed hydrogen content (below ≈ 2000 wppm).

On the other hand, by superposition of the constant hydrogen content curves from Fig. 3 with the brittle-ductile curve in Fig. 7 one can deduce a strong dependence of the critical ECR-BJ (Baker-Just) for the ductile-brittle transition on the hydrogen content, as shown in Fig. 9. This may substantiate new attempts of modification of the post-quench embrittlement criterion in terms of the critical ECR dependence on the *pre-quench* hydrogen content (see, e.g. Fig. 10 from [10, 11]); however, demonstrates practical inconvenience of this approach in comparison with the KAERI and Chung-Kassner advanced criteria formulated purely in terms of oxygen characteristics.

Unfortunately, predictions from Fig. 9 cannot be quantitatively compared with Fig. 10 (in terms of ECR-CP (Cathcart-Pawel)), since no measurements of *post-quench* hydrogen content were presented in [10, 11]. However, they seem qualitatively consistent with the results derived from Fig. 10 demonstrating a similar shift of the critical hydrogen contents, ≈ 250 -300 wppm, between pre-quench (from Fig. 9) and post-quench (from Fig. 10) data at fixed values of ECR-CP (6 and 10%).

These predictions are also consistent with measurements in the recent QUENCH-LOCA tests at the KIT test bundle facility [12], where post-quench brittle failure of ballooned and ruptured claddings was detected at narrow axial bands above and below the burst opening with the local hydrogen concentrations above 1500 wppm. Additional measurements demonstrated that ECR-BJ for those claddings near their burst opening was between 4 and 6% and the mean hydrogen content at these axial locations was in the range 720–750 wppm, in a fair agreement with conclusions derived above from analysis of the KAERI tests in Fig. 9.

These KIT observations offer a complementary criterion for the post-quench cladding embrittlement in terms of so called ‘secondary hydriding’ mechanism:

- Cladding maintains its **mechanical ductility after the LOCA test** when local hydrogen concentration (in the secondary hydriding zones) is **less than 1500 wppm**.

This criterion is consistent with the Chung-Kassner and KAERI advanced criteria (as above explained); however, its practical applications is complicated by necessity of implementation of advanced mechanistic models describing the complex secondary hydriding phenomena and calculating local hydriding levels in the ruptured claddings (as, e.g. realized in the mechanistic code SVECHA/QUENCH, see below Section 4.1).

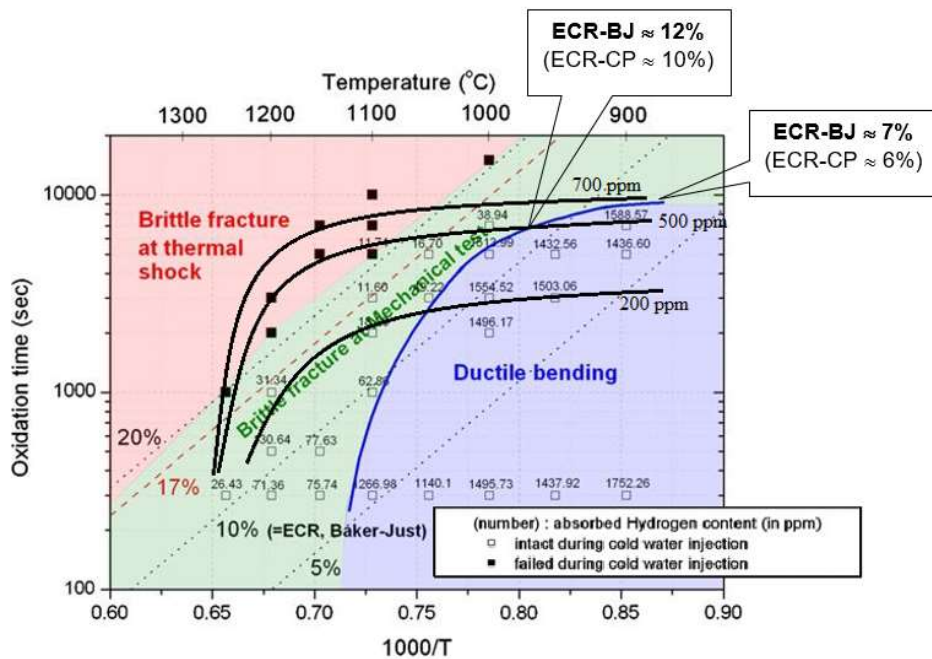


FIG. 9. Superposition of the absorbed hydrogen content curves from Figure 3 with the ductile-to-brittle transition curve from Figure 7, demonstrating a notable dependence of the critical ECR for post-quench embrittlement on absorbed hydrogen.

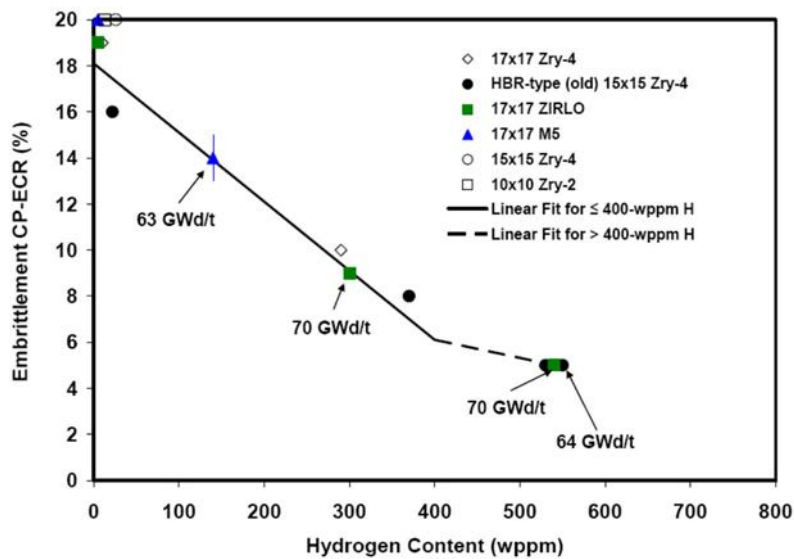


FIG. 10. Ductile-to-brittle transition oxidation level (in terms of ECR-CP) as a function of pre-test hydrogen content in cladding metal for as-fabricated, prehydrided, and high-burnup cladding materials (from [11]).

In summary two qualitative conclusions concerning applicability of the traditional 17% ECR criterion may be derived: (a) the criterion notably underestimates cladding capability to withstand thermal shock during LOCA reflooding (i.e. too conservative), and (b) the criterion notably overestimates ductile-to-brittle transition oxidation level, reflecting cladding post-quench ductility and capability to withstand fuel handling, transport and storage (i.e. too excessive). For this reason, the alternative, more advanced and physically based Chung-Kassner and KAERI criteria as well as the KIT complementary criterion may be used.

4. APPLICATION OF THE ADVANCED CRITERIA

For practical application of the Chung-Kassner criteria, a cladding oxidation model based on the diffusion approach should be utilised, in accordance with the recommendation [6]. In particular, the mechanistic code SVECHA/QUENCH (S/Q) designed for detailed modelling of fuel rod behaviour under re-flooding conditions can be applied. This code, currently a sub-module of the fuel performance and safety code SFPR [13], was initially developed at IBRAE [14] for severe accidents and then adapted for detailed analysis of the single-rod QUENCH rig tests in close cooperation with FZK experimentalists [15, 16]. In the S/Q code, the main physical phenomena occurring during degradation of fuel rods are mechanistically considered: cladding oxidation, cladding mechanical deformation, hydrogen uptake and release by oxidized cladding, fuel rod liquefaction and downward relocation, etc. [15, 16].

In the numerical scheme of S/Q, a fuel rod is divided into meshes along the axial direction. Each mesh comprises a fuel pellet and Zr alloy cladding. For each mesh the cladding is considered as a cylindrical shell consisting of three layers at each surface of the cladding (external and internal): oxide, α -Zr(O) and β -Zr layers. The layers growth kinetics is calculated by the oxidation model which is based on the solution of the oxygen diffusion problem across the multi-layered cladding structure. In particular, the developed diffusion approach allows self-consistent consideration of internal cladding oxidation (and subsequent embrittlement) owing to interactions with the fuel after the gap collapse.

As an example of application of the Chung-Kassner criteria to a LOCA-type scenario using the mechanistic S/Q code, a WWER rod with typical geometry parameters is considered in calculations, Fig. 11.

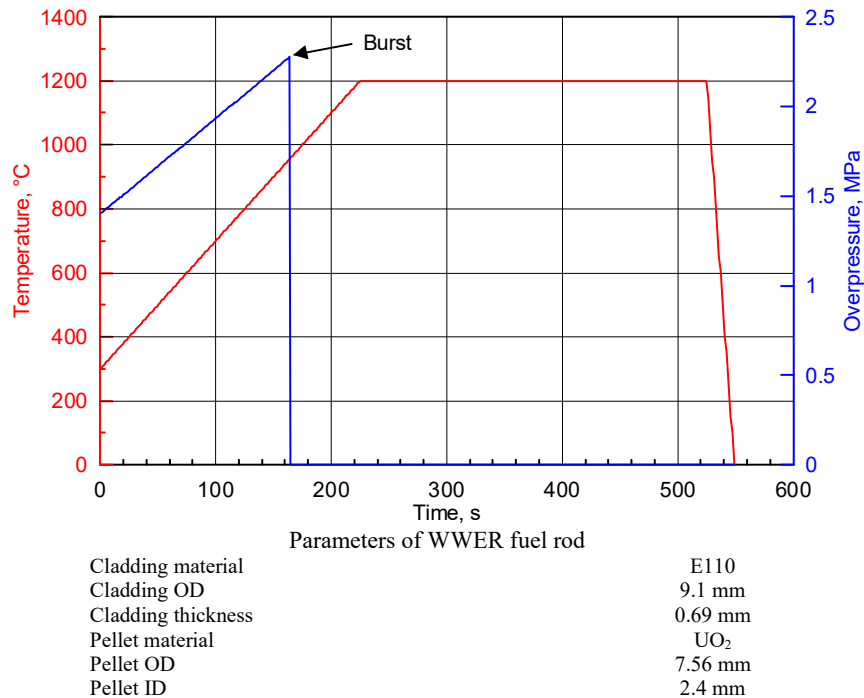


FIG. 11. Temperature scenario of transient (LOCA) test with a WWER fuel rod for calculations.

The code predicts the cladding ballooning, burst and subsequent double-side oxidation at the axial location of the burst opening, as presented in Fig. 12.

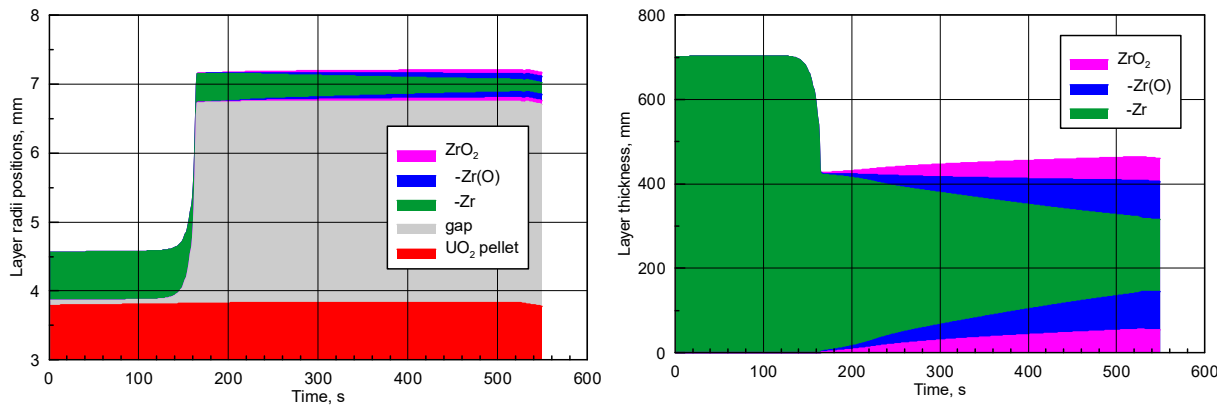


FIG. 12. Calculated by the S/Q code evolution of the oxidized cladding layers radial positions (left) and thicknesses (right) at the axial position of burst opening.

The corresponding evolution of the oxygen concentration profile in the cladding with time is presented in Fig. 13 (left). From the final oxygen distribution in the β -phase layer, Fig. 13 (right), one can see that the oxygen profile in this layer is rather flat and corresponds to the oxygen content of ≈ 0.8 wt% and the thickness of ≈ 0.19 mm. This implies that the calculated thickness of the cladding with ≤ 0.9 wt% oxygen is greater than 0.1 mm, whereas the calculated thickness of the cladding with ≤ 0.7 wt% oxygen is less than 0.3 mm. Therefore, in accordance with the two Chung-Kassner criteria, the cladding withstands the thermal shock on cool-down but fails during post-quench handling and/or transportation.

As expected, the same conclusion may be derived by application of the KAERI criterion [7]: since the absorbed oxygen content in the prior β -layer is **more than 0.5 wt%** (as seen from Fig. 13 (right)), the cladding does not maintain its mechanical ductility after the LOCA test.

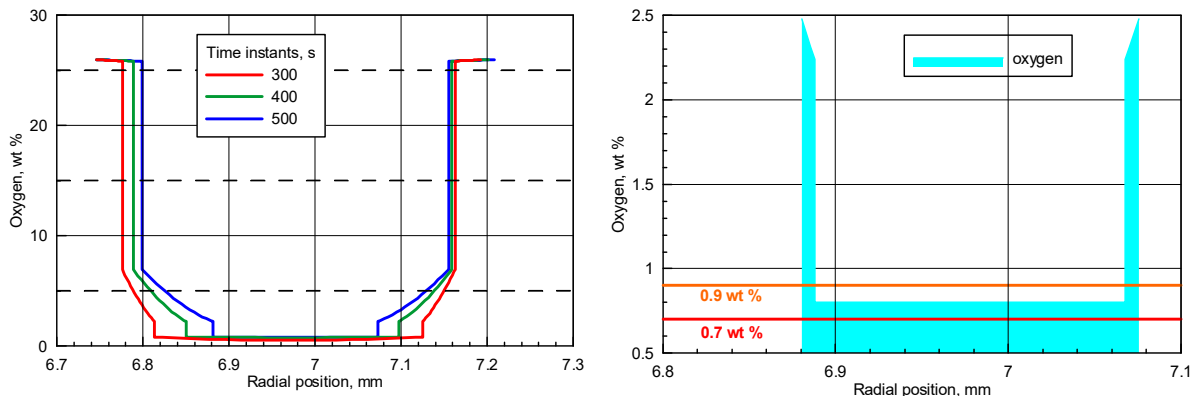


FIG. 13. Evolution of oxygen distribution in cladding layers (left) and the final distribution in the α -phase and β -phase layers (right) at the axial position of the burst opening.

4.1. Secondary hydriding criterion

A series of new out-of-pile QUENCH-LOCA bundle tests were performed at the QUENCH facility in Karlsruhe Institute of Technology (KIT, Germany) [12], as mentioned above in Section 3. Neutron radiography of cladding tubes showed that rather high hydrogen concentrations were attained in narrow bands on the boundaries of the internal oxidized region around burst positions (secondary hydriding). Tensile tests at room temperature evidenced brittle fracture at these bands for several inner rods. Corresponding maximal local hydrogen concentrations measured at the fracture positions were about 1500 wppm and more. Peripheral rods had lower hydrogen contents and were mostly fractured due to stress concentration at burst opening edges. Other tensile tested claddings failed after necking far away from burst region.

In order to simulate the double-side oxidation and hydriding of burst cladding under LOCA conditions, the single-rod SVECHA/QUENCH (S/Q) code has further been developed and verified [18] against various test series. In application to the KIT QUENCH-L0 test [19] the code adequately predicted axial distributions of oxygen and

hydrogen in the cladding, Fig. 14. In particular, the code correctly calculated a rather high hydrogen content in the secondary hydriding zones, > 1500 wppm, and thus, in accordance with the KIT criterion, predicted the brittle fracture of the corresponding rods, in agreement with the observations (see [18]).

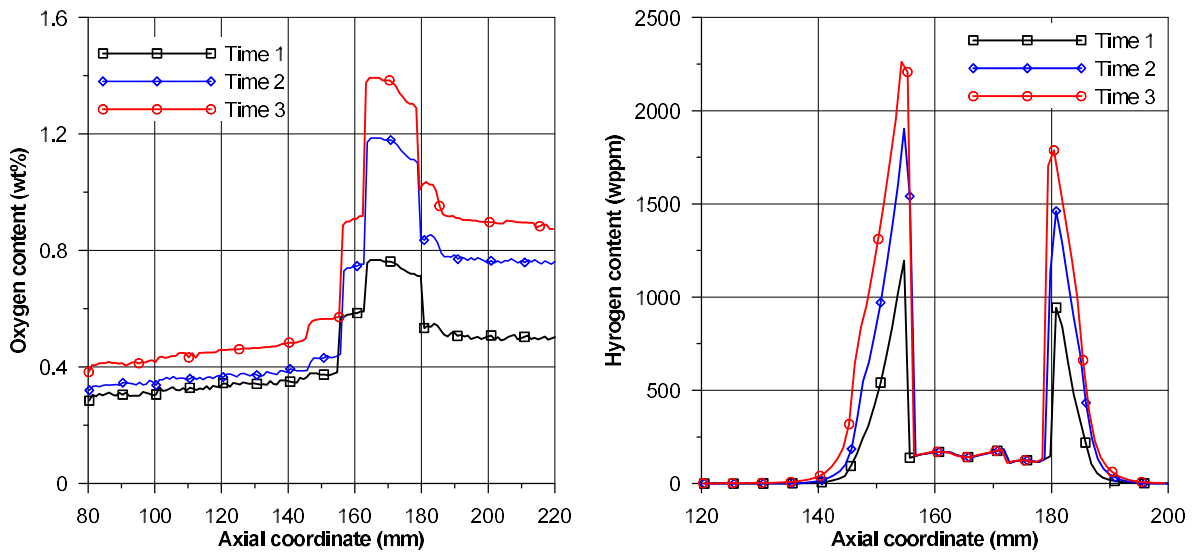


FIG. 14. Calculated axial distribution of the total oxygen content (left) and the total hydrogen content (right) at the moments of 40, 60 and 80 s of the KIT QUENCH-L0 test (Reproduced courtesy of Elsevier [18]).

5. EXTENSION OF THE ADVANCED CRITERIA TO HIGH TEMPERATURES (DEC)

The Chung-Kassner criteria were developed on the base of the oxidation tests performed in a wide temperature interval (far beyond LOCA conditions), up to 1500-1900°C (see Figs 1 (left) and 2). This allows extending their applicability to Design Extension Conditions (DEC), in particular investigated in the FZK tests on high temperature quenching of fuel rod simulators with zircaloy cladding by water or steam at a small-scale rig [16]. The principal ‘input’ experimental parameters were the extent of pre-oxidation and the temperature of the tube before cooldown. A total of 24 experiments has been performed with specimens pre-oxidized at 1400°C with oxide layer thicknesses varying from ≈ 100 to ≈ 350 μm which were rapidly cooled by water or steam from 1100, 1200, 1400 and 1600°C. The main characteristics of the quenched cladding integrity was post test appearance of cracks. Post test detection of through wall cracks with oxidized surfaces was interpreted as the cladding shattering during quenching. In other samples non-oxidized cracks normally penetrated through the oxide and α -phase layers but were arrested in the β -phase layer; these samples were interpreted as the cladding withstanding thermal shock.

S/Q calculated oxygen distributions along radial direction in the β -phase layer of the cladding pre-oxidized at 1400°C to different extents are presented in Fig. 15. One can see that the first Chung-Kassner criterion (on failure during quenching) is valid up to pre-oxidation of ≈ 130 μm . Hence, if pre-oxidation at any location does not exceed 130 μm then the through-wall cracks are not predicted. This conclusion was fairly confirmed by experimental observations [16].

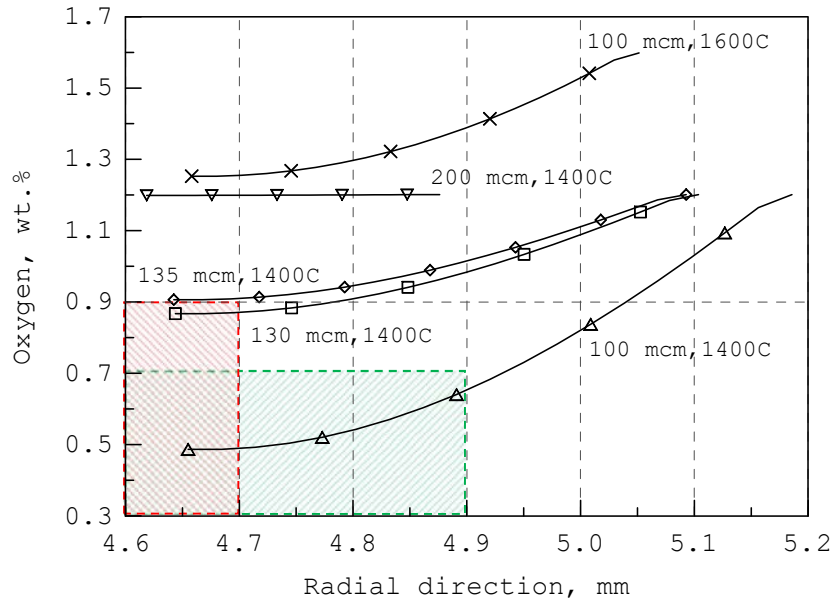


FIG. 15. S/Q simulations for various quenching temperatures and pre-oxidations; red (green) zone represents applicability of the first (second) Chung-Kassner criterion to withstand thermal shock (post test handling).

Later the same approach was applied for interpretations of similar quenching tests with WWER-1000 irradiated fuel rod fragments with maximum burnup of 50–65 MW·d/kgU, performed in RIAR (Dimitrovgrad) [17]. In these samples, cladding oxide layers (external and internal) did not exceed a few μm , typically for the E110 cladding material; this allowed neglecting them with a good accuracy in calculations.

In these tests depending on the extent of pre-oxidation (at 1400°C), different samples were intact (green), broken during quenching (red) or broken during post-quench handling (yellow), as shown in Fig. 16 and Table 1. Predictions of the S/Q code for samples quenched from the pre-oxidation temperature 1400°C, based on the calculations from Fig. 15, are presented in Table 1 and reasonably interpret the observed failure modes using the first and the second Chung-Kassner criteria.

Indeed, in accordance with the first criterion the code predicts that a rod withstands thermal shock (designated in Table 1 as +1) or fails during thermal shock (designated as -1), depending on the oxide thickness (with a threshold of $\approx 130 \mu\text{m}$ as explained above). In accordance with the second criterion, fuel rods survived during quenching will withstand post test handling (designated as +2) or fail (designated as -2) with the oxide thickness threshold of $\approx 100 \mu\text{m}$. Some uncertainty of the fuel rod failure in the two tests with similar oxide layers of $\approx 100 \mu\text{m}$ (tests #36 and #39) was probably connected with the proximity of their thicknesses to the threshold value (as interpreted in Table 1).

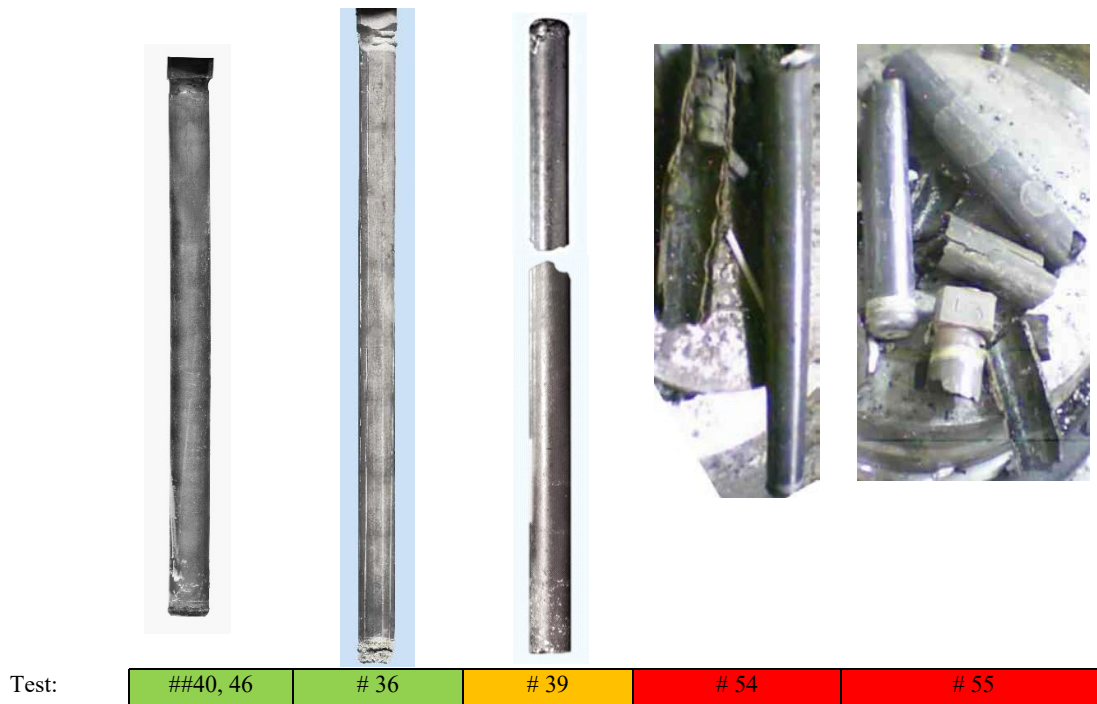


FIG. 16. Post test appearance of irradiated fuel rods in the RIAR tests [17].

TABLE 1. CONDITIONS OF RIAR TESTS [17] WITH FUEL RODS PRESENTED IN FIGURE 16.

Test	##40, 46	# 36	# 39	# 54	# 55
Pre-oxidation temperature/duration	1400°C/ 0 s	1400°C/ ≈ 240 s	1400°C/ ≈ 240 s	1400°C/ 1050 s	1400°C/ 1100 s
Quenching temperature	1400°C	1400°C	1400°C	1400°C	1400°C
Oxide thickness	0 μm	≤ 100 μm	≥ 100 μm	280 μm	300 μm
Failure mode	Intact	Intact	Broken during handling	Broken during quenching	Broken during quenching
Failure criteria	+1/+2	+1/+2	+1/-2	-1	-1

6. EXTENSION OF THE ADVANCED CRITERIA TO COATED ZIRCONIUM CLADDINGS (ATF)

The traditional 17% ECR criterion cannot be directly applied to new designs of Zr alloy claddings with Cr coatings, since the growth of the chromium oxide layer is strongly reduced, whereas oxygen continuously penetrates into the Zr substrate, forms α - and β -phase layers and eventually embrittles the cladding (owing to oxygen saturation of the ductile β -phase layer). For this reason, one may expect, lacking the Zr oxide layer growth, that the Zr cladding embrittlement occurs at ECR much lower than 17%. In particular, this was confirmed in the recent Round Robin tests performed within the IAEA Coordination Research Project (CRP) on Analysis of Options and Experimental Examination of Fuels with Increased Accident Tolerance (ACTOF) [20].

In this situation it is natural to expect that the failure criteria related to the ductility of the β -phase layer are applicable to the modified claddings. In particular, it was shown in the ring compression tests with oxidized claddings (performed by Czech participants, CTU and UJP from Prague) [20] that the cladding embrittlement can be well correlated with the oxygen content in the prior β -phase, Fig. 17; this finding is in a fair accordance with the KAERI criterion [7] presented in Section 4 (cf. Fig. 8). It was assumed in the new tests that the critical value of the oxygen content in E110 alloy is 0.3–0.4 wt%, which slightly modifies the KAERI criterion [7] of ≈ 0.5 wt% for Zry-4 presented in Section 4; however, the latter criterion seems also consistent with the new experimental data [20] (Fig. 17).

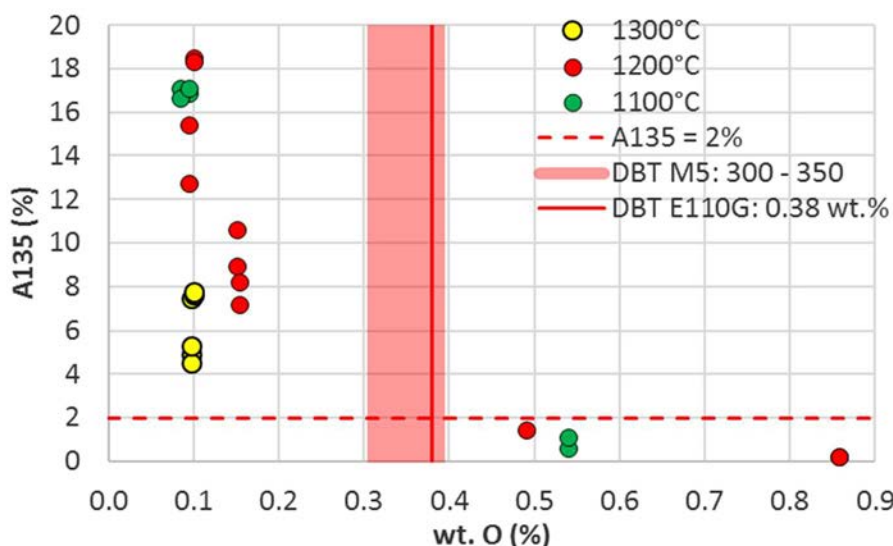


FIG. 17. Residual ductility of the Cr-coated Zr1%Nb samples in relation with oxygen content in prior β -Zr layer (from [20]).

Lacking currently a diffusion model for oxidation of coated claddings, the second Chung-Kassner criterion (on cladding embrittlement) was not verified against these test data; however, considering its mutual consistency with the KAERI criterion (as discussed in Section 3) one may expect its applicability to the coated claddings as well.

Extension of the mechanistic oxidation model to consideration of the coated Zr claddings will also allow verifying applicability of the Chung-Kassner and KAERI criteria (as well as the KIT secondary hydriding criterion) on the base of future tests on the coated Zr cladding quenching, e.g. foreseen in the new IAEA CRP on Testing and Simulation of Advanced Technology Fuels (ATF-TS), planned for 2020–2023.

7. CONCLUSIONS

Basing on the analysis of the experimental data on Zr alloy cladding thermal shock and post-quench ductility tests, it was emphasized that the traditional LOCA safety criterion related to 17% ECR: (a) notably underestimates cladding capability to withstand thermal shock during LOCA reflooding (i.e. is too conservative), and (b) notably overestimates ductile-to-brittle transition oxidation level, reflecting cladding post-quench ductility and capability to withstand fuel handling, transport and storage (i.e. too excessive).

For this reason, the alternative, more advanced and physically based Chung-Kassner criteria as well as the KAERI criterion for post-quench embrittlement are considered for practical applications.

Applicability of the advanced criteria in the majority of the currently existing codes is restricted owing to a simplified approach for evaluation of the cladding oxidation using Baker-Just or Cathcart-Pawel correlations for the weight gain realized in these codes, whereas these criteria require calculation of the oxygen concentration profiles in the different phases (α -Zr(O), β -Zr and ZrO_{2-x}) of the oxidized cladding. This problem can be overcome in more mechanistic fuel performance codes using oxygen diffusion models, validated against isothermal and transient oxidation tests.

As an example of the advanced criteria utilization, the mechanistic fuel performance and safety code SFPR using the thermo mechanical module SVECHA/QUENCH (S/Q) with the oxygen diffusion model for Zr alloy cladding oxidation, is considered. The code predicts cladding ballooning, burst and double-side oxidation during LOCA scenario and allows natural application of the advanced failure criteria by calculation of the oxygen profiles in the cladding.

Being extended to mechanistic consideration of the cladding secondary hydriding phenomenon, the S/Q code allows applying the KIT complementary post-quench embrittlement criterion in practical calculations.

The Chung-Kassner criteria developed on the base of the oxidation tests performed in a wide temperature range (up to 1500–1900°C) that is far beyond LOCA conditions, can be broadened to Design Extension Conditions (DEC). This allowed reasonable predictions of the S/Q code for the fuel rod failure behaviour investigated in the

FZK tests (with fresh Zry-4 claddings) and in the RIAR tests (with irradiated WWER fuel fragments) on high temperature (1400°C) pre-oxidation and quenching by water or steam.

The applicability of the KAERI advanced failure criteria (with some potential modifications) for oxidized Zr alloy claddings with Cr coatings was confirmed in the recent ring compression tests performed within the IAEA Coordination Research Project (CRP) ACTOF. On this base it is assumed that extension of the mechanistic oxidation model to consideration of the coated claddings will allow verifying applicability of the advanced Chung-Kassner and KAERI criteria (as well as the KIT complementary criterion) on the base of future tests on the coated cladding quenching (which are foreseen, e.g. in the subsequent IAEA CRP on ATF in 2020-2023).

ACKNOWLEDGEMENTS

The authors thanks Dr. J.H. Kim (KAERI, Republic of Korea) for presenting additional information on his tests [7] and new figure (Fig. 8), as well as valuable comments to the text; Dr. J. Stuckert (KIT, Germany) for presenting his unpublished data [12] and valuable discussions; Dr. M. Ševeček (CTU, Czech Republic) for sharing his unpublished results (Fig. 17).

REFERENCES

- [1] INTERNATIONAL ATOMIC ENERGY AGENCY, Design of the Reactor Core for Nuclear Power Plants, IAEA Safety Standards, Specific Safety Guide Series SSG-52 (2019).
- [2] INTERNATIONAL ATOMIC ENERGY AGENCY, Design of the Reactor Core for Nuclear Power Plants, IAEA Safety Standards Series No. NS-G-1.12, IAEA, Vienna (2005).
- [3] HACHE, G., CHUNG, H.M., The history of LOCA embrittlement criteria, No. ANL/ET/CP-102703, Argonne National Lab., IL USA (2001).
- [4] Interim Acceptance Criteria for Emergency-Core-Cooling Systems for Light-Water Power Reactor, U.S. Federal Register 36 (125), (1971) 12247-12250.
- [5] Atomic Energy Commission Rule-Making Hearing, Opinion of the Commission, Docket RM-50-1 (28 December 1973).
- [6] CHUNG, H.M., KASSNER, T.F., Embrittlement criteria for Zircaloy fuel cladding applicable to accident situations in light-water reactors. Summary report, No. NUREG/CR-1344; ANL-79-48, Argonne National Lab., IL USA (1980).
- [7] KIM, J.H., LEE, M.H., CHOI, B.K. and JEONG, Y.H., Failure behavior of Zircaloy-4 cladding after oxidation and water quench, *Journal of Nuclear Materials* **362** (2007) 36–45.
- [8] NAGASE, F, FUKETA, T., Effect of pre-hydriding on thermal shock resistance of Zircaloy-4 cladding under simulated loss-of-coolant accident conditions, *Journal of nuclear science and technology* **41** (2004) 723–730.
- [9] KIM, J.H., LEE, M.H., CHOI, B.K., JEONG, Y.H., Embrittlement behavior of Zircaloy-4 cladding during oxidation and water quench, *Nuclear Engineering and Design* **235** (2005) 67-75.
- [10] YAN, Y., BURTSEVA, T.A., BILLONE, M.C., Letter Report from Argonne National Laboratory to NRC “Post-quench Ductility Results for North Anna High-burnup 17×17 ZIRLO Cladding with Intermediate Hydrogen Content”, US NRC ADAMS Accession Number ML091200702 (April 17, 2009)
- [11] CLIFFORD, P.M., FLANAGAN, M.E., Proposed Modification of Cladding Embrittlement Criteria, Proceedings of Top Fuel 2009, Paris, France, September 6-10, 2009, Paper 2120.
- [12] STUCKERT, J., GROSSE, M., STEINBRÜCK, M., WALTER, M., WENSAUER, A., “Results of the QUENCH-LOCA experimental programme at KIT”, ASTM Special Technical Publication in Proceedings of 19th International Symposium “Zirconium in the Nuclear Industry”, STP-1622, Manchester, May 2019 (in press).
- [13] VESHCHUNOV, M.S., BOLDYREV, A.V., OZRIN, V.D., SHESTAK, V.E., TARASOV, V.I., A new mechanistic code SFPR for modeling of single fuel rod performance under various regimes of LWR operation, *Nuclear Engineering and Design* **241** (2011) 2822-2830.
- [14] VESHCHUNOV, M.S., PALAGIN, A.V., VOLCHEK, A.M., YAMSHCHIKOV, N.V., BOLDYREV, A.V., GALIMOV, R.R., KURCHATOV, S.YU., in Transactions of SMiRT-13 Conference, Vol.1 (1995) 159–163.
- [15] HOFMANN, P., NOACK, V., VESHCHUNOV, M.S., BERDYSHEV, A.V., BOLDYREV, A.V., MATWEEV, L.V., PALAGIN, A.V., SHESTAK, V.E., Physico-Chemical Behavior of Zircaloy Fuel Rod Cladding Tubes During LWR Severe Accident Reflood, Report FZKA 5846, Karlsruhe, Germany (1997).
- [16] HOFMANN, P., MIASSOEDOV, A., STEINBOCK, L., STEINBRUECK, M., BERDYSHEV, A.V., BOLDYREV, A.V., PALAGIN, A.V., SHESTAK, V.E., VESHCHUNOV, M.S., Quench Behavior of Zircaloy Fuel Rod Cladding Tubes. Small-Scale Experiments and Modeling of the Quench Phenomena, Report FZKA 6208, INV-COBE (98)-D018, Karlsruhe, Germany (1999).
- [17] GORYACHEV, A.V., VESHCHUNOV, M.S., “Main results of the ISTC Project #1648.2”, 14th International QUENCH Workshop, 2008, Karlsruhe, Germany.

- [18] VESHCHUNOV, M.S., SHESTAK, V.E., Modeling of Zr alloy burst cladding internal oxidation and secondary hydriding under LOCA conditions, *Journal of Nuclear Materials*, 461 (2015)129–142.
- [19] STUCKERT, J., GROßE, M., RÖSSGER, C., KLIMENKOV, M., STEINBRÜCK, M., WALTER, M. QUENCH-LOCA programme at KIT on secondary hydriding and results of the commissioning bundle test QUENCH-L0, *Nuclear Engineering and Design* 255 (2013) 185–201.
- [20] INTERNATIONAL ATOMIC ENERGY AGENCY, Analysis of Options and Experimental Examination of Fuels for Water cooled Reactors with Increased Accident Tolerance (ACTOF), Report of a Coordinated Research Project 2015–2019, IAEA-TECDOC (in press).

LIST OF PARTICIPANTS

- Abe, A. Instituto de Pesquisas Energeticas e Nucleares – IPEN/CNEN – SP
Av. Prof. Mello Moraes 2231, 05508-030,
São Paulo, SP, Brazil,
Email: ayabe@ipen.br
- Bouloire, A. CEA/DEN/DEC Cadarache,
13108 Saint-Paul-lez-Durance,
France
Email: antoine.bouloire@cea.fr
- Chan, P. Royal Military College of Canada
Stn. Forces Kingston, ON K7K 7B4, PO Box 17000, Canada
Email: paul.chan@rmc.ca
- Chen, M. China Nuclear Power Technology Research Institute
Yitian Road; 1312/A, Jiangsu Bldg., Shenzhen 518026 Futian, China
Email: chenmengteng@cgnpc.com.cn
- Gaikwad, A.J. Atomic Energy Regulatory Board
Mumbai, India
Email: avinashg@aerb.gov.in
- Giovedi, C. AMAZUL,
Av. Prof. Lineu Prestes 2468,
São Paulo, SP, Brazil.
Email: claudia.giovedi@labeisco.usp.br
- Ieremenko, M. State Scientific and Technical Centre for Nuclear and Radiation Safety,
35–37, V. Stusa street, 03142, Kyiv, Ukraine
Email: ml_eremenko@sstc.com.ua
- Khodadadi, H. Nuclear Reactors Fuel Company
Roshan Dasht, Isfahan, Islamic Republic of Iran
hakhodadadi1986@gmail.com
- Kim, H.C. Nuclear Fuel Safety Research Division,
Korea Atomic Energy Research Institute,
989–111, Daedeok-daero, Yuseong-gu, Daejeon, 34057,
Republic of Korea
Email: hyochankim@kaeri.re.kr
- Lemes, M. Comisión Nacional de Energía Atómica,
Avenida General Paz 1499, 1650 San Martín,
Provincia de Buenos Aires, Argentina
Email: lemes@cnea.gov.ar

- Liu, S. Nuclear Power Institute of China,
Science and Technology on Reactor System Design Technology
Laboratory,
No. 328 Chang Shun Road, Hua Yang, Chengdu, Sichan, China
Email: hit_lsc@163.com
- Liu, T. China Nuclear Power Technology Research Institute (CNPRI)
Yitian Road; 1312/A, Jiangsu Bldg., Shenzhen 518026 Futian, China
Email: liutong@cgnpc.com.cn
- Loukusa, H. VTT Technical Research Centre of Finland Ltd.
Espoo, Finland
Email: henri.loukusa@vtt.fi
- Lovasz, L. Gesellschaft für Anlagen und Reaktorsicherheit (GRS) gGmbH,
Boltzmann str. 14, 85748, Garching, Germany
Email: liviusz.lovasz@grs.de
- Papp, H. Paks II. Ltd,
H-7030 Paks Gagarin u. 1., Hungary,
Email: papph@paks2.hu
- Ren, Q. China Nuclear Power Technology Research Institute (CNPRI)
Yitian Road; 1312/A, Jiangsu Bldg., Shenzhen 518026 Futian, China
Email: renquisen@cgnpc.com.cn
- Ševeček, M. Czech Technical University in Prague,
Faculty of Nuclear Sciences and Physical Engineering
V.Holesovickach 2, Phaha 8, 180 00, Czech Republic
Email: martin.sevecek@fjfi.cvut.cz
- Shin, C. Nuclear Fuel Safety Research Division,
Korea Atomic Energy Research Institute,
989-111, Daedeok-daero, Yuseong-gu, Daejeon, 34057,
Republic of Korea
Email: shinch@kaeri.re.kr
- Soba, A. Comisión Nacional de Energía Atómica,
Avenida General Paz 1499, 1650 San Martín,
Provincia de Buenos Aires, Argentina
Email: soba@cnea.gov.ar
- Stuckert, J. Karlsruhe Institute of Technology (KIT),
Hermann-von-Helmholtz-Platz 1, 76344 Eggenstein-Leopoldshafen,
Germany
Email: juri.stuckert@kit.edu
- Tang, C. Institute for Applied Materials,
Karlsruhe Institute of Technology,
Hermann-von-Helmholtz-Platz 1, 76344 Eggenstein-Leopoldshafen,
Germany
Email: chongchong.tang@kit.edu

- Vadi, R. Iran Nuclear Regulatory Authority
Atomic Energy Organization of Iran,
End of North Karegan Avenue, 14155–1339,
Tehran, Islamic Republic of Iran
Email: rvadi@aeoi.org.ir
- Veshchunov, M. Nuclear Fuel Cycle and Materials Section
International Atomic Energy Agency
Email: m.veshchunov@iaea.org
- Vlahovic, L. European Commission,
Joint Research Centre,
Hermann-von-Helmholtz Platz 1, 76344, Eggenstein-Leopoldshafen,
Germany
Email: luka.vlahovic@ec.europa.eu
- Zhang, J. Tractebel (ENGIE),
Boulevard Simon Bolivar 34–36, 1000,
Brussels, Belgium
Email: jinzhao.zhang@tractebel.engie.com
- Zhou, Y. Nuclear Power Institute of China,
No. 328 Chang Shun Road, Hua Yang, Chengdu, Sichan, China
Email: 214121048@99.com



ORDERING LOCALLY

IAEA priced publications may be purchased from the sources listed below or from major local booksellers.

Orders for unpriced publications should be made directly to the IAEA. The contact details are given at the end of this list.

NORTH AMERICA

Bernan / Rowman & Littlefield

15250 NBN Way, Blue Ridge Summit, PA 17214, USA

Telephone: +1 800 462 6420 • Fax: +1 800 338 4550

Email: orders@rowman.com • Web site: www.rowman.com/bernan

REST OF WORLD

Please contact your preferred local supplier, or our lead distributor:

Eurospan Group

Gray's Inn House
127 Clerkenwell Road
London EC1R 5DB
United Kingdom

Trade orders and enquiries:

Telephone: +44 (0)176 760 4972 • Fax: +44 (0)176 760 1640

Email: eurospan@turpin-distribution.com

Individual orders:

www.eurospanbookstore.com/iaea

For further information:

Telephone: +44 (0)207 240 0856 • Fax: +44 (0)207 379 0609

Email: info@eurospangroup.com • Web site: www.eurospangroup.com

Orders for both priced and unpriced publications may be addressed directly to:

Marketing and Sales Unit

International Atomic Energy Agency

Vienna International Centre, PO Box 100, 1400 Vienna, Austria

Telephone: +43 1 2600 22529 or 22530 • Fax: +43 1 26007 22529

Email: sales.publications@iaea.org • Web site: www.iaea.org/publications

International Atomic Energy Agency
Vienna
ISBN 978-92-0-108020-2
ISSN 1011-4289